
# Proteomic analysis of the response of murine bone marrow derived macrophages to IFN-γ stimulation and infection with *Staphylococcus aureus*

**Inauguraldissertation**

zur

Erlangung des akademischen Grades

Doktor rerum naturalium (Dr. rer. nat.)

die Mathematisch-Naturwissenschaftliche Fakultät

der Ernst-Moritz-Arndt-Universität Greifswald

Vorgelegt von **Dinh Hoang Dang Khoa**

geboren am 12.06.1981

in Binh Thuan - Vietnam

Greifswald, July 2010

Dekan: Prof. Dr. Klaus Fesser .....

1. Gutachter 1: Prof. Uwe Völker .....

2. Gutachter 2: Prof. Bhanu Sinha .....

Tag der Promotion: 9.12.2010 .....

.....

# Content

# Abbreviations

| | | |
|---|---|---|
| 2-DE | : | Two dimensional gel electrophoresis |
| 2D-DIGE | : | Two-dimensional difference gel electrophoresis |
| ACN | : | Acetonitrile |
| APS | : | Ammonium persulphate |
| BMM | : | Bone marrow derived macrophages |
| CD | : | Cluster of differentiation |
| CyDye | : | CyDye DIGE fluorescent dyes |
| Da | : | Dalton |
| DCs | : | Dendritic cells |
| DIGE | : | Fluorescence difference gel electrophoresis |
| DNA | : | Deoxyribonucleic acid |
| DTT | : | Dithiothreitol |
| ER | : | Endoplasmic reticulum |
| FBS | : | Fetal bovine serum |
| FCS | : | Fetal calf serum |
| Fig. | : | Figure |
| HPLC | : | High performance liquid chromatography |
| IAA | : | Iodoacetamide |
| ID(s) | : | Identifier(s) |
| IEF | : | Isoelectric focusing |
| IFNGR | : | Interferon gamma receptor |
| IFN-γ | : | Interferon gamma |
| IL | | Interleukin |
| iNOS | : | Inducible nitric oxide synthase |
| IPG | : | Immobilized pH gradient |
| IPI | : | International Protein Index |
| kDa | : | Kilodalton |

| | | |
|---|---|---|
| LC | : | Liquid chromatography |
| LC-MS/MS | : | Liquid Chromatography-Tandem Mass Spectrometry |
| LPS | : | Lipopolysaccharide |
| MALDI | : | Matrix-assisted laser desorption/ionization |
| MHC | : | Major histocompatibility complex |
| min | : | Minute |
| *Mr* | : | Molecular mass |
| mRNA | : | Messenger ribonucleic acid |
| MS | : | Mass spectrometry |
| MS/MS | : | Tandem mass spectrometry |
| NADPH | : | Nicotinamide adenine dinucleotide phosphate |
| NCBI | : | National Center for Biotechnology Information |
| NK | : | Natural killer cell |
| NO | : | Nitric oxide |
| NOS | : | Nitric oxide synthase |
| PANTHER | : | Protein Analysis Through Evolutionary Relationships |
| PBS | : | Phosphate buffered saline |
| PCA | : | Principal components analysis |
| *pI* | : | Isoelectric point |
| PTM | : | Post-translational modification |
| RNA | : | Ribonucleic acid |
| RNI | : | Reactive nitrogen intermediate |
| ROI | : | Reactive oxygen intermediate |
| ROS | : | Reactive oxygen species |
| *S. aureus* | : | *Staphylococcus aureus* |
| SDS | : | Sodium dodecyl sulphate |
| SDS-PAGE | : | Sodium dodecyl sulfate polyacrylamide gel electrophoresis |
| STAT | : | Signal transducer and activator of transcription |
| Suppl. | : | Supplements |
| TBS | : | TRIS-buffered saline |

| | | |
|---|---|---|
| TEMED | : | N,N,N',N'-tetramethylethylenediamine |
| TGF-β | : | Transforming growth factor beta |
| TH | : | T helper cell |
| TLR | : | Toll-like receptor |
| TNF | : | Tumor necrosis factor |
| Tris | : | Tris(hydroxymethyl) aminomethane |
| *vs.* | : | versus |

# List of Figures and Tables

## Figures

# Tables

# Summary

Macrophages which are distributed throughout the normal body provide the first line of defence against microbial pathogen infections. With vigorous phagocytosis ability, macrophages can eliminate a wide variety of invading microorganisms including viruses, bacteria, fungi and protozoa. Macrophages also function as professional antigen presenting cells which connect innate and adaptive arms of the immune system. Moreover, many secreted cytokines from macrophages are involved in modulation of the immune response. IFN-γ is well known as a main macrophage stimulator. IFN-γ stimulated macrophages possess higher bactericidal capacity than in normal state. Many physiological and functional changes in IFN-γ stimulated macrophages were reported such as inducing in production of reactive oxygen species (ROI), nitric oxide (NO), and secretion of pro-inflammatory cytokines. However, information about the changes in the proteome of macrophages upon activation by IFN-γ is still limited.

Murine bone marrow derived macrophages (BMMs) are a good model for investigating macrophage biology. In this study, murine BMMs were generated from a well defined standardized serum-free culture system which ensures in comparison to established serum-cultivation improved reproducibility and accuracy of the results. Effects of stimulation with IFN-γ on the proteome of BMMs from an infection-susceptible mouse strain BALB/c and a resistance mouse strain C57BL/6 were studied by complementary 2D-DIGE (gel-based) and LC-MS/MS (gel-free) approaches.

A 2-DE proteome reference map of BMMs was created from protein pools of BMM-BALB/c and BMM-C57BL/6 proteins via 2-DE electrophoresis and MALDI-TOF/TOF-MS. This reference map covers 252 identified protein spots of 145 unique proteins. Functional analysis showed that “protein metabolism and modification”, “immunity and defense”, “cell structure and motility” were the most abundant biological functional groups among the identified proteins.

Applying the 2D-DIGE technique, we identified 18 and 19 proteins spots, respectively, for which spot intensities were significantly changed in BMM-BALB/c and BMM-C57BL/6 due to IFN-γ stimulation. While LC-MS/MS analysis revealed 45 and 53 IFN-γ affected proteins, respectively, in BMM-BALB/c and BMM-C57BL/6. Interestingly, results of the two proteomics analyses showed that BMMs derived from susceptible strain BALB/c and resistance strain C57BL/6 responded to IFN-γ stimulation with a consistent pattern. The functions of the identified IFN-γ regulated proteins could be assigned to transcription regulation (STAT1), microbicidal activity (members of p47 and p65 GTPases), antigen presentation (components of MHC class I and class II molecule, TAP2, lysosomal cathepsins), cell survival (PRDX4, NAMPT, AIF-1), and metabolism (hexokinases, ACSL1).

The activation of macrophage is believed to be a two step process [1]: the first step requires a priming signal (prototypically IFN-γ) which, though capable of inducing a number of changes, is insufficient to endow the responding cell with full functional competence. Exposure to the second triggering signal (lipopolysaccharide, for example) is sufficient to complete the functional activation process. For obtaining an overview of the macrophage activating process, we designed experiments to gain information about changes in the proteome of macrophages in each of the two steps of activation. IFN-γ activated BMM-C57BL/6 were allowed to internalize *Staphylococcus aureus* and changes in the proteome were analyzed 6 h and 24 h after exposure of BMMs to *S. aureus*. With an LC-MS/MS approach, 13 and 45 proteins of IFN-γ activated BMM-C57BL/6 were found to change in amount at the two time points (6 h and 24 h) after *S. aureus* infection, respectively. Functional analysis showed that the proteins displaying changes in intensity upon interaction with *S. aureus* are involved in microbicidal activity (NOS2, OAS1A, GBP5), inflammation regulation (PTGS2, IL1B, CAV1, SQSTM1), cell-cell interaction (CD14), protein and glucose uptake (SLC7A2, SLC3A2, SLC2A1), lipid metabolism (ACSL1, LPL), and cellular iron homeostasis (FTH1, ACO2, HMOX1, ALAS1). Interestingly, we have observed that stimulation with IFN-γ and interaction with *S. aureus* mostly targeted different sets of proteins, while synergistic effect were observed for seven proteins which were regulated by both factors.

In general, mice of the strain C57BL/6 are more resistance to microbial infection than mice of the strain BALB/c. Moreover, BMM-C57BL/6 were reported to possess a higher capacity of killing *B. speudomallei* in comparison with BMM-BALB/c [2]. Therefore, the differences in the proteome and transcriptome of BMMs derived from susceptible BALB/c and resistant C57BL/6 mice may be related to the differences in bactericidal capacity. Surprisingly, while many differences between BMM-BALB/c and BMM-C57BL/6 were found at the protein level, only few differences were observed at the mRNA level. At the protein level, 168 and 204 out of total 914 proteins spots (2D-DIGE analysis); 218 and 308 out of total 946 proteins (LC-MS/MS analysis) were found to be present at different levels in BMM-BALB/c and BMM-C57BL/6 non-stimulated or after IFN-γ treatment, respectively. While at mRNA level, the corresponding numbers of genes differentially expressed between non-stimulated and IFN-γ treated BMMs were 222 and 230 out of 20,074 genes, respectively. The differences between proteomic and transcriptomic data may due to different post-transcriptional mRNA processing, translational regulation and post translational modification (PTM) activities in BMM-BALB/c and BMM-C57BL/6. Interestingly, cellular location analysis showed that most of proteins which were more abundant in BMM-C57BL/6 were located in mitochondria and the lysosome, two cellular compartments important for immunological function of macrophages.

# 1. Introduction

## 1.1. Macrophages

### 1.1.1. Macrophage origin and morphology

Macrophages are distributed throughout the normal body and display regional heterogeneity [3]. They can be found in lung (alveolar macrophages), liver (kupffer cells), spleen (red pulp macrophages), skin (langerhans cells), and intestine. Macrophages differentiate from circulating peripheral blood mononuclear cells, which migrate into tissue in the steady state or in response to inflammation. These peripheral blood mononuclear cells develop from a common myeloid progenitor cell in the bone marrow that is the precursor of many different cell types, including neutrophils, eosinophils, basophils, macrophages, dendritic cells and mast cells. During monocyte development, myeloid progenitor cells (termed granulocyte/macrophage colony-forming units) sequentially give rise to monoblasts, pro-monocytes and finally monocytes, which are released from the bone marrow into the bloodstream [4].

Macrophages are generally large, irregularly shaped cells measuring 25-50 µm in diameter. Electron microscopy demonstrates an eccentric nucleus of variable shape, with chromatin disposed in fine clumps. Clear spaces between membrane-fixed chromatin clumps mark the site of nuclear pores. The cytoplasm contains scattered strands of rough endoplasmic reticulum, a well-developed Golgi complex in a juxtanuclear position, variable number of vesicles, vacuoles and pinocytic vesicles, large mitochondria and electron dense membrane bound lysosomes which can be seen fusing with phagosomes to form secondary lysosomes. Within the secondary lysosomes, ingested cellular, bacterial and non-cellular material can be seen in various stages of degradation and digestion. Microtubules and microfilaments are prominent in macrophages and form a well-organized, three-dimensional cytokeleton which surrounds the nucleus and extends throughout the cytoplasm to the cell periphery [5].

### 1.1.2. Immunological function of macrophages

Microbial pathogens must breach normal host defences to establish invasive infections. With vigorous phagocytic ability, macrophages function as the first line of defense to eliminate the invaders and to maintain sterility of deep tissues. Moreover, through antigen presentation function, macrophages are key regulators of the immune system connecting innate and specific

immune responses. They also participate in the activation of T and B lymphocytes through the secretion of many cytokines.

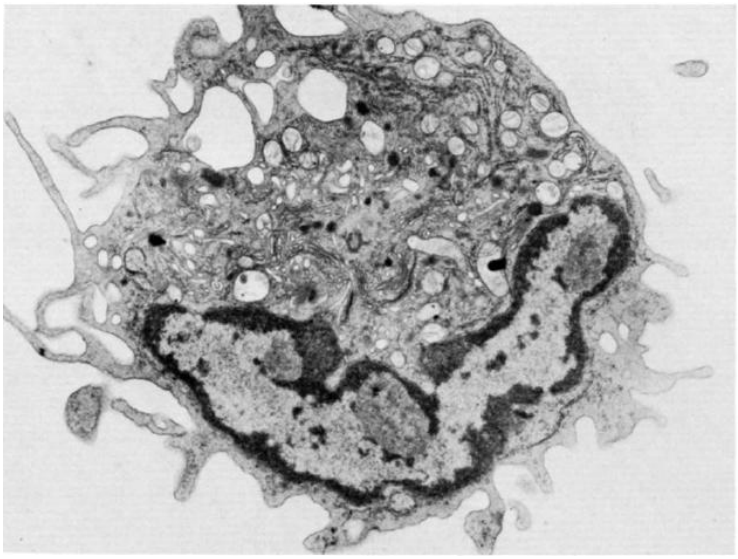

**Figure 1: Typical appearance of macrophage.** The cell surface exhibits many membrane extensions. The cytoplasm contains some dense granules corresponding to lysosomes. The Golgi apparatus is well developed. The nucleus presents its typical lobate shape and a rather thick layer of dense chromatin along its membrane (12,000 x) [6].

### *1.1.2.1. Microbial pathogen phagocytosis*

The central feature of macrophages is the ability to eliminate free or opsonized invading microorganisms through phagocytosis. In viral infection, mononuclear phagocytes (blood monocytes, tissue macrophages, and dendritic cells) have the ability to engulf and eliminate virus from the circulation following a blood-borne infection. Their scavenger function constitutes a first line of defence that reduces the virus load until specific immune responses become available [7]. Phagocytosis and bacterial killing are functions for which macrophages are well suited. They ingest potential pathogens via an array of non-opsonic and opsonic receptors and kill their prey with the oxygen-dependent and oxygen independent mechanisms. In oxygen-dependent mechanisms, macrophages produce reactive oxygen intermediates (ROIs) such as superoxide ($O_2^-$), hydrogen peroxide ($H_2O_2$) and hydroxyl radicals ($OH^-$). ROIs are microbicidal by virtue of the damage they cause to bacterial DNA and membranes [8]. In the second mechanism, macrophages may destroy pathogen with reactive nitrogen intermediates (RNIs), defensins, and lysosomal degradative enzymes [9]. The digested microorganism derived antigens are then

presented to T-cells in regional lymph nodes for initiation of specific immune responses that subsequently clear the infection.

#### *1.1.2.2. Antigen presentation*

The professional antigen presentating cells include macrophages, langerhans cells, dendritic cells and B lymphocytes [10]. Macrophages take up, process and present antigen for lymphocyte recognition involving both major histocompatibility complex (MHC) class I and class II pathways. Through that, they present antigen to surveillance $CD8^+$ and $CD4^+$ T cells creating the initial communication between the innate and acquired arms of the immune system. In general, antigens in the class I pathway originate from cytosolic proteins and antigens in the class II pathway originate in lysosomes. After viral infection of macrophages, viral antigens are processed in the cytosol, transported into the endoplasmic reticulum and presented on the surface of macrophages in association with MHC class I molecules. Binding between receptors of $CD8^+$ T cells and antigen-MHC class I molecule complexes usually results in stimulation of cytotoxic effector mechanism. Antigen-MHC class II molecule complexes are recognized by $CD4^+$ T cells. Activation of $CD4^+$ T cells can initiate a T helper cell response, B-cell activation, and immunoglobulin secretion [11].

#### *1.1.2.3. Immune modulation*

It has become apparent that mononuclear phagocytes, in addition to their phagocytic and immune-modulating properties, have an extensive secretory capacity that includes secretion not only of enzymes but of many other biologically active substances. Over 100 substances have been reported to be secreted by mononuclear phagocytes, with molecular mass ranging from 32 Da (superoxide anions) to 440 000 Da (fibronectin), and biological activity ranging from cell growth to cell death. They are enzymes, enzyme inhibitors, complement components, reactive oxygen intermediates, arachidonic acid intermediates, coagulation factors, and cytokines [1, 12].

Macrophages are known to produce IFN-α in response to viruses, bacteria, and tumor cells. The biological actions of IFN-α include antiviral and antimitotic effects, up-regulation of MHC class II expression, and an increase in natural killer cell activity. Once induced, IFN-α can restrict viral replication in infected macrophages as well as in neighbouring cells [13].

Monocytes, together with many other cells, produce interleukin 1 (IL-1), which is involved in immunoregulation, influencing IL-2, IL-4, IL-6, IL-1 and tumor necrosis factor alpha (TNF-α) production [14]. IL-1 represents a family of polypeptides with a wide range of biological activities including augmentation of cellular immune responses (T-, B-, and NK cells), proliferation of fibroblasts, chemotaxis of monocytes, neutrophils, and lymphocytes; stimulation of prostaglandin $E_2$, increasing in numbers of peripheral blood neutrophils, and neutrophil activation [15].

Human monocytes, together with lymphocytes, hepatocytes, endothelial cells, and dermal fibroblasts, also secrete IL-8 [16]. This cytokine stimulates the chemotaxis of both neutrophils and T-cells, and inhibits IFN-γ release by human NK cells *in vitro* [17]. The expression of the IL-8 gene in monocytes is regulated by known inflammatory agents, such as LPS, $PGE_2$, IL-1, TNF-γ and IFN-γ [18].

### 1.1.3. Other functions of macrophages

Besides immunological functions, it is now known that macrophages are involved in other important processes such as tumor cell control, disposal of damaged or senescent red cells, wound healing and tissue repair. Macrophages infiltrate tumours and lysis of tumour cells by monocytes and macrophages are thought to be a mechanism of host defence against tumours [19]. Cultured human monocytes have been reported to kill tumour cells when activated with cytokines and endotoxin [20]. Macrophages phagocytose aged erythrocytes during their circulation through the spleen. The mechanism whereby macrophages recognize senescent cells is unknown. Senescent red cells are sequestered in the spleen and their destruction presumably occurs because of a subtle abnormality detected by splenic macrophages. Once ingested by macrophages, the erythrocyte is degraded to liberate iron from haem, which is then stored in the protein complexes and transferred to developing erythroblasts [21]. Macrophages are rapidly recruited to wounds after injury, where they can synthesize collagenase and elastase, helping to debride the wound [22, 23]. Macrophages also participate in wound healing and tissue remodeling by releasing substances that induce fibroblast proliferation and neovascularization and in remodeling bone through resorption by osteoclasts [24].

## 1.2. IFN gamma activation of macrophages

### 1.2.1. IFN gamma

Interferons were discovered because of their potent antiviral activity [25]. IFN-γ is also known as type II IFN or immune IFN. In contrast to the large number of type I (α, β and ω) IFN genes and proteins found in mice and human, there is only one IFN-γ gene and protein. IFN-γ maps to a single locus located on the long arm of chromosome 12 in the human, and chromosome 10 in the mouse. Mature IFN-γ messenger ribonucleic acid (mRNA) is ~1.2 kb and encodes a protein of ~17 kDa [26].

IFN-γ is a crucial factor in the clearance of infection as impaired production of IFN-γ or defects in the IFN-γ signaling pathway result in increased susceptibility to various bacterial [27] and viral infections [28]. During the innate inflammatory response, IFN-γ is produced mainly by natural killer cells and subsets of T lymphocytes, including natural killer T cells and $CD8^+$ T cells [29].

IFN-γ primarily signals through the Jak-Stat pathway, a pathway used by over 50 cytokines, growth factors, and hormones to affect gene regulation. After the binding of IFN-γ to its receptor, Jak1 and Jak2 are activated and phosphorylate a specific tyrosine residue on the interferon gamma receptor 1 (IFNGR1) subunit creating a docking site for Stat1. Janus kinases (Jaks) phosphorylate signal transducer and activator of transcription 1 (Stat1) on tyrosine 701 resulting in the dimerization of Stat1 which then translocates into the nucleus and binds to specific DNA elements, known as gamma activated sequence, and regulate gene expression [30].

### 1.2.2. Effects of IFN-γ on macrophages

Macrophage stimulation with IFN-γ induces direct antimicrobial and antitumor mechanisms as well as up-regulating antigen processing and presentation pathways [31].

One of the most important effects of IFN-γ on macrophages is the activation of microbicidal effector functions. Macrophages activated by IFN-γ display increased pinocytosis and receptor mediated phagocytosis as well as enhanced microbial killing ability. IFN-γ-activated microbicidal ability includes induction of the nicotinamide adenine dinucleotide phosphate (NADPH)-dependent phagocyte oxidase (NADPH oxidase) system (“respiratory burst”), priming for nitric oxide (NO) production, tryptophan depletion, and up regulation of lysosomal enzymes promoting microbe destruction [32].

Superoxide and its reactive products are important microbicidal effectors of macrophages. The superoxide anion, $O_2^-$, is generated by an enzyme complex known as reduced nicotinamide adenine dinucleotide phosphate (NADPH) oxidase during a process called "respiratory burst". This enzyme is composed of a membrane associated flavocytochrome $b_{559}$ (a heterodimer consisting of two subunits, $gp91^{phox}$ and $p22^{phox}$) concentrated in the phagosome membrane and four cytosolic components: $p47^{phox}$, $p67^{phox}$, $p40^{phox}$, and the small guanosine triphosphatase (GTPase) Rac. Upon appropriate stimulus (e.g., phagocytosis), the cytosolic components translocate to the membrane to form the active complex, which generates superoxide in the phagosome through transfer of a transported electron to molecular oxygen [33]. The superoxide anion generated by the "respiratory burst" spontaneously reacts to form hydrogen peroxide ($H_2O_2$), hydroxyl radicals (·OH), and hypochlorous acid (HOCl). The toxic oxidants produced by the respiratory burst are also able to react with those produced by inducible nitric oxide synthase (iNOS), thereby forming a large number of different toxic species (e.g., peroxynitrite) to mediate cytotoxicity by a wide variety of mechanisms [34]. The primary mechanism of IFN-γ induced up-regulation of reactive oxygen species (ROS) production in phagocytes is transcriptional induction of the $gp91^{phox}$ and $p67^{phox}$ subunits of the NADPH oxidase complex [35].

Nitric oxide is produced in the NADPH-dependent conversion of L-arginine to L-citrulline by the nitric oxide synthase enzymes (NOS1–3). The NOS2/iNOS isoform alone is inducible by cytokine and/or microbial stimulus. IFN-γ dependent reactive nitrogen intermediate production is associated with increased ability of phagocytic cells to kill ingested pathogens, while mice in which the iNOS gene has been mutated show greater susceptibility to viral, bacterial and parasitic infection. IFN-γ induces RNI production by up-regulating expression of the iNOS enzyme. Maximal induction of iNOS transcription requires "priming" and "triggering" stimuli such as priming with IFN-γ and subsequent triggering with LPS or TNF-α [34].

With ability to modulate both cell-mediated immunity mediated by T helper 1 (TH1) cells and humoral immunity mediated by T helper 2 (TH2) cells, IFN-γ appears as an important regulator of both innate and adaptive immunity. IFN-γ induces antigen presentation of both MHC class I and class II pathways in macrophages [27]. Up-regulation of MHC class I antigen presentation is important for the host response to intracellular pathogens, as it increases the potential for cytotoxic T cell recognition of foreign peptides and thus promotes the induction of cell-mediated immunity. IFN-γ was reported to induce expression of MHC class I component.

Moreover, it also up-regulates the expression of a transporter associated with antigen processing (TAP) which is vital in peptide transport from the cytosol to the endoplasmic reticulum (ER) lumen. TAP transiently associates with class I MHC to aid in efficient peptide loading [27]. IFN-γ induces a replacement of the constitutive proteasome subunits with "immunoproteasome" subunits which in turn increase the quantity, quality, and repertoire of peptides for class I MHC loading [36]. Of the IFNs, IFN-γ alone can efficiently up-regulate the class II antigen presenting pathway and thus promote peptide-specific activation of $CD4^+$ T cells [27]. IFN-γ treatment further up-regulates class II MHC molecules in cells constitutively expressing class II MHC, such as B cells, dendritic cells (DCs), and cells of the monocyte-macrophage lineage [37]. IFN-γ also up-regulates expression of cathepsins B, H, and L, lysosomal proteases which are implicated in production of antigenic peptides for class II MHC loading [38, 39].

## 1.3. Proteomics studies of macrophages

### 1.3.1. Strategies of proteomics analysis

The term "proteome" was first introduced in the mid-1990s by Wilkins and Williams to indicate the entire "protein" complement expressed by a "genome" of a cell, tissue, or entire organism [40]. The proteome of a cell is therefore cell's specific protein complement in a defined physiological context at a specific point in time. Instead of focusing on single proteins, proteomics takes a broader, more comprehensive and systematic approach to the investigation of biological systems.

Proteomics provides information which that can't be accessed by genomic techniques. For example, transcriptomics, a genome-wide measurement of mRNA expression levels, is limited in the fundamental knowledge of protein expression, stability, and post-translational modifications in response to biological or physical signals. Moreover, the mRNA level in a cell or tissue does not necessarily reflect the level of proteins [41]. Often, proteins undergo numerous co- and post-translational modifications such as proteolysis, phosphorylation, glycosylation, acetylation, isoprenylation, etc., to reach their functional active form. Interestingly, these modifications represent an essential source of information that cannot be deduced from the sequence of the corresponding gene. Therefore, it is now clearly that only proteomics analysis can provide a comprehensive and quantitative description of the protein pattern and its changes upon perception of biological or physical signals [42].

Two main strategies for protein separation and identification which are applied in recent proteomic studies are gel-fee and gel-based approaches. Two dimensional gel electrophoresis (2-DE) which was developed more than 30 year ago [43] remains the most powerful integrated separation method for proteins. Based on two independent biochemical characteristics of proteins, 2-DE combines isoelectric focusing, which separates proteins according to their isoelectric point (*pI*), and sodium dodecyl sulfate polyacrylamide gel electrophoresis (SDS-PAGE), which separates them further according to their molecular mass ($M_r$). The next typical steps of the workflow of gel-based proteomics are spot visualization and evaluation, expression analysis and finally protein identification by mass spectrometry. In conventional gel-based proteomic workflows, protein visualization was facilitated by post-2-DE staining of gels by different staining methods such as colloidal coomassie staining and silver staining. Then, the changes in the protein levels were determined by comparing spot intensities from multiple 2-DE gels. However, protein spot detection and quantitation might lack accuracy due to the gel to gel variation and poor reproducibility. Recently, conventional 2-DE has been combined with protein labeling strategies using up to three different fluorescent dyes to allow comparative analysis of different protein samples within a single 2-D gel. In this technique, termed differential in-gel electrophoresis (DIGE), samples are labeled separately then combined and run on the same 2-DE gel minimizing experimental variation and greatly facilitating spot matching. Furthermore, the dyes afford great sensitivity with detection down to 125 pg of a single protein, and a linear response to protein concentration up to five orders of magnitude [44, 45]. However, even with the 2D-DIGE technique there are still some disadvantages such as difficulties in handling hydrophobic proteins, detecting proteins with extreme molecular mass ($M_r$) and isoelectric point (*pI)* values, as well as limited capability for automation and its labour-intense nature [44].

Non-gel-based quantitative proteomics methods have, therefore, also been developed significantly in recent years. As opposed to 2-DE, where the samples are separated at the protein level, most gel-free proteomic approaches are performed at the peptide level. First, the complex protein mixtures are digested by endopeptidases (usually trypsin) to peptides which are then separated according to chemical properties (hydrophobicity and charge) by (1D-3D) liquid chromatography (LC). Then, the eluted peptides can be directly introduced into the mass spectrometer. Thus, this method has advantages in the generation of automated workflows. In gel-free LC-based proteomics, protein quantitation is accomplished by stable isotope labelling or label-free strategies [46, 47].

Stable isotopes can be introduced *in vivo* by feeding cells or an entire organism with a medium enriched with stable isotopes. Alternatively, the isotope can be introduced into the proteins after extraction from the sample, using a covalent coupling reagent that contains either the natural or the heavy form of the isotope. By mixing the differently labeled samples before analysis, experimental procedures can be performed on the mixture of samples. Quantification of changes in protein concentration is then performed by comparing the signal intensities of peptide ions containing the stable isotope versus the natural compound [48]. However, most labeling-based quantification approaches have potential limitations. These include increased time and complexity of sample preparation, requirement for higher sample concentration, high cost of the reagents, incomplete labeling, and the requirement for specific quantification software [49, 50].

More recently, high resolution quantitative approaches have been reported that rely on LC-MS quantitation of peptide concentrations by comparing peak intensities between multiple runs obtained by continuous detection in MS mode. A characteristic of these comparative LC-MS procedures is that they do not rely on the use of stable isotopes; therefore the procedure is often referred to as label-free LC-MS. Major advantages of label-free approaches are that they are simpler, since no additional chemistry or sample labelling steps are required. Furthermore, comparative quantification of multiple samples can be performed in one experiment [50, 51]. In protein-labeling approaches, different protein samples are combined together once labeling is finished and the pooled mixtures are then taken through the sample preparation step before being analyzed by a liquid chromatography-tandem mass spectrometry (LC-MS/MS) experiment. In contrast, in label-free quantitative methods, each sample is separately prepared and then subjected to individual LC-MS/MS runs. Protein quantification is generally based on two categories of measurements. In the first are the measurements of ion intensity changes such as peptide peak areas or peak heights in chromatography. The second is based on the spectral counting of identified proteins after MS/MS analysis. Peptide peak intensity or spectral count are measured for individual LC-MS/MS runs and changes in protein abundance are calculated via a direct comparison between different analyses [50]. It was reported that peak ion intensity measurements yielding greater accuracy than spectral counting in reporting changes in protein abundances [52].

### 1.3.2. Macrophage proteomics

Despite the important roles of macrophages, until now there only some proteomics studies about this cell type have been reported so far. The first 2-DE maps of the human macrophage proteome and secretome were recently published. A total of 127 and 66 distinct intracellular and

secreted protein spots, corresponding to 100 and 38 different proteins, respectively, were identified by mass spectrometry. Functional classification using information from the SWISS-PROT and PUBMED databases showed that most of identified proteins are involved in cell structure (19%), carbohydrate metabolism (16%), cell death/defense (15%), and protein metabolism (13%) [53].

Engulfed invading microbes are killed in phagosomes of macrophages. Using LC-MS/MS technique, Dupont et al., identified 167 IFN-γ-modulated proteins on macrophage phagosomes of which more than 90% were up-regulated. Many of IFN-γ regulated proteins were expected to alter phagosome maturation, enhance microbe degradation, trigger the macrophage immune response, and promote antigen loading on MHC class I molecules. The representative IFN-γ up-regulated proteins which associated with microbicidal function including more than ten different lysosomal hydrolases; four subunits of the V-type proton ATPase (V-ATPase) complex, the proton pump that acidifies the phagosome lumen; and two subunits of NADPH oxidase, the protein complex that generates reactive oxygen species within phagosomes [54].

Microtubules are major structural components of the cytoskeleton that are intricately involved in cell morphology, motility, division and intracellular organization and transport. Most recently, the proteomic analysis of changes in macrophage microtubule cytoskeleton proteins during activation was reported. Microtubule cytoskeleton proteins were extracted from RAW264.7 macrophages which were stimulated with IFN-γ and lipopolysaccharide (LPS). Applying a LC-MS/MS aaproach, the analysis identified 409 proteins that bound directly or indirectly to microtubules. Of these, 52 were up-regulated and 42 were down-regulated 2-fold or greater after IFN-γ/LPS stimulation. Many identified proteins showed preferential recruitment to microtubules depending on the activation status of macrophages [55].

## 1.4. Interaction of *Staphylococcus aureus* and macrophages

*Staphylococcus aureus* (*S. aureus*) is a Gram-positive pathogen and can be found as part of the resident flora of humans. *S. aureus* permanently colonizes the moist squamous epithelium of the anterior nostrils of 20 % of the population, and is transiently associated with another 60 % [56]. However, this member of our benign natural flora can become a formidable intruder when the body defense is compromised, causing diseases ranging in severity from minor superficial skin infections, such as abscesses and impetigo, to life threatening invasive infections, such as septic arthritis, osteomyelitis and endocarditis [57]. In addition, *S. aureus* can also cause toxin-

mediated diseases, such as toxic shock syndrome, staphylococcal food poisoning and staphylococcal scalded skin syndrome.

*S. aureus* was reported to be resistant to bactericidal attack inside the phagocytic vacuoles of neutrophils. Engulfed *S. aureus* may avoid phagocytic killing, by interfering with phagosome endosome fusion and by resistance against released antimicrobial substances [58]. The latter is partially due to the natural modifications of cell wall components, lipoteichoic acid and membrane phospholipid, for example, D-alanine substitutions of ribitol teichoic acid and lipoteichoic acid and L-lysine additions to phosphatidylglycerol. The modifications not only repel the cationic defensins which are released into the neutrophil phagosome but they also protect *S. aureus* from the positively charged antimicrobial proteins in serum, such as phospholipase A2 and lactoferrin [59]. In addition, *S. aureus* can interfere with the lethal effects of free oxygen radicals released by neutrophils during the oxidative burst. For example, the yellow carotenoid pigment of *S. aureus* scavenges oxygen free radicals [60]. *S. aureus* anti-oxidant enzymes such as superoxide dismutase enzymes (Sod A and Sod M) and catalase (KatA) protect *S. aureus* by removing harmful superoxide radicals [61]. Furthermore, to neutralize antimicrobial peptides, *S. aureus* secretes several proteins that can bind and cleave them. Aureolysin cleaves and inactivates the human defensin peptide cathelicidin LL-37 and contributes significantly to resistance to the peptide *in vitro* [62]. Staphylokinase also has potent defensin-peptide-binding activity and contributes to the protection of bacteria [63]. *S. aureus* can also resist lysozyme, and recently the responsible gene, *oatA*, which encodes an integral membrane protein, was identified. The *oatA* deletion mutant had an increased sensitivity to lysozyme [64].

*S. aureus* is known to be able to survive in mice and rat macrophages [65, 66]. Recently, it was reported that significant numbers of *S. aureus* cells which had avoided killing during the first 4–5 days post-phagocytosis were suddenly able to lyse the macrophages in which no signs of apoptosis or necrosis were previously demonstrated. Bacterial survival and escape from phagocytes was dependent not only on α-hemolysin, but also on functional *agr* and $\sigma^B$ loci, as well as on the expression of sortase A and the metalloprotease, aureolysin. Interestingly, macrophages were able to eliminate intracellular staphylococci if pre-stimulated with IFN-γ [67]. However, little is known about how IFN-γ stimulated macrophages respond to internalized *S. aureus*.

## 1.5. A reproducible experimental system - Bone marrow derived macrophages in serum-free culture

Murine bone marrow derived macrophages (BMMs) are a good model for studying macrophage biological processes and functions including macrophage activation, phagocytosis, and secretion. Fetal bovine serum or calf serum (FBS and FCS, respectively) are the most widely used growth supplements for cell culture, primarily because of their high levels of growth stimulatory factors and low levels of growth inhibitory factors. However, it is known that FCS contains several ill-defined substances like transforming growth factor beta (TGF-β) and other cytokines, antigenic peptides, trace elements, endotoxin, glucocorticoids and other hormones which can preactivate and polarise immune cells including macrophages [68-70]. Additionally, a high degree of serum variability was found both within and between suppliers concerning chemical, protein, and endocrine parameters, suggesting that caution should be employed in the interpretation of results from experiments utilizing serum supplements without specific quantitation of possible interfering or modulating factors [71]. Therefore, a standardised serum-free cell culture would be valuable to assure reproducibility as well as more accuracy of results.

There are few studies which dealt with the generating of serum-free cultivation conditions for BMMs. However, the outcomes did not seem satisfying because of the poor adherence and low yield of macrophages obtained [68, 72]. Recently, Eske et al., reported a new standardised cell culture protocol for generating BMMs from mice of strains BALB/c and C57BL/6. With the procedure, serum-free grown macrophages yielded excellent adherence since more than 97% of cells remained attached after washing steps. More than 95% of them possessed macrophage-associated markers including F4/80, CD11b, CD11c and MOMA-2. Moreover, the serum-free system allowed generation of mature BMMs from BALB/c and C57BL/6 mice which exhibited comparable differences in the bactericidal activity against *B. pseudomallei* as previously reported under serum-containing conditions [2]. BALB/c and C57BL/6 BMMs which were generated in the standardised serum-free cell culture system were used in our study for investigation of the effects of IFN-γ stimulation and *S. aureus* engulfment on macrophages.

# 2. Materials and Methods

## 2.1. Materials

### 2.1.1. Chemicals

| Name | Source |
|---|---|
| Acetic acid | Roth or Sigma |
| Acetonitrile (ACN) | Merck |
| Acrylamide/Bisacrylamide (37.5:1) 40% | AppliChem |
| Agarose | Invitrogen |
| Ammonium bicarbonate ($NH_4HCO_3$) | Sigma |
| Ammonium persulphate (APS) | GE HealthCare |
| Ammonium sulphate ($(NH_4)_2SO_4$) | Merck |
| Bradford reagent | Bio-Rad |
| Bromophenol blue | Sigma |
| CHAPS | Sigma |
| Coomassie brilliant blue G-250 | Merck |
| Cy2, Cy3, Cy5 dyes for DIGE | GE HealthCare |
| Di-sodium hydrogen phosphate ($Na_2HPO_4$) | Sigma |
| Dithiothreitol (DTT) | GE HealthCare |
| Ethanol | Merck |
| Formaldehyde 37% | Sigma |
| Glycerol 87% | GE HealthCare |
| Glycine | Roth |
| Immobiline Drystrip cover fluid | GE HealthCare |
| Iodoacetamide (IAA) | Sigma |
| IPG Strips | GE HealthCare |
| Isopropanol | Merck |
| Methanol | Merck |
| Pharmalytes 3-10 and Pharmalytes 8-10.5 | GE HealthCare |
| Phosphoric acid | Roth |

| Name | Source |
|---|---|
| Potassium chloride (KCl) | Merck |
| Potassium dihydrogen phosphate ($KH_2PO_4$) | Roth |
| Silver nitrate ($AgNO_3$) | AppliChem |
| Sodium carbonate ($Na_2CO_3$) | Merck |
| Sodium chloride (NaCl) | Roth |
| Sodium dihydrogen phosphate ($NaH_2PO_4$) | Sigma |
| Sodium dodecyl sulphate (SDS) | Roth |
| Sodium hydroxide (NaOH) | Roth |
| Sodium pyrophosphate | Sigma |
| Sodium thiosulfate pentahydrate ($Na_2S_2O_3 .5H_2O$) | Merck |
| TEMED | GE HealthCare |
| Thiourea | Sigma |
| Trifluoro acetic acid (TFA) | Merck |
| Tris(hydroxymethyl) amino methane | Merck |
| Triton X-100 | Sigma |
| Trypsin | Promega |
| Tween-20 | Sigma |
| Urea | Merck |

### 2.1.2. Instruments

| Name | Source |
|---|---|
| 4700- and 4800- Proteomics Analyzer | Applied Biosystems |
| Centrifuges | Eppendorf |
| Epson Expression 1680 pro scanner | Epson |
| Ettan Spot Handling Workstation | GE HealthCare |
| Exquest™ Spot cutter | Bio-Rad |
| IEF device, Multiphor II | GE HealthCare |
| LTQ-FT-ICR mass spectrometer | Thermo Fisher Scientific |

| Name | Source |
|---|---|
| nanoAcquity UPLC | Waters |
| Spectrophotometer (Ultrospec 2100 pro) | GE HealthCare |
| Typhoon 9400 scanner | GE HealthCare |

### 2.1.3. Software

| Name | Source |
|---|---|
| Delta2D version 3.6 | Decodon, Greifswald, Germany |
| PANTHER | http://www.pantherdb.org |
| PIPE | http://pipe.systemsbiology.net/ |
| Rosetta Elucidator | Rosetta Biosoftware, Seattle, WA, USA |
| UniProt IDs mapping tool | www.uniprot.org/mapping/ |

## 2.2. Methods

### 2.2.1. Sample preparation

#### 2.2.1.1. *Stem cell preparation, cultivation, and differentiation to macrophages*

BMMs cultivation, IFN-γ stimulation, and *S. aureus* infection were performed by staff of the Institute of Medical Microbiology, University of Greifswald, Germany. Preparation and cultivation of mouse stem cells and their differentiation to bone-marrow derived macrophages (BMMs) was conducted as described by Eske [2]. Briefly, bone marrow cells from tibias and femurs of n=3 or n=15 BALB/c or n=4 or n=15 C57BL/6 mice were prepared under sterile conditions, pooled and cultivated for ten days using the serum-free BMM-medium supplemented with granulocyte-macrophage colony-stimulating factor (GM-CSF). Differentiated BMMs were harvested on day 10 for consecutive experiments.

A total of six cell culturing batches of BMMs were used in this project. Four BMM batches were used for proteomic analysis. Two batches (BMM1 and 2) were used to create a 2-DE macrophage proteomic reference map, one batch (BMM2) was used for analyzing IFN-γ effects, the other two batches (BMM5 and 6) were used for studying effects of *S. aureus* engulfment in macrophages (see table 1).

**Table 1: BMM batches used in the study**.

| BMM-batches | BMM-samples | IFN-γ treatment | *S. aureus* infection | Transcriptomic analysis | Proteomic analysis | Purpose |
|---|---|---|---|---|---|---|
| BMM1 | BALB/c C57BL/6 | +/- | - | no | **yes** | 2-DE proteomic map |
| BMM2 | BALB/c C57BL/6 | +/- | - | yes | **yes** | 2-DE proteomic map; IFN-γ effects; strain differences |
| BMM3 | BALB/c C57BL/6 | +/- | - | yes | no | IFN-γ effects; strain differences |
| BMM4 | BALB/c C57BL/6 | +/- | - | yes | no | IFN-γ effects; strain differences |
| BMM5 | C57BL/6 | + | +/- | no | **yes** | *S. aureus* effects |
| BMM6 | C56BL/6 | + | +/- | no | **yes** | *S. aureus* effects |

A total of six BMM sample batches was used in the study. Symbol "+" means that all BMM samples in the BMM batch received a refered treatment (IFN-γ stimulation or *S. aureus* infection), while symbol "-" indicates that none of the samples were treated. Symbol "+/-" means that the BMM batch included both treated and non-treated control sample. "Yes" or "No" mean the corresponding BMM batch was analyzed with a selected technique or not.

#### *2.2.1.2. Interferon-γ activation of bone marrow derived macrophages*

Mature BMMs were seeded in 6-well-plates with 0.8 - 1.5 x $10^6$ cells/well. BMMs in half of the wells were activated for 24 hours by addition of 300 units/ml IFN-γ (Roche, Mannheim, Germany) to serum-free BMM-medium, the other half was cultivated for the same time in the same medium without IFN-γ. For transcriptome analysis 1.6 - 4.5 x $10^6$ cells/sample were available, while proteome analysis needed a higher cell number and therefore had a sample size of 1 - 1.5 x $10^7$ cells.

#### *2.2.1.3. S. aureus infection*

Mature BMM-C57BL/6 were seeded in 48-well plates and stimulated with 300 units/ml IFN-γ for 24 h before *S. aureus* infection. Prior to infection BMMs were washed twice with PBS. S. *aureus* strain Newman was diluted in cell culture medium. In some wells which contained IFN-γ stimulated BMM-C57BL/6, *S. aureus* strain Newman was added at a MOI 200 for 60 min at 37°C. Then, the medium was removed, cells were washed twice with PBS and incubated with medium containing 50 µg/ml gentamycin for 30 min (this point was taken as time zero) and during further incubation to eliminate extracelluar bacteria. Cells were maintained further for several hours until harvesting. IFN-γ stimulated BMM-C57BL/6 with or without *S. aureus* infection were harvested at time point 6 h and 24 h after *S. aureus* engulfment for proteome analyses.

#### *2.2.1.4. BMM protein extraction for proteome analysis*

Cell pellets were resuspended in lysis buffer (8 M Urea, 2 M Thiourea, 2% [wt/vol] CHAPS) by vigorous pipetting. Then, cell mixtures were flash-frozen in liquid nitrogen for 20 s and afterwards thawed by shaking for 10 min at 30°C. The freeze-thaw cycle was repeated 6 times to assure that all cells were completely disrupted. Cell fragments were removed by centrifugation at 13500 rpm, 4°C for 20 min and protein concentrations were determined by Bradford assay.

#### *2.2.1.5. Determination of protein concentration*

For Bradford assays, concentration series of BSA-standard solution were made for preparation of a standard curve as described in the following table.

**Table 2: The serial dilution of BSA-standard solution**

| Amount (µg) | 0 | 1 | 2 | 4 | 6 | 8 | 10 | 12 |
|---|---|---|---|---|---|---|---|---|
| 0.1 µg/µl BSA (µl) | 0 | 10 | 20 | 40 | 60 | 80 | 100 | 120 |
| $H_2O$ (µl) | 800 | 790 | 780 | 760 | 740 | 720 | 700 | 680 |

The assay was started by adding 200 µl of Bradford reagent to each tube. After thorough mixing and incubation for 5 min at room temperature the absorbance was measured at 595 nm using a spectrophotometer. For the measurement of samples, the protein extract was diluted in steps of ten fold and three aliquots of each diluted sample were used for the determination of protein concentration. The mean value of three measurements was used to calculate protein concentrations of samples with the aid of the standard curve.

### 2.2.2. 2D-DIGE approach

#### *2.2.2.1. CyDye labeling reaction for DIGE experiment*

Minimal labelling with CyDye DIGE Fluor minimal dyes was performed according to the manufacturer's instructions (GE Healthcare). The CyDye working solution was prepared by adding one volume of CyDye stock solution to 1.5 volumes of dimethylformamide (DMF). Protein samples were adjusted to a pH of 8.5 with 50 mM NaOH. A protein pool was created by equally contributing aliquots of all different protein samples and used as an internal standard. Protein samples were labeled with Cy3 or Cy5, whereas the protein pool was labeled with Cy2 at

a ratio of 50 µg protein/400 pmol CyDye (1 µl of CyDye working solution). The labelled protein mixtures were incubated on ice in the dark for 30 min and the reaction was stopped by adding an equal (dye) volume of 10 mM lysine and kept on ice for a further 15 min in the dark. In the following 2-DE process, each 2-DE gel was loaded with 150 µg labeled protein which included 50 µg of a Cy3 labeled protein sample, 50 µg of a Cy5 labeled protein sample and 50 µg of the Cy2 labeled protein pool. Before IEF, protein samples were filled up with the rehydration buffer and reduced with dithiothreitol (DTT) as described below in the rehydration step.

#### *2.2.2.2. Rehydration*

For different purposes, a 2-DE gel might be loaded with different amounts of protein. For example, gels loaded with 150 µg (labelled) protein were used in quantitative 2D-DIGE experiments, and gels loaded with 400 µg protein were used as a reparative gel for creating the 2-DE protein reference map. A volume of protein sample solution containing the required amount of protein was mixed with rehydration buffer (8 M urea, 2 M thiourea, 2% CHAPS, 28.5 mM DTT, 1.3% Pharmalytes pH 3-10, and trace of bromphenol blue) to reach a final volume of 450 µl. Protein-rehydration buffer containing eppendof cups were then shaken at 20$^{o}$C in a thermomixer for 1 hour. Sample loading was performed carefully to avoid trapping air bubbles under the gel strips. Finally, all gel strips were covered with mineral oil and rehydrated overnight at 20°C on the surface of a Multiphor II device (Amersham Biosciences).

#### *2.2.2.3. IEF separation*

The rehydrated IPG strips were briefly rinsed with $dH_2O$ and blotted between two sheets of water saturated Whatman paper to remove the excess of mineral oil and rehydration solution. Gel strips were placed on the grooves of the isoelectric focusing tray (gel face up and acidic end toward the anode). Two wet electrode strips were placed at both ends of the gel strips before electrodes were applied and an extra DTT soaked electrode strip was placed next to the cathodic electrode strip. Then, all gel strips were covered with mineral oil to prevent evaporation during the IEF separation process. Isoelectric focusing was performed for a total of 60 kVh in three gradient phases using a Multiphor II device (table 3). After IEF, the gel strips were kept at -20$^{o}$C if not immediately used for equilibration.

**Table 3: IEF program for Immobiline DryStrip pH 4-7, 24 cm**

| Step | Voltage (V) | Vh | Duration (h) |
|---|---|---|---|
| 1 | 500 | 1 | 00:01 |
| 2 | 3500 | 3000 | 01:30 |
| 3 | 3500 | 57000 | 16:20 |
| Total | | 60001 | 17:51 |

#### *2.2.2.4. Equilibration*

Prior to SDS-PAGE, the IPG strips were equilibrated twice for 15 min each time in 5 ml equilibration buffer (375 mM Tris-HCl pH 8.8, 6 M urea, 20% glycerol, 4% SDS) containing first 1% dithiothreitol (DTT), and then 2.5% iodoacetamide (IAA) with traces of bromophenol blue. The gel strips were briefly rinsed with running buffer and placed on a wet Whatman paper for some seconds in order to drain off excess of equilibration buffer.

#### *2.2.2.5. Second dimension separation*

Gels for second dimension (gel size 24 cm x 20 cm x 1.5 mm) were prepared using an Ettan DALT Gel Caster (GE Healthcare). 2D-PAGE was performed using 12.5% acrylamide gels (1.5 M Tris-HCl pH 8.8, 12.5% acrylamide/bisacrylamide [37.5:1], 0.4% SDS, 0.05% APS, 0.0025% TEMED). The IPG strips were placed on top of the gels and covered with 0.5% agarose in 1x electrophoresis running buffer (25 mM Tris, 192 mM glycine, 0.4% SDS). The gel plates were loaded into the electrophoresis tank filled with 1x electrophoresis running buffer. 2D-PAGE was performed in a Dodecan system (BioRad) at 0.5W per gel for 1 hour followed by 2W per gel at 20$^{o}$C until the bromophenol blue tracking front ran off the bottom of the gels.

### 2.2.3. Protein spot visualization

#### *2.2.3.1. CyDye DIGE scanning*

After separation in the second dimension, gel plates were taken out of the 2-DE chamber, cleaned with dH2O and 70% ethanol to avoid interfering background. Gel scanning was performed with a Typhoon 9400 scanner (GE Healthcare) using the parameters suggested by the manufacturer for 2D-DIGE experiments. Gels were scanned at 100 μm resolution with 488/520

Blue, 532/580 Green, 633/670 Red nm excitation/emission wavelengths to obtain the images of the three CyDye channels, Cy2, Cy3 and Cy5, respectively. The signal intensities of all protein spots were optimized between 40-95000 pixels to avoid saturation effects. Gel images were cropped and saved as 16-bit TIFF files using ImageQuant Tools version 5.0 (GE Healthcare).

#### *2.2.3.2. Colloidal coomassie staining*

Gels were removed from the cassette and fixed in 40% methanol and 10% acetic acid for 1 h. After two washing steps with dH2O for a total of 20 min, the gels were stained with CBB-R250 overnight at room temperature with gentle agitation. Colloidal coomassie brilliant blue (CBB) G250 working solution was prepared from stock solution according to the manufacturer's instructions (0.08% CBB, 8% (NH4)2SO4, 0.8% phosphoric acid, 20% methanol). Before scanning, gels were destained with 20% methanol and stored in dH2O.

### 2.2.4. Spot detection and quantification

Analysis of the 2D-DIGE experiments was performed with the Delta2D software version 3.6 (Decodon, Greifswald, Germany). First, different gel images were mapped together through the internal standard gel images (identical protein pool). In a second step, all gel images of the project were merged to generate a fused image which included all protein spots of any individual gel. Spots on the fused gel image were automatically detected by the software, manual edition was applied for some spots to improve the accuracy of the spot detection process. Subsequently, the detected spot pattern of the fused gel image was transferred to each gel image included in the project. Spot intensities were calculated based on the area and pixel intensities of spots. The relative intensity of each spot (% volume) was determined by dividing the intensity of the spot by the sum of the intensities of all spots in the corresponding gel (per gel normalization) and the relative intensity of the corresponding spot on the internal standard gel labeled with Cy2. The mean relative spot intensities of all replicates of the different samples were used to evaluate the changes between groups. A protein spot was considered as up- or down-regulated when the expression ratio changed more than 1.5-fold and the p-value was less than 0.05.

### 2.2.5. Mass spectrometry analysis

#### *2.2.5.1. MALDI-TOF-MS/MS*

##### *2.2.5.1.1. Preparative gels*

For identifying proteins which are contained in protein spots on 2-DE gels by MALDI-MS/MS, preparative gels (each loaded with 400 µg protein) were run with crude extracts from BMM-BALB/c and BMM-C57BL/6. Protein extracts were separated by 2-DE using linear IPG strips 24 cm length, pH 4-7 for the first dimension and 12.5% SDS-PAGE (20 cm x 24 cm) for the second dimension. Preparative gels were stained with colloidal coomassie for visualization of protein spots. Three different preparative gels were created for spot cutting and protein identification by MALDI-MS/MS analysis. One of the three preparative gels was made of a protein pool of two samples BMM-C57BL/6 and BMM-C57BL/6 + IFN-γ from cell cultivation batch 1 (BMM1). The two other preparative gels were made of a protein pool of four samples BMM-BALB/c, BMM-BALB/c + IFN-γ, BMM-C57BL/6 and BMM-C57BL/6 + IFN-γ from cell cultivation batch 2 (BMM2).

##### *2.2.5.1.2. Protein identification by MALDI-TOF/TOF MS*

Protein spots separated on preparative gels were cut manually or with a spot cutter (ExquestTM Spot cutter, Bio-Rad) and transferred into 96 well microtiter plates filled with 200 µl of deionized water in each well. Tryptic in-gel digestion and subsequent spotting of peptide solutions onto the MALDI-targets were performed automatically in an Ettan Spot Handling Workstation (GE, Amersham Biosciences) using a modified standard protocol. Briefly, gel pieces were washed twice with 100 µl of 50 mM $NH_4HCO_3$ in 50% methanol for 30 min and once with 100 µl 75% acetonitrile (ACN) for 10 min. After 17 min drying, 10 µl of trypsin solution (prepared at 4 ng/µl in 20 mM $NH_4HCO_3$) were loaded into each well and incubated at 37 °C for 120 min. For peptide extraction, gel pieces were covered with 60 µl solution (0.1 % TFA and 50 % ACN) and incubated for 30 min at 37 °C. The peptide containing supernatant was transferred into a new microtiter plate and the extraction was repeated with 40 µl of the same solution. The supernatants were dried completely at 40°C for 220 min. Peptides were dissolved in 2.0 µl of matrix solution (3.2 mg/ml α-cyano-4-hydroxy cinnamic acid in 0.5% TFA and 50% ACN) and 0,7 µl of peptide solution spotted on the MALDI-target directly. Prior to the measurement in the MALDI-TOF/TOF instrument the samples were allowed to dry on the target 10 to 15 min.

The MALDI-MS measurement of spotted peptide solutions was carried out on a 4800-Proteomics-Analyzer (Applied Biosystems). The spectra were recorded in reflector mode in a mass range from 900 to 4000 Da with a focus mass of 2000 Da. For one main spectrum 20 sub-spectra with 100 shots per sub-spectrum were accumulated using a random search pattern. If the autolytic fragments of trypsin with the mono-isotopic $(M+H)^+$ m/z at 1045.5 or 2211.104 reached a signal to noise ratio (S/N) of at least 10, an internal calibration was automatically performed using these peaks for an one-point-calibration or a two-point-calibration. The peptide search tolerance was 50 ppm but the actual RMS value was between 5 and 15 ppm. Additionally, a manual calibration was performed if the automatic calibration failed.

MALDI-MS-MS analysis was performed for the five strongest peaks of the MS-spectrum. For one main spectrum 50 sub-spectra with 125 shots per sub-spectrum were accumulated using a random search pattern. The internal calibration was automatically performed as one-point-calibration if the mono-isotopic arginine $(M+H)^+$ m/z at 175.119 or lysine $(M+H)^+$ m/z at 147.107 reached a signal to noise ratio (S/N) of at least 7. Data were processed using the GPS Explorer Software version 3.6 (Applied Biosystems) with the following settings: (i) MALDI-MS: mass range from 900 to 4000 Da; peak density of 50 peaks per range of 200 Da; maximal 200 peaks per protein spot and minimal S/N ratio of 10. (ii) MALDI-MS/MS: mass range from 60 Da to a mass that was 20 Da lower than the precursor mass; peak density of 5 peaks per 200 Da; maximal 20 peaks per precursor and a minimal S/N ratio of 7.

Generated peak lists were searched again the mouse sequence database (SwissProt mouse 56.1) using the Mascot search engine (Version 2.0, Matrix Science Ltd). Proteins which were considered positively identified must have at least 95% of confidence identification (MOWSE score $\geq$ 56) and one MS/MS matched sequence with 95% confidence (ion score $\geq$ 26).

#### *2.2.5.2. Quantitative LC-MS/MS analysis*

Two µg proteins of each sample (in 1xUT-solution) were adjusted to a final concentration of 0.1 µg/µl using 20 mM $NH_4HCO_3$. Trypsin was added at a ratio of 1:25 (trypsin : protein), then protein digestion was allowed to take place for 15h at 37°C. Zip-Tip-C18 (Millipore Corporation) was used to concentrate and purify peptides prior to LC-MS analyses. Contaminations were removed by washing 5 times with 10 µl of 0.1% acetic acid and peptides eluted using 5 times 5 µl 50% and 5 times 5 µl 80% acetonitrile in 0.1% acetic acid. Samples

were concentrated by using a vacuum centrifugation (Eppendorf concentrator) to a volume of 2 µl, and then filled with 18 µl of port-A solution (1% acetic acid, 2% ACN). The sample solution was mixed and 0.3 µg proteins were injected to the LC-MS.

Prior to MS-analysis (Thermo Fisher Scientific Inc., Waltham, MA, U.S.A.) the samples were fractionated using the nanoAcquity UPLC (Waters, Eschborn, Germany) equipped with a $C_{18}$ nano Acquity column (100 µm × 100 mm, 1.7 µm particle size). Separation was achieved in a non-linear gradient within 300 min using 2% acetonitrile in 0.05% acetic acid in water (A) and 0.05% acetic acid in 90% acetonitrile (B) as eluents with a flow rate of 400 nL/min. Four technical replicates of each sample were analyzed immediately after each other. MS-data were generated by LTQ-FT-ICR MS (Thermo Fisher Scientific Inc., Waltham, MA, U.S.A.) equipped with a nanoelectrospray ion source (PicoTip Emitter FS360-20-20-CE-20-C12, New Objective). After a first survey scan in the FTICR (r=50,000) MS2 data were recorded for the five highest mass peaks in the linear ion trap at a collision induced energy (CID) of 35%. The exclusion time was set to 90 s and the minimal signal for MS2 was 1,000.

Differential analysis of label-free MS data was performed with Rosetta Elucidator (http://www.rosettabio.com/products/elucidator/default.htm) (Rosetta Biosoftware, Seattle, WA, USA). The frame and feature annotation was done using the following parameter: retention time minimum cut-off 40 min, retention time maximum cut-off 270 min, m/z minimum cut-off 300 and maximum 1,600. An intensity threshold of 1,000 counts, an instrument mass accuracy of 5 ppm, and an alignment search distance of 10 min were applied. For quantitative analysis, the data were normalized and further grouped. For identification, a complete IPI (International Protein Index) mouse (ipi.MOUSE.v3.56) FASTA sequence database was used (Sorcerer version 3.5, Sage-N Research, Inc.). Tandem MS spectra were searched with precursor ion tolerance of 10 ppm and a fragment ion mass tolerance of 1.00 Da. Oxidation of methionine was specified as variable modification. Peptide identifications were accepted if they exceeded a peptide teller score of 0.95. Ratio data were further merged with the peptide information and filtered prior to quantification using the following parameter settings: quantify only proteins with at least two peptides, one of the peptides needs to be unique, flag those as regulated if $p \leq 0.01$ and fold change $\geq 1.5$.

### 2.2.6. Functional classification of proteins

Protein functional classification was performed using the PANTHER (Protein Analysis Through Evolutionary Relationships) classification system (http://www.pantherdb.org). PANTHER is a unique resource that classifies genes and proteins by their functions, using published scientific experimental evidence and evolutionary relationships abstracted by curators with the goal of predicting function even in the absence of direct experimental evidence [73]. Firstly, lists of protein IPI accession numbers were translated into EntrezGene IDs using the PIPE (http://pipe.systemsbiology.net/pipe) and UniProt identifiers (IDs) (www.uniprot.org) mapping tool. Missing EntrezGene IDs were manually added if possible. Then, deduced EntrezGene ID lists were uploaded into PANTHER for functional classification based on the NCBI M. musculus database.

For information about protein subcellular locolization, deduced EntrezGene ID lists subcellular were uploaded into the web-based tool PIPE-Protein Information and Property Explorer (http://pipe.systemsbiology.net). After uploading, the subcellular localization analyses were performed with setting for M. musculus. The PIPE is interoperable with the Firegoose and the Gaggle, permitting wide-ranging data exploration and analysis. It can maps IPI, Uni- Prot, and NCBI protein identifiers to Entrez Gene IDs, gene symbols, descriptions, Gene Ontology terms, and more. The PIPE currently supports Human, Mouse, Rat, Yeast protein identifiers [74].

### 2.2.7. Transcriptomic analysis

Transcriptomic analyses of BMMs were performed by my colleague – Maren Depke as described below. Transcriptomic analysis was performed based on three biological replicates (BMM2, 3 and 4). Each biological replicate contained 4 different samples: 1) BMM-BALB/c, 2) BMM-BALB + IFN-γ, 3) BMM-C57BL/6, and 4) BMM-C57BL/6 + IFN-γ. Total mRNA from each of the 12 BMM samples was processed and analyzed with GeneChip® Mouse Gene 1.0 ST Array. Labeled cDNA for hybridization was prepared for each sample from 200 ng total RNA using the GeneChip® Whole Transcript (WT) Sense Target Labeling Assay and hybridized to GeneChip® Mouse Gene 1.0 ST Arrays according to the manufacturer's instructions (Affymetrix, Santa Clara, CA, USA). Arrays were washed and stained using the GeneChip® Hybridization, Wash, and Stain Kit in a GeneChip® Fluidics Station 450 and scanned with a GeneChip® Scanner 3000 (all items from Affymetrix, Santa Clara, CA, USA).

Resulting array image files (CEL-files) were imported to Rosetta Resolver® System (Rosetta Biosoftware, Seattle, WA, USA). Signal intensities were extracted using the RMA algorithm and differentially expressed probe sets were accessed with error-weighted one-way Analysis of Variance (ANOVA) including Benjamini Hochberg False Discovery Rate (FDR) multiple testing correction at the analysis levels of Intensity Profiles and sequences. Values of $p^* \leq 0.01$ were regarded as significant. Each statistical test compared two sample groups that consisted of three biological replicates each. Four comparisons were included into statistical testing: 1) BMM-BALB/c + IFN-γ versus BMM-BALB/c to access IFN-γ effects in BMM-BALB/c, 2) BMM-C57BL/6 + IFN-γ versus BMM-C57BL/6 to retrieve IFN-γ effects in BMM-C57BL/6, 3) BMM-C57BL/6 versus BMM-BALB/c to obtain strain differences at the non-activated control level, and 4) BMM-C57BL/6 + IFN-γ versus BMM-BALB/c + IFN-γ to elicit strain differences at the IFN-γ activated level.

The Rosetta Resolver® software allows mapping of 28944 records of sequence level information (i.e. the Affymetrix probe sets) to genes via the EntrezGene nomenclature resulting in 20,074 records. Additionally, the software calculates expression data for genes from the original sequence level values. This function also combines intensities of two or more probe sets for genes that are represented by more than one probe set. The lists of statistically significant differentially expressed probe sets resulting from ANOVA were translated into lists of differentially expressed genes by using the EntrezGene level annotation included in the Rosetta Resolver® software. In order to exclude biologically irrelevant small changes in expression level from the statistically significant lists resulting from ANOVA, expression data on EntrezGene level was restricted to a minimal absolute fold change of 1.5.

The transcriptomic intensity data was then subjected to Principal Component Analysis (PCA). This method calculates the direction of strongest variation from the multidimensional array data set, and reduces it to a new value of the parameter called Principle Component (PC). The remaining variation in the data set is subsequently addressed in the same way until all or a pre-defined fraction of variation is collapsed into new values. This procedure results in a set of PCs, of which each accounts for a fraction of the total variance in the data set. Usually, the first 2 or 3 PCs are displayed in a 2- or 3- dimensional coordinate system, respectively. In such plot the distance of the points, that represent the individual data sets, correlates to the difference between them. In this study the PCA plot was derived from log-transformed intensity data of 12 arrays, analyzing 3 biological replicates of 2 strains and 2 treatment groups.

# 3. Results

The mechanism of macrophage activation has attracted attention of many researches. However, adaptation of the proteome of macrophages due to physiological/biological signals such as IFN-γ stimulation has so far only partially been addressed. In order to gain a better coverage of the proteome of macrophages, we applied two complementing quantitative proteomic techniques: 2D-DIGE and LC-MS/MS for analyzing the response of BMMs to IFN-γ stimulation and *S. aureus* infection. Results of these proteomic analyses are arranged in four main work packages.

**Work package 1:** Creating a 2-DE protein reference map of BMMs (part 3.1): The 2-DE protein reference map contains all separated protein spots on 2-DE gels of BMM-BALB/c and BMM-C57BL/6. Based on the protein reference map, proteins of interest can later directly assessed. Besides that, some physiological/cellular characteristics of macrophages also can be deduced through analysis of biological function, existing level, and cellular location of proteins identified on the protein reference map.

**Work package 2:** Identifying effects of IFN-γ stimulation on the proteome of BMM-BALB/c and BMM-C57BL/6 (part 3.2): Many changes in macrophage cellular characteristics that occur in response to IFN-γ stimulation such as generation of reactive oxygen species, release of arachidonic acid and its metabolism, phagocytic activity and directed cell mobility are well described. However, litte is known about IFN-γ modulated changes in the proteome of macrophages and to which degree these are conserved in different mouse strains. To identify IFN-γ effects, the proteome of IFN-γ stimulated BMMs was compare with that of unstimulated control BMMs. Using 2D-DIGE and LC-MS/MS, we analyzed IFN-γ induced changes in the proteome of BMMs which derived from two different mouse strains: the infection susceptible mouse strain BALB/c and the resistant mouse strain C57BL/6.

**Work package 3:** Comparison of proteomes of BMM-BALB/c and BMM-C57BL/6 (part 3.3): In general, C57BL/6 mice possess a higher infection resistance capacity than BALB/c mice . Moreover, BMM-C57BL/6 were reported to more efficiently kill internalized *Burkholderia pseudomallei* than BMM-BALB/c. Therefore, there may be differences in the proteomes of BMMs which were derived from the two mouse strains. The differences, in turn, may reveal explanations for differences in microbicidal capacity of BMM-BALB/c and BMM-C57BL/6. Using 2D-DIGE and LC-MS/MS, we compared proteomes of BMMs derived from strain BALB/c and strain C57BL/6 without or with IFN-γ treatment.

**Work package 4:** Indentification of changes in proteomes of IFN-γ stimulated BMM-C57BL/6 due to *Staphylococcus aureus* engulfment (part 3.4): It is assumed that the macrophage activation process includes two steps which are responding to the priming signal (IFN-γ) and triggering signal. We wanted to collect information about the adaptation of the proteome of macrophages in each of the two stages of activation. Moreover, recently it was reported that internalized *S. aureus* can survive inside non-stimulated macrophages but not in IFN-γ stimulated macrophages [67]. The proteins displaying changes in intensity in response to interaction with *S. aureus* will be compared with identified IFN-γ regulated proteins to charcaterize the complementary effects of the two signals onto the proteome of BMM-C57BL/6.

Beside proteomic analyses, a parallel transcriptomic analysis was performed using the identical BMM samples. With both transcriptomic and proteomic data sets in hand, one can definitely have a more comprehensive overview of the molecular events inside macrophages. I have performed the proteomic analyses, while transcriptomic analyses were separately done by one of my colleagues – Maren Depke. Some results of this transcriptomic analysis are comparatively discussed with my proteomic data in this thesis.

The workflow of the proteomics/transcriptomics analysis is show in figure 2.

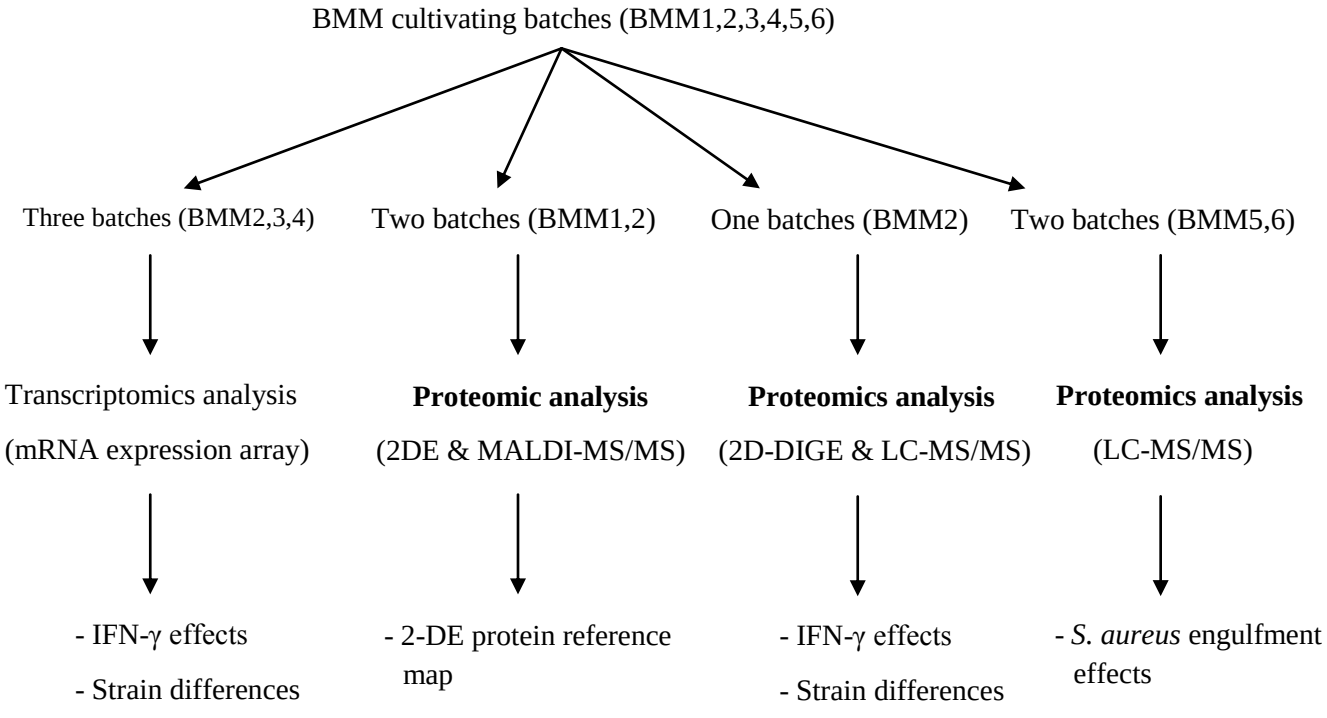


**Figure 2: Overiew of BMMs proteomics and transcriptomics analyses.**

## 3.1. 2-DE protein reference map of BMMs

In gel-based proteomic projects, establishing a two dimensional electrophoresis (2-DE) proteomic reference map is a necessary prerequisite. With a 2-DE proteomic reference map, one can infer included protein of interesting protein spots such as protein spots modulated due to treatment. Besides that, a 2-DE proteomic reference map reveals the composition of the accessible fraction of the extracted complex protein mixture. Based on this information, physiological and cellular characteristic of the corresponding cell type can be reasonably predicted. Therefore, we built a 2-DE proteomic reference map of BMMs using a pool of BMM-BALB/c and BMM-C57BL/6 whole cell extracts.

BMMs of BALB/c and C57BL/6 mice cultured for 10 tens in two independent BMM culturing batches (BMM1 and BMM2) were used for creating the proteomic reference map. Whole cell proteins of BMMs were extracted in Urea/Thiourea solution by the Freeze and Thaw protein extraction method. Protein concentrations were then determined with a Bradford assay. Three preparative gels from which protein spots were cut and analyzed by matrix-assisted laser desorption/ionization coupled with tandem mass spectrometry (MALDI-MS/MS) were created. After coomasie staining, 252 protein spots visible on preparative gels were cut and processed for MALDI-MS/MS measurements (as described in material and methods). Protein searches were performed with a mouse sequence database (SwissProt mouse 56.1) using the Mascot search engine (Version 2.0, Matrix Science Ltd). Proteins which were considered positively identified had to have at least 95% of confidence identification (MOWSE score $\geq$ 56) and one MS/MS matched sequence with 95% confidence (ion score $\geq$ 26).

Identified protein spots of the three preparative gels were mapped to the BMM union fused gel image of the analytical experiments. This BMM union fused image is basically a synthetic gel image created by the Delta2D software by combining several gel images into one. By this way, the BMM union fused image contained all spots of all combined images. In this study, the BMM union fused image was created by combining 16 different gel images which were obtained from the 2D-DIGE experiments (figure 4). Mapping of identified protein spots of the three preparative

gels to corresponding spots on the BMM union fused image was done using the "Gel image warping" function of the Delta2D software.

We have identified 145 distinct proteins in 252 protein spots. The identified protein spots labeled with the name of the corresponding protein are shown in figure 4. A protein reference map with all spots labeled with a spot number and a list of identified proteins are available in supplements (figure A.1 and table A.1). It is important to note that the total number of identified proteins in the 252 protein spots is 290 because some proteins were found in more than one spot. In detail, 99 identified distinct proteins were found in only 1 spot, while 46 distinct proteins were identified in more than one spot (see table 4).

**Table 4: Protein distribution on 2-DE proteomic reference map**.

| Distribution of identified proteins | |
|---|---|
| Number of containing spots | Proteins |
| 1 | 99 |
| 2 | 23 |
| 3 | 7 |
| 4 | 2 |
| 5 | 4 |
| 6 | 1 |
| 7 | 5 |
| 9 | 1 |
| 10 | 1 |
| 17 | 1 |
| 19 | 1 |

One of the most important criteria for quantitative proteomic analysis based on 2-DE technique is good separation capacity. Ideally, each protein spot should contain only one protein. This fact is important because when a regulated (induced/repressed) protein spot contains more than one protein, it is impossible to tell which of them is regulated. Our result showed that 218 protein spots contained only 1 protein/spot, 30 protein spots contained 2 proteins/spot, and 4 protein spots contained 3 proteins/spot.

The resolution range of our 2-DE system (using IPG strip pH 4-7 and 12.5% polyacrylamide gel) covers proteins with *pI* 4-7 and $M_r$ ~10 kDa – 100 kDa. Theoretical molecular mass ($M_r$) and isoelectric point (*pI*) of 136 identified proteins were in the experimental $M_r$/*pI* range. However, 19 identified proteins had theoretical $M_r$ and *pI* out of experimental $M_r$/*pI* range. The existence of the 19 proteins on experimental $M_r$/*pI* range may be due to protein modification, degradation, dimerizaion, and co-migration which lead to changes in $M_r$ and *pI* of the proteins (figure 3).

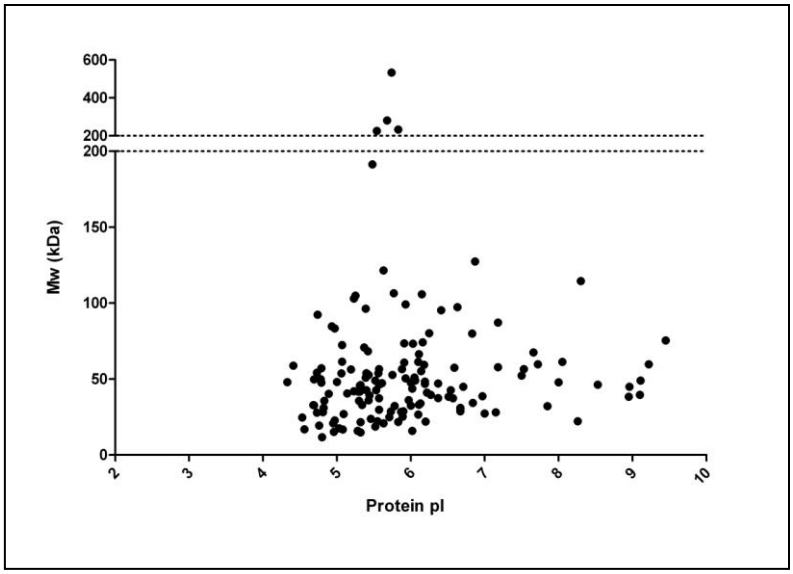


**Figure 3: Molecular mass – isoelectric point plot.** Theoretical *pI* and $M_r$ of 145 identified proteins are plotted on x and y axis, respectively.

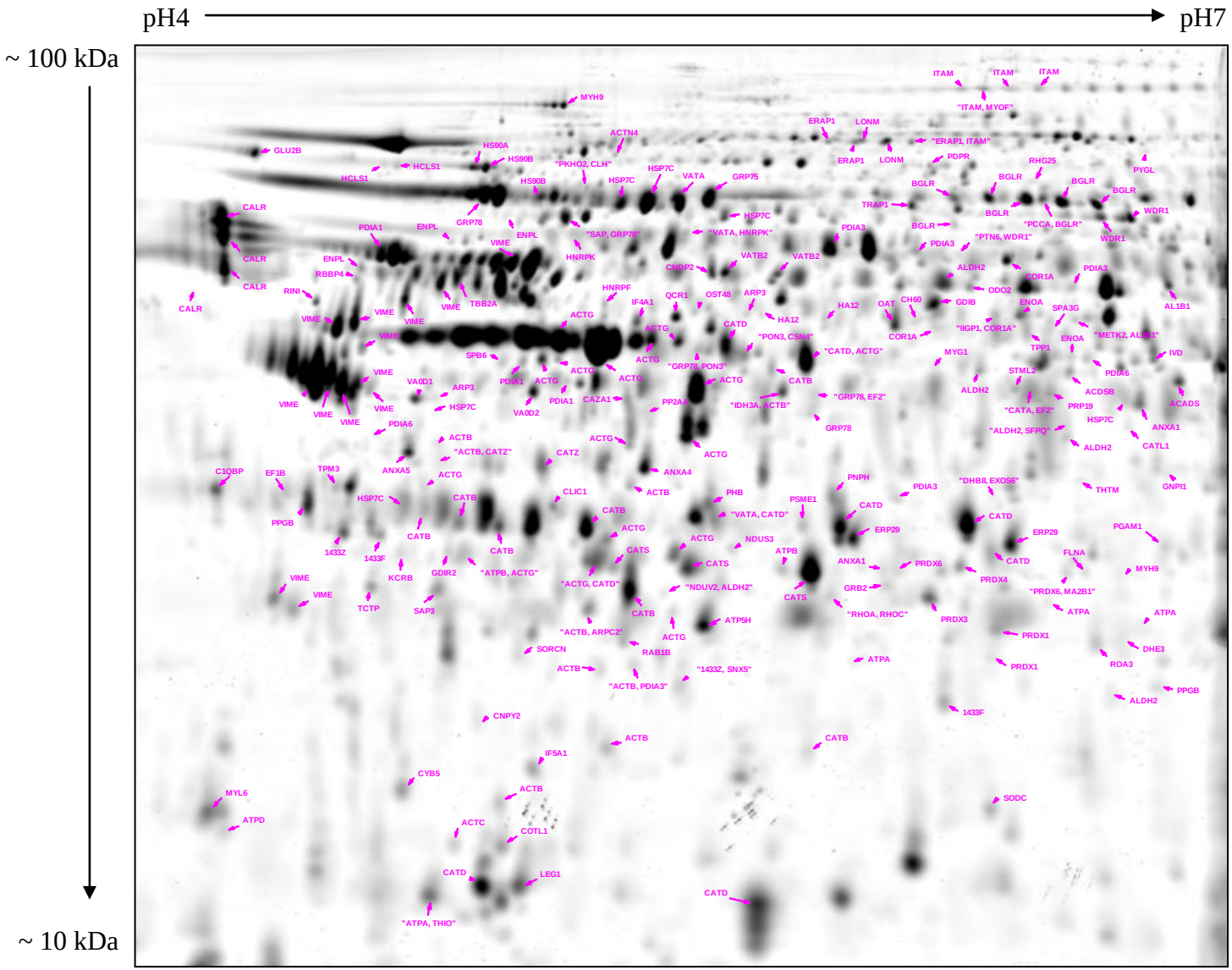


**Figure 4: 2-DE proteome reference map of BMMs.** Fused-gel-image was created by combining 16 gel images of 4 different BMM samples of the 2D-DIGE experiment. On the image, 252 identified protein spots are labeled with protein names. List of identified proteins is provided in suppl.table A.2.

Functional classification of the 145 identified proteins was performed using the PANTHER (Protein Analysis Through Evolutionary Relationships) classificaiton system. At first, UniProt IDs of the proteins were translated to entrez gene IDs by using the PIPE (Protein Information and Property Explorer) web-based software. Then, entrez gene IDs of 145 identified proteins were uploaded to PANTHER (version 6.1). With NCBI mouse databases selected, all 145 entrez gene IDs were mapped with the database and assigned to biological processes. In general, the most abundant biological process groups were "protein metabolism and modification", "immunity and defense", "cell structure and motility". The second abundant biological process groups included "nucleoside, nucleotide and nucleic acid metabolism", "signal transduction", "transport", "intracellular protein traffic", "carbohydrate metabolism", and "electron transport" (figure 5).

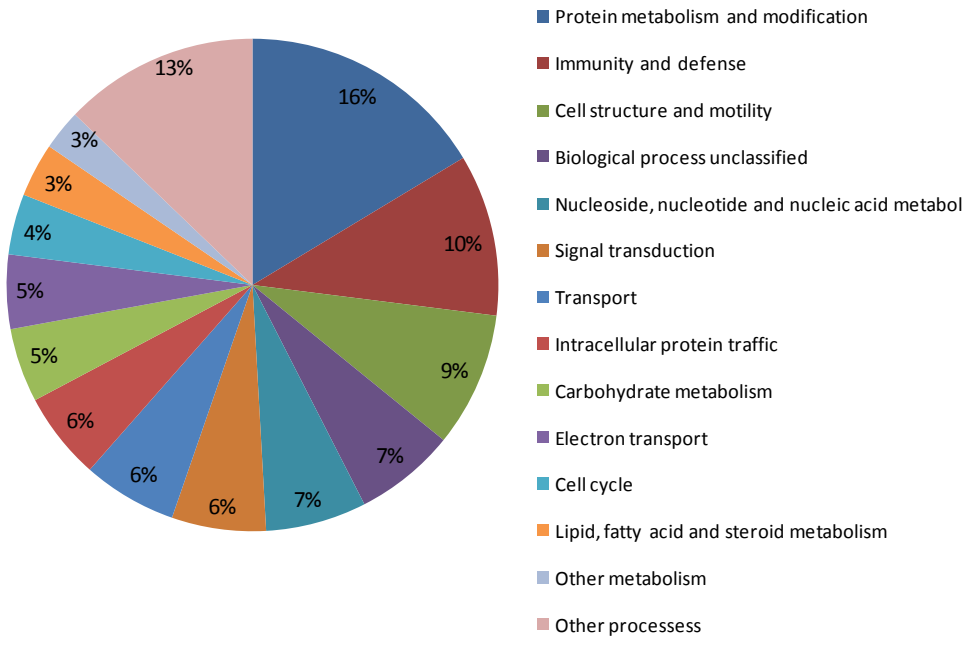


**Figure 5: Functional classification of identified proteins on the 2-DE proteome reference map.** Entrez Gene IDs of 145 identified proteins were uploaded to the PANTHER (version 6.1) classification system. Percentage of a biological process was calculated by its gene number divided by total gene number of all biological processes. On the diagram, 13 biological processes which included highest genes number were separately presented while the others were combined in group "other processes".

The large group of identified proteins was structural proteins. It included the most abundant proteins which existed in many different spots such as: vimentin (VIME), a cytoskeleton protein was found in 17 different spots (spot 381, 432, 453, 454, 461, 548, 555, 558, 574, 578, 589, 698, 792, 828, 829, 896, and 1015); actin cytoplasmic protein 1 and 2 (ACTB and ACTG) existed in a total of 29 spots (521, 526, 535, 536, 566, 567, 571, 577, 591, 594, 604, 657, 663, 673, 687, 712, 717, 767, 773, 776, 782, 802, 833, 846, 885, 886, 898, 920, 945); Tubulin beta-2A chain (TBB2A) which is the major constituent of microtubules was found in two spots (395, 433). Integrin alpha M (ITAM), a protein which participates in various adhesive interactions of monocytes, macrophages and granulocytes was observed in 7 spots (spot 16, 17, 51, 78, 105, 1021, 1051).

Besides that, another large group of identified proteins was lysosomal proteinases such as Cathepsin B (CATB) found in 7 spots (562, 740, 741, 744, 750, 815, 1068); Cathepsin D (CATD) in 9 spots (523, 536, 733, 747, 753, 777, 782, 975, 976); Cathepsin L1 (CATL1) in 1 spot (647); Cathepsin S (CATS) in 5 spots (633, 802, 783, 799, 772); and Cathepsin Z (CATZ) in 2 spots (687, 666). Serine protease inhibitors which control the activity of cathepsins were also observed such as serine protease inhibitor A3G (SPA3G) in spot 511 and Serpin B6 (SPB6) in spot 568.

Heat shock proteins are known to functions as molecular chaperones and involved in processing and transport of secreted proteins. Identified members of this protein group were heat shock protein HSP 90-alpha (HS90A) in spot 169; heat shock protein HSP 90-beta/Endoplasmin (HS90B1) in 5 spots (169, 240, 422, 374, 304); heat shock protein 5 (GRP78 ) in 7 spots (230, 243, 286, 552, 604, 614, 629); heat shock protein 8 (HSP7C) in 6 spots (241, 244, 278, 610, 632, 726); heat shock protein 9 (GRP75) in spot 237; heat shock protein 1 (CH60) in spot 524 and heat shock protein 105 kDa (HS105) in spot 57. Another protein chaperone, calreticulin (CALR) was found in 5 spots (267, 357, 390, 399, and 460).

Peroxiredoxins are involved in redox regulation of the cell. They protect radical-sensitive enzymes from oxidative damage by a radical-generating system. We have observed peroxiredoxin 1 (PRDX1) in 2 spots (859, 880); peroxiredoxin 3 (PRDX3) in spot 823; peroxiredoxin 4 (PRDX4) in spot 797; and peroxiredoxin 6 (PRDX6) in 2 spots (801, 808).

V-ATPase vacuolar ATPase proteins are responsible for acidifying a variety of intracellular compartments in eukaryotic cells. Vacuolar ATP synthase catalytic subunit A (VATA) was found in 3 spots (245, 340, 753), vacuolar proton pump subunit d1 (VA0D1) and d2 (VA0D2) in spot 606 and 598, respectively; vacuolar ATP synthase subunit B (VATB2) in 2 spots (409, 418).

Some of the proteins involved in carbohydrate metabolism such as beta-glucuronidase (BGLR) were found in 7 spots (238, 256, 257, 258, 263, 264, 317); alpha-enolase (ENOA) in 2 spots (1038, 1049); pyruvate kinase isozymes M1/M2 (KPYM) in spot 609; phosphoglycerate mutase 1(PGAM1) in spot 778; and glucosidase 2 subunit beta (GLU2B) in spot 118.

Mitochondrial membrane ATP synthase ($F_1F_0$ ATP synthase or Complex V) produces ATP from ADP in the presence of a proton gradient across the membrane which is generated by electron transport complexes of the respiratory chain. ATP synthase subunit alpha (ATPA) was found in 5 spots (833, 842, 853, 883 and 974); ATP synthase subunit beta (ATPB) in 3 spots (438, 773, and 798); ATP synthase subunit d (ATP5H) in spot 955; ATP synthase subunit d (ATP5H) in spot 837.

## 3.2. IFN-γ effect on BALB/c and C57BL/6 macrophages

High reproducibility between different biological replicates of BMMs samples was clearly depicted through analysis of the transcriptomic results (figure 10-B). Being convinced of the reproducibility of the cultivation and sample processing, we focussed time and efforts on a comprehensive analysis of only one biological replicate. Therefore, we selected BMM2 - one of three biological replicates which have been analyzed by the transcriptomic profiling - to be investigated by proteomic techniques. Quantitative proteomic 2D-DIGE and LC-MS/MS apporaches were applied to analysis whole cell protein extracts of four different samples: BMM-BALB/c, BMM-BALB/c + IFN-γ, BMM-C57BL/6, and BMM-C57BL/6 + IFN-γ of BMM2. The protein expression profiles which resulted from 2D-DIGE and LC-MS/MS analyses were used for idenfying IFN-γ effects as well as strain differences in the proteome of BMMs.

### 3.2.1. IFN-γ regulated proteins identified by 2D-DIGE technique

Extensive application of transcriptomic profiling is now routine for organisms for which the genome sequence is available and the information gained in such studies has provided new information that really extends our understanding of cellular complexity. However, the transcriptomic approach is limited in information of protein expression, stability, and post translation modifications in response to biological signals. Often, proteins undergo numerous co- and post-translational modifications such as proteolysis, phosphorylation, glycosylation, acetylation, isoprenylation, etc. to reach their functional active form.

Until now, two dimensional electrophoresis remains a routinely employed technique for the differential protein expression profiling and quantitative proteomics. This method is able to separate up to thousand of protein spots based on $M_r$ and pI. Moreover, it can easily locate post-translationally modified proteins, as they often appear as distinct rows of spots in the horizontal and/or vertical axis of the 2-DE gel due to differences in $M_r$ and charge as a result of the addition of the modification. However, standard 2-DE techniques also have their drawbacks, and one of that is high degree of gel-to-gel variation in spot patterns particularly between samples. As a result, it is difficult to distinguish any true biological variation from an experimental variation.

The development of the 2D-DIGE technique has largely resolved this problem. The 2D-DIGE technique enables up to three different protein samples to be run on a single 2-DE gel, where the differently fluorescently labeled protein samples are mixed before the first dimension run. The multiplexing procedure of the 2D-DIGE methodology allows the integration of the same internal standard on every 2-DE gel. This internal standard is a mix of all the samples within the experiment, and therefore includes each protein from each sample. It is useful for matching the protein patterns over gels thereby considerably minimizing the problem of inter-gel variation, which is common in standard “one sample per gel” 2-D electrophoresis experiments. Accurate quantitation of differences between samples, with an associated statistical significance, is then possible and the real biological change is easily distinguished from system variation and inherent biological variation. Therefore, the 2D-DIGE technique offers appropriate standardized quantitation for comparative proteomics. Based on fluorescent labeling, 2D-DIGE technique has great sensitivity with detection down to125 pg of a single protein and a linear response to

changes in protein concentration up to five orders of magnitude. In contrast, silver staining detects 1–60 ng of protein with a linear dynamic range of less than two orders of magnitude.

In the 2D-DIGE experiment, each of the four BMM samples was labelled with both fluor minimal dyes Cy3 and Cy5 and run in four technical replicates (2 x Cy3 and 2 x Cy5; figure 6). Independent labelling of each protein sample with the two fluor minimal dyes Cy3 and Cy5 enabled identification and exclusion of dye-specific labelling effects. The internal standard sample which was created from equal aliquots of the four different whole cell protein extracts was labeled with the fluor minimal dye Cy2. Twenty four fluorescent gel images (8 Cy3-, 8 Cy5- and 8 Cy2-labelled protein samples) obtained in this 2D-DIGE experiment were analyzed using the Delta2D software (Decodon, Greifswald, Germany). Quantitative and statistical comparison between control and IFN-γ treated BMM samples was performed based on 4 relative intensity values of each sample. Criteria minimal 1.5 fold change and $p \leq 0.05$ were applied as selection criteria for selecting IFN-γ modulated protein spots.

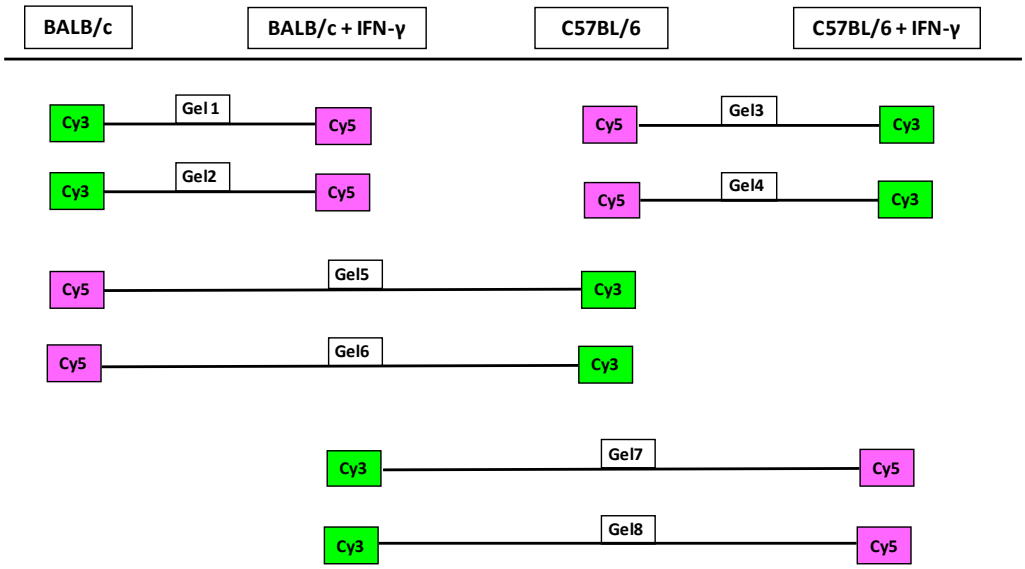


**Figure 6: 2D-DIGE experiment scheme.** Whole cell protein extract of BMM samples (each 50 µg) was labeled with one of two CyDye DIGE Fluor minimal dyes Cy3 and Cy5, respectively. The CyDye DIGE Fluor minimal dye Cy2 was used to label internal standard protein samples. Three labeled protein samples were jointly loaded on IPG strips 24 cm, pH4-7. Labeled proteins were firstly separated by their *pI* in IPG strips then by $M_r$ in 12.5% polyacrylamide gels (20 cm x 24 cm). Each of four BMM samples was labeled two times with Cy3 and two times with Cy5. A total of eight gels were used for separating 24 fluorescent labeled protein samples (8 Cy3-, 8 Cy5- and 8 Cy2-labelled protein samples). Three different fluorescent gel images were separately obtained from each gel by scanning gel at the corresponding excitation and emission wavelength for Cy2, Cy3 and Cy5 using a Typhoon Scanner.Green and pink color boxes mean the corresponding BMM sample was labeled with Cy3 or Cy5, respectively.

Quantitative analysis showed that intensities of 18 and 19 protein spots were significantly changed due to IFN-γ stimulation in BMM-BALB/c and BMM-C57BL/6, respectively. These protein spots were called "IFN-γ modulated protein spots" in this study. In general, the number of IFN-γ modulated protein spots was equal in both mouse strains, and corresponding to approximately 2% of the total of 914 protein spots separated on 2-DE gels. The group of protein spots with increased intensity upon IFN-γ stimulation was more abundance than group of protein spots with reduced intensity. Six IFN-γ modulated protein spots were common between two mouse strains BMM-BALB/c and BMM-C57BL/6 (table 5). There was no protein spot which was modulated by IFN-γ in the opposite direction in the two mouse strains. Based on the 2-DE protein reference map, we could identify 23 out of the 31 IFN-γ modulated protein spots in BMM-BALB/c and/or BMM-C57BL/6. The information about fold change and contained proteins of IFN-γ modulated protein spots in BMM-BALB/c and/or BMM-C57BL/6 is shown in table 6. Representative images for IFN-γ effects observed with 2D-DIGE approach are presented in figure 7 and 8.

**Table 5: IFN-γ modulated protein spots in BMM-BALB/c and BMM-C57BL/6 identified by the 2D-DIGE technique.**

| IFN-γ modulated protein spots | Spots with increased intensity | Spots with reduced intensity | Total |
|---|---|---|---|
| BMM-BALB/c | 12 | 6 | 18 |
| BMM-C57BL/6 | 13 | 6 | 19 |
| Overlap | 6 | 0 | 6 |

Quantitative analysis was performed with Delta2D software based on intensity data of four technical replicates. The threshold for considering as significant modulation was 1.5 fold change, and $p \leq 0.05$. The total number of separated protein spots on 2-DE gels was 914. Fold change and identified protein of IFN-γ modulated protein spots are shown in table 6.

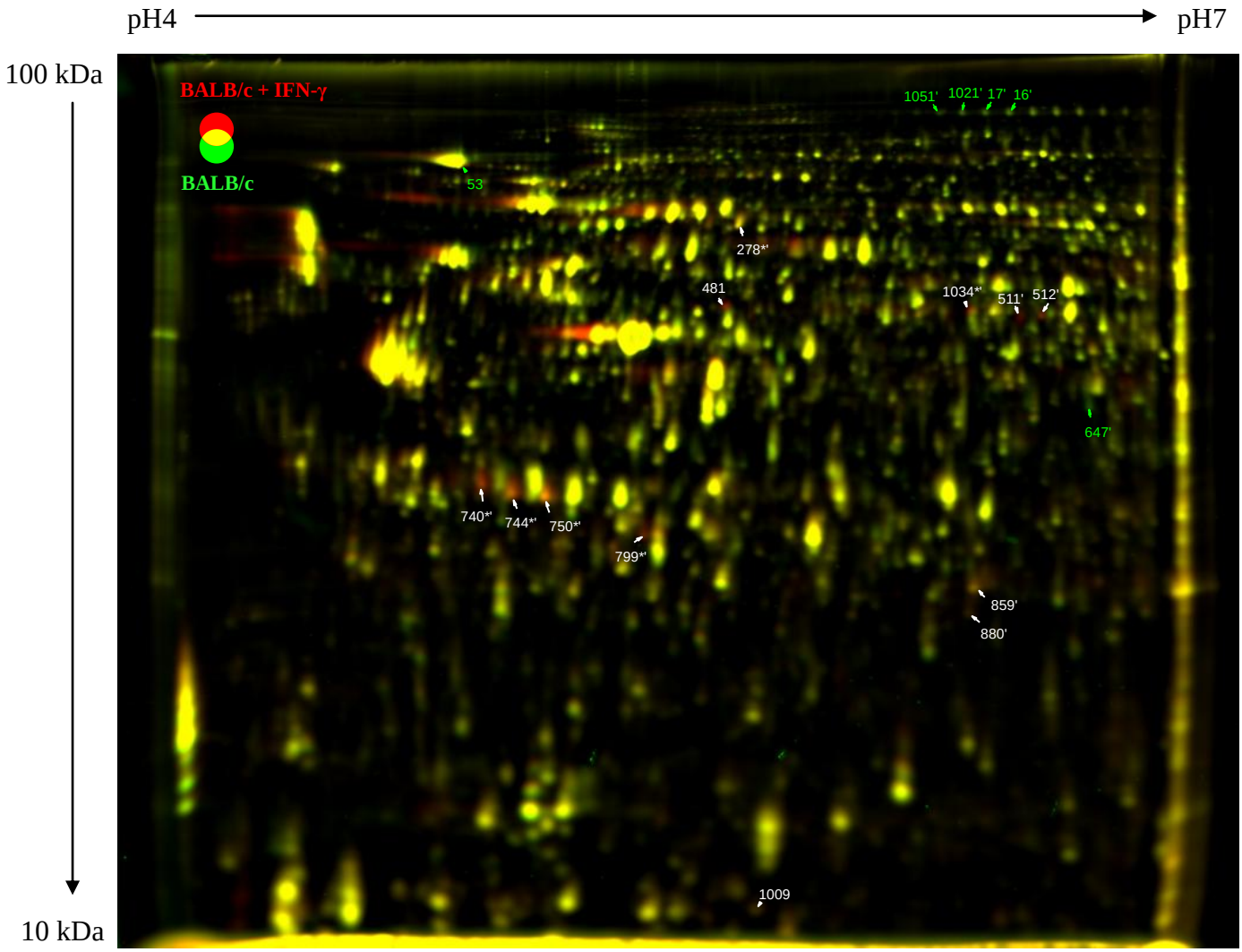


**Figure 7: Representative gel image of the IFN-γ effects on proteome of BMM-BALB/c.** Representative overlay image of protein patterns of the control (green colour) and IFN-γ treated sample (red colour). IFN-γ modulated protein spots were labeled with spot number. Spot colors indicate the effect of IFN-γ on spot intensity: red = increased; green = reduced; yellow = no change. Spots with increased- and reduced-intensity can be also distinguished by white and green letters, respectively. Symbol ***** indicates protein spots which were modulated by IFN-γ in both BMM-BALB/c and BMM-C57BL/6; symbol **'** indicates identified protein spots. The list of identified proteins is shown in table 6.

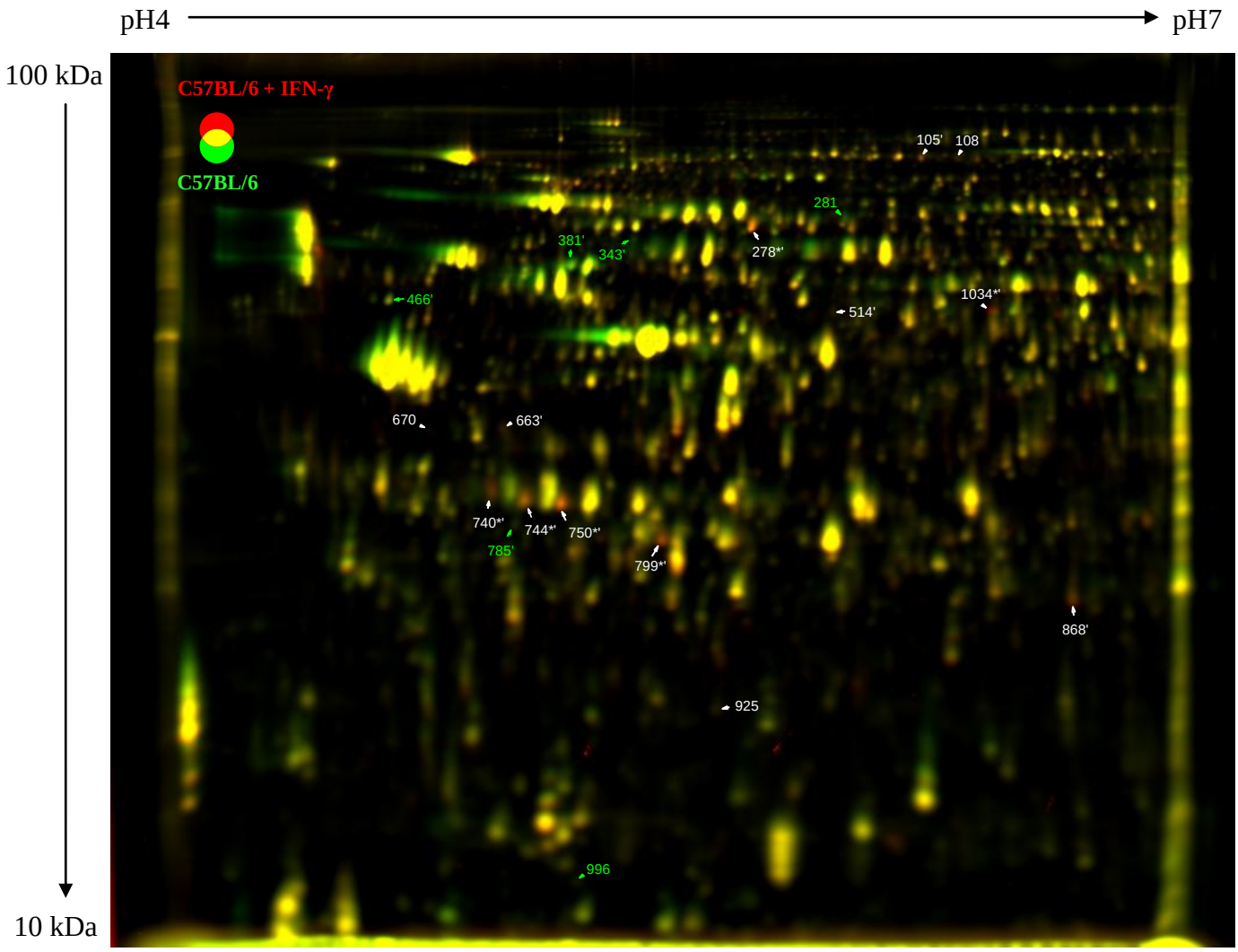


**Figure 8: Representative gel image of the IFN-γ effects on proteome of BMM-C57BL/6.** Representative overlay image of protein patterns of the control (green colour) and IFN-γ treated sample (red colour). IFN-γ modulated protein spots were labeled with spot number. Spot colors indicate the effect of IFN-γ on spot intensity: red = increased; green = reduced; yellow = no change. Spots with increased- and reduced-intensity can be also distinguished by white and green letters, respectively. Symbol ***** indicates protein spots which were modulated by IFN-γ in both BMM-BALB/c and BMM-C57BL/6; symbol **'** indicates identified protein spots. The list of identified proteins is shown in table 6.

Protein identification revealed that 4 IFN-γ modulated spots (spot 105, 512, 1021, and 1034) contained two proteins per spot. Spot 105 which was increased in intensity in BMM-C57BL/6 upon IFN-γ stimulation contained two proteins: endoplasmic reticulum aminopeptidase 1 and integrin alpha-M. Spot 512 was found to be increased and spot 1021 to be reduced in intensity due to IFN-γ stimulation in BMM-BALB/c. Two identified proteins in spot 512 were: S-adenosylmethionine synthetase isoform type-2 and aldehyde dehydrogenase family 3 member B1. Spot 1021 was identified to contain integrin alpha-M and myoferlin. Spot 1034 was found to be increased in intensity in both BMM-BALB/c and BMM-C57BL/6 upon IFN-γ stimulation contained interferon-inducible GTPase 1 and coronin-1A. The co-existence of different proteins in one spot leads to ambiguous statements as off which of them is modulated. Therefore, it was impossible to comfirm any of contained proteins in the four spots as IFN-γ modulated proteins.

In the other 19 IFN-γ modulated spots, each spot contained only one protein. Learned from 2-DE protein reference map of BMMs, one protein might have different protein isoforms which locate in different spots. Therefore, for each protein we considered not only IFN-γ modulated protein isoforms but also the total identified protein isoforms. It was no surprise that IFN-γ modulated proteins were mainly belonging to two groups. The first group contained proteins of which IFN-γ stimulation only modulated some but not all identified protein isoforms. The proteins of this group were abundant proteins which were found in many different spots such as Actin, Vimentin, Integrin, Cathepsin B, Cathepsin S, and Heat shock cognate 71 kDa protein.

While the second group contained proteins of which IFN-γ stimulation caused changes in all identified protein isoforms. All of proteins of the second group were found in only 1 spot (except peroxiredoxin-1 was found in two spots), including serine protease inhibitor A3G, cathepsin L1, ribonuclease inhibitor, rho GDP-dissociation inhibitor 2, and heterogeneous nuclear ribonucleoprotein A3. All of identified proteins in the 19 IFN-γ modulated spots have theoretical $M_r$ and *pI* in the experimental range (pH 4-7, $M_r$ ~10 kDa – 130 kDa) except peroxiredoxin-1which has a theoretical $M_r$/*pI* of 22.2 kDa and 8.26, respectively. Peroxiredoxin-1 was found in the area which corresponds to $M_r$/*pI* of approximately 20-25 kDa and a pI 6.2 - 6.7 on 2D-DIGE gels.

Interestingly, six of the most significantly IFN-γ modulated protein spots were common between BMM-BALB/c and BMM-C57BL/6. The intensities of the six protein spots were all increased upon IFN-γ stimulation. Three of them contained Cathepsin B (spot 740, 744, and 750); one contained Cathepsin S (spot 799) (figure 9); one contained Heat shock cognate 71 kDa protein (spot 278); and one contained two different proteins coronin-1A, and interferon-inducible GTPase 1 (spot 1034).

**Table 6: Proteins identified in IFN-γ modulated protein spots**

| *Spot* | *Accession Number* | *Gene entrez ID* | *Protein Name* | *BALB/c+IFN-γ v.s BALB/c* | *C57BL/6+IFN-γ vs. C57BL/6* | *Theoretical $M_r$ (kDa)* | *Theoretical pI* | *Regulated-/total- protein isoforms* |
|---|---|---|---|---|---|---|---|---|
| 16 | ITAM_MOUSE | 16409 | Integrin alpha-M | -1.59 | - | 127.4 | 6.87 | 3/7 |
| 17 | ITAM_MOUSE | 16409 | Integrin alpha-M | -1.77 | - | 127.4 | 6.87 | 3/7 |
| *105* | *ERAP1_MOUSE* | *80898* | *Endoplasmic reticulum aminopeptidase 1* | - | *1.63* | *106.5* | *5.77* | *3* |
| *105* | *ITAM_MOUSE* | *16409* | *Integrin alpha-M* | - | *1.63* | *127.4* | *6.87* | *7* |
| 278* | HSP7C_MOUSE | 15481 | Heat shock cognate 71 kDa protein | 1.52 | 1.55 | 70.8 | 5.37 | 1/6 |
| 343 | HNRPK_MOUSE | 15387 | Heterogeneous nuclear ribonucleoprotein K | - | -2.14 | 50.9 | 5.39 | 1/2 |
| 381 | VIME_MOUSE | 22352 | Vimentin | - | -1.83 | 53.7 | 5.06 | 1/17 |
| 466 | RINI_MOUSE | 107702 | Ribonuclease inhibitor | - | -1.61 | 49.8 | 4.69 | 1/1 |
| 511 | SPA3G_MOUSE | 20715 | Serine protease inhibitor A3G | 2.04 | - | 49.0 | 6.06 | 1/1 |
| *512* | *METK2_MOUSE* | *232087* | *S-adenosylmethionine synthetase isoform type-2* | *1.59* | - | *43.7* | *6.02* | *1* |
| *512* | *AL3B1_MOUSE* | *67689* | *Aldehyde dehydrogenase family 3 member B1* | *1.59* | - | *52.3* | *7.5* | *1* |
| 514 | HA12_MOUSE | 14964 | H-2 class I histocompatibility antigen, D-D alpha chain | - | 2.06 | 41.1 | 6.22 | 1/3 |
| 647 | CATL1_MOUSE | 13039 | Cathepsin L1 | -2.25 | - | 37.5 | 6.37 | 1/1 |
| 663 | ACTB_MOUSE | 11461 | Actin, cytoplasmic 1 | - | 1.57 | 41.7 | 5.29 | 1/10 |
| 740* | CATB_MOUSE | 13030 | Cathepsin B | 2.12 | 1.92 | 37.3 | 5.57 | 3/7 |
| 744* | CATB_MOUSE | 13030 | Cathepsin B | 1.73 | 1.62 | 37.3 | 5.57 | 3/7 |
| 750* | CATB_MOUSE | 13030 | Cathepsin B | 1.60 | 1.61 | 37.3 | 5.57 | 3/7 |
| 785 | GDIR2_MOUSE | 11857 | Rho GDP-dissociation inhibitor 2 | - | -1.66 | 22.8 | 4.97 | 1/1 |
| 799* | CATS_MOUSE | 13040 | Cathepsin S | 1.93 | 2.03 | 38.4 | 6.51 | 1/5 |
| 859 | PRDX1_MOUSE | 18477 | Peroxiredoxin-1 | 1.50 | - | 22.2 | 8.26 | 2/2 |
| 868 | ROA3_MOUSE | 229279 | Heterogeneous nuclear ribonucleoprotein A3 | - | 1.90 | 39.6 | 9.1 | 1/1 |
| 880 | PRDX1_MOUSE | 18477 | Peroxiredoxin-1 | 1.67 | - | 22.2 | 8.26 | 2/2 |
| *1021* | *ITAM_MOUSE* | *16409* | *Integrin alpha-M* | *-1.82* | - | *127.4* | *6.87* | *7* |
| *1021* | *MYOF_MOUSE* | *226101* | *Myoferlin* | *-1.82* | - | *233.2* | *5.83* | *1* |
| *1034** | *COR1A_MOUSE* | *12721* | *Coronin-1A* | *1.73* | *1.96* | *51.0* | *6.05* | *3* |
| *1034** | *IIGP1_MOUSE* | *60440* | *Interferon-inducible GTPase 1* | *1.73* | *1.96* | *47.5* | *6* | *1* |
| 1051 | ITAM_MOUSE | 16409 | Integrin alpha-M | -1.98 | - | 127.4 | 6.87 | 3/7 |
| 53 | Not identified | | | -1.55 | | | | |
| 108 | Not identified | | | | 1.61 | | | |
| 281 | Not identified | | | | -1.50 | | | |
| 481 | Not identified | | | 2.30 | | | | |
| 670 | Not identified | | | | 9.94 | | | |
| 925 | Not identified | | | | 1.56 | | | |
| 996 | Not identified | | | | -2.12 | | | |
| 1009 | Not identified | | | 1.52 | | | | |

In total, 31 unique IFN-γ modulated protein spots were observed in the 2-DE protein expression profiles of BMM-BALB/c and/or BMM-C57BL/6. In 23 out of 31 spots, proteins were successfully identified with MALDI-MS/MS. For each protein, number of identifed IFN-γ modulated protein spots (modulated protein isoforms) versus number of all spots in which the protein was identified (total identified protein isoforms) was listed. Italic characters were used to distinguish 4 proteins spots which contain 2 proteins per spot. Symbol * indicates protein spots modulated by IFN-γ in both BMM-BALB/c and BMM-C57BL/6. Symbol "–" means that protein spot was not changed or changes were below thresholds applied.

| protein | spot | $M_r$ (kDa)/ pI | BALB/c control | BALB/c + IFN-γ | C57BL/6 control | C57BL/6 + IFN-γ | IFN-γ effect |
|---|---|---|---|---|---|---|---|
| Cathepsin B | 740 | 45/5.00 |  | 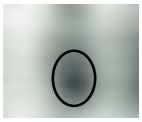 |  |  | induction |
| | 744 | 45/5.05 |  | 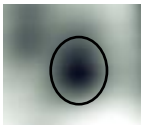 |  | 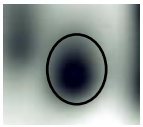 | induction |
| | 750 | 45/5.10 |  | 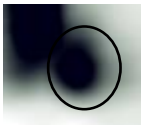 |  |  | induction |
| | 741 | 45/5.30 |  |  | 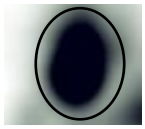 |  | no change |
| Cathepsin S | 799 | 30/5.32 |  |  |  | 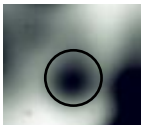 | induction |
| | 783 | 35/5.50 | 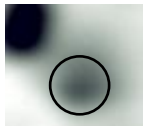 | 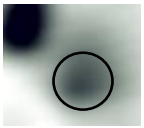 | 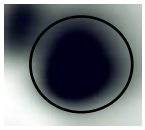 | 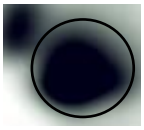 | no change |

**Figure 9: Induction of cathepsin B and cathepsin S protein isoforms due to IFN-γ stimulation.** Cathepsin B was identified in a total of 7 different proteins spots and Cathepsin S in 5 different spots on the 2-DE protein reference map. After IFN-γ-treatment, 3 Cathepsin B spots and 1 cathepsin S spot had a higher intensity while the other 4 Cathepsin B and 4 Cathepsin S spots were not affected. The image shows all IFN-γ modulated protein spots and one un-affected protein spots of Cathepsin B and S.

### 3.2.2. IFN-γ regulated proteins identified by LC-MS/MS and comparison with transcriptomic results.

With the sensitive and high resolution 2D-DIGE technique, we have identified total 14 proteins which were affected in some or all of their protein isoforms by IFN-γ stimulation. It was known that hundreds of genes were regulated in macrophages due to IFN-γ stimulation [75]. Transcriptomic analysis in this study identified 442 and 396 IFN-γ regulated genes in BMM-BALB/c and BMM-C57BL/6, respectively. This means that many IFN-γ regulated genes and the proteins encoded were out of the observation window of 2D-DIGE technique. In order to obtain more information about IFN-γ effects on the proteome of macrophages, we have applied another quantitative proteomic technique: label free Liquid Chromatography coupled with Tandem Mass Spectrometry (LC-MS/MS). This method has a better ability to access proteins which are extremely big or small, acidic or basic, and hydrophobic. Therefore, we decided to use quantitative LC-MS/MS as a complementary method for identifying IFN-γ effects in the proteome of BMMs.

It should be mentioned that results of transcriptomic analysis were only compared with proteomic LC-MS/MS results and not with 2D-DIGE results. The reason is that the 2D-DIGE technique has the ability to separate different modified forms (isoforms) of one protein. Therefore, in case a protein exists in different isoforms, each of them is independently quantified by the 2D-DIGE technique, whereas the LC-MS/MS technique quantifies the sum of the protein isoforms as a single protein. Therefore, results of transcriptomic analysis which quantify the total amount of mRNA were directly compared with results of the LC-MS/MS analysis; while results of the proteomic 2D-DIGE analysis were analyzed independently.

Transcriptomic analysis was performed based on three biological replicates (BMM2, 3 and 4) by my colleague – Maren Depke as described in the materials and methods part. Each biological replicate contained 4 different samples: 1) BMM-BALB/c, 2) BMM-BALB + IFN-γ, 3) BMM-C57BL/6, and 4) BMM-C57BL/6 + IFN-γ. The obtained transcriptomic intensity data was subjected to Principal Component Analysis (PCA) using Rosetta Resolver® System (Rosetta Biosoftware, Seattle, WA, USA). The result of PCA analysis clearly depicts the high reproducibility of biological replicates obtained from the serum-free model of BMM differentiation, cultivation and IFN-γ-activation: The 3 biological replicates of each group are arranged together, while the BMM of different strains and treatments are separated (Fig. 8-B).

As mentioned above, whole cell protein extracts of four samples BMM-BALB/c, BMM-BALB/c + IFN-γ, BMM-C57BL/6, and BMM-C57BL/6 + IFN-γ of the biological sample series BMM2 were selected to be analyzed with 2D-DIGE and LC-MS/MS technique. Four technical

replicate LC-MS/MS measurements were performed for each sample (following the LC-MS/MS protocol described in material and method part). With the "Quality Control function" of Rosetta Elucidator software, one can assess the quality of LC-MS/MS measurements. Using this option the three best measurements of each sample were selected for quantitative analysis. Thresholds for significant differently expression were set as minimum 1.5 fold change and $p \leq 0.01$.

In the LC-MS/MS experiment, 946 identified proteins met the required criteria for usage in quantitative analysis (protein teller $\geq 0.95$, at least two peptides). Principal component analysis (PCA) was performed based on intensities of these 946 identified proteins. The purpose of the PCA analysis was to discover the trends in data as well as verifying the reproducibility of technical replicates. The PCA analyses of both transcriptomic and proteomic data showed that there were differences between control and IFN-γ treatment samples, as well as between BMMs derived from strain BALB/c and C57BL/6. Taken together, the good reproducibility of 3 biological replicates was shown in PCA analysis of transcriptomic data (figure 10-B), while high reproducibility of LC-MS/MS replicated measurements was shown in PCA analysis of proteomic data (figure 10-A).

Quantitative and statistical analysis of proteomic LC-MS/MS data showed that there were 45 IFN-γ regulated proteins (41 induced and 4 repressed) in BMM-BALB/c and 53 IFN-γ regulated proteins (44 induced and 9 repressed) in BMM-C57BL/6. Of which, 29 IFN-γ regulated proteins (17 induced and 5 repressed) were common in both BMM-BALB/c and BMM-C57BL/6 (table 7A, 7C). There was no protein which was regulated by IFN-γ in opposite directions in the two mouse strains. Taken together, the LC-MS/MS results showed that increases in the level of proteins were the prominent response of macrophages to stimulation with IFN-γ, and that BMMs derived from the two different mouse strains consistently responded to IFN-γ stimulation.

In the transcriptomic study, the comparison between IFN-γ treatment and control macrophages showed that there were 442 IFN-γ regulated genes (388 induced and 54 repressed) in BMM-BALB/c and 396 IFN-γ regulated genes (330 induced and 66 repressed) in BMM-C57BL/6. Of these, 307 genes were regulated by IFN-γ in both mouse strains (281 induced and 26 repressed) (table 7A,7B). None of the identified IFN-γ regulated genes was regulated in opposite directions in the two different mouse strains. Induction of gene expression was also the prominent effect of IFN-γ in the transcritome analysis of BMMs derived from both mouse strains, and high similarity in the IFN-γ responses of BMMs derived from the two mouse strains was clearly demonstrated.

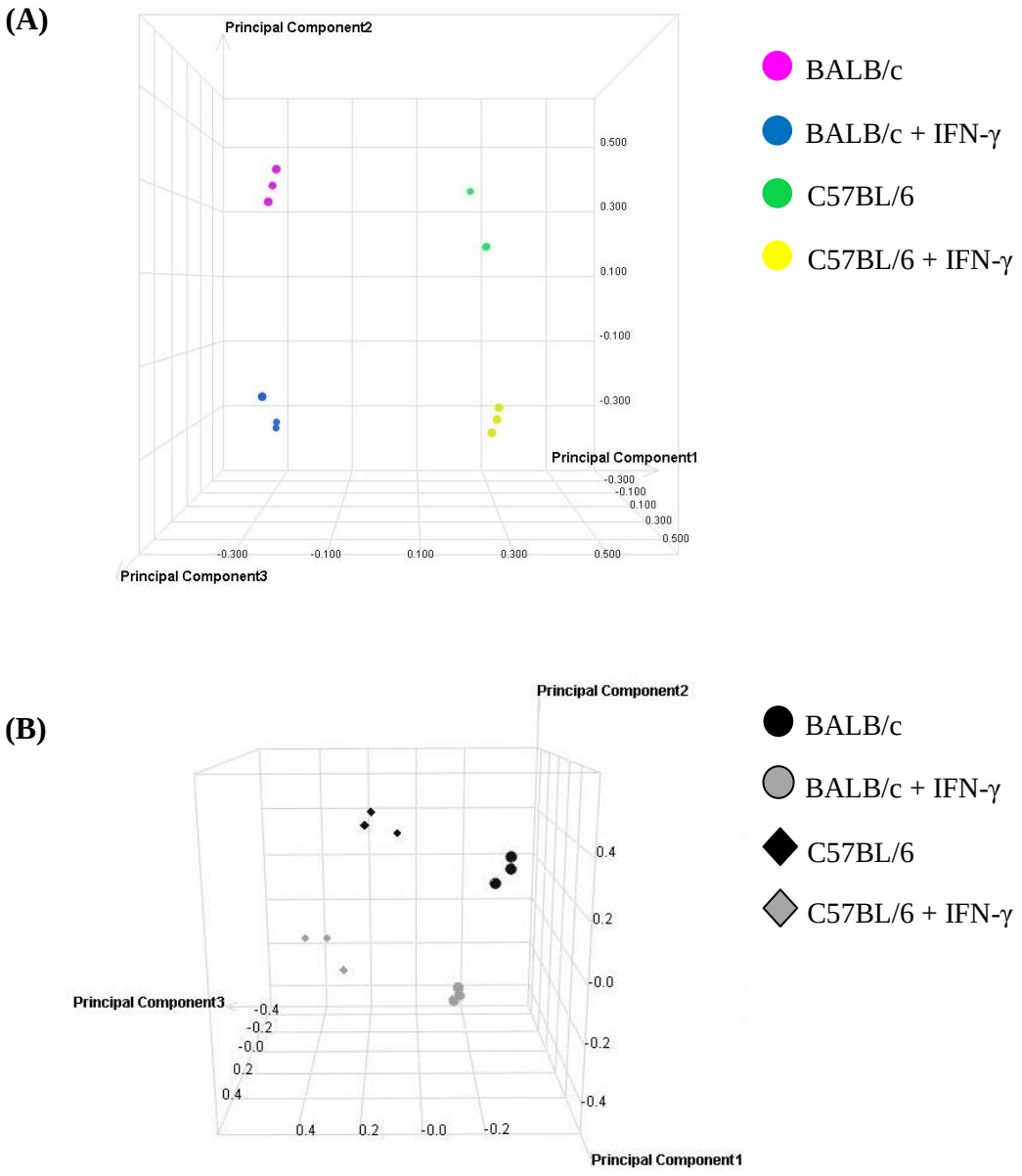


**Figure 10: Principal component analysis of proteomic LC-MS/MS and transcriptomic data.**

(A) **Proteome analysis by LC-MS/MS**: The biological samples series BMM2 was selected for proteomic LC-MS/MS analysis. Intensity data of 12 LC-MS/MS measurements (3 measurements/sample x 4 samples) were uploaded to Elucidator Resolver sofware. PCA analysis was performed based on intensity values of 946 identified proteins. Dot colors are used to cite 4 different samples: pink _ BMM-BALB/c, blue_BMM-BALB/c + IFN-γ, green_BMM-C57BL/6, and yellow_BMM-C57BL/6 + IFN-γ.

(B) **Transcriptom**e profiling: Three biological samples series BMM2, 3, and 4 were used for transcriptomic analysis. Intensity data of 12 arrays (1 measurement/sample x 3 biological replicate x 4 samples) were uploaded to Rosetta Resolver software. PCA analysis was performed based on intensity values of 20,074 genes on GeneChip® Mouse Gene 1.0 ST Arrays. Arrays of BMM-BALB/c samples are represented by dots (●), arrays of BMM-C57BL/6 samples by rhombi (◆). IFN-γ-activated samples are indicated in gray and non-activated control level samples are colored in black.

**Table 7: Summary of genes and proteins identified by transcriptomic and proteomic LC-MS/MS technique as IFN-γ regulated.**

**(A) Overview of IFN-γ regulated genes/proteins identified by transcriptomic and LC-MS/MS proteomic approaches.**

**(B) IFN-γ regulated genes in BMM-BALB/c and BMM-C57BL/6 identified by transcriptome profiling.**

**(C) IFN-γ regulated proteins in BMM-BALB/c and BMM-C57BL/6 identified by LC-MS/MS**.

**(A)**

| | Total number of detected genes or proteins | **IFN-γ effects** | |
|---|---|---|---|
| | | in BMM-BALB/c | in BMM-C57BL/6 |
| microarray | 20,074 | 442 (2.2%) | 396 (2.0%) |
| LC-MS/MS | 946 | 45 (4.8%) | 53 (5.5%) |

**(B)**

| IFN-γ regulated genes | Induced | Repressed | Total |
|---|---|---|---|
| BMM-BALB/c | 388 | 54 | 442 |
| BMM-C57BL/6 | 330 | 66 | 396 |
| Overlap | 281 | 26 | 307 |

**(C)**

| IFN-γ regulated proteins | Induced | Repressed | Total |
|---|---|---|---|
| BMM-BALB/c | 41 | 4 | 45 |
| BMM-C57BL/6 | 44 | 9 | 53 |
| Overlap | 27 | 2 | 29 |

Intensity data from 12 arrays (1 measurement/sample x 4 samples x 3 biological replicates) were processed and analyzed with Rosetta Resolver software. In total quantitative analysis of 20,074 genes on GeneChip® Mouse Gene 1.0 ST Arrays identified 442 and 396 IFN-γ regulated genes in BMM-BALB/c and BMM-C57BL/6, respectively. Protein intensity data of 12 LC-MS/MS measurements (3 measurements/sample x 4 samples) were processed and analyzed with Elucidator Resolver software. In total 946 proteins were identified in the LC-MS/MS experiment of which 45 and 53 IFN-γ regulated proteins were identified in BMM-BALB/c and BMM-C57BL/6, respectively. Thresholds for considering regulation as significant in both transcriptomic and proteomic quantitative analysis were a minimum 1.5 fold change and $p \leq 0.01$. Percentages of IFN-γ regulated genes/proteins of total genes/proteins covered/identified are shown in brackets.

Fold changes of identified IFN-γ regulated proteins in BMM-BALB/c and BMM-C57BL/6 were used to build ratio plots. On a ratio plot, each data point depicts a fold change value of a protein due to IFN-γ stimulation in BMM-BALB/c on the x axis and in BMM-C57BL/6 on the y axis. Using such ratio plots, one can easily visualize how well changes in levels of individual proteins in response to IFN-γ stimulation are conserved or specific to BMM-BALB/c as well as in BMM-C57BL/6. Such ratio plots were especially useful when a protein was considered as significantly influenced by IFN-γ in BMMs from one of two mouse strains only. In such cases a ratio plot will reveal if the protein responds in the same direction to IFN-γ stimulation in BMMs derived from the other mouse strain and just missed the cut-off level or not. Using the same procedure, ratio plot of IFN-γ regulated genes (transcriptomics) were constructed in order to compare with ratio plot of IFN-γ regulated proteins (proteomics; figure 11). Ratio plots of both IFN-γ regulated genes and proteins showed that almost all IFN-γ regulated proteins/genes consistenly responded to IFN-γ stimulation in both mouse strains. Only a few proteins/genes responded to IFN-γ stimulation in one strain and did not in the other. The dominance of induction of gene expression and increases of protein intensities over repression of gene expression and reductions in protein levels was also obvious from these ratio plots. There was no opposite response to IFN-γ due to strain difference observed in both proteomic and transcritpomic data sets.

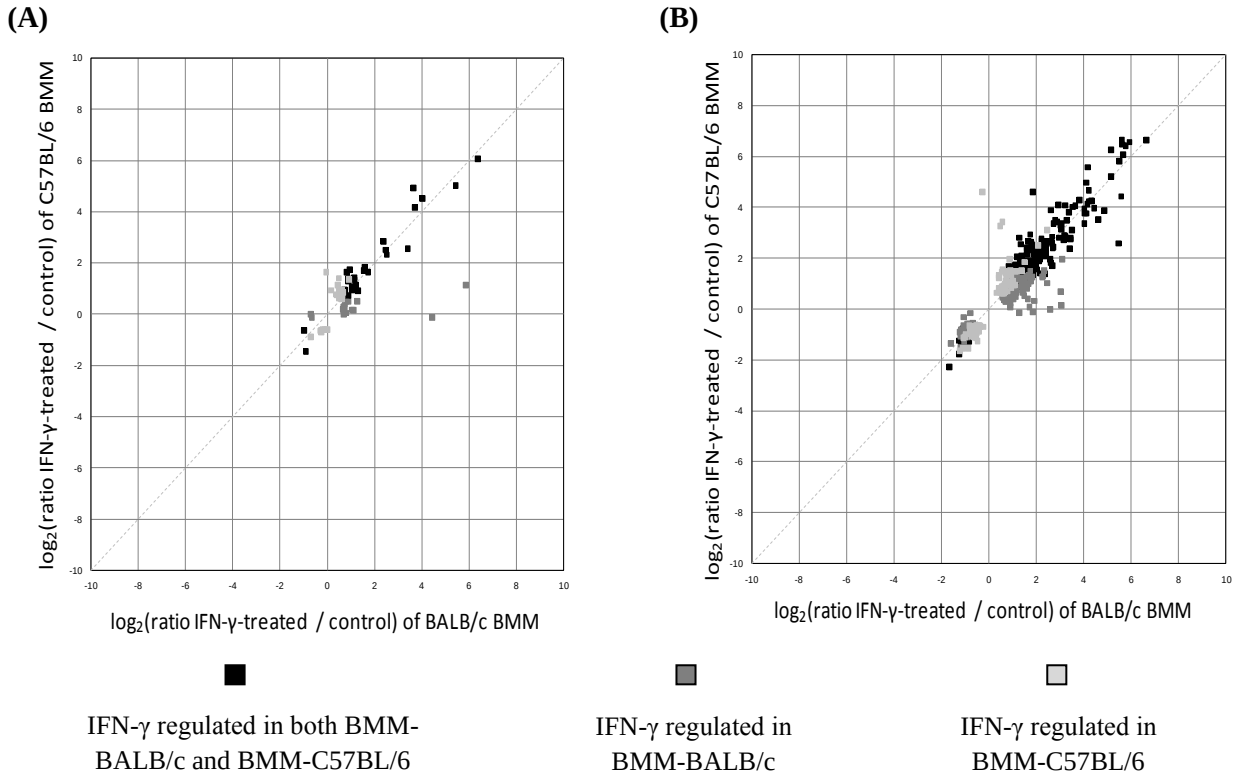


**Figure 11: Ratio plots of identified IFN-γ regulated genes and proteins.**

Quantitative LC-MS/MS and transcriptomic analysis identified a total of 69 and 531 distinct IFN-γ regulated proteins and genes, respectively. $Log_2$-transformed ratio data of the 69 proteins or 531 genes were used to create ratio plots. $Log_2$-transformed ratio data "IFN-γ-treated BMM-BALB/c" / "control BMM-BALB/c" were plotted on the x-axis and $log_2$-transformed ratio data "IFN-γ-treated BMM-C57BL/6" / "control BMM-C57BL/6" on the y-axis. Coloring distinguishes three different groups of regulated genes/proteins: genes/proteins with significant differential regulations by IFN-γ only in BMM-BALB/c were shown in dark gray, while that with significant differential expression by IFN-γ only in BMM-C57BL/6 were displayed in light gray. Genes/proteins significantly regulated by IFN-γ in both BMM-BALB/c and BMM-C57BL/6 were colored in black.

**(A) Ratio plot of IFN-γ regulated proteins identified by LC-MS/MS.** In total 69 distinct IFN-γ regulated proteins in BMM-BALB/c and/or BMM-C57BL/6 were identified by LC-MS/MS. $Log_2$-transformed ratio data of the 69 proteins was used to create a ratio plot. All LC-MS/MS ratio data were derived from mean intensities of three LC-MS/MS technical replicates.

**(B) Ratio plot of IFN-γ regulated genes identified by transcriptomics.** A total of 531 distinct IFN-γ regulated genes in BMM-BALB/c and/or BMM-C57BL/6 were identified by transcriptional profiling. $Log_2$-transformed ratio data of the 531 genes was used to create the ratio plot. All transcriptome ratio data were derived from mean intensities of three biological replicates.

In total, 69 IFN-γ regulated proteins in BMM-BALB/c and/or BMM-C57BL/6 were identified with LC-MS/MS. Biological functions of IFN-γ regulated proteins were assigned using the PANTHER (version 6.1) classification system. At first, UniProt IDs of the proteins were translated to entrez gene ID by using PIPE (Protein Information and Property Explorer) classification system. Then, entrez gene IDs of 69 IFN-γ regulated proteins were uploaded to PANTHER (version 6.1) for biological processes classification. Searching against NCBI mouse databases, information about biological process of 52 out of 69 entrez gene IDs of IFN-γ regulated proteins was available. These entrez gene IDs then were assigned to biological processes they are involved in. In order to compare with proteomic LC-MS/MS results, gene entrez IDs of a total of 531 distinct IFN-γ regulated genes identified in BMM-BALB/c and/or BMM-C57BL/6 by transcriptomic analysis were also uploaded to PANTHER, and information about biological process of 513 gene entrez IDs was available.

It was not surprised to find that the most abundant biological process of IFN-γ regulated proteins/genes was "immune and defense". In general, the distribution of IFN-γ regulated genes identified in BMM-BALB and BMM-C57BL/6 was consistent (figure 12-B). The distribution of identified IFN-γ regulated proteins in BMM-BALB and BMM-C57BL/6 showed small differences in some biological processes (figure 12-A). However, the small differences may be due to the small size of analyzed groups of IFN-γ regulated proteins. Morevore, we observed that most IFN-γ regulated proteins responded to IFN-γ stimulation in the same direction in the two strains. Therefore, the differences in distribution of some biological processes might not really reflect truly different responses to IFN-γ stimulation of BMMs derived from BALB/c and C57BL/6.

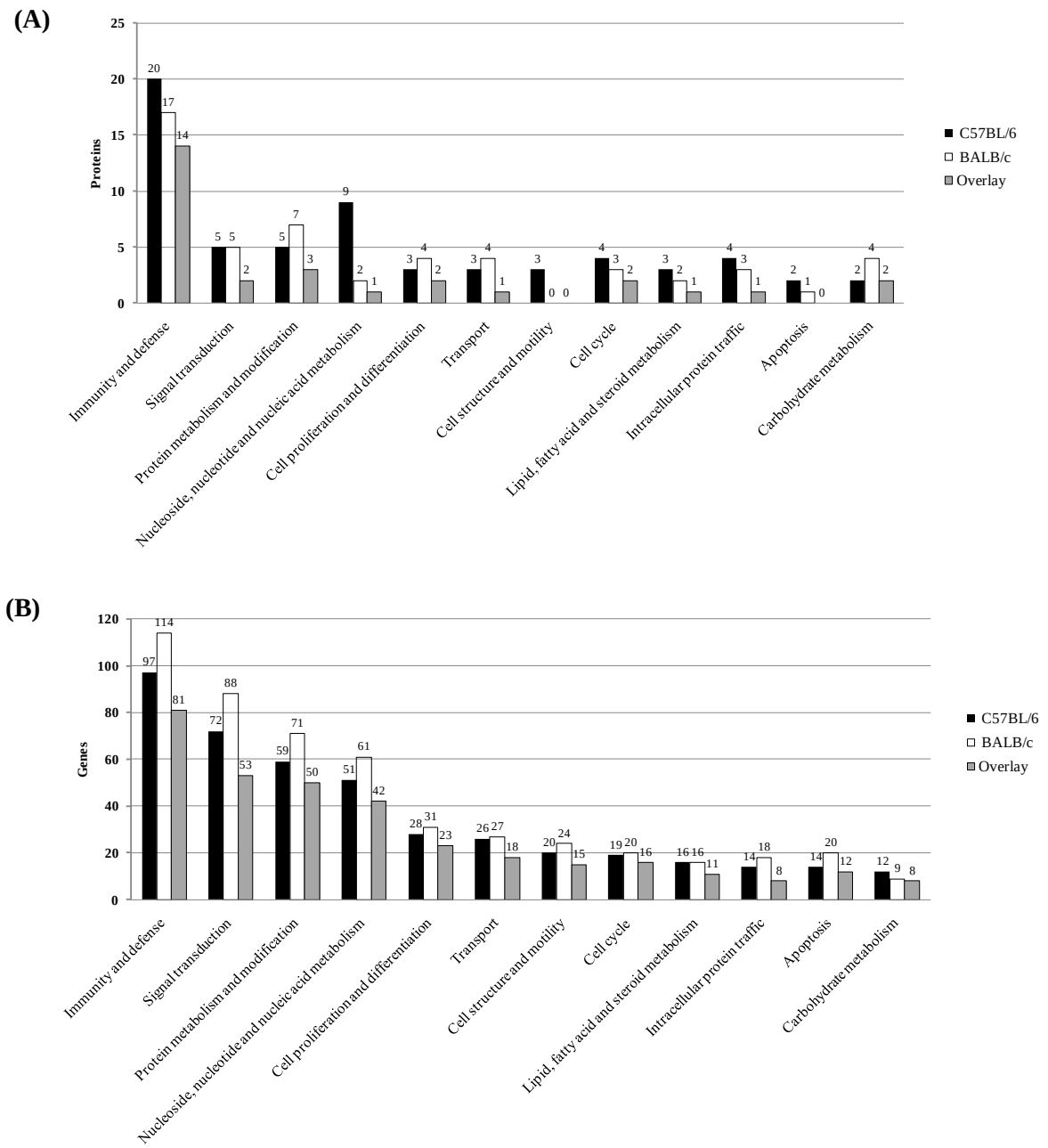


**Figure 12: Functional classification of IFN-γ regulated proteins and genes identified by proteomic LC-MS/MS and transcriptomic technique.**

**(A) Functional classification of IFN-γ regulated proteins identified by LC-MS/MS technique.** There were total 69 distinct IFN-γ regulated proteins in BMM-BALB/c and/or BMM-C57BL/6 identified by LC-MS/MS technique. Entrez Gene IDs of the 69 proteins were uploaded to PANTHER (Version 6.1) for functional classification. Information of biological process was available for 52 out of 69 proteins. In the picture, 12 biological processes which have highest number of proteins are showed.

**(B) Functional classification of IFN-γ regulated genes identified by transcriptomic technique.** There were a total of 531 distinct IFN-γ regulated genes in BMM-BALB/c and/or BMM-C57BL/6 identified by transcriptomic analysis. Entrez Gene IDs of the 531 genes were uploaded to PANTHER (Version 6.1) for functional classification. Information of biological process was available for 513 out of the 531 genes. In the picture, 12 biological processes which have highest number of genes are showed.

To this point, the comparison between proteomic - and transcriptomic - analysis was performed based on whole set of data accessible to each technique. Transcriptomics allowed monitoring of 20,074 genes while only 946 proteins were identified by LC-MS/MS. Two questions that could be addressed are: "How many genes were indeed on both the mRNA and protein level?" and "How many of them were indeed found to be regulated by IFN-γ at mRNA and protein level?"

In order to compare the LC-MS and transcriptomic results, initially identified proteins must be mapped with genes covered by the affymetrix array. Therefore, protein IPI identifiers were translated into EntrezGene IDs using the PIPE (http://pipe.systemsbiology.net/pipe) and UniProt ID (www.uniprot.org) mapping tools. Missing EntrezGene IDs were manually added if possible. The resulting list of deduced EntrezGene IDs was imported into the Rosetta Resolver software and compared with genes on the Affymetrix array based on the annotation of the Rosetta Resolver software. The comparision showed that 900 out of 946 identified proteins could be mapped to the 20,074 EntrezGene records that were specified to be represented on the Affymetrix GeneChip® Mouse Gene 1.0 ST array (figure 13).

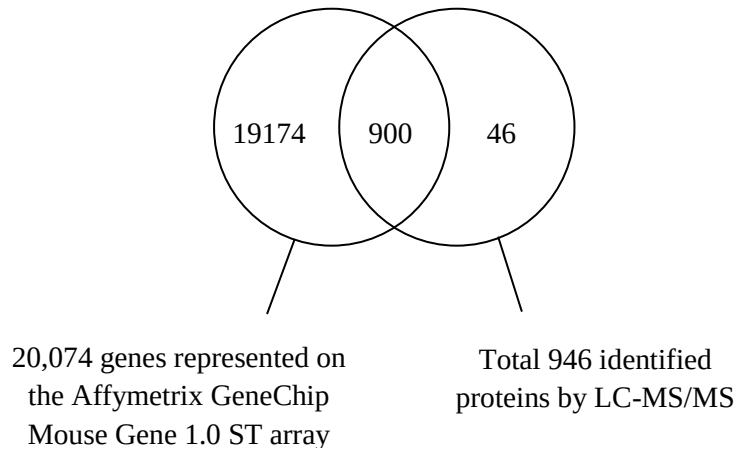


**Figure 13: Overlay between identified genes and proteins.** Comparison of 20,074 genes covered by the Affymetrix GeneChip Mouse Gene 1.0 ST array with 946 proteins identified by LC-MS/MS approach. Protein IPI identifiers were translated into EntrezGene IDs using the PIPE (http://pipe.systemsbiology.net/pipe) and UniProt ID (www.uniprot.org) mapping tools. Missing EntrezGene IDs were manually added if possible. The resulting list of proteins was imported into the Rosetta Resolver software and compared with genes on the Affymetrix array based on the annotation of the Rosetta Resolver software.

In these 900 genes/proteins, more than 50% of the identified IFN-γ regulated proteins overlay with IFN-γ regulated genes (Table 8). Comparing between two mouse trains, 17 genes were found regulated by IFN-γ in both mouse strains at both transcriptional and translational level (table 12).

**Table 8: Overlay of genes and proteins influenced by IFN-γ treatment.**

| IFN-γ treatment effects | | | |
|---|---|---|---|
| | LC-MS/MS | Microarray | Overlap |
| BALB/c BMM | | | |
| Induced | 39 | 41 | 24 |
| Repressed | 4 | 11 | 0 |
| Total | 43 | 52 | 24 |
| C57BL/6 BMM | | | |
| Induced | 42 | 41 | 20 |
| Repressed | 8 | 12 | 0 |
| Total | 50 | 53 | 20 |

Interestingly, we have observed that total mRNA and protein level of some genes which have important functions in anti-microbial activities of macrophages were not changed upon IFN-γ stimulation (figure 14, table 9). Some examples of these genes are lysosome-associated membrane glycoprotein 1 (LAMP1), and ras-related protein Rab-7a (RAB7), which play important roles in fusion of phagosome and lysosome; Peroxiredoxin-1 (PRDX1), which protect macrophages by reducing peroxides; Lysosomal proteases such as cathepsin B (CATB), cathepsin D (CATD), cathepsin S (CATS),…The genes and their predominant functions are shown in figure 14. We also observed that these proteins were present at high level in BMMs, which probably reflects their "ready to go" status for anti-microbial activities of BMMs.

**Table 9: Functions of immune related genes for which total mRNA and protein amount were not influenced by IFN-γ stimulation**

| *Gene* | *Protein name* | *Function* |
|---|---|---|
| **Anpep** | Aminopeptidase N, CD13 | The final digestion of peptides |
| **Capg** | Macrophage-capping protein | May play a role in regulating cytoplasmic and/or nuclear structures |
| **Cltc** | Clathrin, heavy polypeptide | Major role in the formation of coated vesicles |
| **Ctsb** | Cathepsin B | Intracellular degradation and turnover of proteins |
| **Ctsd** | Cathepsin D | Intracellular degradation and turnover of proteins |
| **Ctss** | Cathepsin S | Intracellular degradation and turnover of proteins |
| **Itgam** | Integrin alpha M | Adhesive interactions of macrophages and mediating the uptake of complement-coated particles |
| **Itgb2** | Integrin beta | Integrin alpha-L/beta-2 is a receptor for ICAM1, ICAM2, ICAM3 and ICAM4 |
| **Lamp1** | Lysosome-associated membrane glycoprotein 1 | Required for fusion of lysosomes with phagosomes |
| **Lyz2** | Lysozyme C-2 | Bacteriolytic function |
| **Myof** | Isoform 1 of Myoferlin | Rapid resealing of membranes disrupted by mechanical stress |
| **Prdx1** | Peroxiredoxin-1 | Reduces peroxides |
| **Rab7** | Ras-related protein Rab-7a | Regulates vesicle traffic in the late endosomes to lysosomes |

**(A)**

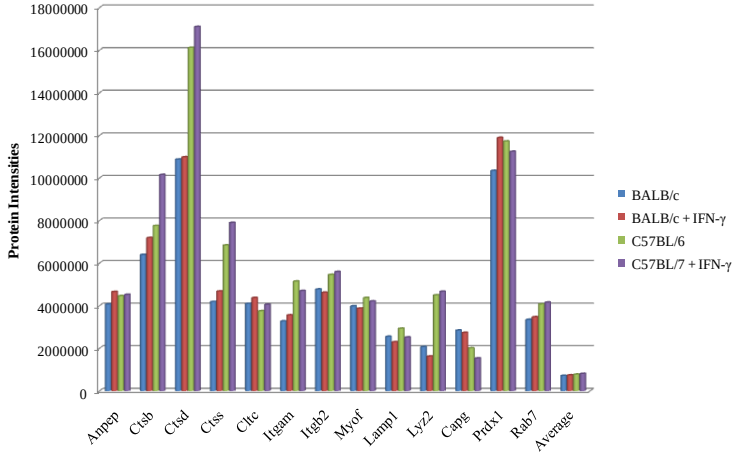


**(B)**

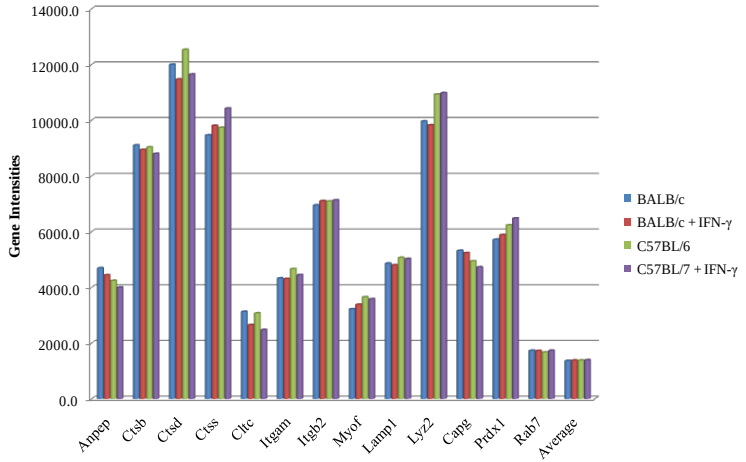


**Figure 14: mRNA and protein level of thirdteen immune related genes.**

**(A): Protein intensities of 13 immune related genes measured by LC-MS/MS.** Mean intensity values of proteins were derived from 3 technical replicates. The average intensity value of all 946 identified proteins was used to compare with intensity of 13 immune related proteins.

**(B): mRNA intensities of 13 immune related genes measured by** GeneChip® Mouse Gene 1.0 ST Arrays**.** Mean intensity values of genes were derived from 3 biological replicates. The average intensity value of all 20,074 identified genes was used to compare with intensity of 13 immune related genes.

**Table 10: List of a total of 69 IFN-γ regulated proteins in BMM-BALB/c and/or BMM-C57BL/6 identified by LC-MS/MS technique**.

| *Primary Protein Name* | *Gene Entrez ID* | *Gene Symbol* | *Protein name* | *BALB/c-fold change* | *C57BL/6-fold change* |
|---|---|---|---|---|---|
| IPI00857226* | 14081 | Acsl1 | Long-chain-fatty-acid--CoA ligase 1 | 2.2 | 2.5 |
| IPI00230440 | 269378 | Ahcy | Adenosylhomocysteinase | - | 1.5 |
| IPI00116339* | 11629 | Aif1 | Allograft inflammatory factor 1 | 1.9 | 3.3 |
| IPI00221613 | 11840 | Arf3 | ADP-ribosylation factor 3 | 1.6 | - |
| IPI00221616 | 11845 | Arf6 | ADP-ribosylation factor 6 | 1.8 | - |
| IPI00109966* | 12010 | B2m | beta-2-microglobulin | 1.7 | 1.9 |
| IPI00409462 | 53817 | Bat1a | Spliceosome RNA helicase Bat1 | - | 1.8 |
| IPI00111560 | 434632 | BC085271 | cDNA sequence BC085271 | - | 2.0 |
| IPI00124820 | 23790 | Coro1c | Coronin-1C | - | 1.7 |
| IPI00118987 | 13036 | Ctsh | Cathepsin H | 1.6 | - |
| IPI00128154* | 13039 | Ctsl | Cathepsin L1 | -2.0 | -1.6 |
| IPI00420363 | 13207 | Ddx5 | Probable ATP-dependent RNA helicase DDX5 | - | 1.9 |
| IPI00753434 | 100047333 | Evl | Isoform 2 of Ena/VASP-like protein | 1.6 | - |
| IPI00116705 | 11770 | Fabp4 | Fatty acid-binding protein, adipocyte | -1.6 | - |
| IPI00132217 | 66437 | Fis1 | 16 kDa protein | 1.7 | - |
| IPI00117063 | 233908 | Fus | 53 kDa protein | - | 2.2 |
| IPI00112129 | 67092 | Gatm | Glycine amidinotransferase, mitochondrial | 1.7 | - |
| IPI00124675 | 14468 | Gbp1 | Interferon-induced guanylate-binding protein 1 | 21.7 | - |
| IPI00323251* | 14469 | Gbp2 | Interferon-induced guanylate-binding protein 2 | 12.5 | 30.3 |
| IPI00403729* | 229898 | Gbp5 | Guanylate-binding protein 5 | 83.3 | 66.7 |
| IPI00172039* | 14960 | H2-Aa | H-2 class II histocompatibility antigen, I-E alpha chain (Fragment) | 1.8 | 3.1 |
| IPI00110805 | 14964 | H2-D1 | H-2 class I histocompatibility antigen, D-D alpha chain | - | 2.7 |
| IPI00124741 | 14998 | H2-DMa | MAd protein | - | 2.6 |
| IPI00121908* | 14999 | H2-DMb1 | Class II histocompatibility antigen, M beta 1 chain | 2.2 | 2.7 |
| IPI00113299 | 14969 | H2-Eb1 | H-2 class II histocompatibility antigen, I-A beta chain | - | 3.2 |
| IPI00850057* | 100044874 | H2-K1 | H-2 class I histocompatibility antigen, K-D alpha chain | 2.1 | 2.0 |
| IPI00109996 | 14980 | H2-L | H-2 class I histocompatibility antigen, L-D alpha chain | 2.1 | - |
| IPI00624138* | 14964 | H2-L | H-2D cell surface glycoprotein (Fragment) | 2.0 | 2.1 |
| IPI00283611* | 15275 | Hk1 | Isoform HK1-SA of Hexokinase-1 | 1.6 | 1.9 |
| IPI00114342* | 15277 | Hk2 | Hexokinase-2 | 1.8 | 2.4 |
| IPI00751595 | 212032 | Hk3 | Hexokinase-3 | 1.7 | - |
| IPI00226073 | 98758 | Hnrnpf | Isoform 2 of Heterogeneous nuclear ribonucleoprotein F | - | 1.6 |
| IPI00465574 | 15387 | Hnrnpk | Isoform 1 of Heterogeneous nuclear ribonucleoprotein K | - | 1.6 |

| *Primary Protein Name* | *Gene Entrez ID* | *Gene Symbol* | *Protein name* | *BALB/c-fold change* | *C57BL/6-fold change* |
|---|---|---|---|---|---|
| IPI00122973* | 15894 | Icam1 | Isoform 2 of Intercellular adhesion molecule 1 | 2.9 | 3.2 |
| IPI00123570* | 15953 | Ifi47 | Interferon gamma inducible protein 47 | 10.6 | 5.8 |
| IPI00308971 | 16004 | Igf2r | Cation-independent mannose-6-phosphate receptor | - | -1.8 |
| IPI00457501* | 16145 | Igtp | interferon gamma induced GTPase | 13.2 | 17.9 |
| IPI00323496* | 60440 | Iigp1 | Interferon-inducible GTPase 1 | 43.5 | 32.3 |
| IPI00111285* | 16365 | Irg1 | Immune-responsive gene 1 protein | 16.4 | 22.7 |
| IPI00120264* | 15944 | Irgm1 | Isoform 1 of Immunity-related GTPase family M protein | 5.2 | 7.1 |
| IPI00125091 | 16796 | Lasp1 | LIM and SH3 protein 1 | - | -1.5 |
| IPI00119809 | 19039 | Lgals3bp | Galectin-3-binding protein | - | 1.8 |
| IPI00130627 | 19141 | Lgmn | Legumain | - | 1.7 |
| IPI00119063 | 16971 | Lrp1 | Prolow-density lipoprotein receptor-related protein 1 | - | -1.5 |
| IPI00319270 | 66905 | M6prbp1 | Mannose-6-phosphate receptor-binding protein 1 | - | -1.5 |
| IPI00321648* | 17381 | Mmp12 | Macrophage metalloelastase | -1.9 | -2.8 |
| IPI00658632* | 17476 | Mpeg1 | macrophage expressed gene 1 | 2.3 | 2.2 |
| IPI00111258 | 78388 | Mvp | Major vault protein | - | -1.5 |
| IPI00123181 | 17886 | Myh9 | Myosin-9 | - | -1.6 |
| IPI00109044 | 67268 | Mylc2b | Myosin regulatory light chain MRLC2 | - | -1.6 |
| IPI00320188* | 59027 | Nampt | Nicotinamide phosphoribosyltransferase | 2.1 | 1.9 |
| IPI00321058 | 246730 | Oas1a | 2'-5'-oligoadenylate synthetase 1A | - | 1.8 |
| IPI00329896 | 27226 | Pla2g7 | phospholipase A2, group VII | - | 1.7 |
| IPI00315452 | 18950 | Pnp1 | Purine nucleoside phosphorylase | 2.4 | - |
| IPI00116254 | 53381 | Prdx4 | Peroxiredoxin-4 | - | 1.5 |
| IPI00225419 | 15170 | Ptpn6 | Isoform 2 of Tyrosine-protein phosphatase non-receptor type 6 | 1.7 | - |
| IPI00110910* | 14961 | Rmcs5 | H-2 class II histocompatibility antigen, A-D beta chain | 2.2 | 2.0 |
| IPI00850840 | 16785 | Rpsa | 40S ribosomal protein SA | 1.6 | - |
| IPI00875198* | 56045 | Samhd1 | SAM domain and HD domain-containing protein 1 | 1.8 | 2.6 |
| IPI00669817 | 20715 | Serpina3g | Serine protease inhibitor A3G | 58.8 | - |
| IPI00222763 | 225027 | Sfrs7 | Isoform 2 of Splicing factor, arginine/serine-rich 7 | - | 1.9 |
| IPI00395151* | 327978 | Slfn5 | Schlafen family member 5 | 5.7 | 5.0 |
| IPI00719950 | 20779 | Src | Neuronal proto-oncogene tyrosine-protein kinase Src | 2.1 | - |
| IPI00467004* | 20846 | Stat1 | Signal transducer and activator of transcription 1 | 5.5 | 5.6 |
| IPI00121842* | 21355 | Tap2 | TAP2 | 3.0 | 3.5 |
| IPI00620227* | 21356 | Tapbp | Isoform Short of Tapasin | 3.3 | 3.1 |
| IPI00126861* | 21817 | Tgm2 | Protein-glutamine gamma-glutamyltransferase 2 | 1.9 | 1.6 |
| IPI00135068* | 21856 | Timm44 | translocase of inner mitochondrial membrane 44 | 2.5 | 1.9 |
| IPI00122548 | 22335 | Vdac3 | Voltage-dependent anion-selective channel protein 3 | -1.6 | - |

Thresholds for considering regulation as significantly were 1.5 fold change, and $p \leq 0.01$. Symbol * indicates protein spots which were regulated by IFN-γ in both mouse strains. Symbol "–" means that protein was not changed or the changing was below significant threshold.

**Table 11: Twenty seven genes for which changes by IFN-γ stimulation were observed at both transcriptional and translational level**.

| *Primary Protein Name* | *EntrezGene* | *Gene Symbol* | *Protein name* | *BALB/c - Protein* | *BALB/c - Gene* | *C57BL/6-Protein* | *C57BL/6-Gene* |
|---|---|---|---|---|---|---|---|
| IPI00857226* | ***14081*** | ***Acsl1*** | Long-chain-fatty-acid--CoA ligase 1 | 2.2 | 3.7 | 2.5 | 3.5 |
| IPI00116339* | **11629** | Aif1 | Allograft inflammatory factor 1 | 1.9 | 4.6 | 3.3 | 5.1 |
| IPI00118987 | **13036** | Ctsh | Cathepsin H | 1.6 | 2.2 | - | - |
| IPI00112129 | **67092** | Gatm | Glycine amidinotransferase, mitochondrial | 1.7 | 2.5 | - | 3.2 |
| IPI00124675 | **14468** | Gbp1 | Interferon-induced guanylate-binding protein 1 | 21.7 | 43.9 | - | 6.0 |
| IPI00323251* | **14469** | Gbp2 | Interferon-induced guanylate-binding protein 2 | 12.5 | 17.2 | 30.3 | 31.2 |
| IPI00403729* | **229898** | Gbp5 | Guanylate-binding protein 5 | 83.3 | 50.7 | 66.7 | 66.8 |
| IPI00124741 | **14998** | H2-DMa | MAd protein | - | - | 2.6 | 2.1 |
| IPI00121908 | **14999** | H2-DMb1 | Class II histocompatibility antigen, M beta 1 chain | - | - | 2.7 | 2.1 |
| IPI00114342 | **15277** | Hk2 | Hexokinase-2 | 1.8 | - | 2.4 | 1.9 |
| IPI00751595 | **212032** | Hk3 | Hexokinase-3 | 1.7 | 1.8 | - | - |
| IPI00122973* | **15894** | Icam1 | Isoform 2 of Intercellular adhesion molecule 1 | 2.9 | 2.3 | 3.2 | 2.2 |
| IPI00123570* | **15953** | Ifi47 | Interferon gamma inducible protein 47 | 10.6 | 10.4 | 5.8 | 13.9 |
| IPI00457501* | **16145** | Igtp | interferon gamma induced GTPase | 13.2 | 17.4 | 17.9 | 13.5 |
| IPI00323496* | **60440** | Iigp1 | Interferon-inducible GTPase 1 | 43.5 | 100.0 | 32.3 | 100.0 |
| IPI00111285* | **16365** | Irg1 | Immune-responsive gene 1 protein | 16.4 | 17.7 | 22.7 | 17.4 |
| IPI00120264* | **15944** | Irgm1 | Isoform 1 of Immunity-related GTPase family M protein | 5.2 | 6.9 | 7.1 | 11.2 |
| IPI00320188* | **59027** | Nampt | Nicotinamide phosphoribosyltransferase | 2.1 | 2.3 | 1.9 | 2.5 |
| IPI00315452 | **18950** | Pnp1 | Purine nucleoside phosphorylase | 2.4 | 3.2 | - | 2.5 |
| IPI00225419 | **15170** | Ptpn6 | Isoform 2 of Tyrosine-protein phosphatase non-receptor type 6 | 1.7 | 2.2 | - | 2.0 |
| IPI00875198* | **56045** | Samhd1 | SAM domain and HD domain-containing protein 1 | 1.8 | 2.1 | 2.6 | 2.4 |
| IPI00669817 | **20715** | Serpina3g | Serine protease inhibitor A3G | 58.8 | 35.5 | - | 76.5 |
| IPI00395151* | **327978** | Slfn5 | Schlafen family member 5 | 5.7 | 2.0 | 5.0 | 2.3 |
| IPI00467004* | **20846** | Stat1 | Signal transducer and activator of transcription 1 | 5.5 | 4.7 | 5.6 | 6.5 |
| IPI00121842* | **21355** | Tap2 | TAP2 | 3.0 | 3.3 | 3.5 | 3.0 |
| IPI00620227* | **21356** | Tapbp | Isoform Short of Tapasin | 3.3 | 1.9 | 3.1 | 2.0 |
| IPI00126861* | **21817** | Tgm2 | Protein-glutamine gamma-glutamyltransferase 2 | 1.9 | 3.4 | 1.6 | 3.6 |

Symbol * indicates proteins which were regulated by IFN-γ in both BMM-BALB/c and BMM-C57BL/6. Symbol "–" means that protein was not changed or the changing was below significant threshold.

**Table 12: Immune related proteins which were not changed in total amount due to IFN-γ stimulation.**

| *Primary Protein Name* | *EntrezGene* | *Gene Symbol* | *Protein name* | *BALB/c - Protein* | *BALB/c - Gene* | *C57BL/6-Protein* | *C57BL/6-Gene* |
|---|---|---|---|---|---|---|---|
| IPI00319509 | 16790 | Anpep | Aminopeptidase N, CD13 | 1.16 | -1.06 | 1.01 | -1.06 |
| IPI00113517 | 13030 | Ctsb | Cathepsin B | 1.14 | -1.02 | 1.25 | -1.03 |
| IPI00404551 | 13033 | Ctsd | Cathepsin D | 1.00 | -1.05 | 1.05 | -1.08 |
| IPI00309520 | 13040 | Ctss | Cathepsin S | 1.14 | 1.04 | 1.16 | 1.07 |
| IPI00648173 | 67300 | Cltc | Clathrin, heavy polypeptide | 1.08 | -1.18 | 1.07 | -1.24 |
| IPI00761784 | 16409 | Itgam | Integrin alpha M | 1.10 | -1.01 | -1.11 | -1.05 |
| IPI00320605 | 16414 | Itgb2 | Integrin beta | -1.03 | 1.02 | 1.02 | 1.01 |
| IPI00849670 | 226101 | Fer1l3 | Isoform 1 of Myoferlin | -1.02 | 1.05 | -1.05 | -1.02 |
| IPI00469218 | 16783 | Lamp1 | Lysosome-associated membrane glycoprotein 1 | -1.11 | -1.01 | -1.18 | -1.01 |
| IPI00107952 | 17105 | Lyz2 | Lysozyme C-2 | -1.26 | -1.01 | 1.03 | 1.00 |
| IPI00277930 | 12332 | Capg | Macrophage-capping protein | -1.04 | -1.02 | -1.31 | -1.05 |
| IPI00121788 | 18477 | Prdx1 | Peroxiredoxin-1 | 1.16 | 1.03 | -1.05 | 1.04 |
| IPI00408892 | 19349 | Rab7 | Ras-related protein Rab-7a | 1.05 | -1.00 | 1.01 | 1.04 |

## 3.3. Comparative proteome analysis of BALB/c and C57BL/6 macrophages

Mice of the BALB/c strain are considered more susceptible for microbial infection in comparison to strain C57BL/6. It is clear that the progression and outcome of infections are determined by the responses of host defense mechanisms and the expression of pathogen virulence factors. Therefore, the outcome of host-pathogen interaction depends on both the particular infecting pathogen and the physiological status of the host. Even if in general, C57BL/6 mice are considered more resistant to microbial infection than BALB/c, there are also some exceptions. Some examples are C57BL/6 mice are more resistance than BALB/c mice to *Burkholderia speudomallei* [76], *Listeria monocytogenes* [77], or protozoan parasite *Leishmania major* [78], however the BALB/c mice showed more resistance against the protozoan parasite *Trypanosoma cruzi* than C57BL/6 mice [79]. Moreover, none marrow derived macrophages from C57BL/6 had a higher capacity of killing intracellular *Burkholderia pseudomallei* compared to BALB/c, especially after stimulation with IFN-γ [76]. Because the two mouse strains show different in bacterial killing capacity, they usually used as complementary models for investigating the host pathogen interacting process and identification of factors which determine outcome.

Our goal in this study was to identify the similarities and differences in transcriptomic and proteomic profiles of BMMs derived from the two mouse strains in the control as well as in IFN-γ treatment condition. To my knowledge, this was the first combined transcriptome and proteome analysis of BMMs derived from the two mouse strains BALB/c and C57BL/c. Results of such a comparison would be meaningful for other investigations addressing host-pathogen interactions of BMMs derived from the two mouse strains.

As mention above, protein expression profiles of four different BMM samples (biological samples series BMM2) which were obtained in 2D-DIGE and LC-MS/MS experiments were used to identify IFN-γ-effects as well as strain differences.

### 3.3.1. Differences in proteomic profiles of BMM-BALB/c and BMM-C57BL/6 identified with the 2D – DIGE technique

2D-DIGE protein expression profiles of BMM-BALB/c were compared to those of BMM-C57BL/6 to find out strain differences in the unstimulated control condition. By the same way, protein expression profiles of BMM-BALB/c + IFN-γ were compared to those of BMM-C57BL/6 + IFN-γ to identify strain differences in IFN-γ treatment condition. Thresholds for significant differences were minimum 1.5 fold changes and $p \leq 0.05$. In general, the 2D-DIGE results showed that 2-DE protein expression patterns of BMMs derived from the two mouse strain were not identical. We found that 168 and 204 proteins spots for which intensities were different between BMM-BALB/c and BMM-C57BL/6 in control and IFN-γ treatment condition, respectively (suppl. fig A.2 and A.3). These protein spots were called "strain different protein spots" in this study. Comparing the two sets of protein spots in control and in IFN-γ treatment conditions, we found that 130 protein spots were differing in intensity between BMMs of the two mouse strains in both conditions (table 13).

**Table 13: Protein spots identified by 2D-DIGE technique and displaying strain-specific differences in intensity.**

| Strain different protein spots | Higher in BMM-C57BL/6 | Higher in BMM-BALB/c | Total |
|---|---|---|---|
| Control condition | 55 | 113 | 168 |
| IFN-γ treatment condition | 71 | 133 | 204 |
| Overlap | 43 | 87 | 130 |

Quantitative analysis was performed with Delta2D software based on intensity data of four technical replicates. Thresholds for considering intensities as significantly different were a minimum of 1.5 fold change, and $p \leq 0.05$. The total number of separated protein spots on 2-DE gels was 914.

Based on the 2-DE protein reference map, we could identify the corresponding proteins in 106 out of the total of 242 strain different protein spots in control and/or IFN-γ treatment conditions. Protein identification result showed that 81 distinct proteins were found in the 106 strain different protein spots. Representative images which display differences in the 2-DE protein profiles of BMMs derived from strain BALB/c and C57BL/6 are shown in figure 15.

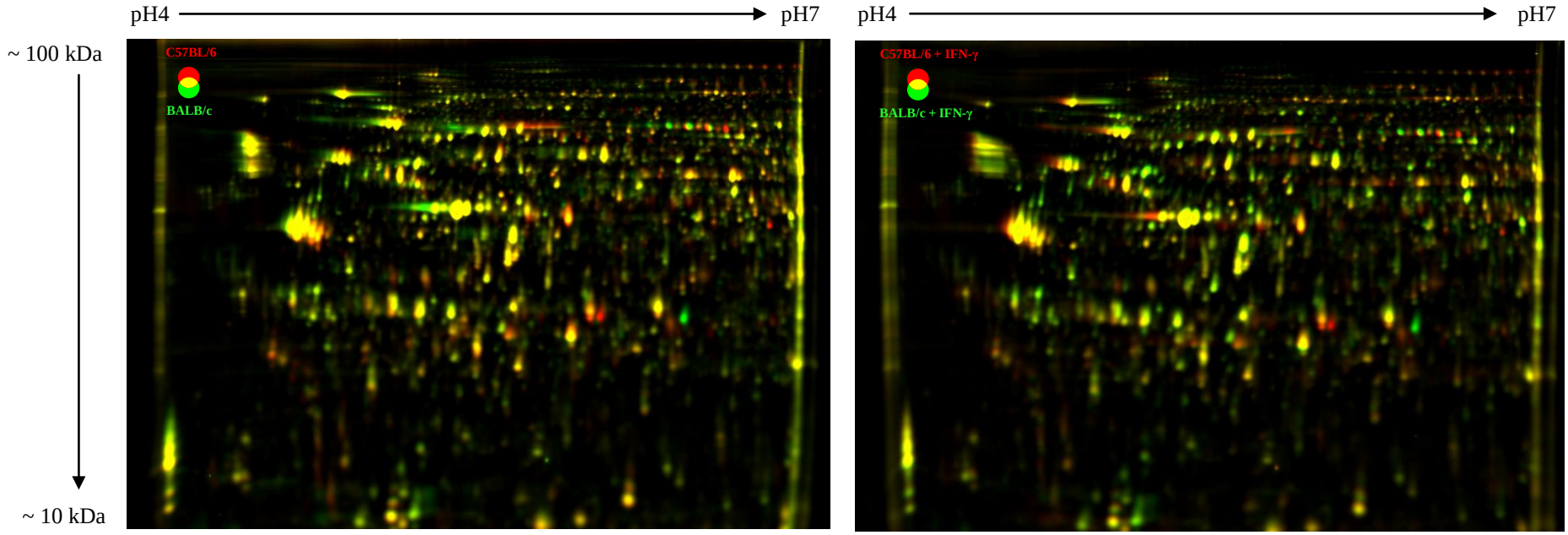


**Figure 15: Representative gels of differences in 2-DE protein expression profiles of BMM-BALB/c and BMM-C57BL/6.** The overlay images of BMM-BALB/c and BMM-C57BL/6 in control and IFN-γ treatment conditions are presented on the left image and right image, repectively. Protein patterns of BMM-BALB/c are colored in green while those of BMM-C57BL/6 are colored in red. Spot color indicates the different in protein abundance between the two mouse strains: red = higher in BMM-C57BL/6; green = lower in BMM-C57BL/6; yellow = equal between BMM-BALB/c and BMM-C57BL/6.

Protein identification of 106 strain different protein spots showed that 13 protein spots contained more than 1 protein per spot. The presence of different proteins prevented identification of the protein which was indeed regulated. Therefore, the 25 proteins which were identified in those 13 spots were not considered in the comparison of BMMs of the two mouse strains (suppl.table A.2).

The other 93 strain different protein spots contained only one protein per spot. In total 63 unique proteins were identified in the 93 spots. From the 2-DE protein reference map of BMMs, we knew that one protein may have different protein isoforms which locate in different spots. Therefore, for each protein we considered not only strain different isoforms but also the total identified isoforms of the protein. This was important because for one protein some of its isoforms might exist at higher level in one strain but the total amount of all protein isoforms might not have been significantly different. In a validation we verified that 63 proteins belonged to one of the following three groups.

- **Group 1**: Proteins for which the total amount was equal, however their protein isoforms were differently distributed in 2-DE protein profiles of BMM-BALB/c and BMM-C57BL/6. This group contained 5 proteins found in 26 spots: Actin cytoplasmic 1 (ACTB), Actin cytoplasmic 2 (ACTG), vimentin (VIME), beta-glucuronidase (BGLR), and endoplasmic reticulum protein ERp29 (ERP29) (suppl.table A.3). Of them actin and vimentin have a total of 29 and 17 protein isoforms, respectively. We believe that the different distribution of protein spcecies of the two proteins seemed to be random events. Interestingly, we recognized that protein isoforms of beta-glucuronidase (BGLR) and endoplasmic reticulum protein ERp29 (ERP29) were systematically differently distributed between two strains in control as well as IFN-γ treatment condition (figure 16).
- **Group 2:** Proteins for which total amount might be significantly different, because a portion but not all protein isoforms were higher in one strain. These proteins had more than 1 protein isoforms; and some but not all of their protein isoforms were present at higher level in one strain. This group included 23 proteins found in 30 spots. For example, in this group 3 protein isoforms of cathepsin D and and 3 protein isoforms of cathepsin S were present in higher amount in BMM-C57BL/6 while, 6 other protein isoforms of cathepsin D and 3 protein isoforms of cathepsin S showed no difference in intensity between the two mouse strains (suppl.table A.4).

- **Group 3**: Proteins for which the total amount was significant different, due to a higher abundance of all protein isoforms in one strain. These proteins had one or more protein isoforms and all of their protein isoforms were present at higher levels in one strain. This group contained 35 proteins found in 37 spots (suppl.table A.5). For example, elongation factor 1-beta (EF1B), and eukaryotic translation initiation factor 5A-1 (EF5A1) were found at higher level in BMM-BALB/c; while pyruvate dehydrogenase phosphatase regulatory subunit (PDPR), and short/branched chain specific acyl-CoA dehydrogenase (ACDSB) were found at higher levels in BMM-C57BL/6.

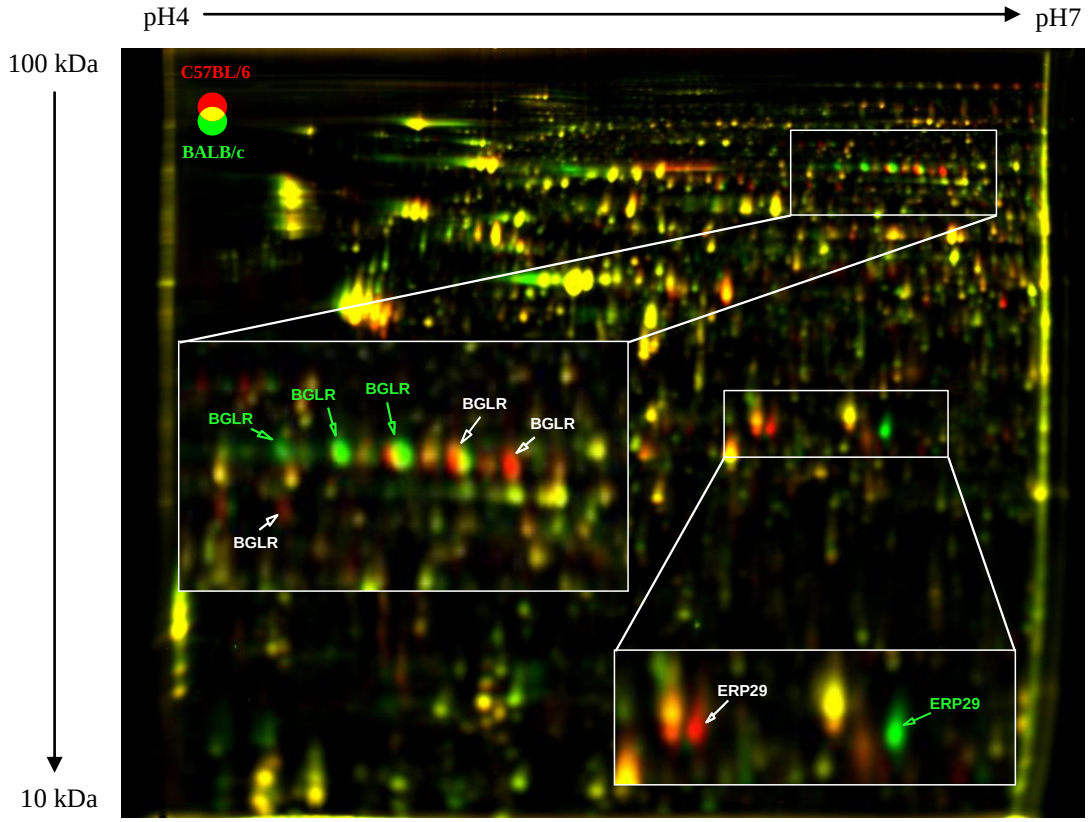


**Figure 16: Different distribution of protein isoforms of BGLR and ERP29 in BMM-BALB/c and BMM-C57BL/6**. Gel areas which contain BGLR and ERP29 protein isoforms are enlarged in two insets. Representative overlay images show 2-DE protein patterns of the BMM-BALB/c (green colour) and BMM-C57BL/6 (red colour) in the control condition. Spot colour indicates the difference in protein abundance between the two mouse strains: red = higher in BMM-C57BL/6; green = lower in BMM-C57BL/6; yellow = equal between BMM-BALB/c and BMM-C57BL/6. Spots which display different intensities in BMM-C57BL/6 and BMM-BALB/c can be also distinguished by white and green letters, respectively.

Taken together, a total of 242 strain different spots were identified in the 2-DE protein profiles of BMM-BALB/c and BMM-C57BL/6; most of the differences in control condition were reserved in IFN-γ treatment condition. The protein identification then proved that at least 35 proteins existed in different amounts; while some other proteins existed in different modified forms in BMM-BALB/c and BMM-C57BL/6.

### 3.3.2. Comparison of LC-MS/MS and transcriptomic data

Supporting the 2D-DIGE data, proteome analysis by LC-MS/MS showed that there were many differences in the proteome of BMMs derived from mouse strain BALB/c and C57BL/6. Applying the strict threshold values of a minimum 1.5 fold change, and $p \leq 0.01$, LC-MS/MS analysis showed that 218 and 308 proteins which were corresponding to 23% and 32% of a total of 946 identified proteins were present at different levels in the two mouse strains in control and IFN-γ treatment conditions, respectively. Of those, 183 proteins were found to be present at different levels in two strains in both conditions (table 14-C). In total, 343 proteins which were present at different levels in the two mouse strains in control and/or IFN-γ treatment conditions were identified (suppl.table A.7).

Surprisingly, in contrast to the results of both proteomic analyses, only minor difference between BMM-BALB/c and BMM-C57BL/6 was observed with transcriptomic analysis at the mRNA level. While both proteomic techniques showed many differences between the two mouse strains, transcriptomic analysis revealed that only 1% of the total 20,074 genes on the microarray was differentially expressed in the two mouse strains. The thresholds for considering significant different in the transcriptomic analysis was the same as with the proteomic LC-MS/MS: minimum 1.5 fold change, and $p \leq 0.01$. The number of genes identified as differentially expressed in BMMs of the two mouse strains in control macrophages was 222, and in IFN-γ stimulated macrophages was 230. Of those, 128 genes were found differently expressed in both conditions (table 14-B).

**Table 14: Summary of genes and proteins displaying strain specific expression levels identified by transcriptomics and LC-MS/MS techniques.**

**(A) Overview of differences in BMM-BALB/c and BMM-C57BL/6 at mRNA and protein levels identified by transcriptomics and LC-MS/MS.**

**(B) Genes expressed at different levels in BMM-BALB/c and BMM-C57BL/6**

**(C) Proteins present at different levels in BMM-BALB/c and BMM-C57BL/6 (identified by LC-MS/MS)**

**(A)**

| | Total number of detected genes or proteins | **Strain differences** | |
|---|---|---|---|
| | | in Control condition | in IFN-γ treament condition |
| microarray | 20,074 | 222 (1.1%) | 230 (1.1%) |
| LC-MS/MS | 946 | 218 (23%) | 308 (32%) |

**(B)**

| Strain diff. genes | Higher C57BL/6 | Higher BALB/c | Total |
|---|---|---|---|
| Control condition | 100 | 122 | 222 |
| IFN-γ treatment | 93 | 137 | 230 |
| Overlap | 64 | 64 | 128 |

**(C)**

| Strain diff. proteins | Higher C57BL/6 | Higher BALB/c | Total |
|---|---|---|---|
| Control condition | 112 | 106 | 218 |
| IFN-γ treatment | 135 | 173 | 308 |
| Overlap | 88 | 95 | 183 |

Intensity data from 12 arrays (1 measurement/sample x 3 biological replicate x 4 samples) were processed and analyzed with the Rosetta Resolver software. Result of quantitative analysis based on intensity data of 20,074 genes showed that 222 and 230 genes displaying strain dependent expression patterns in control and IFN-γ treatment condition, respectively. Protein intensity data of 12 LC-MS/MS measurements (3 measurements/sample x 4 samples) were processes and analyzed with Elucidator Resolver software. Performing quantitative analysis based on intensity data of 946 identified proteins, we identified 218 and 308 proteins being present at different levels in a strain dependent manner in control and IFN-γ treatment condition, respectively. Thresholds for considering differences as significant in both transcriptomic and proteomic analysis were a minimum 1.5 fold change, and $p \leq 0.01$. Percentage of IFN-γ regulated genes/proteins of total identified genes/proteins is showed in brackets.

Despite the different magnitude of strain differences identified by transcriptomic and LC-MS/MS analyses, the two analyses were consistent in two observations. The first was that strain differences were mostly not affected by IFN-γ stimulation. The second was that the number of genes/proteins being present in higher levels in BMM-BALB/c was equal with number of genes/proteins existed in higher levels in BMM-C57BL/6. The two observations can clearly be seen on the ratio plot diagram of proteins and mRNAs displaying different intensities in the two strains (figure 17)

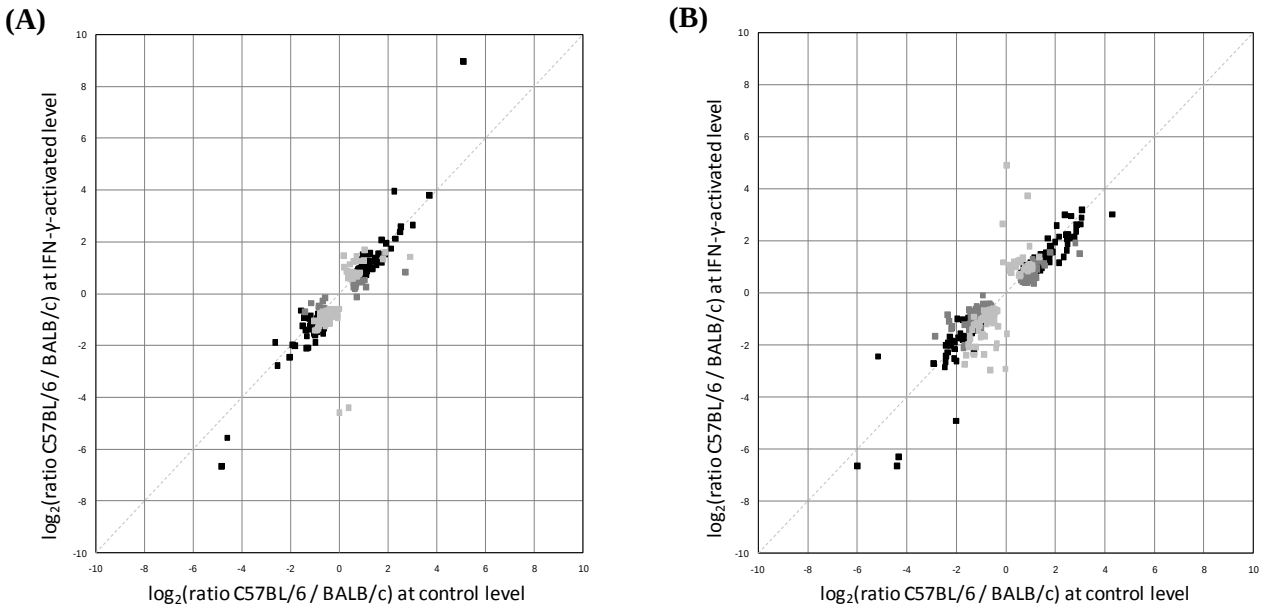


**Figure 17: Ratio plot of mRNAs and proteins being present at different levels in a strain-dependent manner.** Quantitative LC-MS/MS and transcriptomic analysis identified 343 proteins and 324 genes displaying strain dependent expression patterns, respectively. $Log_2$-transformed ratio data of the 343 proteins or 324 genes was used to create a ratio plot. Log2-transformed ratio data "control BMM-C57BL/6" / "control BMM-BALB/c" was plotted on the x-axis and log2-transformed ratio data "IFN-γ-treated BMM-C57BL/6" / "IFN-γ-treated BMM-BALB/c" on the y-axis. Coloring distinguishes three different groups of regulated proteins: proteins with significant strain difference only at control level were shown in dark gray, while that with significant strain difference only at IFN-γ-treated level were displayed in light gray. Proteins significantly different between BMM-BALB/c and -C57BL/6 on both conditions were colored in black.

**(A) Ratio plot of IFN-γ regulated proteins identified by LC-MS/MS.** In total 343 distinct proteins were identified as present at different levels in BMM-BALB/c and BMM-C57BL/6 in control and/or IFN-γ treatment conditions. $Log_2$-transformed ratio data of the 343 proteins were used to create a ratio plot. All LC-MS/MS ratio data were derived from mean intensities of three measurements of each sample.

**(B) Ratio plot of IFN-γ regulated genes identified by transcriptomics.** A total of 324 genes, displaying strain dependent expression patterns in BMM-BALB/c and BMM-C57BL/6 in control and/or IFN-γ treatment conditions were identified. $Log_2$-transformed ratio data of the 324 genes were used to create a ratio plot. All transcriptomic ratio data were derived from mean intensities of three biological replicates.

In the 900 genes/proteins which have been observed in both the transcriptomic and proteomic approaches, the overlap of differentially expressed proteins and differentially expressed genes was low in absolute numbers (12 at control level and 19 at IFN-γ-activated level) but it still contained 60% (control level) and 79% (IFN-γ-activated level) of the genes that were both differentially expressed in the array data set and accessible by proteome analysis (table 15).

**Table 15: Overlay of genes and proteins showing different expression or levels**

| **Strain differences** | | | |
|---|---|---|---|
| | LC-MS/MS | Microarray | Overlap |
| **Control condition** | | | |
| Higher C57BL/6 | 102 | 10 | 7 |
| Higher BALB/c | 101 | 10 | 4 |
| Total | 203 | 20 | 12 |
| **Treatment condition** | | | |
| Higher C57BL/6 +IFN-γ | 123 | 13 | 10 |
| Higher BALB/c +IFN-γ | 165 | 11 | 7 |
| Total | 288 | 24 | 19 |

Transcriptomic analysis showed that approximately 1% of 20,074 genes were differently expressed in BMM-BALB/c and BMM-C57BL/6. Therefore, the difference in anti-microbial potential of BMM-BALB/c and BMM-C57BL/6 seemed to be primarily resulting from differences at the protein level because these for found to occur for approximately 30% of a total of 946 proteins identified in the LC-MS/MS analysis. We performed further functional analysis for 343 proteins displaying strain-dependent differences in level either in controls and/or after IFN-γ treatment. First, protein IPI identifiers were translated into EntrezGene IDs using the PIPE (The Protein Information and Property Explorer_ http://pipe.systemsbiology.net) and UniProt ID (www.uniprot.org) mapping tools. Missing EntrezGene IDs were manually added if possible. The resulting list of gene entrez IDs was imported into PANTHER (version 6.1) classification system for identifying which biological processes the 343 proteins involve in. Information of biological

process was available for 291 out of 343 proteins. Panther biological classification results showed that different distributions occured in the two sets of proteins. Proteins belonging to the biological processes “cell cycle”, “cell structure and cell motility”, “signal transduction”, “nucleoside, nucleotide and nucleic acid metabolism”, “cell proliferation and differentiation” were more abundant in BMM-BALB/c, while more abundant proteins in BMM-C57BL/6 were found for “lipid, fatty acid and steroid metabolism” (figure 18-A).

The same gene entrez IDs list was uploaded into PIPE (The Protein Information and Property Explorer_ http://pipe.systemsbiology.net) classification system to figure out the cellular localization of proteins showing strain-dependent abundances. Information of cellular localization was available for 304 out of 343 proteins. PIPE analysis showed that most of the proteins which were more abundant in BMM-C57BL/6 were located in “Mitochondrion”, “Mitochondrial membrane”, and “Lysosome”, while more abundant proteins in BMM-BALB/c were found mostly in “Cytosol”, “Cytoskeleton”, “Cytoplasm”, and “Nucleus” (figure 18-B).

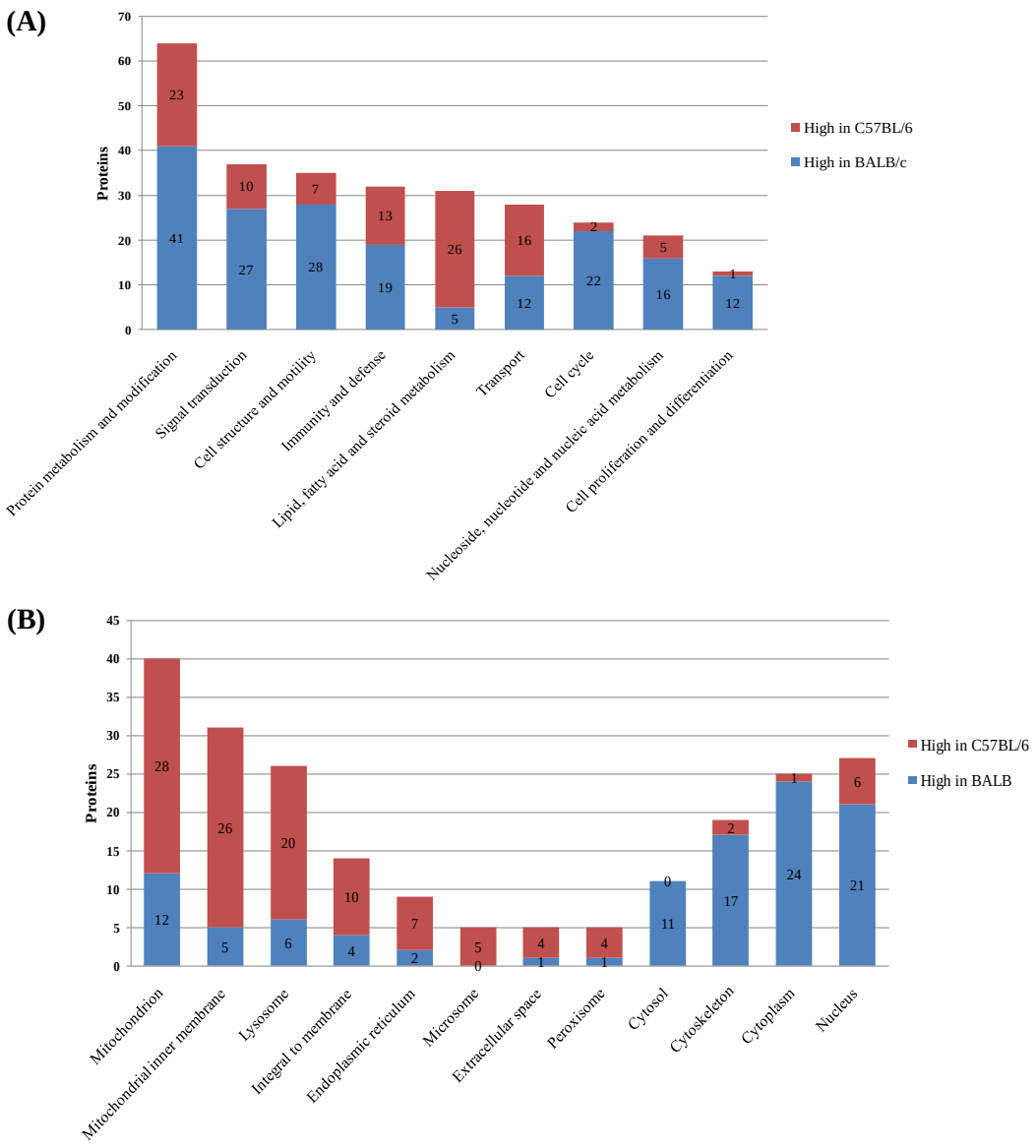


**Figure 18: Functional classification and cellular localization of the 343 proteins identified as different levels in BMM-BALB/c and BMM-C57BL/6.**

**(A) Functional classification.** Entrez Gene IDs of the 343 proteins were uploaded to PANTHER (Version 6.1) classification system. Information of biological process was available for 291 out of 343 proteins. Nine biological processes which displayed the highest number of proteins were selected for the diagram.

**(B) Cellular localization.** Entrez Gene IDs of the 343 proteins were uploaded to The Protein Information and Property Explorer (http://pipe.systemsbiology.net) Classification System. Information of cellular location was available for 304 out of 343 proteins. Nine cellular locations which contained largest number of proteins were showed on diagram. Note: Protein number of group Cytoskeleton shown on diagram was sum of five groups "actin cytoskeleton", "microtubule", "cortical actin cytoskeleton", "cytoskeleton", and "cortical cytoskeleton".

## 3.4. Effects of *S. aureus* infection on the proteome pattern of IFN-γ stimulated BMM-C57BL/6

Classically, macrophage activation was defined as a two stages process. In the model, the first stage is initiated with a "priming" signal (such as IFN-γ) which, though capable of inducing a number of changes, is insufficient to endow the responding cell with full functional competence. Exposure to the second "triggering" signal (such as LPS) is sufficient to complete the functional activation process [1]. There is evidence supporting this classical macrophage activation model. For example, IFN-γ priming is insufficient to stimulate macrophages to realease proinflammatory cytokines, although priming sensitizes macrophages, resulting in enhanced secretion of proinflammatory cytokines to subsequent LPS treatment [80, 81]. Another example is that maximal induction of inducible nitric oxide synthase (iNOS) transcription requires both "priming" and "triggering" stimuli such as priming with IFN-γ and subsequent triggering with LPS or TNF-α [82, 83].

However, the complementary effects between the "priming" and "triggering" factors in macrophage activation are not clearly understood. In this study, we wanted to define the effects of "priming" factors as well as "triggering" factors on the macrophage proteome. The identified IFN-γ effects on BMMs were already described in the previous part. In this part, the effects of a "triggering" factor – *S. aureus* engulfment event– will be presented. Protein profiles of IFN-γ stimulated macrophages were compared with IFN-γ stimulated macrophages containing intracellular *S. aureus* to identified *S. aureus* induced changes in the protein profile. BMM samples were collected at 6 h and 24 h after *S. aureus* engulfment event (figure 19). The infection resistant mouse strain C57BL/6 was selected for identifying *S. aureus* effects on IFN-γ stimulated macrophages. Two biologically independent samples series of BMM-C57BL/6 were used for the LC-MS/MS experiment. Whole cell extract proteins of IFN-γ stimulated BMM-C57BL/6 and IFN-γ stimulated BMM-C57BL/6 containing intracellular *S. aureus* were processed and analyzed by LC-MS/MS following the protocol described in material and methods part.

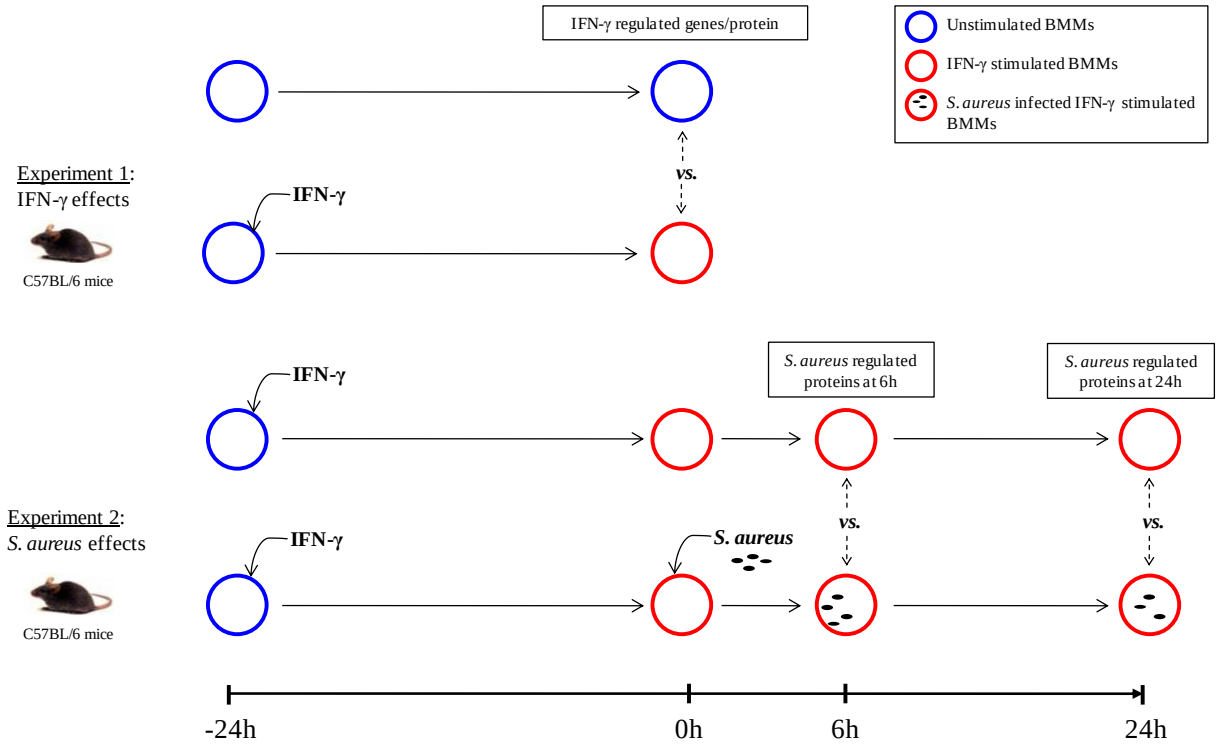


**Figure 19: Experimental setting for identifying IFN-γ effects and *S. aureus* effects in BMM-C57BL/6.** Experiment 1 (identifying IFN-γ effects) and experiment 2 (identifying *S. aureus* engulfment effects) were independently performed. In experiment 1, IFN-γ effects in BMMs from both mouse strains BALB/c and C57BL/6 was studied (in the figure, BMM-BALB/c is not shown) using biological samples series BMM2. *S. aureus* engulfment effects on BMM-C57BL/6 were studied in experiment 2 using two biologically independent samples series BMM5 and BMM6. The characters "**vs.**" between dot arrows was used to mark the comparisons from which corresponding IFN-γ regulated proteins, and *S. aureus* regulated proteins at 6 h and 24 h were identified.

Quantitative analysis was performed based on intensity values of the 939 proteins identified in LC-MS/MS experiment. Thresholds for significant regulation were atleast of 1.5 fold change and $p \leq 0.01$. In total 13 and 45 proteins were found to be present at different levels in IFN-γ stimulated BMM-C57BL/6 with and without intracellular *S. aureus* 6 h and 24 h after *S. aureus* infection, respectively. The proteins being present at different level due to *S. aureus* engulfment were called in short "*S. aureus* regulated proteins" in this study. The increase in protein level due to *S. aureus* engulfment was the prominent effect at both time points studied. We found that 10 proteins were significantly changed in amount due to *S. aureus* engulfment at both examined time points (table 16). Only for one out of 10 proteins, protein C receptor (Procr) opposite regulation was found between the two time points. The list of identified *S. aureus* regulated proteins is presented in table 17.

**Table 16: Proteins regulated by infection with *S. aureus* in IFN-γ stimulated BMM-C57BL/6**.

| *S. aureus* regulated proteins | 6 h after engulfment | 24 h after engulfment | Overlap |
|---|---|---|---|
| Induced | 10 | 31 | 8 |
| Repressed | 3 | 14 | 2 |
| Total | 13 | 45 | 10 |

LC-MS/MS intensity data were processed and analyzed with Rosetta Elucidator software. In total 939 proteins were identified in the LC-MS/MS experiment. Protein expression profiles of IFN-γ stimulated BMM-C57BL/6 were compared with those of IFN-γ stimulated BMM-C57BL/6 containing intracellular *S. aureus* 6 h and 24 h after *S. aureus* engulfment. Quantitative comparisons were based on 6 LC-MS/MS intensity data (two biological replicates x 3 technical replicates/sample). Thresholds for significant regulation were 1.5 fold change, and $p \leq 0.01$.

For finding complementary effects of IFN-γ stimulation and *S. aureus* engulfment in the proteome of BMM-C57BL/6, the identified *S. aureus* regulated proteins had to be compared with the identified IFN-γ regulated genes/proteins. In total, three experiments were independently performed for identifying effects of IFN-γ stimulation and *S. aureus* engulfment onto the proteome of BMM-C57BL/6. The first experiment - transcriptomic analysis – identified 442 IFN-γ regulated genes in a total of 20,074 genes. The second experiment – LC-MS/MS analysis – identified 53 IFN-γ regulated proteins in a total of 946 proteins. The third experiment – LC-MS/MS analysis – identified 48 S. *aureus* regulated proteins in a total of 939 proteins. Identified genes/proteins of the three experiments were mapped to the others through gene entrez IDs. For this purpose, IPI identifiers of identified proteins in the LC-MS/MS experiments were translated to EntrezGene IDs and mapping with transcriptomic data. Firstly, protein IPI identifiers were translated into EntrezGene IDs using the PIPE (http://pipe.systemsbiology.net/pipe) and UniProt ID (www.uniprot.org) mapping tools. Missing EntrezGene IDs were manually added if possible. The mapping results showed that 54 IFN-γ regulated genes and 44 IFN-γ regulated proteins were also covered in the 939 proteins of the third experiment. Of these IFN-γ regulated genes/proteins, 6 genes and 7 proteins were regulated by both factors, while 48 genes and 37 proteins were not affected by *S. aureus* engulfment. In the other side, 44 *S. aureus* regulated proteins were covered in the 20,074 genes of the first experiment, of which 6 proteins were regulated in both data sets, while 38 proteins were only regulated by *S. aureus* and not by IFN-γ stimulation. By the same way, we found that 27 *S. aureus* regulated proteins were covered in the 946 proteins of the second experiment, of which 7 proteins were regulated in both data sets, while 20 proteins were only regulated by *S. aureus* and not by IFN-γ stimulation (figure 20). Taken together, the

comparisons showed that IFN-γ stimulation and *S. aureus* engulfment events largely targeted different groups of proteins. Most of IFN-γ regulated genes were subsequently not affected by *S. aureus* engulfment, while the main portion of *S. aureus* regulated proteins had not previously been shown to be regulated by IFN-γ treatment. However, a synergistic effect of IFN-γ stimulation and *S. aureus* engulfment was observed for proteins which were regulated by both factors (figure 20, table 18).

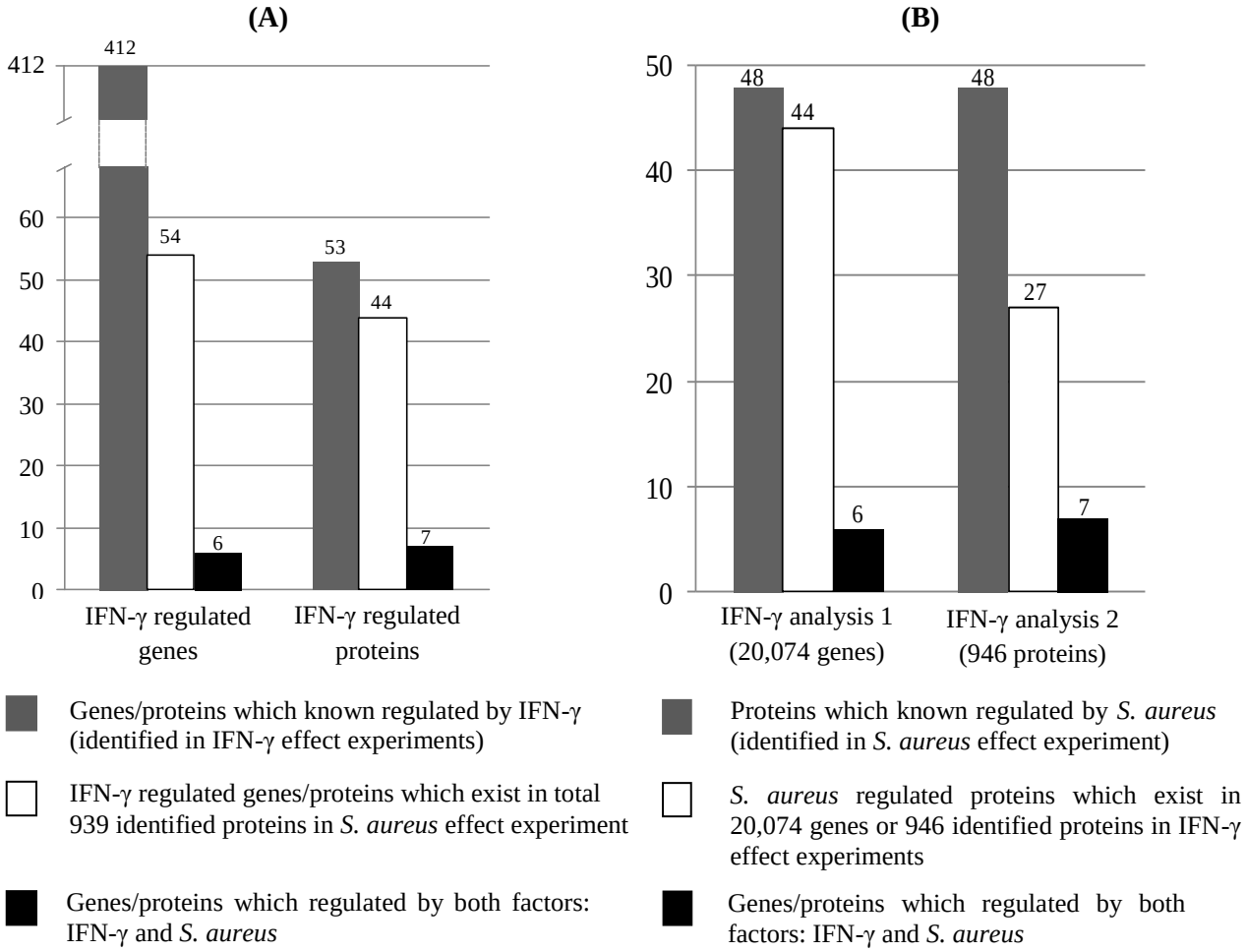


**Figure 20: Mapping of IFN-γ regulated genes/proteins and *S. aureus* regulated proteins in BMM-C57BL/6.**

**(A)** Mapping of IFN-γ regulated genes/proteins to all proteins identified in the LC-MS/MS experiment for the analysis of the *S. aureus* effect. Gene entrez IDs of 442 IFN-γ regulated genes and 53 IFN-γ regulated proteins identified in C57BL/6 were mapped with gene entrez IDs of 939 proteins identified in the LC-MS/MS experiment designed to study the *S. aureus* effect.

**(B)** Mapping of *S. aureus* regulated proteins to all genes accessible to the microarray analysis or all proteins identified in transcriptomic and LC-MS/MS experiment designed to study the IFN-γ effect. Gene entrez IDs of 48 *S. aureus* regulated proteins were mapped onto gene entrez IDs of 20,074 genes on the microarray and 946 identified proteins in the LC-MS/MS experiments for studying the effect of IFN-γ.

**Table 17: Proteins influenced in abundance by infection with *S. aureus* at 6 h and/or 24 h post infection**.

| *Protein* | *Gene Entrez ID* | *Gene Symbol* | *Protein name* | *Fold change 6 h-(S. aureus /control)* | *Fold change 24 h-(S. aureus /control)* |
|---|---|---|---|---|---|
| **IPI00116074** | 11429 | Aco2 | Aconitate hydratase, mitochondrial | - | -2.0 |
| **IPI00135015** | 18412 | Acpp | Isoform 1 of Prostatic acid phosphatase | 1.9 | 2.8 |
| **IPI00857226** | 14081 | Acsl1 | Long-chain-fatty-acid--CoA ligase 1 | - | 2.2 |
| **IPI00121287** | 11655 | Alas1 | aminolevulinic acid synthase 1 | - | 3.7 |
| **IPI00828225** | 27061 | Bcap31 | B-cell receptor-associated protein 31, isoform CRA_c | - | 1.5 |
| **IPI00408495** | 12215 | Bsg | Isoform 2 of Basigin | - | 4.7 |
| **IPI00117829** | 16956 | Cav1 | Isoform Alpha of Caveolin-1 | 2.4 | 8.4 |
| **IPI00308990** | 12475 | Cd14 | Monocyte differentiation antigen CD14 | - | 5.7 |
| **IPI00129594** | 12523 | Cd84 | Isoform 1 of SLAM family member 5 | - | -1.5 |
| **IPI00229834** | 12847 | Copa | Coatomer subunit alpha | - | 1.6 |
| **IPI00126083** | 13660 | Ehd1 | EH domain-containing protein 1 | - | 1.6 |
| **IPI00122411** | 13733 | Emr1 | EGF-like module-containing mucin-like hormone receptor-like 1 | - | 1.8 |
| **IPI00875145** | 50527 | Ero1l | ERO1-like | - | 2.6 |
| **IPI00187353** | 67475 | Ero1lb | ERO1-like protein beta | - | 2.3 |
| **IPI00230145** | 14319 | Fth1 | Ferritin heavy chain | - | 1.7 |
| **IPI00229277** | 229898 | Gbp5 | Guanylate-binding protein 5 | - | 2.1 |
| **IPI00126721** | 66092 | Ghitm | Growth hormone-inducible transmembrane protein | - | 1.5 |
| **IPI00126346** | 18126 | H2-Aa | H-2 class II histocompatibility antigen, A-B alpha chain | 1.7 | - |
| **IPI00110806** | 14972 | H2-K1 | 42 kDa protein | - | 1.5 |
| **IPI00131577** | 15368 | Hmox1 | Heme oxygenase 1 | - | 6.3 |
| **IPI00114067** | 14960 | Il1b | Interleukin-1 beta | 13.3 | 19.3 |
| **IPI00111285** | 16365 | Irg1 | Immune-responsive gene 1 protein | - | 2.0 |
| **IPI00132474** | 16412 | Itgb1 | Integrin beta-1 | - | 1.8 |
| **IPI00129265** | 16889 | Lipa | lysosomal acid lipase A | - | -1.8 |
| **IPI00849349** | 100048461 | LOC100048461 | similar to dendritic cell-associated C-type lectin-1; DECTIN-1 | - | -2.0 |
| **IPI00319188** | 11988 | Lpl | lipoprotein lipase | -1.5 | -1.9 |
| **IPI00119063** | 16971 | Lrp1 | Prolow-density lipoprotein receptor-related protein 1 | - | -1.6 |
| **IPI00321648** | 17381 | Mmp12 | Macrophage metalloelastase | - | -1.7 |
| **IPI00848818** | 19225 | Mtap4 | Isoform 1 of Microtubule-associated protein 4 | -1.6 | - |
| **IPI00116748** | 67273 | Ndufa10 | NADH dehydrogenase [ubiquinone] 1 alpha subcomplex subunit 10, mitochondrial | - | -1.8 |
| **IPI00125929** | 17992 | Ndufa4 | NADH dehydrogenase [ubiquinone] 1 alpha subcomplex subunit 4 | - | -1.5 |
| **IPI00308882** | 227197 | Ndufs1 | NADH-ubiquinone oxidoreductase 75 kDa subunit, mitochondrial | - | -1.5 |
| **IPI00130460** | 17995 | Ndufv1 | NADH dehydrogenase [ubiquinone] flavoprotein 1, mitochondrial | - | -1.8 |
| **IPI00125726** | 19124 | Nos2 | Nitric oxide synthase, inducible | 2.7 | 16.2 |
| **IPI00321058** | 246730 | Oas1a | 2'-5'-oligoadenylate synthetase 1A | - | 1.5 |
| **IPI00475158** | 624814 | OTTMUSG00000005734 | similar to NADH dehydrogenase (ubiquinone) Fe-S protein 3 | - | -2.1 |
| **IPI00119551** | 56193 | Plek | P Pleckstrin-2 | - | 1.6 |
| **IPI00473190** | 16176 | Procr | Protein C receptor, endothelial, isoform CRA_b | -1.6 | 2.3 |
| **IPI00308785** | 17758 | Ptgs2 | Prostaglandin G/H synthase 2 | 17.4 | 22.9 |
| **IPI00169485** | 56318 | Rab11fip1 | RAB11 family interacting protein 1 | 1.9 | 2.8 |

| *Protein* | *Gene Entrez ID* | *Gene Symbol* | *Protein name* | *Fold change 6 h-(S. aureus /control)* | *Fold change 24 h-(S. aureus /control)* |
|---|---|---|---|---|---|
| **IPI00126585** | 12389 | H2-Ab1 | H-2 class II histocompatibility antigen, A beta chain | 1.8 | - |
| **IPI00338536** | 67680 | Sdhb | Succinate dehydrogenase [ubiquinone] iron-sulfur subunit, mitochondrial | - | -1.6 |
| **IPI00884508** | 20525 | Slc2a1 | solute carrier family 2 (facilitated glucose transporter), member 1 | - | 1.7 |
| **IPI00114641** | 17254 | Slc3a2 | CD98 heavy chain | - | 2.1 |
| **IPI00894970** | 14961 | Slc7a2 | Isoform 2 of Low affinity cationic amino acid transporter 2 | 3.2 | 19.8 |
| **IPI00776208** | 57319 | Smpdl3a | acid sphingomyelinase-like phosphodiesterase 3a | - | -1.5 |
| **IPI00117534** | 100340 | Smpdl3b | Acid sphingomyelinase-like phosphodiesterase 3b | - | 2.2 |
| **IPI00133374** | 75767 | Sqstm1 | Isoform 2 of Sequestosome-1 | 1.8 | 7.1 |

LC-MS/MS data were processed and analyzed with Rosetta Elucidator software. Quantitative analyses were based on two biological replicates and 3 technical replicates. Thresholds for considering proteins as significantly regulated were a minimum of 1.5 fold change and $p \leq 0.01$.

**Table 18: Proteins influenced in abundance by infection with *S. aureus* and IFN-γ stimulation**.

| | | | | *IFN-γ effect* | | *S. aureus effect* | |
|---|---|---|---|---|---|---|---|
| **Primary Protein Name** | **Entrez gene nr.** | **Gene symbol** | **Protein name** | **Transcriptomic** | **LC-MS** | **6 h** | **24 h** |
| **IPI00857226** | 14081 | Acsl1 | Long-chain-fatty-acid--CoA ligase 1 | 3.5 | 2.5 | - | 2.2 |
| **IPI00229277** | 229898 | Gbp5 | Guanylate-binding protein 5 | 66.8 | 66.7 | - | 2.1 |
| **IPI00126346** | 14960 | H2-Aa | H-2 class II histocompatibility antigen, A-B alpha chain | - | 3.1 | 1.7 | - |
| **IPI00111285** | 16365 | Irg1 | Immune-responsive gene 1 protein | 17.4 | 22.7 | - | 2.0 |
| **IPI00119063** | 16971 | Lrp1 | Prolow-density lipoprotein receptor-related protein 1 | n.i | -1.5 | - | -1.6 |
| **IPI00321648** | 17381 | Mmp12 | Macrophage metalloelastase | - | -2.8 | - | -1.7 |
| **IPI00125726** | 18126 | Nos2 | Nitric oxide synthase, inducible | 25.5 | n.i | 2.7 | 16.2 |
| **IPI00321058** | 246730 | Oas1a | 2'-5'-oligoadenylate synthetase 1A | - | 1.8 | - | 1.5 |
| **IPI00308785** | 19225 | Ptgs2 | Prostaglandin G/H synthase 2 | 15.4 | n.i | 17.4 | 22.9 |
| **IPI00117534** | 100340 | Smpdl3b | Acid sphingomyelinase-like phosphodiesterase 3b | 6.1 | n.i | - | 2.2 |

"**-**" indicates that the changes observed were not significant.

"**n.i**" - indicates gene/protein was not identified in a particular experiment.

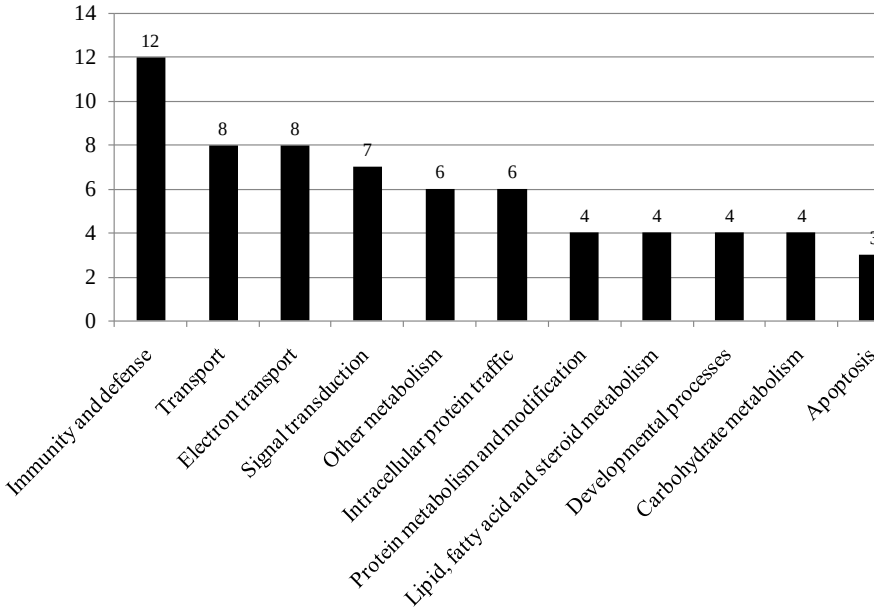


**Figure 21: Functional classification of *S. aureus* regulated proteins.** 48 proteins were influenced in abundance by *S. aureus* infection in IFN-γ stimulated BMM-C57BL/6 6 h and/or 24 h post infection. Entrez Gene IDs of the 48 proteins were uploaded to the PANTHER (Protein Analysis Through Evolutionary Relationships) classification system. Biological process information was available for 47 out of 48 proteins. Eleven biological processes which were covered by the highest number of proteins were selected for the diagram.

Classification of biological function of the 48 distinct identified *S. aureus* regulated proteins 6 h and/or 24 h post infection was performed with the PANTHER classification system (version 6.1). Using NCBI mouse databases, biological process information was available for 47 out of 48 uploaded entrez gene IDs of *S. aureus* regulated proteins. The analysis result showed that the most abundant biological process of IFN-γ regulated proteins/genes was "immune and defense". However, different from the 69 IFN-γ regulated proteins in which most of proteins accumulated to one biological process "immune and defense", the 48 *S. aureus* regulated proteins were rather equally distributed also in different biological processes. The other biological processes which included *S. aureus* regulated proteins were "transport" "electron transport", "signal transduction", "intracellular protein traffic". Other *S. aureus* regulated proteins belonged to metabolic processes such as "protein metabolism and modification", "lipid, fatty acid and steroid metabolism", and "carbohydrate metabolism" (figure 21).

The most strongly regulated proteins due to *S. aureus* engulfment were already changed at the early time point 6 h p.i. and continuously changed in the same direction as observed at time point 24 h p.i. These proteins were inducible NO synthase (NOS2), prostaglandin G/H synthase 2 (PTGS2), interleukin-1 beta (IL1B), low affinity cationic amino acid transporter 2 (SLC7A2), isoform alpha of Caveolin-1 (CAV1), RAB11 family interacting protein 1 (RAB11FIP1), and Sequestosome-1 (SQSTM1). Interestingly, most of them were observed significantly induced only after *S. aureus* engulfment. Especially, despite the observed induction of mRNA level due to IFN-γ stimulation, two proteins inducible NO synthase (NOS2) and prostaglandin G/H synthase 2 (PTGS2) were only found at low level in IFN-γ stimulated BMM-C57BL/6 until *S. aureus* engulfment.

It is important to note that, the synergistic effect of IFN-γ and *S. aureus* infection was clearly depicted in 10 proteins which were regulated by the both factors. *S. aureus* infection magnified the effects of IFN-γ stimulation on these proteins. The most significantly changed proteins in this group were Inducible NO synthase (NOS2), prostaglandin G/H synthase 2 (PTGS2), immune-responsive gene 1 protein (IRG1), guanylate-binding protein 5 (GBP5), and long-chain-fatty-acid-CoA ligase 1 (ACSL1). Changes of the levels of some interesting *S. aureus* regulated proteins are presented in figure 22.

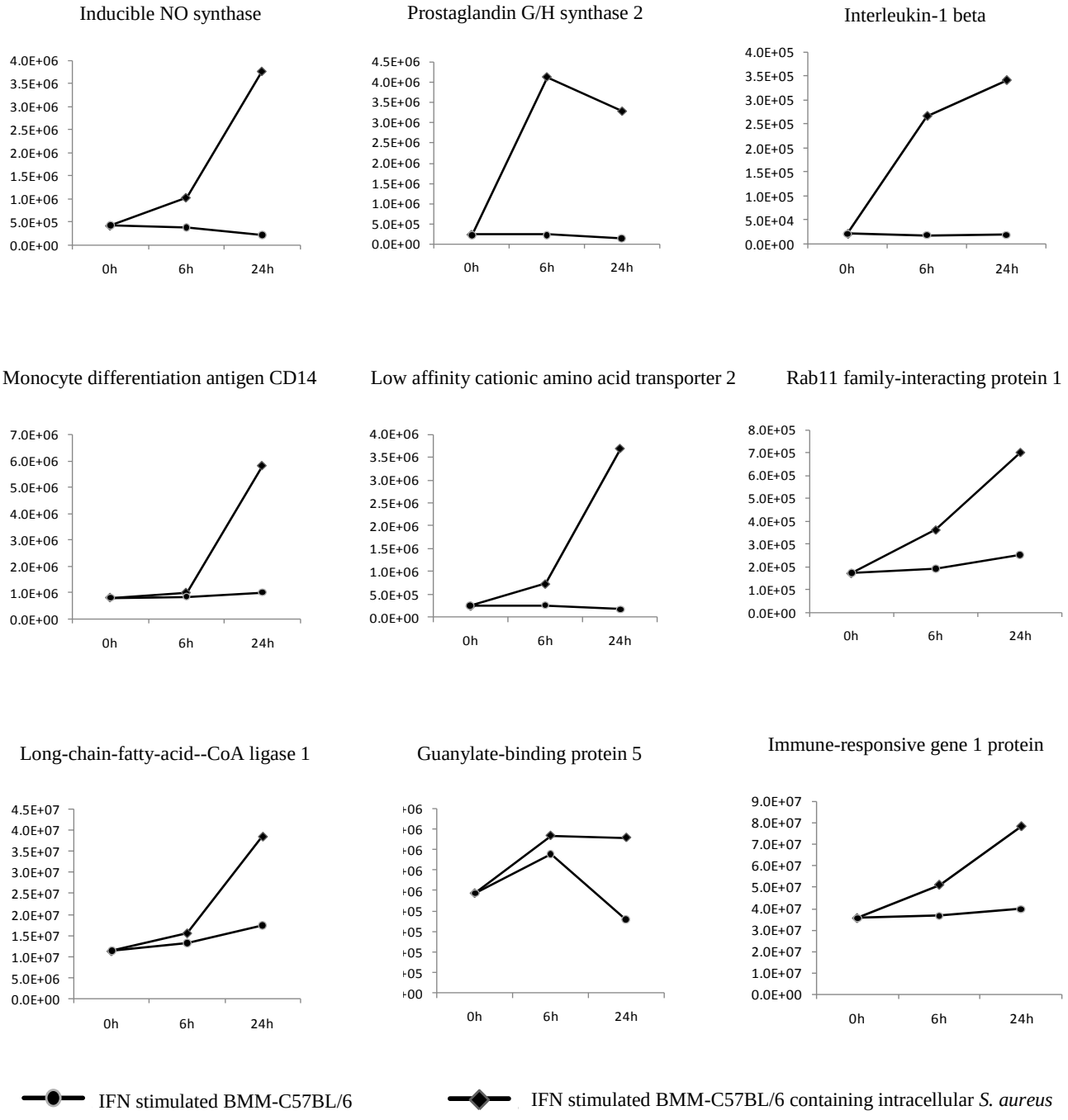


**Figure 22: Time-resolved analysis of the intensity changes of some selected proteins influenced by infection with *S. aureus***. The black line with circles shows intensity data of IFN-γ stimulated BMM-C57BL/6 without *S. aureus* interaction. Black lines with diamond symbols represent intensity data of IFN-γ stimulated BMM-C57BL/6 containing intracellular *S. aureus*. Mean of intenstiy of each protein was calculated from 6 correponding intensity values obtained from LC-MS/MS measurements (2 biological replicates x 3 technical replicates).

# 4. Discussion

## 4.1. 2-DE proteome reference map of bone marrow derived macrophages

Until now, only few 2-DE protein reference maps of macrophages have been published. Recently, the first human macrophage 2-DE protein reference map which covered 125 distinct proteins was published [53]. This time, we could separate whole cell protein extract of bone marrow derived macrophages into 914 protein spots on a 2-DE gel. From those 145 distinct proteins were identified in the 252 most abundant protein spots with MALDI-MS/MS. The identified proteins on the 2-DE protein reference map revealed many specific characteristics of macrophages.

Macrophage movement and phagocytosis require the participating of cytoskeleton and microtubule proteins [84, 85]. The most abundant proteins that have been observed on 2-DE protein reference map were naturally structural proteins such as vimentin (VIME), actin cytoplasmic protein 1 and 2 (ACTB and ACTG), and tubulin beta-2A chain (TBB2A).

Macrophages are known to possess large amounts of lysosomal proteases which participate in antigen processing and proteolytic proprotein activation [86]. The observed proteins of this group were cathepsin B (CATB), cathepsin D (CATD), cathepsin L1 (CATL1), cathepsin S (CATS), and cathepsin Z (CATZ). Serine protease inhibitors which control activity of cathepsins [87] were also observed such as serine protease inhibitor A3G (SPA3G) and Serpin B6 (SPB6).

Macrophages utilize reactive oxygen species (ROS) and nitric oxide (NO) for killing engulfed microorganisms, however, these agents when accumulating in large amounts can result in cell death [88]. Therefore, balancing the level of toxic agents is very important for survival of macrophages themselfes. Peroxiredoxins involved in redox regulation of the cell, protect cells from oxidative damage by reactive oxygen and nitrogen species [89]. Four members of the peroxiredoxin family peroxiredoxin 1 (PRDX1), peroxiredoxin 3 (PRDX3), peroxiredoxin 4 (PRDX4), and peroxiredoxin 6 (PRDX6) were identified in this study.

Heat shock proteins have recently been indicated in having the ability to modulate the cellular immune response. These proteins serve as cellular chaperones, participate in protein synthesis and transport through the various cellular compartments [90, 91]. Heat shock protein HSP 90-alpha (HS90A), heat shock protein HSP 90-beta/Endoplasmin (HS90B1), heat shock protein 1 (CH60), heat shock protein 5 (GRP78), heat shock protein 8 (HSP7C), heat shock

protein 9 (GRP75), and heat shock protein 105 kDa (HS105) were found here. We also observed calreticulin (CALR) which promotes folding, oligomeric assembly and quality control in the endoplasmic reticulum via the calreticulin/calnexin cycle [92].

Many identified proteins have functions in carbohydrate metabolism such as beta-glucuronidase (BGLR), alpha-enolase (ENOA), pyruvate kinase isozymes M1/M2 (KPYM), phosphoglycerate mutase 1 (PGAM1), and glucosidase 2 subunit beta (GLU2B). This may reflect high level of metabolic activity of macrophages [5]. Mitochondrial membrane ATP synthase produces ATP from ADP in the presence of a proton gradient across the membrane which is generated by electron transport complexes of the respiratory chain [93]. Three components of ATP synthase were identified including ATP synthase subunit alpha (ATPA), ATP synthase subunit beta (ATPB), and ATP synthase subunit d (ATP5H).

It should be noted that some proteins were found in more than one spot on the 2-DE protein reference map. The differently modified forms of a protein which locate in different spots were referred as protein isoforms. The existence of different protein isoforms was also reported by other studies which utilize the 2-DE technique [53, 94]. In most cases, the reasons and biological meanings of this phenomenon are not understood. Some explanations for the phenomenon in previous studies were "*we do not yet know the exact reason(s) or biological significance of the differences observed*" [53] and "*the presence of such multiple spots for procathepsins D and B are most likely due to the heterogeneity of their carbohydrate moieties*" [94]. The existence of different protein isoforms may come from different mRNA splicing and post translational modification. However, further detail protein sequencing and functional analysis are required for understanding the mechanisms and biological meanings of this phenomenon.

## 4.2. IFN-γ effects on BMM-BALB/c and BMM-C57BL/6 identified by proteomic 2D-DIGE and LC-MS/MS approaches

Difference in anti-microbial capacity of the two mouse strains BALB/c and C57BL/6 are well described. Recently, it was reported that bone marrow derived macrophages from C57BL/6 mice have a higher capacity of killing intracellular *Burkholderia speudomallei* than those derived from BALB/c mice, especially after stimulation with IFN-γ [76]. Despite difference in anti-microbial defense capacity, we have found that BMMs derived from the two strains consistently

responded to IFN-γ stimulation (Figure 11). Remarkably, there was high concordance between LC-MS/MS and transcriptomic analysis in the identified IFN-γ effects on BMMs.

Both proteomic and transcriptomic analyses showed that induction of gene expression and increases in protein level were prominent effects of IFN-γ stimulation (Figure 11). Immune related genes/proteins constituted the most abundant functional group of all identified IFN-γ regulated genes and proteins (Figure 12). Approximately 50% of the identified IFN-γ regulated proteins were also identified by transcriptomic analysis (Table 8). The good agreement between proteomic and transcriptomic results supported that both analyses were precisely performed and predominantly reflected biological changes in macrophages than technical variation.

A consistent response to IFN-γ stimulation in BMM-BALB/c and BMM-C57BL/6 was observed with both proteomic and transcriptomics, analyses. More than 60% of the IFN-γ regulated proteins and 70% of IFN-γ regulated genes were common between the two mouse strains. Particularly, there was no IFN-γ regulated gene/protein which was changed in opposite directions after IFN-γ treatment in the two mouse strains. Ratio plots clearly indicated that almost all IFN-γ regulated proteins identified in BMM-BALB/c and BMM-C57BL/6 changed in the same direction after IFN-γ treatment (Figure 11). Only two proteins, interferon-induced guanylate-binding protein 1 (Gbp1) and serine protease inhibitor A3G (Serpina3g) were observed as strongly induced by IFN-γ only in BMM-BALB/c. Because of high consistence in IFN-γ responses of BMM-BALB/c and BMM-C57BL/6, the identified IFN-γ effects were considered common in both BMM-BALB/c and BMM-C57BL/6. The two proteins which differently responded to IFN-γ between BMM-BALB/c and BMM-C57BL/6 will be discussed in the corresponding functional context.

The changes identified in the proteome of BMMs by gel based 2D-DIGE and gel-free LC-MS/MS techniques were combined and discussed in functional contexts.

### 4.2.1. Transcription regulation

Hundreds of genes in macrophages are differently expressed due to IFN-γ stimulation [75]. In this study, 531 IFN-γ regulated genes were identified in BMM-BALB/c and/or BMM-C57BL/6 with a transcriptomic analysis. We have observed the induction of signal transducer and activator of transcription 1 protein (STAT1) in both mRNA and protein level after IFN-γ stimulation. The Jak-Stat1 pathway plays a central role in the regulation of gene expression in

response to IFN-γ [95]. After the binding of IFN-γ to its receptor, Jak1 and Jak2 are activated and phosphorylate a specific tyrosine residue on the IFNGR1 subunit creating a docking site for Stat1. Jaks phosphorylate Stat1 on tyrosine 701 resulting in the dimerization of Stat1 which then translocates into the nucleus and binds to specific DNA elements, known as gamma activated sequence, and regulate gene expression. Many of the induced genes are in fact transcription factors (for example, IRF-1 [96]), which are able to further drive regulation of the next wave of transcription [29]. The key function of Stat1 in IFN-γ signal transduction was demonstrated with Stat1 deficient mice. STAT1-deficient mice display a complete lack of responsiveness to either IFN-α or IFN-γ and are highly sensitive to infection by microbial pathogens and viruses [97].

### 4.2.2. p47 and p65 GTPases

In this study, we have observed many proteins which belong to two GTPases families: p47-immunity-related GTPases (p47 IRGs) and p65 guanylate-binding proteins (p65 GBPs), such as LRG-47/Irgm1, IIGP1/Irga6, IRG-47/ ifi47, IGTP/Irgm3, Gbp1, Gbp2, Gbp5 and that are strongly induced in both transcriptional and translational levels in bone marrow derived macrophages after IFN-γ treatment. Our finding are in agreement with previous studies that members of the two GTPases families are strongly induced after IFN-γ treatment [98, 99]. The p47 family members primarily respond to IFN-γ in a STAT-1 dependent manner [98, 100] while Gbps transcription requires secondary transcription factors such as interferon regulatory factor–1 (IRF-1) to initiate promoter activity [98]. These two GTPases families are now emerging as new host defense effectors which provide cell-autonomous resistance against many bacterial, eukaryotic and viral pathogens [review in 101, 102]. The anti-microbial activity of p47 members is supported by many evidences at both cellular as well as organism level. At cellular level, IGTP/Irgm3 and LRG-47/Irgm1 are required for IFN-γ-induced inhibition of *T. gondii* growth in macrophages [103]; IIGP1/Irga6 and IGTP/Irgm3 are required for restriction of *T. gondii* growth in mouse astrocytes [104, 105]; Irgm1 for control of *M. tuberculosis* [100] and *Trypanosoma cruzi* [106] in macrophages. Studies on p47 genes-deficient mice revealed the important role of these genes in host protection at the whole organism levels. These finding were well described [102, 107], for example LRG-47/Irgm1 deficient mice are susceptible for *Toxoplasma gondii*, *Listeria monocytogenes*, *Mycobacterium tuberculosis*; IGTP/Irgm3 deficient mice are susceptible for *T. gondii*, *Leishmania major* and *Chlamydia trachomatis*. Only little is known about antimicrobial activity of p65 GBPs members. Gbp1 mediates an antiviral effect

against both vesicular stomatitis virus (VSV) and encephalomyocarditis virus (EMCV) in Hela cells [108] while GBP-2 inhibits the replication of these both viruses in NIH 3T3 cells [109]. The antimicrobial mechanisms of p47 and p65 GTPases proteins appear to be linked to their role in processing pathogen-containing vacuoles. LRG-47/Irgm1 was found on *M. tuberculosis* phagosomes [100], IIGP1/Irga6 and IGTP/Irgm3 accumulate at vacuoles containing *T. gondii* [104, 110]. Recently, the accumulation of Gbp1, 2, 3, 6, 7, and 9 around the parasitophorous vacuole *T.gondii* was observed [99]. Interestingly, we have found that Gbp1 and 2 were differently expressed between BMM-BALB/c and BMM-C57BL/6. Gbp1 was only induced in BMM-BALB/c and not in BMM-C57BL/6 while Gbp2 levels were higher in BMM-C57BL/6 than in BMM-BALB/c after IFN-γ treatment. Our observation agrees with other previous studies that Gbp1 is only expressed in BALB/c mice and not in C57BL/6 mice after IFN-γ treatment [111-113]. Taken together, with complementing proteomic and transcriptomic approaches, we could identify and confirm the induction of members of the p47 and p65 GTPases families, which are new host effectors against microbial pathogens. Until now, the activity mechanisms of members of the two GTPases families are still unclear and need further investigation. Our result placed the changes of the two families of GTPases p47 IRGs and p65 GBPs due to IFN-γ treatment in the context of regulation of other genes and proteins. Therefore, it should be useful for other studies devoted to the analysis of activation mechanisms of members of the two GTPases families.

### 4.2.3. Antigen presentation

Macrophages play an important role in immune response through their phagocytosis and antigen presentation functions. As professional phagocytes, macrophages possess both MHC class I and class II for presenting intracellular and extracellular antigens, respectively [114]. Antigen presentation activities are induced in IFN-γ activated macrophages [29]. We found that proteins involved in MHC class I and class II antigen presentation pathways were induced after IFN-γ stimulation.

Endogenous antigens are generated within the cells. These would include proteins encoded by genes of viruses in infected cells or aberrant proteins that are encoded by mutant genes such as in cancer cells. Endogenous antigens are degraded into peptide fragments which bind to class I MHC molecules. After that, the peptide - MHC class I molecule complex is presented on the cell surface. CD8+ T cells recognize antigens associated with class I MHC molecules, the toxic T

cells attack and kill cells which present antigen - MHC class I molecule complex. In this study we found that components of MHC class I including H2-K1, H2-L, and beta-2 microglobulin (B2M) [115, 116]; antigen processing transporter 2 (TAP2) which is responsible for transporting small peptides from the cytosol to the endoplasmic reticulum lumen where they can associate with MHC class I molecules [117]; and tapasin (also known as TAP binding protein TAPBP) of which chaperone function is necessary for efficient loading of antigen peptide in MHC I molecules were induced due to IFN-γ stimulation.

Exogenous antigens are antigens that have entered the cells from outside through endocytosis or phagocytosis. Antigen presenting cells (macrophages, dendritic cells, and B cells) process the exogenous antigens to peptide fragments, which are then combined with class II MHC molecules to form peptide- MHC class II molecules complex. Class II MHC molecules are only expressed in antigen presenting cells. CD4+ T cells (T helper cells) recognize peptides which are presented in class II MHC molecules. After T helper cells interact with peptide - MHC class II molecule complex they become activated and secret many cytokines. The secreted cytokines are involved in activating B cells, T toxic cels, macrophages. In this study we found that many components of MHC class II were induced by IFN-γ treatment such as H2-Aa, H2-Eb1, H2-Dmb1. Besides that the induction of cathepsin H was identified with LC-MS/MS, while induction in some protein isoforms of cathepsin B and S was observed with the 2D-DIGE technique. The induction of the lysosomal proteases may implicate subsequent increases in protein degradation to produce antigenic peptides for class II MHC loading [86, 118].

We observed that intercellular adhesion molecule 1 (ICAM1) was induced by IFN-γ treatment. ICAM1 is a ligand for the beta2 integrin molecule present on leukocytes. ICAM-1 is expressed at low levels on endothelial cells, lymphocytes and monocytes, its expression was known to significantly increase after IFN-γ stimulation. ICAM-1 participates in trafficking of inflammatory cells, and in cell:cell interactions during antigen presentation. The interaction of T lymphocytes bearing specific T cell receptors (TCR) with antigen-presenting cells (e.g., macrophage) displaying MHC-presented antigen requires receptor:ligand pairs such as LFA-1:ICAM-1, CD2:CD48, and CD28:CD80. Thereofore, ICAM1 has an important function as interaction molecule in the activation of T cell signal transduction pathways [119].

### 4.2.4. Metabolism

We found that proteins which are involved in different metabolic processes such as hexokinases (glucose metabolism), long-chain acyl CoA synthetase 1 (fatty acids metabolism), and purine nucleoside phosphorylase (nucleosides and nucleotides metabolism) were induced after IFN-γ stimulation.

Glucose is an important source for generation of energy and precursors for biosynthesis of other cellular constituents. Activated macrophages greatly increase oxygen uptake, and begin to produce large amounts of superoxide ($O_2^-$) and hydrogen peroxide ($H_20_2$); at the same time the activated macrophages metabolize large quantities of glucose by usage of the hexose monophosphate shunt. This series of changes has come to be known as the "respiratory burst." The main purpose of glucose metabolism in “respiratory burst” is not to produce energy, but to generate powerful microbicidal agents by the partial reduction of oxygen. Glucose is metabolized through the hexose monophosphate shunt in order to regenerate the NADPH that has been consumed by the $O_2^-$-forming enzyme and by a glutathione-dependent $H_20_2$-detoxifying system that is found in the cytoplasm of the phagocyte [120]. Hexokinases play an important role in glucose metabolism through initiating the first step in metabolism of glucose by phosphorylation to form glucose-6-phosphate [121]**.** In this study, hexokinase 1, hexokinase 2, hexokinase 3 were found induced due to IFN-γ stimulation.

Lipids play an important role in phagocytosis. They were involved in phagosome formation, the generation and transduction of signals, remodeling the cytoskeleton, and guiding the fusion and fission events that define phagosome maturation. Defects in lipid metabolism can cause infectious, inflammatory, and autoimmune disorders [122, 123]. For almost all further metabolic reactions, fatty acids have to be activated by esterification with CoA before they can be utilized. Long-chain acyl CoA synthetases (ACSLs) play a critical role in fatty acid homeostasis. These enzymes controls both uptake and activation of fatty acids for intracellular metabolism [124]. Inhibition of these enzymes caused lipotoxicity in macrophages [125].

The role of purine nucleoside phosphorylase (PNP) - the enzyme which reversibly catalyzes the phosphorolysis of purine nucleosides - in macrophage activation is still unknown. PNP has been noted because the deficiency in this gene caused to a severe T-cell immunodeficiency in children [126], however the underlying mechanism is still unclear. More recently, it was proposed that accumulation of dGTP in the mitochondria of T lymphocytes of PNP-deficient

mice initiates apoptosis of the cells by interfering with the repair of mitochondrial DNA [127]. We have found that amount of PNP protein was increased upon IFN-γ stimulation in BMM-BALB/c, therefore the protein may play an significant role in macrophage activation. For this reason, the PNP protein may be a good candidate for further functional analysis.

### 4.2.5. Cell survival

Upon infection with microbial pathogens, the macrophages may be exposed to toxic bacterial products which can cause cell death [128]. Besides that, the reactive oxygen and nitrogen species which are synthesized by macrophages to combat microbial pathogens also can be toxic for the cell [88, 129]. Therefore, the ability of macrophages to resistance to apoptosis is important for effective host innate immune responses. We have found proteins which are involved in controlling cell viability such as peroxiredoxin 4 (PRDX4), nicotinamide phosphoribosyltransferase (NAMPT), serine protease inhibitor A3G (SERPINA3G), allograft inflammatory factor-1 (AIF-1), and protein-glutamine gamma-glutamyltransferase 2 (TGM2) induced after IFN-γ treatment.

Activated macrophages induce expression of genes which are responsible the synthesis of reactive oxygen and nitrogen species (NO, O2-, H2O2 and peroxynitrite). The molecules play important roles in killing intracellular pathogens, however when accumulation at high concentrations, can cause cell death [88, 129]. Peroxiredoxins are a family of thiol peroxidases. They are expressed at high levels in cells and play an important role in cell peroxide and peroxynitrite detoxification [89].

Nicotinamide phosphoribosyl transferase (NAMPT)/pre-B cell colony-enhancing factor (PBEF)/visfatin is a proteins which display several function such as regulate B cell development, apoptosis, glucose metabolism, and NAD biosynthesis. NAMPT is involved in cellular resistance to genotoxic/oxidative stress, and through that function it induces the ability of cell survival during stressful situations such as inflammation [130, 131].

Serine protease inhibitor A3G (SERPINA3G) which is also known as serine protease inhibitor 2A (SPI2A) protects cells from lysosome-mediated apoptosis. The release of cysteine cathepsins from the lysosome into the cytoplasm can trigger programs of cell death. Spi2A protects cells from caspase-independent programs of cell death by inhibiting lysosomal executioner proteases after they are released into the cytoplasm [87]. Surprisingly, although the

mRNA of this gene was strongly induced after IFN-γ treatment in both BMM-BALB/c and BMM-C57BL/6, results of proteomic 2D-DIGE and LC-MS/MS analysis showed that increases on protein level were only observed in BMM-BALB/c and not in BMM-C57BL/6.

Allograft inflammatory factor 1 (AIF-1) is known as specifically expressed in cells of the monocyte/macrophage lineage, and augmented by IFN-γ [132]. AIF-1 expression is involved in determining the survival, migration and proinflammatory properties of macrophages. It was reported that blocking the expression of AIF-1 induced apoptosis of macrophages [133]. AIF-1 is also known as an important molecule in membrane ruffling and the phagocytosis of macrophages [134].

Protein-glutamine gamma-glutamyltransferase 2 (TGM2) is a specific protein which can both facilitate and inhibit apoptosis, while the GTP-bound form of the enzyme generally protects cells against death. It is also involved in prevention of inflammation, tissue injury and autoimmunity once the apoptosis has already been initiated [135].

### 4.2.6. Secretion of cathepsin L and metalloelastase

Secretion of proteases is critical for degradation of the extracellular matrix during an inflammatory response. Degradation of the extracellular matrix could be important for the activated antigen presenting cells to migrate to lymph nodes to meet the appropriate T lymphocyte, as well as for the recruitment of effectors of inflammation, e.g., neutrophils and eosinophils. Cathepsin L (CATL) is one of the major elastinolytic cysteine proteases in mouse macrophages. Extracellular accumulation of mature CATL is up-regulated by inflammatory stimuli as observed in IFN-γ treated macrophages and lipopolysaccharide activated dendritic cells. Indeed, secreted active CATL has been shown to play a role in degrading the extracellular matrix and to enhance migration of activated human macrophages [136]. Macrophage matrix metalloproteinase 12 (MMP12) (also known as elastase) is an enzyme predominantly expressed in mature tissue macrophages. MMPs have been extensively studied for their role in tissue remodeling during development, growth and tissue repair [137]. We have observed that the intracellular amount of cathepsin L and macrophage metalloelastase were reduced by both IFN-γ treatment and *S. aureus* engulfment factors. The observation might suggest that BMMs induced secretion of CATL and MMP12 in responding to IFN-γ stimulation and *S. aureus* engulfment.

### 4.2.7. Well known, immunologically important proteins not influenced by IFN-γ treatment

Interestingly, looking for well known immunological related proteins, we found that many of them were not induced by IFN-γ stimulation, but already exist in high amount in macrophages.

Total amounts of cathepsin B, D, and S were not significantly different between control and activated BMMs as observed by LC-MS/MS measurement, despite induction in some protein isoforms of cathepsin B and S identified by 2D-DIGE. This observation proofs the complementarity of different proteomic approaches and indicates that modifications of cathepsins might be more important than changes in their level.

Peroxiredoxins protect cells from reactive oxygen and nitrogen species. Peroxiredoxin 1 (PRDX1) which is the most abundant and ubiquitously distributed member of the mammalian peroxiredons [138] was found unaffected by IFN-γ stimulation. Ras-related protein Rab-7a (RAB7) and lysosome-associated membrane glycoprotein 1(LAMP1) which play important roles in phagosome maturation [139]. Lysozyme C2 (LYZ2) has a primary function in lysis of bacteria and is known to be expressed in macrophages [140]. The constant existence in high level of these proteins revealed specific characteristic which enable macrophages quickly and efficiently eliminate invading microorganism.

## 4.3. Changes in the proteome of IFN-γ stimulated BMM-C57BL/6 due to *S. aureus* infection

Proteomic analysis of *S. aureus* effects in IFN-γ stimulated BMM-C57BL/6 showed that approximately 1% and 5% of the identified proteins were changed in amount at time point 6 h and 24 h after *S. aureus* infection, respectively. Increases of protein level were prominent effects of *S. aureus* engulfment in IFN-γ stimulated BMM-C57BL/6. Interestingly, we discovered IFN-γ stimulation and *S. aureus* engulfment targeted different sets of proteins in BMM-C57BL/6 (Figure 20).

### 4.3.1. Anti-microbial proteins

*S. aureus* engulfment caused increased levels of proteins which are involved in anti-microbial responses such as nitric oxide synthase 2 (NOS2), 2'-5' oligoadenylate synthetase 1A (OAS1A), and guanylate binding protein 5 (GBP5).

Nitric oxide (NO) plays an important role in microbicidal activity of macrophages against viruses, bacteria, fungi, protozoa, helminths. NO is produced in the NADPH-dependent conversion of L-arginine to L-citrulline by the nitric oxide synthase (NOS) enzymes (NOS1–3). The NOS2 isoform alone is inducible by cytokine and/or microbial stimulus [34]. Synergistic effects of IFN-γ and LPS in stimulation of NOS2 were known before [83]. Interestingly, in this study despite induction of mRNA levels of NOS2 was observed due to IFN-γ stimulation, the protein level of NOS2 remained at low level and only strongly increased after *S. aureus* engulfment. This observation might reflect the control of NO production of macrophages, because NO is not only a bactericidal factor but also causes cell death. In combination with hypoxia NO may induce necrosis if glycolysis is limiting and, combined with superoxide or $H_2O_2$, it may induce necrosis via peroxynitrite. In the absence of antioxidants, sustained exposure to NO results in production of reactive oxygen species (ROS) and reactive nitrogen species (RNS) that induce apoptosis or necrosis [88, 129].

Initially identified as IFN-induced proteins that generate low-molecular weight inhibitors of cell-free protein synthesis, 2'-5' oligoadenylate synthetase 1A (OAS1A) is a key intermediate in the cellular defense against infection, leading to degradation of viral and cellular RNAs by activating the interferon induced ribonuclease [141, 142]. We found synergistic effects of IFN-γ stimulation and *S. aureus* engulfment in inducing expression of OAS1A.

Two families of GTPases p47 immunity-related GTPases (p47 IRGs) and p65 guanylate-binding proteins (p65 GBPs) were known to provide cell-autonomous resistance against a variety of bacterial, eukaryotic and viral pathogens [101]. We found many members of both groups were strongly induced by IFN-γ stimulation such as LRG-47/Irgm1, IIGP1/Irga6, IRG-47/ ifi47, IGTP/Irgm3, Gbp1, Gbp2, Gbp5. The subsequent *S. aureus* engulfment event only induced expression of Gbp5 and not the others. This observation reflected that the two families of GTPases are early responding genes which almost fully activated by IFN-γ stimulation alone.

### 4.3.2. Inflammatory regulation proteins

Tissue damage caused by a wound or by an invading pathogenic microorganism induces a complex sequence of events collectively known as the inflammatory response. Major events of an inflammatory response are microvascular caliber, enhanced vascular permeability, leukocyte recruitment, and release of inflammatory mediators. The end result of inflammation may be the

mobilizing of a specific immune response to the invasion or clearance of the invader by components of the innate immune system. Macrophages play a critical role in the initiation, maintenance, and resolution of inflammation [143]. We have observed the induction of proteins which initiate inflammation such as prostaglandin G/H synthase 2 (PTGS2) and interleukin-1 beta (IL1B), as well as proteins which inhibit inflammation such as caveolin-1 (CAV1) and sequestosome 1 (SQSTM1).

Activated macrophages are known to release prostaglandin and other arachidonic acid metabolites [1]. Prostaglandins have diverse physiological effects, including increased vascular permeability, increased vascular dilation, and induction of neutrophil chemotaxis [144]. Prostaglandin G/H synthase 2 (PTGS2) which catalyzes the committed step in prostaglandin formation was found induced after *S. aureus* engulfment. Interleukin-1 (IL-1) is an important proinflammatory cytokine which induces a cascade of proinflammatory effector molecules. IL-1 stimulates the expression of genes associated with inflammation such as prostaglandin G/H synthase 2 (PTGS2), type 2 phospholipase A and inducible nitric oxide synthase (iNOS). This cytokine also known stimulate proliferation of T and B cells, and increases the infiltration of immunocompetent cells by inducing expression of adhesion molecules such as intercellular adhesion molecule-1 (ICAM-1) [14, 145].

Inflammation is the physiologic response to damaging influences, but when allowed to continue unopposed, the subsequent cascade of events can lead to serious host injury. Inhibition of inflammation by removal or deactivation of mediators and inflammatory effector cells permits the host to repair damages tissues. Caveolin-1 (CAV1) is involved in controlling of the inflammatory response by suppression of proinflammatory cytokine (TNF-α and IL-6) production and augmentation of anti-inflammatory cytokine (IL-10) [146]. Apoptosis is the normal process by which inflammatory cells are removed from healing sites, and CAV1 was known to increase in macrophages undergoing apoptosis [147]. Sequestosome 1 (SQSTM1) is involved in controlling of excessive inflammatory responses after macrophage activation. SQSTM1 was indicated as a broad negative regulator of cytokine expression in stimulated macrophages. Over-expression of SQSTM1 inhibited expression of multiple cytokines, IL-12p40, TNF-alpha, IL-1beta, IL-6, and IFN-beta, whereas SQSTM1 under-expression markedly elevated their expression [148].

### 4.3.3. Cell-cell interaction

In this study cell surface CD14 receptor was found late induced in IFN-γ stimulated BMM-C57BL/6 only at time point 24 h after *S. aureus* engulfment. The CD14 receptor is expressed on monocytes/macrophages and to a lesser extent on granulocytes. It is a pattern recognition molecule that can interact with LPS from gram negative bacteria and components of gram positive bacteria and fungi. The molecule plays an important role in innate immunity through involving in monocyte activation, leucocyte–endothelial cell interactions, and regulation of apoptosis of monocytes [149].

### 4.3.4. Metabolism

#### 4.3.4.1. *Protein and glucose uptake*

*S. aureus* engulfment induced expression of proteins which are involved in amino acid and glucose uptake in IFN-γ stimulated BMM-C57BL/6 such as low affinity cationic amino acid transporter 2 (SLC7A2/CAT2), CD98 heavy chain (SLC3A2/CD98), and solute carrier family 2 member 1 (SLC2A1/GLUT1). We also observed the RAB11 family interacting protein 1 (RAB11FIP1) which is involved in targeting of cycling endosomes induced after *S. aureus* engulfment.

Abundant NO synthesis by macrophages requires extracellular arginine uptake via the CAT2 transporter. Three closely related cationic amino acid transporter genes (CAT1–3) encode the transporters that mediate most arginine uptake in mammalian cells. Cat2 deficiency caused significantly reduce in NO production and L-Arg uptake in activated macrophages [150, 151]. The CD98 heavy chain, encoded by the Slc3a2 gene, was described 25 years ago as a lymphocyte activation antigen [152]. The 80kD CD98 heavy chain is covalently linked with one of several 40 kD light chains, which function as amino acid transporters [153]. Leucine and isoleucine transport is mediated by the CD98 heterodimer, and these amino acids are important regulators of the mTOR pathway that governs nutrient-regulated lymphocyte function [154].

Solute carrier family 2, member 1 (SLC2A1) is also known as glucose transporter 1 (GLUT1). Macrophage glucose uptake and the level of glucose transporter 1 (GLUT1) induced in LPS or TNF-alpha activated macrophages [155]. Glucose transporter 1 (GLUT1) is responsible for rapidly and sustained increasing of glucose uptake into macrophages. GLUT1 has been

reported induced in LPS or TNF-alpha activated macrophages parallel with induction of glucose uptake [155, 156].

After endocytic internalization, most membrane proteins and lipids return to the plasma membrane after passing through one or several endosomal compartments, such as the sorting endosome and the endocytic recycling endosome [157]. Proteins that specifically regulate transport from the endocytic recycling compartment include the small GTPase Rab11 [158] and EH domain-containing protein 1 (EHD1) [159]. RAB11 family interacting protein 1 (RAB11FIP1), as a predominantly membrane-associated protein, was known to be involved in the targeting of Rab11- mediated complex to the correct compartment [160]. Interestingly, we have found EHD1 and RAB11FIP1 proteins at increased levels after *S. aureus* engulfment.

#### *4.3.4.2. Lipid metabolism*

As mentioned above, long-chain acyl CoA synthetases (ACSLs) play a critical role in fatty acid homeostasis [124]. This study showed the synergistic effect of IFN-γ and *S. aureus* engulfment in increasing the level ACSL1. Lipoprotein lipase (LPL) is a 60-kD glycoprotein that plays a central role in plasma triglyceride metabolism by hydrolysis of triglyceride-rich chylomicrons and very low density lipoproteins [161]. This time, LPL was found reduced in IFN-γ activated BMM-C57BL/6 after *S. aureus* engulfment. It was known that macrophages in culture synthesize and secrete LPL [162], and activation dramatically alters macrophage LPL secretion [163]. Therefore, the observation may reflect that *S. aureus* infected macrophages increased LPL secretion.

#### *4.3.4.3. Cellular iron homeostasis*

Iron is essential for fundamental cell functions but nonprotein bound “free” iron is toxic for cells by forming highly reactive radicals that damage membranes and DNA. Iron present in heme, iron-sulfur clusters, or directly associated with proteins plays a central role in a large number of essential cellular functions, such as oxygen transport, mitochondrial energy metabolism, electron transport, deoxynucleotide synthesis, or detoxification. Cellular iron levels are therefore carefully regulated in order to ensure iron supply but to prevent accumulation of excess iron [164].

The iron storage protein, ferritin, plays a key role in iron metabolism. Its ability to sequester the element gives ferritin the dual functions of iron detoxification and iron reserve. It is

composed of a protein shell that can accommodate up to 4,500 atoms of iron in its cavity. The protein shell has a molecular mass between 430 and 460 kDa and is made up of 24 symmetrically arranged subunits of two types, a light subunit (L) and a heavy subunit (H) with sizes of 19 and 21 kDa, respectively. Both recombinant H- and L-homopolymers can incorporate iron, but H-ferritin is several times more efficient than L-ferritin [165]. Induction of ferritin synthesis was reported in IFN-γ/LPS- stimulated RAW 264.7 macrophages [166]. We have observed that the level of ferritin heavy chain (FTH1) was increased after *S. aureus* engulfment.

Aconitase (ACO2) has recently been recognized not only as an enzyme of Krebs cycle but also an iron responsive elements-binding protein (IRE-BP) which plays important roles in cellular iron homeostasis. Biosynthetic rates of ferritin, an iron sequestration protein, and the transferrin receptor, a protein involved in iron acquisition, are regulated by levels of intracellular iron. Iron responsive elements (IREs) are RNA stem loop structures found within the 5' UTR of the mRNA of ferritin and within the 3' UTR of the transferrin receptor mRNA. IREs function as binding sites for an iron-sensing protein, the IRE binding protein (IRE-BP). The IRE-BP binds to IREs when the cell is iron-depleted and simultaneously inhibits translation of ferritin mRNA and degradation of transferrin receptor mRNA. A Fe-S cluster in the structure of cytosolic aconitase may be responsible for switching between aconitase and IRE-BP functions [167, 168]. We found that ACO2 was reduced after *S. aureus* engulfment through which could be accelerating synthesis of ferritin.

Heme is a complex of iron with protoporphyrin IX that is essential for the function of all aerobic cells. Heme serves as the prosthetic group of numerous hemoproteins which include nitric oxide synthase. Heme depletion leads to loss of NOS2 enzyme activity in activated macrophages [151]. Cellular heme levels are tightly controlled through balancing between heme biosynthesis and catabolism. 5-aminolevulinic acid synthase (ALA-S, the first enzyme in heme biosynthesis) is responsible for the differences in regulation and rates of heme synthesis in erythroid and nonerythroid cells [169]. Haem oxygenase-1 (HMOX1) catabolizes heme to generate bilirubin, carbon monoxide, and free iron. HMOX1 also known to augmenst iron efflux to prevent cellular iron toxification by accumulation of free iron [170]. Moreover, HMOX1 has been shown to have anti-inflammatory, antiapoptotic, and antiproliferative effects [171]. Interestingly, we have found that both proteins HMOX1 and ALAS1 were increased in level at 24 h after *S. aureus* engulfment.

### 4.3.5. Immune-responsive gene 1 protein

The function of immune-responsive gene 1 protein (IRG1) is not well understood. However, it was found induced in activated macrophages by bacterial LPS [172] and identified as a critical regulator of the early events in implantation [173]. In this study, IRG1 was found strongly induced by IFN-γ and further continuously induced by consequent *S. aureus* engulfment. The observation suggests that IRG1 may play a significant role in immune responses of macrophages.

## 4.4. Differences in proteome of BMMs derived from strain BALB/c and C57BL/6

To my knowledge, this was the first study which combined proteomics and transcriptomics approaches for the study of BMM-BALB/c and BMM-C57BL/6. Results of proteomic and transcriptomic analyses were consistent in identifying responses of BMMs to IFN-γ stimulation. There were only few genes/proteins which were found differently responding to IFN-γ stimulation between BMM-BALB/c and BMM-C57BL/6. Therefore, the differences in nature of macrophages which derived from different strains may account for physiological differences such as capacity for killing intracellular *B. speudomallei* [76]. Surprisingly, results of proteomic and transcriptomic analysis were not consistent in comparing BMM-BALB/c with BMM-C57BL/6. Both 2D-DIGE and LC-MS/MS based proteomic approaches showed many differences at the protein level, while few differences at mRNA level were identified by transcriptomic analysis.

In the analysis of IFN-γ effects on BMMs, results of proteomic and transcriptomic analysis were highly consistent to one another. Moreover, many of the identified IFN-γ regulated genes/proteins agreed with previous publications of IFN-γ effects on macrophages such as p47 and p65 GTPases, hexokinases, class I and II MHC molecules etc. Therefore, it was reasonable to assume that both proteomic and transcriptomic were properly performed and merely reveal real biological changes than technical errors. Beside of that, the recent studies to find correlations between mRNA and protein expression levels have sometimes shown that both only minimal and partially correlate. At least three reasons could be responsible for the poor correlations between mRNA level and protein level: translational regulation, differences in protein *in vivo* half-lives,

and the significant amount of experimental error, including differences with respect to the experimental conditions [41, 174, 175].

Because minor differences were found with transcriptomic analysis, post transcription mRNA processing and translational regulations seem to be responsible for identified differences in proteomic analysis. Beside of that, some presumable differences in post translational modifications between macrophages derived from the two strains were revealed by 2D-DIGE analysis. 2D-DIGE analysis clearly depicted differently modified forms of two proteins beta-glucuronidase (BGLR) and endoplasmic reticulum protein (ERp29) in BMM-BALB/c and BMM-C57BL/6 (Figure 18). Interestingly, cellular localization analysis of proteins present at different levels in both strains showed that almost all proteins abundant in BMM-BALB/c are located in cytoskeleton, cytoplasm and nucleus while proteins abundant in BMM-C57BL/6 locate to mitochondria and lysosome. Notably, the results showed differences in proteins of mitochondria and lysosome, the two cellular organelles which play important roles in determining the outcome of host-pathogen interaction. Lysosomes act as the primary component of the intracellular digestive system in virtually all eukaryotic cells. The lysosome contains more than 50 acid hydrolases. They are responsible for breaking down the sugar, lipid, glycolipids, glycosaminoglycans, nucleic acids and proteins. These enzymes work together to contribute to the total catabolic function of the lysosome. Phagosome-lysosome membrane fusion is a highly regulated event that is essential for intracellular killing of microorganisms. Subsequently, dozens of different types of hydrolases (proteases, DNases, lipases, etc.), which are capable of digesting most biological macromolecules, are released from lysosomes into the phagosome, contributing to the demise and digestion of the particle [176, 177]. The mitochondrion is at the core of cellular energy metabolism, being the site of most ATP generation. On the other hand, mitochondria play a central role in regulation of metabolism, cell-cycle control, development, antiviral responses and cell death [178]. Further molecular and cellular analyses are required for understand how the identified differences in the proteomes may contribute to anti-bactericidal capacity of BMM-BALB/c and BMM-C57BL/6.

# Conclusion

Macrophage activation has been an interesting phenomenon for biologists since it was discovered more than 100 years ago [179]. However, the molecular mechanism of macrophage activation process still remains a subject for investigation. In this study, applying new quantitative proteomics techniques 2D-DIGE and LC-MS/MS allowed us to access the changes in the proteome of macrophages during their activation process. We analyzed the proteome of bone marrow derived macrophages (BMMs) from the infection susceptible mouse strain BALB/c and the resistant strain C57BL/6 in response to IFN-γ stimulation and subsequent *S. aureus* infection. IFN-γ stimulation caused significant alterations in the proteome of BMMs, of which increases in protein levels was the prominent effect. Interestingly, BMMs from the susceptible mouse strain BALB/c and the resistant strain C57BL/6 were found to consistently respond to IFN-γ stimulation. Functional analysis revealed that IFN-γ regulated proteins are involved in many important functional processes of macrophages. Of those, induction in transcriptional regulation, microbicidal capacity, and antigen presentation were clearly depicted. Quantitative proteomic LC-MS/MS analysis also revealed that macrophages are inherently rich in proteins which have important functions in phagocytosis and digestion. The subsequent *S. aureus* engulfment induced not only the microbicidal capacity but also immune modulation activities of IFN-γ stimulated BMM-C57BL/6. Taken together, the "priming signal" IFN-γ seemed merely prepare BMMs for killing invading microbes, while bacteria engulfment triggered immune modulation activities of BMMs. Beside of that, strong induction of immune responsive protein 1 (IRG1) during macrophage activation suggested that the protein may have a significant roles in macrophage-pathogen interaction.

Proteomic and transcriptomic analyses showed that there were more differences between BMMs from the susceptible mouse strain BALB/c and resistant mouse strain C57BL/6 at protein level compared with the mRNA level. This observation suggested that post transcriptional mRNA processing, translational control, and post translational modification seem to be important. The exact mechanism is unknown; it requires further molecular, functional, and cellular research for better understanding.

Making use of new proteomic approaches, this research not simply rediscovers but also integrates previous knowledge about macrophage activation in a comprehensive biological context, as well as indicates new potential protein candidates for further investigation. It would be a useful reference for further BMMs macrophage-pathogen interaction studies.

# References


1. Adams, D.O. and T.A. Hamilton, *The cell biology of macrophage activation.* Annu Rev Immunol, 1984. **2**: p. 283-318.
2. Eske, K., et al., *Generation of murine bone marrow derived macrophages in a standardised serum-free cell culture system.* J Immunol Methods, 2009. **342**(1-2): p. 13-9.
3. Gordon, S., S. Keshav, and L.P. Chung, *Mononuclear phagocytes: tissue distribution and functional heterogeneity.* Curr Opin Immunol, 1988. **1**(1): p. 26-35.
4. Gordon, S. and P.R. Taylor, *Monocyte and macrophage heterogeneity.* Nat Rev Immunol, 2005. **5**(12): p. 953-64.
5. Bernard Burke, C.E.L., *The macrophage*. 2002: Oxford University Press, 2002.
6. Ryter, A., *Relationship between ultrastructure and specific functions of macrophages.* Comp Immunol Microbiol Infect Dis, 1985. **8**(2): p. 119-33.
7. Morahan, P.S., J.R. Connor, and K.R. Leary, *Viruses and the versatile macrophage.* Br Med Bull, 1985. **41**(1): p. 15-21.
8. Hampton, M.B., A.J. Kettle, and C.C. Winterbourn, *Inside the neutrophil phagosome: oxidants, myeloperoxidase, and bacterial killing.* Blood, 1998. **92**(9): p. 3007-17.
9. Langermans, J.A., W.L. Hazenbos, and R. van Furth, *Antimicrobial functions of mononuclear phagocytes.* J Immunol Methods, 1994. **174**(1-2): p. 185-94.
10. Bell, D., J.W. Young, and J. Banchereau, *Dendritic cells.* Adv Immunol, 1999. **72**: p. 255-324.
11. Cresswell, P., *Antigen processing and presentation.* Immunol Rev, 2005. **207**: p. 5-7.
12. Nathan, C.F., *Secretory products of macrophages.* J Clin Invest, 1987. **79**(2): p. 319-26.
13. Pestka, S., et al., *Interferons and their actions.* Annu Rev Biochem, 1987. **56**: p. 727-77.
14. Dinarello, C.A., *Interleukin-1 and interleukin-1 antagonism.* Blood, 1991. **77**(8): p. 1627-52.
15. Dinarello, C.A., *An update on human interleukin-1: from molecular biology to clinical relevance.* J Clin Immunol, 1985. **5**(5): p. 287-97.
16. Mielke, V., et al., *Detection of neutrophil-activating peptide NAP/IL-8 and NAP/IL-8 mRNA in human recombinant IL-1 alpha- and human recombinant tumor necrosis factor-alpha-stimulated human dermal fibroblasts. An immunocytochemical and fluorescent in situ hybridization study.* J Immunol, 1990. **144**(1): p. 153-61.
17. Larsen, C.G., et al., *The neutrophil-activating protein (NAP-1) is also chemotactic for T lymphocytes.* Science, 1989. **243**(4897): p. 1464-6.
18. *Cytokines and lipocortins in inflammation and differentiation. Proceedings of the International Conference on Molecular and Cellular Biology of IL-1, TNF, and Lipocortins in Inflammation and Differentiation. Siena, Italy, October 22-25, 1989. Proceedings.* Prog Clin Biol Res, 1990. **349**: p. 1-444.
19. Wood, G.W. and K.A. Gollahon, *Detection and quantitation of macrophage infiltration into primary human tumors with the use of cell-surface markers.* J Natl Cancer Inst, 1977. **59**(4): p. 1081-7.
20. Grabstein, K.H., et al., *Induction of macrophage tumoricidal activity by granulocyte-macrophage colony-stimulating factor.* Science, 1986. **232**(4749): p. 506-8.

21. Kay, M.M., *Mechanism of removal of senescent cells by human macrophages in situ.* Proc Natl Acad Sci U S A, 1975. **72**(9): p. 3521-5.

22. Werb, Z. and S. Gordon, *Secretion of a specific collagenase by stimulated macrophages.* J Exp Med, 1975. **142**(2): p. 346-60.

23. Werb, Z. and S. Gordon, *Elastase secretion by stimulated macrophages. Characterization and regulation.* J Exp Med, 1975. **142**(2): p. 361-77.

24. Knighton, D.R. and V.D. Fiegel, *The macrophages: effector cell wound repair.* Prog Clin Biol Res, 1989. **299**: p. 217-26.

25. Isaacs, A. and J. Lindenmann, *Virus interference. I. The interferon.* Proc R Soc Lond B Biol Sci, 1957. **147**(927): p. 258-67.

26. Shtrichman, R. and C.E. Samuel, *The role of gamma interferon in antimicrobial immunity.* Curr Opin Microbiol, 2001. **4**(3): p. 251-9.

27. Boehm, U., et al., *Cellular responses to interferon-gamma.* Annu Rev Immunol, 1997. **15**: p. 749-95.

28. Novelli, F. and J.L. Casanova, *The role of IL-12, IL-23 and IFN-gamma in immunity to viruses.* Cytokine Growth Factor Rev, 2004. **15**(5): p. 367-77.

29. Schroder, K., et al., *Interferon-gamma: an overview of signals, mechanisms and functions.* J Leukoc Biol, 2004. **75**(2): p. 163-89.

30. Subramaniam, P.S., B.A. Torres, and H.M. Johnson, *So many ligands, so few transcription factors: a new paradigm for signaling through the STAT transcription factors.* Cytokine, 2001. **15**(4): p. 175-87.

31. Mosser, D.M. and J.P. Edwards, *Exploring the full spectrum of macrophage activation.* Nat Rev Immunol, 2008. **8**(12): p. 958-69.

32. Decker, T., et al., *IFNs and STATs in innate immunity to microorganisms.* J Clin Invest, 2002. **109**(10): p. 1271-7.

33. Mizrahi, A., et al., *Assembly of the phagocyte NADPH oxidase complex: chimeric constructs derived from the cytosolic components as tools for exploring structure-function relationships.* J Leukoc Biol, 2006. **79**(5): p. 881-95.

34. MacMicking, J., Q.W. Xie, and C. Nathan, *Nitric oxide and macrophage function.* Annu Rev Immunol, 1997. **15**: p. 323-50.

35. Gupta, J.W., et al., *Induction of expression of genes encoding components of the respiratory burst oxidase during differentiation of human myeloid cell lines induced by tumor necrosis factor and gamma-interferon.* Cancer Res, 1992. **52**(9): p. 2530-7.

36. Groettrup, M., et al., *Interferon-gamma inducible exchanges of 20S proteasome active site subunits: why?* Biochimie, 2001. **83**(3-4): p. 367-72.

37. Mach, B., et al., *Regulation of MHC class II genes: lessons from a disease.* Annu Rev Immunol, 1996. **14**: p. 301-31.

38. Lah, T.T., et al., *Gamma-interferon causes a selective induction of the lysosomal proteases, cathepsins B and L, in macrophages.* FEBS Lett, 1995. **363**(1-2): p. 85-9.

39. Lafuse, W.P., et al., *IFN-gamma increases cathepsin H mRNA levels in mouse macrophages.* J Leukoc Biol, 1995. **57**(4): p. 663-9.

40. Wilkins, M.R., et al., *Progress with proteome projects: why all proteins expressed by a genome should be identified and how to do it.* Biotechnol Genet Eng Rev, 1996. **13**: p. 19-50.

41. Gygi, S.P., et al., *Correlation between protein and mRNA abundance in yeast.* Mol Cell Biol, 1999. **19**(3): p. 1720-30.

42. Hegde, P.S., I.R. White, and C. Debouck, *Interplay of transcriptomics and proteomics.* Curr Opin Biotechnol, 2003. **14**(6): p. 647-51.

43. O'Farrell, P.H., *High resolution two-dimensional electrophoresis of proteins.* J Biol Chem, 1975. **250**(10): p. 4007-21.

44. Ali-Khan, N., X. Zuo, and D.W. Speicher, *Overview of proteome analysis.* Curr Protoc Protein Sci, 2003. **Chapter 22**: p. Unit 22 1.

45. Larbi, N.B. and C. Jefferies, *2D-DIGE: comparative proteomics of cellular signalling pathways.* Methods Mol Biol, 2009. **517**: p. 105-32.

46. Unwin, R.D., C.A. Evans, and A.D. Whetton, *Relative quantification in proteomics: new approaches for biochemistry.* Trends Biochem Sci, 2006. **31**(8): p. 473-84.

47. Kolkman, A., M. Slijper, and A.J. Heck, *Development and application of proteomics technologies in Saccharomyces cerevisiae.* Trends Biotechnol, 2005. **23**(12): p. 598-604.

48. America, A.H. and J.H. Cordewener, *Comparative LC-MS: a landscape of peaks and valleys.* Proteomics, 2008. **8**(4): p. 731-49.

49. Patel, V.J., et al., *A comparison of labeling and label-free mass spectrometry-based proteomics approaches.* J Proteome Res, 2009. **8**(7): p. 3752-9.

50. Zhu, W., J.W. Smith, and C.M. Huang, *Mass spectrometry-based label-free quantitative proteomics.* J Biomed Biotechnol, 2010. **2010**: p. 840518.

51. Bantscheff, M., et al., *Quantitative mass spectrometry in proteomics: a critical review.* Anal Bioanal Chem, 2007. **389**(4): p. 1017-31.

52. Old, W.M., et al., *Comparison of label-free methods for quantifying human proteins by shotgun proteomics.* Mol Cell Proteomics, 2005. **4**(10): p. 1487-502.

53. Dupont, A., et al., *Two-dimensional maps and databases of the human macrophage proteome and secretome.* Proteomics, 2004. **4**(6): p. 1761-78.

54. Jutras, I., et al., *Modulation of the phagosome proteome by interferon-gamma.* Mol Cell Proteomics, 2008. **7**(4): p. 697-715.

55. Patel, P.C., et al., *Proteomic Analysis of Microtubule-associated Proteins during Macrophage Activation.* Mol Cell Proteomics, 2009. **8**(11): p. 2500-14.

56. Kluytmans, J., A. van Belkum, and H. Verbrugh, *Nasal carriage of Staphylococcus aureus: epidemiology, underlying mechanisms, and associated risks.* Clin Microbiol Rev, 1997. **10**(3): p. 505-20.

57. Foster, T.J., *Immune evasion by staphylococci.* Nat Rev Microbiol, 2005. **3**(12): p. 948-58.

58. Gresham, H.D., et al., *Survival of Staphylococcus aureus inside neutrophils contributes to infection.* J Immunol, 2000. **164**(7): p. 3713-22.

59. Peschel, A., et al., *Staphylococcus aureus resistance to human defensins and evasion of neutrophil killing via the novel virulence factor MprF is based on modification of membrane lipids with l-lysine.* J Exp Med, 2001. **193**(9): p. 1067-76.

60. Liu, G.Y., et al., *Staphylococcus aureus golden pigment impairs neutrophil killing and promotes virulence through its antioxidant activity.* J Exp Med, 2005. **202**(2): p. 209-15.

61. Das, D., S.S. Saha, and B. Bishayi, *Intracellular survival of Staphylococcus aureus: correlating production of catalase and superoxide dismutase with levels of inflammatory cytokines.* Inflamm Res, 2008. **57**(7): p. 340-9.

62. Sieprawska-Lupa, M., et al., *Degradation of human antimicrobial peptide LL-37 by Staphylococcus aureus-derived proteinases.* Antimicrob Agents Chemother, 2004. **48**(12): p. 4673-9.

63. Jin, T., et al., *Staphylococcus aureus resists human defensins by production of staphylokinase, a novel bacterial evasion mechanism.* J Immunol, 2004. **172**(2): p. 1169-76.

64. Bera, A., et al., *Why are pathogenic staphylococci so lysozyme resistant? The peptidoglycan O-acetyltransferase OatA is the major determinant for lysozyme resistance of Staphylococcus aureus.* Mol Microbiol, 2005. **55**(3): p. 778-87.

65. Baughn, R. and P.F. Bonventre, *Phagocytosis and intracellular killing of Staphylococcus aureus by normal mouse peritoneal macrophages.* Infect Immun, 1975. **12**(2): p. 346-52.

66. Michailova, L., et al., *Interaction of alveolar macrophages with Staphylococcus aureus and induction of microbial L-forms during infection in rats.* Int J Med Microbiol, 2000. **290**(3): p. 259-67.

67. Kubica, M., et al., *A potential new pathway for Staphylococcus aureus dissemination: the silent survival of S. aureus phagocytosed by human monocyte-derived macrophages.* PLoS One, 2008. **3**(1): p. e1409.

68. Flesch, I., A. Fruh, and E. Ferber, *Functional comparison of bone marrow-derived macrophages obtained by cultivation in serum-free or serum-supplemented medium.* Immunobiology, 1986. **173**(1): p. 72-81.

69. Flesch, I.E. and S.H. Kaufmann, *Effect of fetal calf serum on cytokine release by bone marrow-derived macrophages during infection with intracellular bacteria.* Immunobiology, 1999. **200**(1): p. 120-7.

70. Elenkov, I.J., *Glucocorticoids and the Th1/Th2 balance.* Ann N Y Acad Sci, 2004. **1024**: p. 138-46.

71. Honn, K.V., J.A. Singley, and W. Chavin, *Fetal bovine serum: a multivariate standard.* Proc Soc Exp Biol Med, 1975. **149**(2): p. 344-7.

72. Vogel, S.N., et al., *Use of serum-free, compositionally defined medium for analysis of macrophage differentiation in vitro.* J Leukoc Biol, 1988. **44**(2): p. 136-42.

73. Thomas, P.D., et al., *PANTHER: a library of protein families and subfamilies indexed by function.* Genome Res, 2003. **13**(9): p. 2129-41.

74. Ramos, H., P. Shannon, and R. Aebersold, *The protein information and property explorer: an easy-to-use, rich-client web application for the management and functional analysis of proteomic data.* Bioinformatics, 2008. **24**(18): p. 2110-1.

75. Ehrt, S., et al., *Reprogramming of the macrophage transcriptome in response to interferon-gamma and Mycobacterium tuberculosis: signaling roles of nitric oxide synthase-2 and phagocyte oxidase.* J Exp Med, 2001. **194**(8): p. 1123-40.

76. Breitbach, K., et al., *Role of inducible nitric oxide synthase and NADPH oxidase in early control of Burkholderia pseudomallei infection in mice.* Infect Immun, 2006. **74**(11): p. 6300-9.

77. Cheers, C., et al., *Production of colony-stimulating factors (CSFs) during infection: separate determinations of macrophage-, granulocyte-, granulocyte-macrophage-, and multi-CSFs.* Infect Immun, 1988. **56**(1): p. 247-51.

78. Laskay, T., et al., *Early parasite containment is decisive for resistance to Leishmania major infection.* Eur J Immunol, 1995. **25**(8): p. 2220-7.

79. Roggero, E., et al., *Differential susceptibility to acute Trypanosoma cruzi infection in BALB/c and C57BL/6 mice is not associated with a distinct parasite load but cytokine abnormalities.* Clin Exp Immunol, 2002. **128**(3): p. 421-8.

80. Gifford, G.E. and M.L. Lohmann-Matthes, *Gamma interferon priming of mouse and human macrophages for induction of tumor necrosis factor production by bacterial lipopolysaccharide.* J Natl Cancer Inst, 1987. **78**(1): p. 121-4.

81. Schroder, K., M.J. Sweet, and D.A. Hume, *Signal integration between IFNgamma and TLR signalling pathways in macrophages.* Immunobiology, 2006. **211**(6-8): p. 511-24.

82. Kamijo, R., et al., *Generation of nitric oxide and induction of major histocompatibility complex class II antigen in macrophages from mice lacking the interferon gamma receptor.* Proc Natl Acad Sci U S A, 1993. **90**(14): p. 6626-30.

83. Kamijo, R., et al., *Requirement for transcription factor IRF-1 in NO synthase induction in macrophages.* Science, 1994. **263**(5153): p. 1612-5.

84. Kantengwa, S. and B.S. Polla, *Phagocytosis of Staphylococcus aureus induces a selective stress response in human monocytes-macrophages (M phi): modulation by M phi differentiation and by iron.* Infect Immun, 1993. **61**(4): p. 1281-7.

85. Aderem, A. and D.M. Underhill, *Mechanisms of phagocytosis in macrophages.* Annu Rev Immunol, 1999. **17**: p. 593-623.

86. Brix, K., et al., *Cysteine cathepsins: cellular roadmap to different functions.* Biochimie, 2008. **90**(2): p. 194-207.

87. Liu, N., Y. Wang, and P.G. Ashton-Rickardt, *Serine protease inhibitor 2A inhibits caspase-independent cell death.* FEBS Lett, 2004. **569**(1-3): p. 49-53.

88. Borutaite, V. and G. Brown, *What else has to happen for nitric oxide to induce cell death?* Biochem Soc Trans, 2005. **33**(Pt 6): p. 1394-6.

89. Abbas, K., J. Breton, and J.C. Drapier, *The interplay between nitric oxide and peroxiredoxins.* Immunobiology, 2008. **213**(9-10): p. 815-22.

90. Moseley, P., *Stress proteins and the immune response.* Immunopharmacology, 2000. **48**(3): p. 299-302.

91. Multhoff, G. and L.E. Hightower, *Cell surface expression of heat shock proteins and the immune response.* Cell Stress Chaperones, 1996. **1**(3): p. 167-76.

92. Williams, D.B., *Beyond lectins: the calnexin/calreticulin chaperone system of the endoplasmic reticulum.* J Cell Sci, 2006. **119**(Pt 4): p. 615-23.

93. Weber, J., *ATP synthase--the structure of the stator stalk.* Trends Biochem Sci, 2007. **32**(2): p. 53-6.

94. Yanagawa, M., et al., *Cathepsin E deficiency induces a novel form of lysosomal storage disorder showing the accumulation of lysosomal membrane sialoglycoproteins and the elevation of lysosomal pH in macrophages.* J Biol Chem, 2007. **282**(3): p. 1851-62.

95. Takaoka, A. and H. Yanai, *Interferon signalling network in innate defence.* Cell Microbiol, 2006. **8**(6): p. 907-22.

96. Ramana, C.V., et al., *Complex roles of Stat1 in regulating gene expression.* Oncogene, 2000. **19**(21): p. 2619-27.

97. Meraz, M.A., et al., *Targeted disruption of the Stat1 gene in mice reveals unexpected physiologic specificity in the JAK-STAT signaling pathway.* Cell, 1996. **84**(3): p. 431-42.

98. Boehm, U., et al., *Two families of GTPases dominate the complex cellular response to IFN-gamma.* J Immunol, 1998. **161**(12): p. 6715-23.

99. Degrandi, D., et al., *Extensive characterization of IFN-induced GTPases mGBP1 to mGBP10 involved in host defense.* J Immunol, 2007. **179**(11): p. 7729-40.

100. MacMicking, J.D., G.A. Taylor, and J.D. McKinney, *Immune control of tuberculosis by IFN-gamma-inducible LRG-47.* Science, 2003. **302**(5645): p. 654-9.

101. Shenoy, A.R., et al., *Emerging themes in IFN-gamma-induced macrophage immunity by the p47 and p65 GTPase families.* Immunobiology, 2007. **212**(9-10): p. 771-84.

102. Taylor, G.A., C.G. Feng, and A. Sher, *Control of IFN-gamma-mediated host resistance to intracellular pathogens by immunity-related GTPases (p47 GTPases).* Microbes Infect, 2007. **9**(14-15): p. 1644-51.

103. Butcher, B.A., et al., *p47 GTPases regulate Toxoplasma gondii survival in activated macrophages.* Infect Immun, 2005. **73**(6): p. 3278-86.

104. Martens, S., et al., *Disruption of Toxoplasma gondii parasitophorous vacuoles by the mouse p47-resistance GTPases.* PLoS Pathog, 2005. **1**(3): p. e24.

105. Halonen, S.K., G.A. Taylor, and L.M. Weiss, *Gamma interferon-induced inhibition of Toxoplasma gondii in astrocytes is mediated by IGTP.* Infect Immun, 2001. **69**(9): p. 5573-6.

106. Santiago, H.C., et al., *Mice deficient in LRG-47 display enhanced susceptibility to Trypanosoma cruzi infection associated with defective hemopoiesis and intracellular control of parasite growth.* J Immunol, 2005. **175**(12): p. 8165-72.

107. MacMicking, J.D., *IFN-inducible GTPases and immunity to intracellular pathogens.* Trends Immunol, 2004. **25**(11): p. 601-9.

108. Anderson, S.L., et al., *Interferon-induced guanylate binding protein-1 (GBP-1) mediates an antiviral effect against vesicular stomatitis virus and encephalomyocarditis virus.* Virology, 1999. **256**(1): p. 8-14.

109. Carter, C.C., V.Y. Gorbacheva, and D.J. Vestal, *Inhibition of VSV and EMCV replication by the interferon-induced GTPase, mGBP-2: differential requirement for wild-type GTP binding domain.* Arch Virol, 2005. **150**(6): p. 1213-20.

110. Ling, Y.M., et al., *Vacuolar and plasma membrane stripping and autophagic elimination of Toxoplasma gondii in primed effector macrophages.* J Exp Med, 2006. **203**(9): p. 2063-71.

111. Nguyen, T.T., et al., *Murine GBP-5, a new member of the murine guanylate-binding protein family, is coordinately regulated with other GBPs in vivo and in vitro.* J Interferon Cytokine Res, 2002. **22**(8): p. 899-909.

112. Staeheli, P., et al., *Genetic control of interferon action: mouse strain distribution and inheritance of an induced protein with guanylate-binding property.* Virology, 1984. **137**(1): p. 135-42.

113. Vestal, D.J., et al., *Murine GBP-2: a new IFN-gamma-induced member of the GBP family of GTPases isolated from macrophages.* J Interferon Cytokine Res, 1998. **18**(11): p. 977-85.

114. Leenen, P.J., et al., *Markers of mouse macrophage development detected by monoclonal antibodies.* J Immunol Methods, 1994. **174**(1-2): p. 5-19.

115. Martayan, A., et al., *Class I HLA folding and antigen presentation in beta 2-microglobulin-defective Daudi cells.* J Immunol, 2009. **182**(6): p. 3609-17.

116. Berko, D., et al., *Membrane-anchored beta 2-microglobulin stabilizes a highly receptive state of MHC class I molecules.* J Immunol, 2005. **174**(4): p. 2116-23.

117. Abele, R. and R. Tampe, *The ABCs of immunology: structure and function of TAP, the transporter associated with antigen processing.* Physiology (Bethesda), 2004. **19**: p. 216-24.

118. Hsieh, C.S., et al., *A role for cathepsin L and cathepsin S in peptide generation for MHC class II presentation.* J Immunol, 2002. **168**(6): p. 2618-25.

119. Hubbard, A.K. and R. Rothlein, *Intercellular adhesion molecule-1 (ICAM-1) expression and cell signaling cascades.* Free Radic Biol Med, 2000. **28**(9): p. 1379-86.

120. Babior, B.M., *The respiratory burst of phagocytes.* J Clin Invest, 1984. **73**(3): p. 599-601.

121. Wilson, J.E., *Isozymes of mammalian hexokinase: structure, subcellular localization and metabolic function.* J Exp Biol, 2003. **206**(Pt 12): p. 2049-57.

122. Steinberg, B.E. and S. Grinstein, *Pathogen destruction versus intracellular survival: the role of lipids as phagosomal fate determinants.* J Clin Invest, 2008. **118**(6): p. 2002-11.

123. Yeung, T. and S. Grinstein, *Lipid signaling and the modulation of surface charge during phagocytosis.* Immunol Rev, 2007. **219**: p. 17-36.

124. Digel, M., et al., *Acyl-CoA synthetases: fatty acid uptake and metabolic channeling.* Mol Cell Biochem, 2009. **326**(1-2): p. 23-8.

125. Saraswathi, V. and A.H. Hasty, *Inhibition of long-chain acyl coenzyme A synthetases during fatty acid loading induces lipotoxicity in macrophages.* Arterioscler Thromb Vasc Biol, 2009. **29**(11): p. 1937-43.

126. Giblett, E.R., et al., *Nucleoside-phosphorylase deficiency in a child with severely defective T-cell immunity and normal B-cell immunity.* Lancet, 1975. **1**(7914): p. 1010-3.

127. Arpaia, E., et al., *Mitochondrial basis for immune deficiency. Evidence from purine nucleoside phosphorylase-deficient mice.* J Exp Med, 2000. **191**(12): p. 2197-208.

128. Zychlinsky, A. and P. Sansonetti, *Perspectives series: host/pathogen interactions. Apoptosis in bacterial pathogenesis.* J Clin Invest, 1997. **100**(3): p. 493-5.

129. Estevez, A.G. and J. Jordan, *Nitric oxide and superoxide, a deadly cocktail.* Ann N Y Acad Sci, 2002. **962**: p. 207-11.

130. Rongvaux, A., et al., *Nicotinamide phosphoribosyl transferase/pre-B cell colony-enhancing factor/visfatin is required for lymphocyte development and cellular resistance to genotoxic stress.* J Immunol, 2008. **181**(7): p. 4685-95.

131. Grant, R.S., et al., *Evidence for increased de novo synthesis of NAD in immune-activated RAW264.7 macrophages: a self-protective mechanism?* Arch Biochem Biophys, 1999. **372**(1): p. 1-7.

132. Sibinga, N.E., et al., *Macrophage-restricted and interferon gamma-inducible expression of the allograft inflammatory factor-1 gene requires Pu.1.* J Biol Chem, 2002. **277**(18): p. 16202-10.

133. Yang, Z.F., et al., *Allograft inflammatory factor-1 (AIF-1) is crucial for the survival and pro-inflammatory activity of macrophages.* Int Immunol, 2005. **17**(11): p. 1391-7.

134. Ohsawa, K., et al., *Involvement of Iba1 in membrane ruffling and phagocytosis of macrophages/microglia.* J Cell Sci, 2000. **113 ( Pt 17)**: p. 3073-84.

135. Fesus, L. and Z. Szondy, *Transglutaminase 2 in the balance of cell death and survival.* FEBS Lett, 2005. **579**(15): p. 3297-302.

136. Fiebiger, E., et al., *Invariant chain controls the activity of extracellular cathepsin L.* J Exp Med, 2002. **196**(9): p. 1263-9.

137. He, J.Q. and M.L. Campagne, *Macrophage metalloelastase: stretching therapeutic opportunities.* J Mol Cell Biol, 2009. **1**(2): p. 55-7.

138. Immenschuh, S. and E. Baumgart-Vogt, *Peroxiredoxins, oxidative stress, and cell proliferation.* Antioxid Redox Signal, 2005. **7**(5-6): p. 768-77.

139. Scott, C.C., R.J. Botelho, and S. Grinstein, *Phagosome maturation: a few bugs in the system.* J Membr Biol, 2003. **193**(3): p. 137-52.

140. Markart, P., et al., *Comparison of the microbicidal and muramidase activities of mouse lysozyme M and P.* Biochem J, 2004. **380**(Pt 2): p. 385-92.

141. Sadler, A.J. and B.R. Williams, *Interferon-inducible antiviral effectors.* Nat Rev Immunol, 2008. **8**(7): p. 559-68.

142. Samuel, C.E., *Antiviral actions of interferons.* Clin Microbiol Rev, 2001. **14**(4): p. 778-809, table of contents.

143. Fujiwara, N. and K. Kobayashi, *Macrophages in inflammation.* Curr Drug Targets Inflamm Allergy, 2005. **4**(3): p. 281-6.

144. Richard A. Goldsby, T.J.K., Barbara A. Osborne, *Kuby Immunology*. 2000: W.H. Freeman & Company.

145. Dinarello, C.A., *The IL-1 family and inflammatory diseases.* Clin Exp Rheumatol, 2002. **20**(5 Suppl 27): p. S1-13.

146. Wang, X.M., et al., *Caveolin-1 confers antiinflammatory effects in murine macrophages via the MKK3/p38 MAPK pathway.* Am J Respir Cell Mol Biol, 2006. **34**(4): p. 434-42.

147. Gargalovic, P. and L. Dory, *Cellular apoptosis is associated with increased caveolin-1 expression in macrophages.* J Lipid Res, 2003. **44**(9): p. 1622-32.

148. Kim, J.Y. and K. Ozato, *The sequestosome 1/p62 attenuates cytokine gene expression in activated macrophages by inhibiting IFN regulatory factor 8 and TNF receptor-associated factor 6/NF-kappaB activity.* J Immunol, 2009. **182**(4): p. 2131-40.

149. Arroyo-Espliguero, R., et al., *CD14 and toll-like receptor 4: a link between infection and acute coronary events?* Heart, 2004. **90**(9): p. 983-8.

150. Nicholson, B., et al., *Sustained nitric oxide production in macrophages requires the arginine transporter CAT2.* J Biol Chem, 2001. **276**(19): p. 15881-5.

151. Vodovotz, Y., et al., *Inactivation of nitric oxide synthase after prolonged incubation of mouse macrophages with IFN-gamma and bacterial lipopolysaccharide.* J Immunol, 1994. **152**(8): p. 4110-8.

152. Kehrl, J.H. and A.S. Fauci, *Identification, purification, and characterization of antigen-activated and antigen-specific human B lymphocytes.* J Exp Med, 1983. **157**(5): p. 1692-7.

153. Torrents, D., et al., *Identification and characterization of a membrane protein (y+L amino acid transporter-1) that associates with 4F2hc to encode the amino acid transport activity y+L. A candidate gene for lysinuric protein intolerance.* J Biol Chem, 1998. **273**(49): p. 32437-45.

154. Mondino, A. and D.L. Mueller, *mTOR at the crossroads of T cell proliferation and tolerance.* Semin Immunol, 2007. **19**(3): p. 162-72.

155. Fukuzumi, M., et al., *Endotoxin-induced enhancement of glucose influx into murine peritoneal macrophages via GLUT1.* Infect Immun, 1996. **64**(1): p. 108-12.

156. Gamelli, R.L., et al., *Augmentations of glucose uptake and glucose transporter-1 in macrophages following thermal injury and sepsis in mice.* J Leukoc Biol, 1996. **59**(5): p. 639-47.

157. Maxfield, F.R. and T.E. McGraw, *Endocytic recycling.* Nat Rev Mol Cell Biol, 2004. **5**(2): p. 121-32.

158. Chen, W., et al., *Rab11 is required for trans-golgi network-to-plasma membrane transport and a preferential target for GDP dissociation inhibitor.* Mol Biol Cell, 1998. **9**(11): p. 3241-57.

159. Lin, S.X., et al., *Rme-1 regulates the distribution and function of the endocytic recycling compartment in mammalian cells.* Nat Cell Biol, 2001. **3**(6): p. 567-72.

160. Lindsay, A.J., et al., *Rab coupling protein (RCP), a novel Rab4 and Rab11 effector protein.* J Biol Chem, 2002. **277**(14): p. 12190-9.

161. Goldberg, I.J., *Lipoprotein lipase and lipolysis: central roles in lipoprotein metabolism and atherogenesis.* J Lipid Res, 1996. **37**(4): p. 693-707.

162. Goldman, R., *Control of lipoprotein lipase secretion by macrophages: effect of macrophage differentiation agents.* J Leukoc Biol, 1990. **47**(1): p. 79-86.

163. Behr, S.R. and F.B. Kraemer, *Effects of activation on lipoprotein lipase secretion by macrophages. Evidence for autoregulation.* J Exp Med, 1986. **164**(4): p. 1362-7.

164. Hentze, M.W. and L.C. Kuhn, *Molecular control of vertebrate iron metabolism: mRNA-based regulatory circuits operated by iron, nitric oxide, and oxidative stress.* Proc Natl Acad Sci U S A, 1996. **93**(16): p. 8175-82.

165. Harrison, P.M. and P. Arosio, *The ferritins: molecular properties, iron storage function and cellular regulation.* Biochim Biophys Acta, 1996. **1275**(3): p. 161-203.

166. Kim, S. and P. Ponka, *Nitrogen monoxide-mediated control of ferritin synthesis: implications for macrophage iron homeostasis.* Proc Natl Acad Sci U S A, 2002. **99**(19): p. 12214-9.

167. Klausner, R.D. and T.A. Rouault, *A double life: cytosolic aconitase as a regulatory RNA binding protein.* Mol Biol Cell, 1993. **4**(1): p. 1-5.

168. Beinert, H. and M.C. Kennedy, *Aconitase, a two-faced protein: enzyme and iron regulatory factor.* Faseb J, 1993. **7**(15): p. 1442-9.

169. Ponka, P., *Cell biology of heme.* Am J Med Sci, 1999. **318**(4): p. 241-56.

170. Ferris, C.D., et al., *Haem oxygenase-1 prevents cell death by regulating cellular iron.* Nat Cell Biol, 1999. **1**(3): p. 152-7.

171. Morse, D. and A.M. Choi, *Heme oxygenase-1: the "emerging molecule" has arrived.* Am J Respir Cell Mol Biol, 2002. **27**(1): p. 8-16.

172. Lee, C.G., et al., *Cloning and analysis of gene regulation of a novel LPS-inducible cDNA.* Immunogenetics, 1995. **41**(5): p. 263-70.

173. Cheon, Y.P., et al., *Immune-responsive gene 1 is a novel target of progesterone receptor and plays a critical role during implantation in the mouse.* Endocrinology, 2003. **144**(12): p. 5623-30.

174. Greenbaum, D., et al., *Comparing protein abundance and mRNA expression levels on a genomic scale.* Genome Biol, 2003. **4**(9): p. 117.

175. Nie, L., G. Wu, and W. Zhang, *Correlation of mRNA expression and protein abundance affected by multiple sequence features related to translational efficiency in Desulfovibrio vulgaris: a quantitative analysis.* Genetics, 2006. **174**(4): p. 2229-43.

176. Bainton, D.F., *The discovery of lysosomes.* J Cell Biol, 1981. **91**(3 Pt 2): p. 66s-76s.

177. Haas, A., *The phagosome: compartment with a license to kill.* Traffic, 2007. **8**(4): p. 311-30.

178. McBride, H.M., M. Neuspiel, and S. Wasiak, *Mitochondria: more than just a powerhouse.* Curr Biol, 2006. **16**(14): p. R551-60.

179. Metchnikoff, E., *On the Present State of the Question of Immunity in Infectious Diseases.* The Nobel Lectures, 1908.

# Erklärung

Hiermit erkläre ich, daß diese Arbeit bisher von mir weder an der Mathematisch Naturwissenschaftlichen Fakultät der Ernst-Moritz-Arndt-Universität Greifswald noch einer anderen wissenschaftlichen Einrichtung zum Zwecke der Promotion eingereicht wurde.

Ferner erkläre ich, daß ich diese Arbeit selbständig verfaßt und keine anderen als die darin angegebenen Hilfsmittel benutzt habe.

Greifswald, July 2010 Unterschrift

Dinh Hoang Dang Khoa

# Curriculum Vitae

## Personal information:

| | | |
|---|---|---|
| Name | : | **Dinh Hoang Dang Khoa** |
| Sex | : | Male |
| Date of Birth | : | 12 June 1981 |
| Place of Birth | : | Binh Thuan, Vietnam |
| Nationality | : | Vietnamese |

## Education and Training:

| | | |
|---|---|---|
| 1999 – 2003 | : | Bachelor course in Biotechnology, Faculty of Biology, University of Natural Sciences, Ho Chi Minh city, Vietnam |
| 2004-2005 | : | Researcher, Department of Animal physiology, Faculty of Biology, University of Natural Sciences, Ho Chi Minh city, Vietnam |
| 2005 – 2006 | : | Student of Diploma Equivalent course, Life Science, Joint Graduate Education Program (JGEP) cooperated between Ernst-Moritz-Arndt University of Greifswald, Germany; Hanoi University of Science and Institute of Biotechnology; and Vietnamese Academy of Science and Technology. |
| 2007 – 2010 | : | Ph.D. student of Interfaculty Institute for Genetics and Functional Genomics, Ernst-Moritz-Arndt Universität Greifswald, Germany |

## Publication:

1. Maren Depke, **Dinh Hoang Dang Khoa**, Katrin Breitbach, Antje Bast, Lars Brinkmann, Manuela Gesell-Salazar, Elke Hammer, Leif Steil, Frank Schmidt, Ivo Steinmetz, and Uwe Völker. "Transcriptomic and proteomic characterization of mouse BMM after IFN¬γ-activation in a serum-free system". *Manuscript in preparing*.

# Acknowledgments

First of all, I would like to express my special gratitude to my supervisor Prof. Dr. Uwe Völker for his excellent supervision. I have learned a lot from him through scientific discussions, comments and advices. Furthermore, I strongly appreciated for his kind supports not only for my scientific research but also life during the last four years.

I am also especially grateful to Dr. Frank Schmidt and Dr. Leif Steil – my direct advisors – They have guided and strongly supported me throughout the PhD study with well-qualified discussion and lectures, as well as valuable advices and encouragements. I am very grateful.

I would like to express my thanks to Dr. Truong Quoc Phong for his kindly guiding about experimental techniques at the starting time of my study in Greifswald.

I wish to express my gratitude to Dr. Manuela Gesell Salazar, Dr. Elke Hammer and Dr. Vishnu Dhople for their perfect support in mass spectrometry experiments. I would like to thank Lars Brinkmann for his effective collaboration in data analysis and computer works.

I would like to express my thankfulness to Prof. Dr. Ivo Steinmetz, Dr. Katrin Breitbach, and Dr. Antje Bast of Friedrich Loeffler Institute of Medical Microbiology, for macrophage sample preparations and useful scientific discussions.

I would like to express my thanks to Maren Depke for providing transcriptome data which is a meaningful complementary information resource for my research.

I wish to thank Karsta Barnekow, Ulrike Lissner, Kastrin Schoknecht, Beatrice Bardorek, Kastrin Passow, Manja Möller for perfect technical assistance.

My thanks go to Nicholas Ehlers for his kind support in document works, to Malanie Gutjahr and all members of Laboratory for Functional Genomics in Greifswald for their friendship and collaboration during my research in Germany.

I also thank the Joint Graduate Education Program (JGEP) coordinators Dr. Jörn Kasbohm and Dr. Le Thi Lai for their support.

I would like to thank the Ministry of Education and Training of Vietnam (MOET), German Academic Exchange Service (DAAD) for financial support.

Grateful thanks to all my friends, especially to VietGreif group members, for their support and friendship. Thank you all so much.

Last but not least I would like to express my deepest gratitude to my parents and my family members for their love.

# Supplements

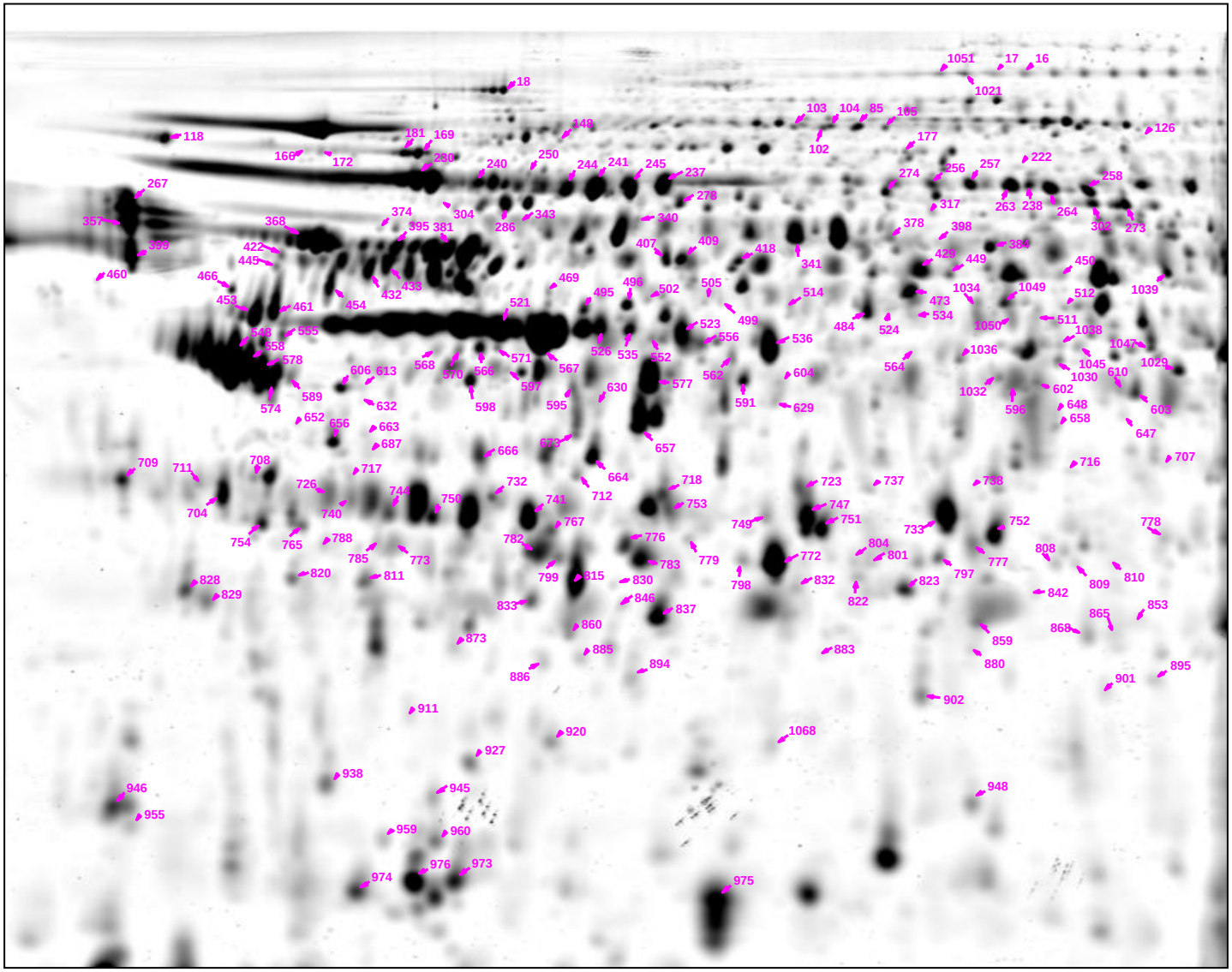


**Figure A.1: 2DE proteome reference map of BMMs.** Fused-gel-image was created by combining 16 gel images of 4 different BMM samples in 2D-DIGE experiment. On the image, 252 identified protein spots are labelled with spot number.

**Table A.1: Identified proteins in 252 protein spots on 2DE proteome reference map of BMMs.**

| *Spot* | *Accession Number* | *Gene entrez ID* | *Protein Name* | *Protein Score* | *Total Ion Score* | *Sequence coverage* | *Peptide Count* | *Theoretical MW (kDa)* | *Theoretical pI* |
|---|---|---|---|---|---|---|---|---|---|
| 16 | ITAM_MOUSE | 16409 | Integrin alpha-M | 704 | 466.1 | 38% | 38 | 127.4 | 6.87 |
| 17 | ITAM_MOUSE | 16409 | Integrin alpha-M | 681 | 457.3 | 39% | 37 | 127.4 | 6.87 |
| 18 | MYH9_MOUSE | 17886 | Myosin-9 | 621 | 492.7 | 23% | 34 | 226.2 | 5.54 |
| 51 | ITAM_MOUSE | 16409 | Integrin alpha-M | 418 | 336.9 | 24% | 21 | 127.4 | 6.87 |
| 57 | HS105_MOUSE | 15505 | Heat shock protein 105 kDa | 426 | 198.6 | 46% | 38 | 96.3 | 5.39 |
| 78 | ITAM_MOUSE | 16409 | Integrin alpha-M | 119 | 94.4 | 16% | 13 | 127.4 | 6.87 |
| 85 | LONM_MOUSE | 74142 | Lon protease homolog, mitochondrial | 747 | 438.9 | 45% | 42 | 105.8 | 6.15 |
| 98 | ACTN1_MOUSE | 109711 | Alpha-actinin-1 | 365 | 159.6 | 45% | 33 | 103.0 | 5.23 |
| 102 | ERAP1_MOUSE | 80898 | Endoplasmic reticulum aminopeptidase 1 | 684 | 380.3 | 51% | 41 | 106.5 | 5.77 |
| 103 | ERAP1_MOUSE | 80898 | Endoplasmic reticulum aminopeptidase 1 | 654 | 378.4 | 50% | 39 | 106.5 | 5.77 |
| 104 | LONM_MOUSE | 74142 | Lon protease homolog, mitochondrial | 712 | 388.4 | 44% | 43 | 105.8 | 6.15 |
| 105 | ERAP1_MOUSE | 80898 | Endoplasmic reticulum aminopeptidase 1 | 626.0 | 348.9 | 50% | 39 | 106.5 | 5.77 |
| 105 | ITAM_MOUSE | 16409 | Integrin alpha-M | 65.3 | 50.7 | 13% | 10 | 127.4 | 6.87 |
| 118 | GLU2B_MOUSE | 19089 | Glucosidase 2 subunit beta | 355 | 250.0 | 40% | 18 | 58.8 | 4.41 |
| 126 | PYGL_MOUSE | 110095 | Glycogen phosphorylase, liver form | 602 | 303.6 | 48% | 42 | 97.4 | 6.63 |
| 148 | ACTN4_MOUSE | 60595 | Alpha-actinin-4 | 172 | 43.0 | 39% | 25 | 104.9 | 5.25 |
| 166 | HCLS1_MOUSE | 15163 | Hematopoietic lineage cell-specific protein | 457 | 342.4 | 41% | 19 | 54.2 | 4.73 |
| 169 | HS90B_MOUSE | 15516 | Heat shock protein HSP 90-beta | 519 | 320.2 | 46% | 29 | 83.3 | 4.97 |
| 172 | HCLS1_MOUSE | 15163 | Hematopoietic lineage cell-specific protein | 653 | 448.4 | 56% | 27 | 54.2 | 4.73 |
| 177 | PDPR_MOUSE | 319518 | Pyruvate dehydrogenase phosphatase regulatory subunit | 666 | 310.7 | 52% | 44 | 99.2 | 5.93 |
| 181 | HS90A_MOUSE | 15519 | Heat shock protein HSP 90-alpha | 392 | 228.8 | 41% | 28 | 84.7 | 4.93 |
| 190 | P5CS_MOUSE | 56454 | Delta-1-pyrroline-5-carboxylate synthetase | 561 | 304.9 | 50% | 36 | 87.2 | 7.18 |
| 222 | RHG25_MOUSE | 232201 | Rho GTPase-activating protein 25 | 744 | 472.8 | 64% | 34 | 73.3 | 6.03 |
| 230 | GRP78_MOUSE | 14828 | 78 kDa glucose-regulated protein | 831 | 553.4 | 57% | 36 | 72.4 | 5.07 |
| 237 | GRP75_MOUSE | 15526 | Stress-70 protein, mitochondrial | 805 | 564.3 | 58% | 32 | 73.5 | 5.91 |
| 238 | PCCA_MOUSE | 110821 | Propionyl-CoA carboxylase alpha chain, mitochondrial | 177.0 | 53.0 | 47% | 23 | 79.9 | 6.83 |
| 238 | BGLR_MOUSE | 110006 | Beta-glucuronidase | 149 | 52.5 | 37% | 19 | 74.2 | 6.16 |
| 240 | HS90B_MOUSE | 15516 | Heat shock protein HSP 90-beta | 309 | 156.4 | 41% | 25 | 83.3 | 4.97 |
| 241 | HSP7C_MOUSE | 15481 | Heat shock cognate 71 kDa protein | 972 | 743.4 | 60% | 31 | 70.8 | 5.37 |
| 243 | GRP78_MOUSE | 14828 | 78 kDa glucose-regulated protein | 814 | 593.6 | 53% | 31 | 72.4 | 5.07 |
| 244 | HSP7C_MOUSE | 15481 | Heat shock cognate 71 kDa protein | 537 | 343.2 | 57% | 27 | 70.8 | 5.37 |
| 245 | VATA_MOUSE | 11964 | Vacuolar ATP synthase catalytic subunit A | 666 | 503.1 | 57% | 24 | 68.3 | 5.42 |
| 250 | PKHO2_MOUSE | 102595 | Pleckstrin homology domain-containing family O member 2 | 376.0 | 268.5 | 49% | 17 | 53.8 | 5.40 |
| 250 | CLH_MOUSE | 67300 | Clathrin heavy chain 1 | 194.0 | 134.4 | 24% | 24 | 191.4 | 5.48 |
| 256 | BGLR_MOUSE | 110006 | Beta-glucuronidase | 629 | 413.4 | 45% | 30 | 74.2 | 6.16 |

| *Spot* | *Accession Number* | *Gene entrez ID* | *Protein Name* | *Protein Score* | *Total Ion Score* | *Sequence coverage* | *Peptide Count* | *Theoretical MW (kDa)* | *Theoretical pI* |
|---|---|---|---|---|---|---|---|---|---|
| 257 | BGLR_MOUSE | 110006 | Beta-glucuronidase | 767 | 497.7 | 54% | 34 | 74.2 | 6.16 |
| 258 | BGLR_MOUSE | 110006 | Beta-glucuronidase | 745 | 427.5 | 56% | 38 | 74.2 | 6.16 |
| 263 | BGLR_MOUSE | 110006 | Beta-glucuronidase | 836 | 527.0 | 57% | 37 | 74.2 | 6.16 |
| 264 | BGLR_MOUSE | 110006 | Beta-glucuronidase | 722 | 403.7 | 60% | 38 | 74.2 | 6.16 |
| 267 | CALR_MOUSE | 12317 | Calreticulin | 221 | 99.8 | 47% | 18 | 48.0 | 4.33 |
| 273 | WDR1_MOUSE | 22388 | WD repeat-containing protein 1 | 969 | 738.0 | 65% | 30 | 66.4 | 6.11 |
| 274 | TRAP1_MOUSE | 68015 | Heat shock protein 75 kDa, mitochondrial | 461 | 240.2 | 55% | 31 | 80.2 | 6.25 |
| 278 | HSP7C_MOUSE | 15481 | Heat shock cognate 71 kDa protein | 651 | 400.4 | 57% | 32 | 70.8 | 5.37 |
| 286 | SAP_MOUSE | 19156 | Sulfated glycoprotein 1 | 132.0 | 79.1 | 31% | 13 | 61.4 | 5.07 |
| 286 | GRP78_MOUSE | 14828 | 78 kDa glucose-regulated protein | 123 | 79.1 | 27% | 12 | 72.4 | 5.07 |
| 298 | NCF2_MOUSE | 17970 | Neutrophil cytosol factor 2 | 619 | 434.4 | 55% | 26 | 59.4 | 6.18 |
| 302 | WDR1_MOUSE | 22388 | WD repeat-containing protein 1 | 567 | 357.8 | 64% | 28 | 66.4 | 6.11 |
| 304 | ENPL_MOUSE | 22027 | Endoplasmin | 198 | 114.7 | 31% | 21 | 92.4 | 4.74 |
| 317 | BGLR_MOUSE | 110006 | Beta-glucuronidase | 657 | 437.3 | 55% | 30 | 74.2 | 6.16 |
| 340 | VATA_MOUSE | 11964 | Vacuolar ATP synthase catalytic subunit A | 307.0 | 195.1 | 49% | 20 | 68.3 | 5.42 |
| 340 | HNRPK_MOUSE | 15387 | Heterogeneous nuclear ribonucleoprotein K | 151.0 | 64.6 | 39% | 16 | 50.9 | 5.39 |
| 340 | PLEC1_MOUSE | 18810 | Plectin-1 | 117 | 69.3 | 12% | 38 | 533.9 | 5.74 |
| 341 | PDIA3_MOUSE | 14827 | Protein disulfide-isomerase A3 | 730 | 495.3 | 62% | 30 | 56.6 | 5.88 |
| 343 | HNRPK_MOUSE | 15387 | Heterogeneous nuclear ribonucleoprotein K | 403 | 158.8 | 58% | 29 | 50.9 | 5.39 |
| 357 | CALR_MOUSE | 12317 | Calreticulin | 213 | 95.6 | 49% | 18 | 48.0 | 4.33 |
| 368 | PDIA1_MOUSE | 18453 | Protein disulfide-isomerase | 458 | 246.5 | 55% | 28 | 57.1 | 4.79 |
| 374 | ENPL_MOUSE | 22027 | Endoplasmin | 247 | 167.1 | 29% | 20 | 92.4 | 4.74 |
| 378 | PDIA3_MOUSE | 14827 | Protein disulfide-isomerase A3 | 392 | 212.5 | 55% | 26 | 56.6 | 5.88 |
| 381 | VIME_MOUSE | 22352 | Vimentin | 900 | 578.0 | 78% | 35 | 53.7 | 5.06 |
| 384 | COR1A_MOUSE | 12721 | Coronin-1A | 324 | 187.6 | 50% | 20 | 51.0 | 6.05 |
| 390 | CALR_MOUSE | 12317 | Calreticulin | 217 | 97.5 | 39% | 18 | 48.0 | 4.33 |
| 395 | TBB2A_MOUSE | 22151 | Tubulin beta-2A chain | 851 | 522.6 | 77% | 34 | 49.9 | 4.78 |
| 398 | PTN6_MOUSE | 15170 | Tyrosine-protein phosphatase non-receptor type 6 | 266.0 | 88.4 | 55% | 27 | 67.5 | 7.66 |
| 398 | WDR1_MOUSE | 22388 | WD repeat-containing protein 1 | 139 | 46.9 | 41% | 17 | 66.4 | 6.11 |
| 399 | CALR_MOUSE | 12317 | Calreticulin | 125 | 54.6 | 36% | 13 | 48.0 | 4.33 |
| 407 | CNDP2_MOUSE | 66054 | Cytosolic non-specific dipeptidase | 282 | 120.0 | 52% | 23 | 52.7 | 5.43 |
| 409 | VATB2_MOUSE | 11966 | Vacuolar ATP synthase subunit B, brain isoform | 773 | 463.1 | 73% | 33 | 56.5 | 5.57 |
| 418 | VATB2_MOUSE | 11966 | Vacuolar ATP synthase subunit B, brain isoform | 910 | 541.2 | 79% | 37 | 56.5 | 5.57 |
| 422 | ENPL_MOUSE | 22027 | Endoplasmin | 294 | 213.5 | 28% | 20 | 92.4 | 4.74 |
| 429 | ALDH2_MOUSE | 11669 | Aldehyde dehydrogenase, mitochondrial | 235 | 147.6 | 40% | 16 | 56.5 | 7.53 |

| *Spot* | *Accession Number* | *Gene entrez ID* | *Protein Name* | *Protein Score* | *Total Ion Score* | *Sequence coverage* | *Peptide Count* | *Theoretical MW (kDa)* | *Theoretical pI* |
|---|---|---|---|---|---|---|---|---|---|
| 432 | VIME_MOUSE | 22352 | Vimentin | 702 | 444.1 | 76% | 30 | 53.7 | 5.06 |
| 433 | TBB2A_MOUSE | 22151 | Tubulin beta-2A chain | 456 | 227.6 | 73% | 27 | 49.9 | 4.78 |
| 438 | ATPB_MOUSE | 11947 | ATP synthase subunit beta, mitochondrial | 759 | 549.9 | 72% | 26 | 56.3 | 5.19 |
| 445 | RBBP4_MOUSE | 19646 | Histone-binding protein RBBP4 | 220 | 190.7 | 27% | 7 | 47.6 | 4.79 |
| 449 | ODO2_MOUSE | 78920 | Dihydrolipoyllysine-residue succinyltransferase component of 2-oxoglutarate dehydrogenase complex, mitochondrial | 678 | 513.2 | 51% | 22 | 49.0 | 9.11 |
| 450 | PDIA3_MOUSE | 14827 | Protein disulfide-isomerase A3 | 379 | 230.6 | 51% | 23 | 56.6 | 5.88 |
| 453 | VIME_MOUSE | 22352 | Vimentin | 586 | 353.1 | 69% | 28 | 53.7 | 5.06 |
| 454 | VIME_MOUSE | 22352 | Vimentin | 707 | 443.7 | 73% | 30 | 53.7 | 5.06 |
| 460 | CALR_MOUSE | 12317 | Calreticulin | 217 | 129.0 | 36% | 15 | 48.0 | 4.33 |
| 461 | VIME_MOUSE | 22352 | Vimentin | 689 | 466.0 | 72% | 27 | 53.7 | 5.06 |
| 466 | RINI_MOUSE | 107702 | Ribonuclease inhibitor | 1090 | 764.5 | 89% | 35 | 49.8 | 4.69 |
| 469 | HNRPF_MOUSE | 98758 | Heterogeneous nuclear ribonucleoprotein F | 800 | 593.8 | 64% | 24 | 45.7 | 5.31 |
| 473 | GDIB_MOUSE | 14569 | Rab GDP dissociation inhibitor beta | 463 | 257.0 | 74% | 27 | 50.5 | 5.93 |
| 477 | CNDP2_MOUSE | 66054 | Cytosolic non-specific dipeptidase | 271.0 | 139.5 | 53% | 20 | 52.7 | 5.43 |
| 477 | PDIA6_MOUSE | 71853 | Protein disulfide-isomerase A6 | 147.0 | 79.1 | 36% | 13 | 48.1 | 5.00 |
| 477 | HA12_MOUSE | 14964 | H-2 class I histocompatibility antigen, D-D alpha chain | 96 | 53.4 | 29% | 10 | 41.1 | 6.22 |
| 484 | OAT_MOUSE | 18242 | Ornithine aminotransferase, mitochondrial | 515 | 341.6 | 60% | 23 | 48.3 | 6.19 |
| 495 | IF4A1_MOUSE | 13681 | Eukaryotic initiation factor 4A-I | 694 | 438.9 | 76% | 29 | 46.1 | 5.32 |
| 496 | QCR1_MOUSE | 22273 | Cytochrome b-c1 complex subunit 1, mitochondrial | 647 | 478.3 | 48% | 23 | 52.7 | 5.75 |
| 499 | HA12_MOUSE | 14964 | H-2 class I histocompatibility antigen, D-D alpha chain | 576 | 365.2 | 57% | 26 | 41.1 | 6.22 |
| 502 | OST48_MOUSE | 13200 | Dolichyl-diphosphooligosaccharide--protein glycosyltransferase 48 kDa subunit | 532 | 409.4 | 50% | 19 | 49.0 | 5.52 |
| 505 | ARP3_MOUSE | 74117 | Actin-related protein 3 | 578 | 351.4 | 61% | 27 | 47.3 | 5.61 |
| 511 | SPA3G_MOUSE | 20715 | Serine protease inhibitor A3G | 496 | 273.6 | 65% | 27 | 49.0 | 6.06 |
| 512 | METK2_MOUSE | 232087 | S-adenosylmethionine synthetase isoform type-2 | 289.0 | 178.5 | 51% | 17 | 43.7 | 6.02 |
| 512 | AL3B1_MOUSE | 67689 | Aldehyde dehydrogenase family 3 member B1 | 145.0 | 63.3 | 41% | 16 | 52.3 | 7.50 |
| 513 | IF4A1_MOUSE | 13681 | Eukaryotic initiation factor 4A-I | 80.7 | 27.4 | 44% | 11 | 46.1 | 5.32 |
| 514 | HA12_MOUSE | 14964 | H-2 class I histocompatibility antigen, D-D alpha chain | 628 | 405.1 | 57% | 27 | 41.1 | 6.22 |
| 521 | ACTG_MOUSE | 11465 | Actin, cytoplasmic 2 | 693 | 505.4 | 72% | 23 | 41.8 | 5.31 |
| 523 | CATD_MOUSE | 13033 | Cathepsin D | 505 | 427.0 | 43% | 13 | 44.9 | 6.71 |
| 524 | CH60_MOUSE | 15510 | 60 kDa heat shock protein, mitochondrial | 771 | 603.8 | 47% | 25 | 60.9 | 5.91 |
| 526 | ACTG_MOUSE | 11465 | Actin, cytoplasmic 2 | 618 | 455.1 | 72% | 21 | 41.8 | 5.31 |
| 534 | COR1A_MOUSE | 12721 | Coronin-1A | 275 | 158.6 | 43% | 18 | 51.0 | 6.05 |
| 535 | ACTG_MOUSE | 11465 | Actin, cytoplasmic 2 | 562 | 456.0 | 56% | 16 | 41.8 | 5.31 |
| 536 | CATD_MOUSE | 13033 | Cathepsin D | 325.0 | 225.8 | 43% | 15 | 44.9 | 6.71 |
| 536 | ACTG_MOUSE | 11465 | Actin, cytoplasmic 2 | 249.0 | 136.8 | 60% | 17 | 41.8 | 5.31 |

| *Spot* | *Accession Number* | *Gene entrez ID* | *Protein Name* | *Protein Score* | *Total Ion Score* | *Sequence coverage* | *Peptide Count* | *Theoretical MW (kDa)* | *Theoretical pI* |
|---|---|---|---|---|---|---|---|---|---|
| 548 | VIME_MOUSE | 22352 | Vimentin | 550 | 360.5 | 60% | 25 | 53.7 | 5.06 |
| 552 | GRP78_MOUSE | 14828 | 78 kDa glucose-regulated protein | 229.0 | 166.4 | 30% | 15 | 72.4 | 5.07 |
| 552 | PON3_MOUSE | 269823 | Serum paraoxonase/lactonase 3 | 163 | 131.6 | 31% | 7 | 39.3 | 5.44 |
| 555 | VIME_MOUSE | 22352 | Vimentin | 515 | 289.2 | 70% | 28 | 53.7 | 5.06 |
| 556 | PON3_MOUSE | 269823 | Serum paraoxonase/lactonase 3 | 217.0 | 169.0 | 35% | 9 | 39.3 | 5.44 |
| 556 | CSN4_MOUSE | 26891 | COP9 signalosome complex subunit 4 | 108 | 46.0 | 45% | 12 | 46.3 | 5.57 |
| 558 | VIME_MOUSE | 22352 | Vimentin | 514 | 280.0 | 70% | 28 | 53.7 | 5.06 |
| 562 | CATB_MOUSE | 13030 | Cathepsin B | 202 | 123.6 | 49% | 13 | 37.3 | 5.57 |
| 564 | MYG1_MOUSE | 60315 | UPF0160 protein MYG1 | 273 | 120.1 | 71% | 21 | 42.7 | 6.54 |
| 566 | ACTG_MOUSE | 11465 | Actin, cytoplasmic 2 | 575 | 408.8 | 69% | 21 | 41.8 | 5.31 |
| 567 | ACTG_MOUSE | 11465 | Actin, cytoplasmic 2 | 736 | 533.9 | 72% | 24 | 41.8 | 5.31 |
| 568 | SPB6_MOUSE | 20719 | Serpin B6 | 248 | 110.2 | 62% | 20 | 42.6 | 5.53 |
| 570 | PDIA1_MOUSE | 18453 | Protein disulfide-isomerase | 443 | 268.6 | 56% | 25 | 57.1 | 4.79 |
| 571 | ACTG_MOUSE | 11465 | Actin, cytoplasmic 2 | 615 | 448.3 | 68% | 21 | 41.8 | 5.31 |
| 574 | VIME_MOUSE | 22352 | Vimentin | 551 | 345.8 | 62% | 26 | 53.7 | 5.06 |
| 577 | ACTG_MOUSE | 11465 | Actin, cytoplasmic 2 | 755 | 576.4 | 66% | 22 | 41.8 | 5.31 |
| 578 | VIME_MOUSE | 22352 | Vimentin | 465 | 265.2 | 59% | 26 | 53.7 | 5.06 |
| 587 | PDIA1_MOUSE | 18453 | Protein disulfide-isomerase | 283 | 163.7 | 46% | 20 | 57.1 | 4.79 |
| 589 | VIME_MOUSE | 22352 | Vimentin | 401 | 246.2 | 60% | 22 | 53.7 | 5.06 |
| 591 | IDH3A_MOUSE | 67834 | Isocitrate dehydrogenase [NAD] subunit alpha, mitochondrial | 272.0 | 129.2 | 48% | 21 | 39.6 | 6.27 |
| 591 | ACTB_MOUSE | 11461 | Actin, cytoplasmic 1 | 122 | 82.7 | 39% | 9 | 41.7 | 5.29 |
| 594 | ACTG_MOUSE | 11465 | Actin, cytoplasmic 2 | 83.7 | 43.5 | 48% | 9 | 41.8 | 5.31 |
| 595 | CAZA1_MOUSE | 12340 | F-actin-capping protein subunit alpha-1 | 424 | 353.4 | 66% | 11 | 32.9 | 5.34 |
| 596 | CATA_MOUSE | 12359 | Catalase | 197.0 | 115.3 | 40% | 16 | 59.7 | 7.72 |
| 596 | EF2_MOUSE | 13629 | Elongation factor 2 | 186 | 151.4 | 20% | 14 | 95.3 | 6.41 |
| 597 | PDIA1_MOUSE | 18453 | Protein disulfide-isomerase | 573 | 386.4 | 60% | 26 | 57.1 | 4.79 |
| 598 | VA0D2_MOUSE | 242341 | Vacuolar proton pump subunit d 2 | 561 | 347.4 | 74% | 26 | 40.5 | 5.14 |
| 602 | PRP19_MOUSE | 28000 | Pre-mRNA-processing factor 19 | 169 | 88.3 | 43% | 14 | 55.2 | 6.14 |
| 603 | ANXA1_MOUSE | 16952 | Annexin A1 | 322 | 186.5 | 69% | 20 | 38.7 | 6.97 |
| 604 | GRP78_MOUSE | 14828 | 78 kDa glucose-regulated protein | 227.0 | 171.4 | 27% | 14 | 72.4 | 5.07 |
| 604 | EF2_MOUSE | 13629 | Elongation factor 2 | 83.3 | 42.4 | 27% | 14 | 95.3 | 6.41 |
| 604 | ACTB_MOUSE | 11461 | Actin, cytoplasmic 1 | 57.1 | 30.1 | 33% | 7 | 41.7 | 5.29 |
| 606 | VA0D1_MOUSE | 11972 | Vacuolar proton pump subunit d 1 | 408 | 208.1 | 58% | 24 | 40.3 | 4.89 |
| 609 | KPYM_MOUSE | 18746 | Pyruvate kinase isozymes M1/M2 | 383 | 191.5 | 54% | 27 | 57.8 | 7.18 |
| 610 | HSP7C_MOUSE | 15481 | Heat shock cognate 71 kDa protein | 742 | 551.8 | 42% | 27 | 70.8 | 5.37 |

| *Spot* | *Accession Number* | *Gene entrez ID* | *Protein Name* | *Protein Score* | *Total Ion Score* | *Sequence coverage* | *Peptide Count* | *Theoretical MW (kDa)* | *Theoretical pI* |
|---|---|---|---|---|---|---|---|---|---|
| 613 | ARP3_MOUSE | 74117 | Actin-related protein 3 | 217 | 144.1 | 34% | 13 | 47.3 | 5.61 |
| 614 | GRP78_MOUSE | 14828 | 78 kDa glucose-regulated protein | 363.0 | 267.5 | 29% | 19 | 72.4 | 5.07 |
| 614 | ESYT1_MOUSE | 23943 | Extended-synaptotagmin-1 | 90.2 | 76.1 | 11% | 10 | 121.5 | 5.63 |
| 629 | GRP78_MOUSE | 14828 | 78 kDa glucose-regulated protein | 710 | 557.9 | 33% | 25 | 72.4 | 5.07 |
| 630 | PP2AA_MOUSE | 19052 | Serine/threonine-protein phosphatase 2A catalytic subunit alpha isoform | 333 | 249.1 | 54% | 13 | 35.6 | 5.30 |
| 632 | HSP7C_MOUSE | 15481 | Heat shock cognate 71 kDa protein | 509 | 401.1 | 38% | 19 | 70.8 | 5.37 |
| 633 | CATS_MOUSE | 13040 | Cathepsin S | 380.0 | 283.4 | 55% | 17 | 38.4 | 6.51 |
| 633 | TALDO_MOUSE | 21351 | Transaldolase | 156.0 | 50.8 | 46% | 17 | 37.4 | 6.57 |
| 647 | CATL1_MOUSE | 13039 | Cathepsin L1 | 406 | 338.0 | 39% | 13 | 37.5 | 6.37 |
| 648 | ALDH2_MOUSE | 11669 | Aldehyde dehydrogenase, mitochondrial | 530.0 | 374.4 | 43% | 23 | 56.5 | 7.53 |
| 648 | SFPQ_MOUSE | 71514 | Splicing factor, proline- and glutamine-rich | 120.0 | 79.5 | 21% | 15 | 75.4 | 9.45 |
| 652 | PDIA6_MOUSE | 71853 | Protein disulfide-isomerase A6 | 665 | 556.0 | 43% | 17 | 48.1 | 5.00 |
| 654 | WDR1_MOUSE | 22388 | WD repeat-containing protein 1 | 229.0 | 172.6 | 33% | 12 | 66.4 | 6.11 |
| 654 | ALD2_MOUSE | 14187 | Aldose reductase-related protein 2 | 87.5 | 36.9 | 42% | 9 | 36.1 | 5.97 |
| 656 | ANXA5_MOUSE | 11747 | Annexin A5 | 651 | 433.9 | 68% | 24 | 35.7 | 4.83 |
| 657 | ACTG_MOUSE | 11465 | Actin, cytoplasmic 2 | 797 | 646.4 | 55% | 20 | 41.8 | 5.31 |
| 658 | ALDH2_MOUSE | 11669 | Aldehyde dehydrogenase, mitochondrial | 618 | 424.1 | 52% | 26 | 56.5 | 7.53 |
| 663 | ACTB_MOUSE | 11461 | Actin, cytoplasmic 1 | 100 | 78.2 | 30% | 6 | 41.7 | 5.29 |
| 664 | ANXA4_MOUSE | 11746 | Annexin A4 | 529 | 337.8 | 67% | 25 | 36.0 | 5.43 |
| 666 | CATZ_MOUSE | 64138 | Cathepsin Z | 347 | 304.6 | 34% | 8 | 34.0 | 6.13 |
| 673 | ACTG_MOUSE | 11465 | Actin, cytoplasmic 2 | 744 | 591.9 | 61% | 20 | 41.8 | 5.31 |
| 687 | ACTB_MOUSE | 11461 | Actin, cytoplasmic 1 | 236.0 | 195.3 | 42% | 9 | 41.7 | 5.29 |
| 687 | CATZ_MOUSE | 64138 | Cathepsin Z | 131 | 87.4 | 32% | 8 | 34.0 | 6.13 |
| 691 | ANXA5_MOUSE | 11747 | Annexin A5 | 363 | 189.8 | 69% | 21 | 35.7 | 4.83 |
| 698 | VIME_MOUSE | 22352 | Vimentin | 254.0 | 116.2 | 52% | 22 | 53.7 | 5.06 |
| 698 | TPM1_MOUSE | 22003 | Tropomyosin alpha-1 chain | 74.1 | 46.2 | 35% | 8 | 32.7 | 4.69 |
| 699 | TPM3_MOUSE | 59069 | Tropomyosin alpha-3 chain | 73.2 | 61.0 | 20% | 6 | 32.8 | 4.68 |
| 702 | ALDH2_MOUSE | 11669 | Aldehyde dehydrogenase, mitochondrial | 537 | 402.7 | 38% | 21 | 56.5 | 7.53 |
| 704 | PPGB_MOUSE | 19025 | Lysosomal protective protein | 145 | 112.5 | 25% | 9 | 53.8 | 5.56 |
| 707 | GNPI1_MOUSE | 26384 | Glucosamine-6-phosphate isomerase 1 | 106 | 31.2 | 57% | 11 | 32.5 | 6.00 |
| 708 | TPM3_MOUSE | 59069 | Tropomyosin alpha-3 chain | 57.6 | 39.6 | 25% | 6 | 32.8 | 4.68 |
| 709 | C1QBP_MOUSE | 12261 | Complement component 1 Q subcomponent-binding protein, mitochondrial | 171 | 120.0 | 47% | 8 | 31.0 | 4.82 |
| 711 | EF1B_MOUSE | 55949 | Elongation factor 1-beta | 94.5 | 61.1 | 44% | 6 | 24.7 | 4.53 |
| 712 | ACTB_MOUSE | 11461 | Actin, cytoplasmic 1 | 611 | 455.0 | 73% | 20 | 41.7 | 5.29 |
| 716 | THTM_MOUSE | 246221 | 3-mercaptopyruvate sulfurtransferase | 683 | 485.1 | 73% | 22 | 33.0 | 6.11 |

| *Spot* | *Accession Number* | *Gene entrez ID* | *Protein Name* | *Protein Score* | *Total Ion Score* | *Sequence coverage* | *Peptide Count* | *Theoretical MW (kDa)* | *Theoretical pI* |
|---|---|---|---|---|---|---|---|---|---|
| 717 | ACTG_MOUSE | 11465 | Actin, cytoplasmic 2 | 507 | 414.2 | 50% | 15 | 41.8 | 5.31 |
| 718 | PHB_MOUSE | 18673 | Prohibitin | 807 | 588.5 | 84% | 23 | 29.8 | 5.57 |
| 723 | PNPH_MOUSE | 18950 | Purine nucleoside phosphorylase | 452 | 289.9 | 75% | 19 | 32.3 | 5.78 |
| 726 | HSP7C_MOUSE | 15481 | Heat shock cognate 71 kDa protein | 93.9 | 43.2 | 33% | 12 | 70.8 | 5.37 |
| 729 | PDIA1_MOUSE | 18453 | Protein disulfide-isomerase | 293 | 173.6 | 34% | 20 | 57.1 | 4.79 |
| 732 | CLIC1_MOUSE | 114584 | Chloride intracellular channel protein 1 | 637 | 465.4 | 67% | 19 | 27.0 | 5.09 |
| 733 | CATD_MOUSE | 13033 | Cathepsin D | 451 | 385.7 | 37% | 12 | 44.9 | 6.71 |
| 737 | PDIA3_MOUSE | 14827 | Protein disulfide-isomerase A3 | 242 | 137.8 | 39% | 18 | 56.6 | 5.88 |
| 738 | DHB8_MOUSE | 14979 | Estradiol 17-beta-dehydrogenase 8 | 447.0 | 364.2 | 63% | 12 | 26.6 | 6.10 |
| 738 | EXOS6_MOUSE | 72544 | Exosome complex exonuclease MTR3 | 120.0 | 69.1 | 36% | 9 | 28.4 | 5.87 |
| 740 | CATB_MOUSE | 13030 | Cathepsin B | 411 | 351.0 | 30% | 11 | 37.3 | 5.57 |
| 741 | CATB_MOUSE | 13030 | Cathepsin B | 697 | 581.5 | 45% | 16 | 37.3 | 5.57 |
| 744 | CATB_MOUSE | 13030 | Cathepsin B | 446 | 366.1 | 39% | 13 | 37.3 | 5.57 |
| 747 | CATD_MOUSE | 13033 | Cathepsin D | 423 | 324.1 | 43% | 15 | 44.9 | 6.71 |
| 749 | PSME1_MOUSE | 19186 | Proteasome activator complex subunit 1 | 164 | 108.9 | 40% | 10 | 28.7 | 5.73 |
| 750 | CATB_MOUSE | 13030 | Cathepsin B | 420 | 348.9 | 39% | 12 | 37.3 | 5.57 |
| 751 | ERP29_MOUSE | 67397 | Endoplasmic reticulum protein ERp29 | 499 | 270.8 | 72% | 23 | 28.8 | 5.90 |
| 752 | ERP29_MOUSE | 67397 | Endoplasmic reticulum protein ERp29 | 440 | 284.5 | 55% | 18 | 28.8 | 5.90 |
| 753 | VATA_MOUSE | 11964 | Vacuolar ATP synthase catalytic subunit A | 211.0 | 136.7 | 38% | 15 | 68.3 | 5.42 |
| 753 | CATD_MOUSE | 13033 | Cathepsin D | 189.0 | 134.8 | 28% | 11 | 44.9 | 6.71 |
| 753 | OSTF1_MOUSE | 20409 | Osteoclast-stimulating factor 1 | 92.2 | 35.6 | 61% | 9 | 23.8 | 5.46 |
| 754 | 1433Z_MOUSE | 22631 | 14-3-3 protein zeta/delta | 405 | 272.6 | 67% | 17 | 27.8 | 4.73 |
| 765 | 1433F_MOUSE | 22629 | 14-3-3 protein eta | 263 | 189.5 | 57% | 12 | 28.2 | 4.81 |
| 767 | ACTG_MOUSE | 11465 | Actin, cytoplasmic 2 | 512 | 360.0 | 64% | 20 | 41.8 | 5.31 |
| 772 | CATS_MOUSE | 13040 | Cathepsin S | 407 | 316.3 | 54% | 14 | 38.4 | 6.51 |
| 773 | ATPB_MOUSE | 11947 | ATP synthase subunit beta, mitochondrial | 350.0 | 297.7 | 36% | 11 | 56.3 | 5.19 |
| 773 | ACTG_MOUSE | 11465 | Actin, cytoplasmic 2 | 84.7 | 69.5 | 26% | 5 | 41.8 | 5.31 |
| 776 | ACTG_MOUSE | 11465 | Actin, cytoplasmic 2 | 524 | 407.0 | 50% | 17 | 41.8 | 5.31 |
| 777 | CATD_MOUSE | 13033 | Cathepsin D | 438 | 384.6 | 24% | 11 | 44.9 | 6.71 |
| 778 | PGAM1_MOUSE | 18648 | Phosphoglycerate mutase 1 | 216 | 119.3 | 55% | 13 | 28.8 | 6.67 |
| 779 | NDUS3_MOUSE | 68349 | NADH dehydrogenase [ubiquinone] iron-sulfur protein 3, mitochondrial | 675 | 450.8 | 68% | 24 | 30.1 | 6.67 |
| 782 | ACTG_MOUSE | 11465 | Actin, cytoplasmic 2 | 349.0 | 256.6 | 39% | 15 | 41.8 | 5.31 |
| 782 | CATD_MOUSE | 13033 | Cathepsin D | 99.7 | 67.4 | 23% | 8 | 44.9 | 6.71 |
| 783 | CATS_MOUSE | 13040 | Cathepsin S | 741 | 590.8 | 61% | 21 | 38.4 | 6.51 |
| 785 | GDIR2_MOUSE | 11857 | Rho GDP-dissociation inhibitor 2 | 472 | 388.6 | 76% | 10 | 22.8 | 4.97 |
| 788 | KCRB_MOUSE | 12709 | Creatine kinase B-type | 425 | 339.1 | 33% | 14 | 42.7 | 5.40 |
| 792 | VIME_MOUSE | 22352 | Vimentin | 701 | 548.7 | 45% | 22 | 53.7 | 5.06 |
| 797 | PRDX4_MOUSE | 53381 | Peroxiredoxin-4 | 443 | 322.7 | 66% | 15 | 31.0 | 6.67 |

| *Spot* | *Accession Number* | *Gene entrez ID* | *Protein Name* | *Protein Score* | *Total Ion Score* | *Sequence coverage* | *Peptide Count* | *Theoretical MW (kDa)* | *Theoretical pI* |
|---|---|---|---|---|---|---|---|---|---|
| 798 | ATPB_MOUSE | 11947 | ATP synthase subunit beta, mitochondrial | 568 | 457.6 | 44% | 18 | 56.3 | 5.19 |
| 799 | CATS_MOUSE | 13040 | Cathepsin S | 601 | 495.6 | 54% | 17 | 38.4 | 6.51 |
| 801 | PRDX6_MOUSE | 11758 | Peroxiredoxin-6 | 801 | 533.9 | 87% | 25 | 24.9 | 5.71 |
| 802 | ACTG_MOUSE | 11465 | Actin, cytoplasmic 2 | 371.0 | 296.6 | 48% | 13 | 41.8 | 5.31 |
| 802 | CATS_MOUSE | 13040 | Cathepsin S | 175 | 116.3 | 48% | 12 | 38.4 | 6.51 |
| 804 | ANXA1_MOUSE | 16952 | Annexin A1 | 301 | 206.1 | 49% | 15 | 38.7 | 6.97 |
| 805 | DGUOK_MOUSE | 27369 | Deoxyguanosine kinase, mitochondrial | 294 | 181.0 | 57% | 15 | 32.2 | 7.85 |
| 808 | PRDX6_MOUSE | 11758 | Peroxiredoxin-6 | 571.0 | 356.4 | 84% | 22 | 24.9 | 5.71 |
| 808 | MA2B1_MOUSE | 17159 | Lysosomal alpha-mannosidase | 66.9 | 59.8 | 8% | 7 | 114.5 | 8.30 |
| 809 | FLNA_MOUSE | 192176 | Filamin-A | 84.5 | 70.8 | 11% | 15 | 281.0 | 5.68 |
| 810 | MYH9_MOUSE | 17886 | Myosin-9 | 144 | 106.4 | 12% | 20 | 226.2 | 5.54 |
| 811 | SAP3_MOUSE | 14667 | Ganglioside GM2 activator | 101 | 82.8 | 30% | 4 | 20.8 | 5.63 |
| 815 | CATB_MOUSE | 13030 | Cathepsin B | 548 | 472.3 | 38% | 12 | 37.3 | 5.57 |
| 820 | TCTP_MOUSE | 22070 | Translationally-controlled tumor protein | 328 | 255.3 | 44% | 10 | 19.4 | 4.76 |
| 822 | GRB2_MOUSE | 14784 | Growth factor receptor-bound protein 2 | 207 | 118.1 | 65% | 13 | 25.2 | 5.89 |
| 823 | PRDX3_MOUSE | 11757 | Thioredoxin-dependent peroxide reductase, mitochondrial | 349 | 270.3 | 53% | 11 | 28.1 | 7.15 |
| 828 | VIME_MOUSE | 22352 | Vimentin | 134 | 78.9 | 32% | 13 | 53.7 | 5.06 |
| 829 | VIME_MOUSE | 22352 | Vimentin | 442 | 294.6 | 39% | 23 | 53.7 | 5.06 |
| 830 | NDUV2_MOUSE | 72900 | NADH dehydrogenase [ubiquinone] flavoprotein 2, mitochondrial | 522.0 | 405.6 | 61% | 15 | 27.3 | 7.00 |
| 830 | ALDH2_MOUSE | 11669 | Aldehyde dehydrogenase, mitochondrial | 130 | 83.2 | 20% | 12 | 56.5 | 7.53 |
| 832 | RHOA_MOUSE | 11848 | Transforming protein RhoA | 79.8 | 61.3 | 29% | 5 | 21.8 | 5.83 |
| 832 | RHOC_MOUSE | 11853 | Rho-related GTP-binding protein RhoC | 78.9 | 61.3 | 29% | 4 | 22.0 | 6.20 |
| 833 | ACTB_MOUSE | 11461 | Actin, cytoplasmic 1 | 436.0 | 298.2 | 53% | 19 | 41.7 | 5.29 |
| 833 | ARPC2_MOUSE | 76709 | Actin-related protein 2/3 complex subunit 2 | 115 | 86.9 | 25% | 7 | 34.3 | 6.84 |
| 837 | ATP5H_MOUSE | 71679 | ATP synthase subunit d, mitochondrial | 150 | 59.3 | 73% | 11 | 18.7 | 5.52 |
| 842 | ATPA_MOUSE | 11946 | ATP synthase subunit alpha, mitochondrial | 459 | 346.0 | 33% | 19 | 59.7 | 9.22 |
| 846 | ACTG_MOUSE | 11465 | Actin, cytoplasmic 2 | 388 | 241.1 | 58% | 20 | 41.8 | 5.31 |
| 853 | ATPA_MOUSE | 11946 | ATP synthase subunit alpha, mitochondrial | 574 | 506.8 | 29% | 13 | 59.7 | 9.22 |
| 859 | PRDX1_MOUSE | 18477 | Peroxiredoxin-1 | 623 | 450.0 | 76% | 18 | 22.2 | 8.26 |
| 860 | RAB1B_MOUSE | 76308 | Ras-related protein Rab-1B | 422 | 277.1 | 84% | 16 | 22.2 | 5.55 |
| 865 | DHE3_MOUSE | 14661 | Glutamate dehydrogenase 1, mitochondrial | 159 | 141.6 | 18% | 7 | 61.3 | 8.05 |
| 868 | ROA3_MOUSE | 229279 | Heterogeneous nuclear ribonucleoprotein A3 | 405 | 242.1 | 39% | 21 | 39.6 | 9.10 |
| 873 | SORCN_MOUSE | 109552 | Sorcin | 174 | 131.4 | 47% | 7 | 21.6 | 5.32 |
| 880 | PRDX1_MOUSE | 18477 | Peroxiredoxin-1 | 519 | 355.9 | 78% | 17 | 22.2 | 8.26 |
| 883 | ATPA_MOUSE | 11946 | ATP synthase subunit alpha, mitochondrial | 258 | 217.6 | 26% | 10 | 59.7 | 9.22 |
| 885 | ACTB_MOUSE | 11461 | Actin, cytoplasmic 1 | 112.0 | 90.3 | 27% | 6 | 41.7 | 5.29 |
| 885 | PDIA3_MOUSE | 14827 | Protein disulfide-isomerase A3 | 97 | 53.2 | 31% | 11 | 56.6 | 5.88 |
| 886 | ACTB_MOUSE | 11461 | Actin, cytoplasmic 1 | 510 | 452.6 | 38% | 11 | 41.7 | 5.29 |

| *Spot* | *Accession Number* | *Gene entrez ID* | *Protein Name* | *Protein Score* | *Total Ion Score* | *Sequence coverage* | *Peptide Count* | *Theoretical MW (kDa)* | *Theoretical pI* |
|---|---|---|---|---|---|---|---|---|---|
| 894 | 1433Z_MOUSE | 22631 | 14-3-3 protein zeta/delta | 680.0 | 528.7 | 68% | 20 | 27.8 | 4.73 |
| 894 | SNX5_MOUSE | 69178 | Sorting nexin-5 | 162 | 117.7 | 28% | 10 | 46.8 | 6.19 |
| 895 | PPGB_MOUSE | 19025 | Lysosomal protective protein | 429 | 366.5 | 24% | 14 | 53.8 | 5.56 |
| 896 | VIME_MOUSE | 22352 | Vimentin | 491 | 380.2 | 41% | 18 | 53.7 | 5.06 |
| 898 | ACTG_MOUSE | 11465 | Actin, cytoplasmic 2 | 201 | 160.9 | 40% | 9 | 41.8 | 5.31 |
| 901 | ALDH2_MOUSE | 11669 | Aldehyde dehydrogenase, mitochondrial | 271 | 205.2 | 26% | 14 | 56.5 | 7.53 |
| 902 | 1433F_MOUSE | 22629 | 14-3-3 protein eta | 63.2 | 40.9 | 36% | 5 | 28.2 | 4.81 |
| 911 | CNPY2_MOUSE | 56530 | Protein canopy homolog 2 | 184 | 112.4 | 71% | 10 | 20.8 | 4.95 |
| 920 | ACTB_MOUSE | 11461 | Actin, cytoplasmic 1 | 235 | 179.0 | 31% | 11 | 41.7 | 5.29 |
| 927 | IF5A1_MOUSE | 276770 | Eukaryotic translation initiation factor 5A-1 | 363 | 289.0 | 59% | 10 | 16.8 | 5.08 |
| 938 | CYB5_MOUSE | 109672 | Cytochrome b5 | 485 | 393.0 | 56% | 10 | 15.2 | 4.96 |
| 945 | ACTB_MOUSE | 11461 | Actin, cytoplasmic 1 | 297 | 257.8 | 30% | 9 | 41.7 | 5.29 |
| 946 | MYL6_MOUSE | 17904 | Myosin light polypeptide 6 | 399 | 303.3 | 66% | 12 | 16.9 | 4.56 |
| 948 | SODC_MOUSE | 20655 | Superoxide dismutase [Cu-Zn] | 305 | 238.7 | 49% | 8 | 15.9 | 6.02 |
| 955 | ATPD_MOUSE | 66043 | ATP synthase subunit delta, mitochondrial | 138 | 106.7 | 41% | 5 | 17.6 | 5.03 |
| 959 | ACTC_MOUSE | 11464 | Actin, alpha cardiac muscle 1 | 210 | 169.1 | 20% | 9 | 42.0 | 5.23 |
| 960 | COTL1_MOUSE | 72042 | Coactosin-like protein | 202 | 112.7 | 69% | 11 | 15.9 | 5.28 |
| 973 | LEG1_MOUSE | 16852 | Galectin-1 | 502 | 361.4 | 77% | 14 | 14.9 | 5.32 |
| 974 | ATPA_MOUSE | 11946 | ATP synthase subunit alpha, mitochondrial | 146.0 | 97.2 | 25% | 12 | 59.7 | 9.22 |
| 974 | THIO_MOUSE | 22166 | Thioredoxin | 122 | 85.0 | 62% | 6 | 11.7 | 4.80 |
| 975 | CATD_MOUSE | 13033 | Cathepsin D | 212 | 193.5 | 16% | 6 | 44.9 | 6.71 |
| 976 | CATD_MOUSE | 13033 | Cathepsin D | 359 | 346.6 | 13% | 4 | 44.9 | 6.71 |
| 1015 | VIME_MOUSE | 22352 | Vimentin | 441 | 278.5 | 60% | 23 | 53.7 | 5.06 |
| 1021 | ITAM_MOUSE | 16409 | Integrin alpha-M | 421.0 | 244.7 | 37% | 33 | 127.4 | 6.87 |
| 1021 | MYOF_MOUSE | 226101 | Myoferlin | 331.0 | 36.1 | 32% | 55 | 233.2 | 5.83 |
| 1029 | ACADS_MOUSE | 11409 | Short-chain specific acyl-CoA dehydrogenase, mitochondrial | 707 | 439.3 | 67% | 30 | 44.9 | 8.96 |
| 1030 | ACDSB_MOUSE | 66885 | Short/branched chain specific acyl-CoA dehydrogenase, mitochondrial | 740 | 459.9 | 70% | 31 | 47.8 | 8.00 |
| 1032 | STML2_MOUSE | 66592 | Stomatin-like protein 2 | 232 | 141.9 | 53% | 14 | 38.4 | 8.95 |
| 1034 | IIGP1_MOUSE | 60440 | Interferon-inducible GTPase 1 | 646.0 | 428.1 | 63% | 27 | 47.5 | 6.00 |
| 1034 | COR1A_MOUSE | 12721 | Coronin-1A | 115.0 | 50.4 | 32% | 13 | 51.0 | 6.05 |
| 1036 | ALDH2_MOUSE | 11669 | Aldehyde dehydrogenase, mitochondrial | 439 | 280.8 | 49% | 23 | 56.5 | 7.53 |
| 1038 | ENOA_MOUSE | 13806 | Alpha-enolase | 273 | 106.8 | 62% | 22 | 47.1 | 6.37 |
| 1039 | AL1B1_MOUSE | 72535 | Aldehyde dehydrogenase X, mitochondrial | 307 | 201.3 | 44% | 18 | 57.5 | 6.59 |
| 1045 | PDIA6_MOUSE | 71853 | Protein disulfide-isomerase A6 | 558 | 458.0 | 36% | 16 | 48.1 | 5.00 |
| 1047 | IVD_MOUSE | 56357 | Isovaleryl-CoA dehydrogenase, mitochondrial | 212 | 152.9 | 38% | 12 | 46.3 | 8.53 |
| 1049 | ENOA_MOUSE | 13806 | Alpha-enolase | 345 | 162.5 | 68% | 23 | 47.1 | 6.37 |
| 1050 | TPP1_MOUSE | 12751 | Tripeptidyl-peptidase 1 | 394 | 379.4 | 14% | 6 | 61.3 | 6.10 |
| 1051 | ITAM_MOUSE | 16409 | Integrin alpha-M | 160 | 77.4 | 26% | 22 | 127.4 | 6.87 |
| 1068 | CATB_MOUSE | 13030 | Cathepsin B | 84.4 | 67.1 | 21% | 5 | 37.3 | 5.57 |

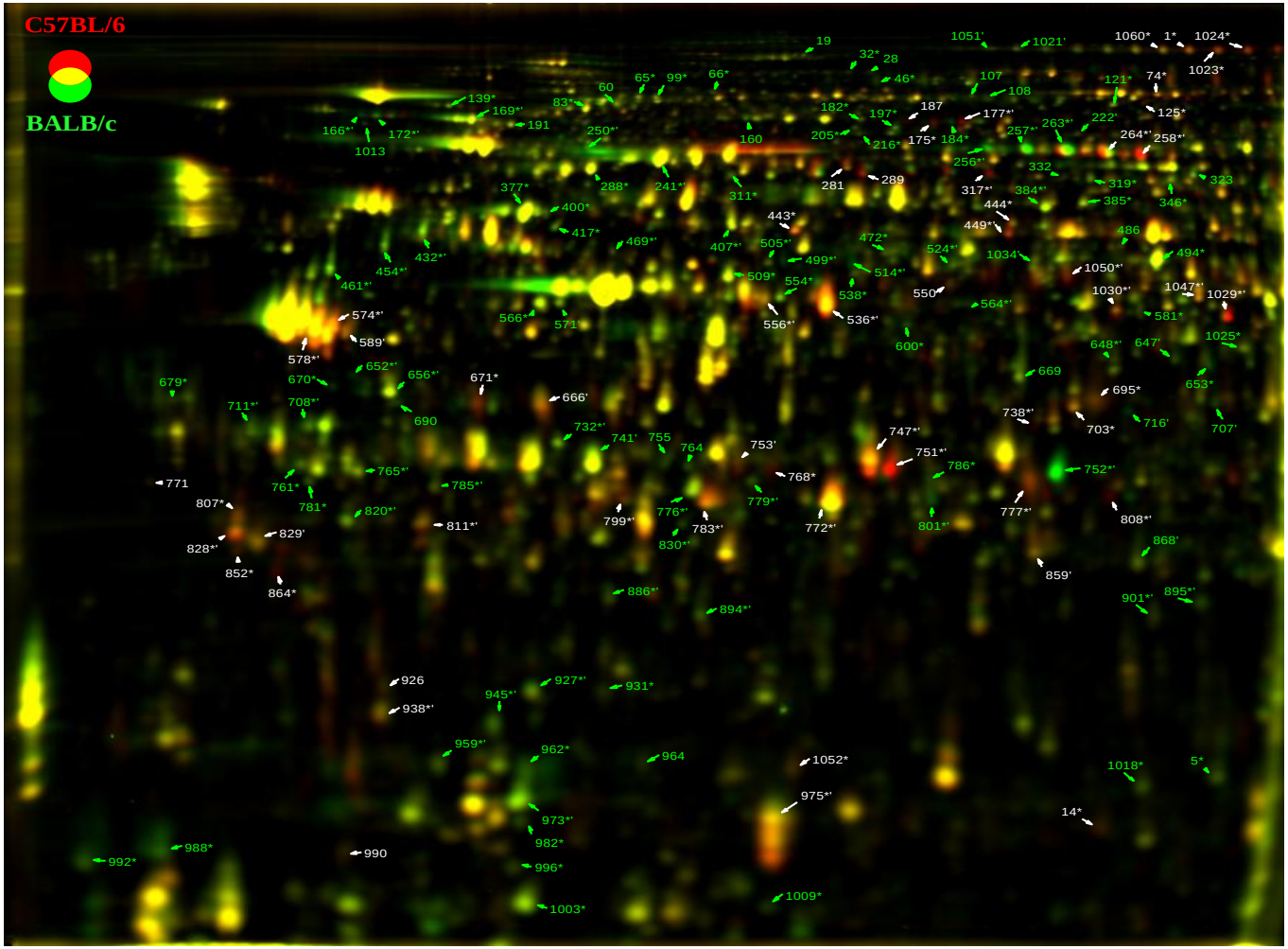


**Figure A.2: Representative gel image BMM-BALB/c versus BMM-C57BL/6 in control condition.** Representative overlay image of protein patterns of the control BMM-BALB/c (green colour) and control BMM-C57BL/6 (red colour). 168 protein spots identified at different levels in control BMM-BALB/c and control BMM-C57BL/6 are labeled with spot number. 82 protein spots were successfully identified with MALDI-MS/MS. Spot colour indicates the different in protein abundance between to mouse strains: red = higher in control BMM-C57BL/6; green = lower in control BMM-C57BL/6; yellow = equal between control BMM-BALB/c and control BMM-C57BL/6. Higher- and lower-existing protein spots in control BMM-C57BL/6 can be also distinguished by white and green letters, respectively. Symbol ***** indicate protein spots which identified at different levels in BMM-BALB/c and BMM-C57BL/6 in both control and IFN-γ treatment condition. Symbol **'** indicates successfully identified proteins spots with MALDI-MS/MS.

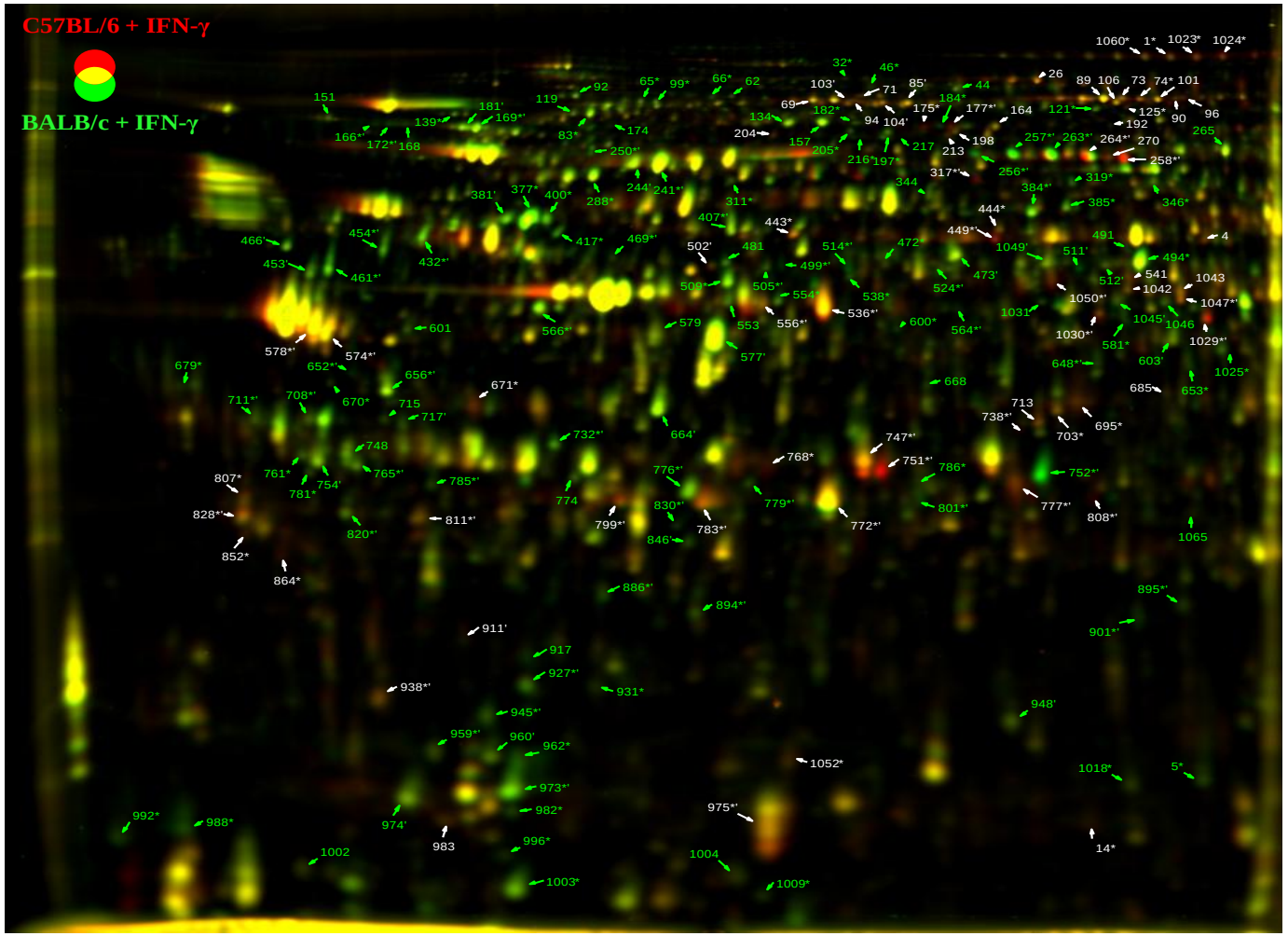


**Figure A.3: Representative gel image BMM-BALB/c versus BMM-C57BL/6 in IFN-γ treatment condition.** Representative overlay image of 2D protein expression patterns of the IFN-γ stimulated BMM-BALB/c (green colour) and IFN-γ stimulated BMM-C57BL/6 (red colour). 204 protein spots identified at different levels in IFN-γ stimulated BMM-BALB/c and IFN-γ stimulated BMM-C57BL/6 are labeled with spot number. 91 protein spots were successfully identified with MALDI-MS/MS. Spot colour indicates the different in protein abundance between to mouse strains: red = higher in IFN-γ stimulated BMM-C57BL/6; green = lower in IFN-γ stimulated BMM-C57BL/6; yellow = equal between IFN-γ stimulated BMM-BALB/c and IFN-γ stimulated BMM-C57BL/6. Higher- and lower-existing protein spots in IFN-γ stimulated BMM-C57BL/6 can be also distinguished by white and green letters, respectively. Symbol ***** indicate protein spots which identified at different levels in BMM-BALB/c and BMM-C57BL/6 in both control and IFN-γ treatment condition. Symbol **'** indicates successfully identified proteins spots with MALDI-MS/MS.

**Table A.2: Thirteen protein spots identified as different level in BMM-BALB/c and BMM-C57BL/6 which contained more than 1 protein/spot.**

| *Spot* | *Accession Number* | *Gene entrez ID* | *Protein Name* | *Fold change ('C57BL/6' /'BALB/c')* | *Fold change ('C57BL/6+IFN' /'BALB/c+IFN')* | *MW (kDa)* | *Protein pI* |
|---|---|---|---|---|---|---|---|
| 250* | CLH_MOUSE | 67300 | Clathrin heavy chain 1 | -1.92 | -1.91 | 191.4 | 5.48 |
| 250* | PKHO2_MOUSE | 102595 | Pleckstrin homology domain-containing family O member 2 | -1.92 | -1.91 | 53.8 | 5.4 |
| 512 | AL3B1_MOUSE | 67689 | Aldehyde dehydrogenase family 3 member B1 | - | -1.59 | 52.3 | 7.5 |
| 512 | METK2_MOUSE | 232087 | S-adenosylmethionine synthetase isoform type-2 | - | -1.59 | 43.7 | 6.02 |
| 536* | ACTG_MOUSE | 11465 | Actin, cytoplasmic 2 | 2.51 | 2.42 | 41.8 | 5.31 |
| 536* | CATD_MOUSE | 13033 | Cathepsin D | 2.51 | 2.42 | 44.9 | 6.71 |
| 556* | CSN4_MOUSE | 26891 | COP9 signalosome complex subunit 4 | 1.56 | 1.63 | 46.3 | 5.57 |
| 556* | PON3_MOUSE | 269823 | Serum paraoxonase/lactonase 3 | 1.56 | 1.63 | 39.3 | 5.44 |
| 648* | ALDH2_MOUSE | 11669 | Aldehyde dehydrogenase, mitochondrial | -1.62 | -1.83 | 56.5 | 7.53 |
| 648* | SFPQ_MOUSE | 71514 | Splicing factor, proline- and glutamine-rich | -1.62 | -1.83 | 75.4 | 9.45 |
| 738* | DHB8_MOUSE | 14979 | Estradiol 17-beta-dehydrogenase 8 | 1.82 | 3.13 | 26.6 | 6.1 |
| 738* | EXOS6_MOUSE | 72544 | Exosome complex exonuclease MTR3 | 1.82 | 3.13 | 28.4 | 5.87 |
| 753 | CATD_MOUSE | 13033 | Cathepsin D | 1.58 | - | 44.9 | 6.71 |
| 753 | OSTF1_MOUSE | 20409 | Osteoclast-stimulating factor 1 | 1.58 | - | 23.8 | 5.46 |
| 753 | VATA_MOUSE | 11964 | Vacuolar ATP synthase catalytic subunit A | 1.58 | - | 68.3 | 5.42 |
| 808* | MA2B1_MOUSE | 17159 | Lysosomal alpha-mannosidase | 4.48 | 8.71 | 114.5 | 8.3 |
| 808* | PRDX6_MOUSE | 11758 | Peroxiredoxin-6 | 4.48 | 8.71 | 24.9 | 5.71 |
| 830* | ALDH2_MOUSE | 11669 | Aldehyde dehydrogenase, mitochondrial | -3.10 | -2.73 | 56.5 | 7.53 |
| 830* | NDUV2_MOUSE | 72900 | NADH dehydrogenase [ubiquinone] flavoprotein 2, mitochondrial | -3.10 | -2.73 | 27.3 | 7 |
| 894* | 1433Z_MOUSE | 22631 | 14-3-3 protein zeta/delta | -1.83 | -1.62 | 27.8 | 4.73 |
| 894* | SNX5_MOUSE | 69178 | Sorting nexin-5 | -1.83 | -1.62 | 46.8 | 6.19 |
| 974 | ATPA_MOUSE | 11946 | ATP synthase subunit alpha, mitochondrial | - | -1.61 | 59.7 | 9.22 |
| 974 | THIO_MOUSE | 22166 | Thioredoxin | - | -1.61 | 11.7 | 4.8 |
| 1021 | ITAM_MOUSE | 16409 | Integrin alpha-M | -1.56 | - | 127.4 | 6.87 |
| 1021 | MYOF_MOUSE | 226101 | Myoferlin | -1.56 | - | 233.2 | 5.83 |
| 1034 | COR1A_MOUSE | 12721 | Coronin-1A | -1.53 | - | 51.0 | 6.05 |
| 1034 | IIGP1_MOUSE | 60440 | Interferon-inducible GTPase 1 | -1.53 | - | 47.5 | 6 |

The 13 protein spots contained total 25 proteins. These proteins were identified as different levels between two mouse strains and contained two proteins/spot. Symbol ***** indicate protein spots which identified at different levels in BMM-BALB/c and BMM-C57BL/6 in both control and IFN-γ treatment condition. Positive fold change value means higher in BMM-C57BL/6, negative value means lower in BMM-C57BL/6.

**Table A.3: Five proteins of which total amount were equal, however their protein isoforms were differently distributed in two mouse strains**.

| *Spot* | *Accession Number* | *Gene entrez ID* | *Protein Name* | *Fold change ('C57BL/6' /'BALB/c')* | *Fold change ('C57BL/6+IFN' /'BALB/c+IFN')* | *MW (kDa)* | *Protein pI* |
|---|---|---|---|---|---|---|---|
| 886* | ACTB_MOUSE | 11461 | Actin, cytoplasmic 1 | -1.76 | -2.06 | 41.7 | 5.29 |
| 945* | ACTB_MOUSE | 11461 | Actin, cytoplasmic 1 | -2.09 | -2.90 | 41.7 | 5.29 |
| 566* | ACTG_MOUSE | 11465 | Actin, cytoplasmic 2 | -1.61 | -1.84 | 41.8 | 5.31 |
| 571 | ACTG_MOUSE | 11465 | Actin, cytoplasmic 2 | -1.50 | - | 41.8 | 5.31 |
| 577 | ACTG_MOUSE | 11465 | Actin, cytoplasmic 2 | - | -1.65 | 41.8 | 5.31 |
| 717 | ACTG_MOUSE | 11465 | Actin, cytoplasmic 2 | - | -1.72 | 41.8 | 5.31 |
| 776* | ACTG_MOUSE | 11465 | Actin, cytoplasmic 2 | -1.53 | -1.82 | 41.8 | 5.31 |
| 846 | ACTG_MOUSE | 11465 | Actin, cytoplasmic 2 | - | -2.10 | 41.8 | 5.31 |
| 256* | BGLR_MOUSE | 110006 | Beta-glucuronidase | -2.08 | -1.80 | 74.2 | 6.16 |
| 257* | BGLR_MOUSE | 110006 | Beta-glucuronidase | -5.06 | -4.91 | 74.2 | 6.16 |
| 258* | BGLR_MOUSE | 110006 | Beta-glucuronidase | 3.21 | 3.48 | 74.2 | 6.16 |
| 263* | BGLR_MOUSE | 110006 | Beta-glucuronidase | -2.33 | -2.27 | 74.2 | 6.16 |
| 264* | BGLR_MOUSE | 110006 | Beta-glucuronidase | 1.86 | 1.94 | 74.2 | 6.16 |
| 317* | BGLR_MOUSE | 110006 | Beta-glucuronidase | 1.72 | 2.12 | 74.2 | 6.16 |
| 751* | ERP29_MOUSE | 67397 | Endoplasmic reticulum protein ERp29 | 4.90 | 5.57 | 28.8 | 5.9 |
| 752* | ERP29_MOUSE | 67397 | Endoplasmic reticulum protein ERp29 | -11.40 | -9.06 | 28.8 | 5.9 |
| 381 | VIME_MOUSE | 22352 | Vimentin | - | -2.42 | 53.7 | 5.06 |
| 432* | VIME_MOUSE | 22352 | Vimentin | -1.82 | -2.04 | 53.7 | 5.06 |
| 453 | VIME_MOUSE | 22352 | Vimentin | - | -2.06 | 53.7 | 5.06 |
| 454* | VIME_MOUSE | 22352 | Vimentin | -3.07 | -3.31 | 53.7 | 5.06 |
| 461* | VIME_MOUSE | 22352 | Vimentin | -2.95 | -3.81 | 53.7 | 5.06 |
| 574* | VIME_MOUSE | 22352 | Vimentin | 2.21 | 1.58 | 53.7 | 5.06 |
| 578* | VIME_MOUSE | 22352 | Vimentin | 2.42 | 1.89 | 53.7 | 5.06 |
| 589 | VIME_MOUSE | 22352 | Vimentin | 1.92 | - | 53.7 | 5.06 |
| 828* | VIME_MOUSE | 22352 | Vimentin | 2.51 | 2.03 | 53.7 | 5.06 |
| 829 | VIME_MOUSE | 22352 | Vimentin | 1.68 | - | 53.7 | 5.06 |

The 25 protein spots which were identified as different levels in BMM-BALB/c and BMM-C57BL/6 contained 5 proteins. Each of 5 proteins had some isoforms existed in higher levels in BMMs of one strain, however some other of it isoform existed in higher levels in the other strain. Symbol ***** indicate protein spots which identified at different levels in BMM-BALB/c and BMM-C57BL/6 in both control and IFN-γ treatment condition. Positive fold change value means higher in BMM-C57BL/6, negative value means lower in BMM-C57BL/6.

**Table A.4: Twenty three proteins of which total amount might be significant different in two strains.**

| *Spot* | *Accession Number* | *Gene entrez ID* | *Protein Name* | *Fold change ('C57BL/6' /'BALB/c')* | *Fold change ('C57BL/6+IFN' /'BALB/c+IFN')* | *MW (kDa)* | *Protein pI* |
|---|---|---|---|---|---|---|---|
| **765*** | 1433F_MOUSE | 22629 | 14-3-3 protein eta | -1.61 | -1.66 | 28.2 | 4.81 |
| **754** | 1433Z_MOUSE | 22631 | 14-3-3 protein zeta/delta | - | -1.53 | 27.8 | 4.73 |
| **505*** | ARP3_MOUSE | 74117 | Actin-related protein 3 | -1.66 | -1.86 | 47.3 | 5.61 |
| **901*** | ALDH2_MOUSE | 11669 | Aldehyde dehydrogenase, mitochondrial | -1.63 | -2.51 | 56.5 | 7.53 |
| **1049** | ENOA_MOUSE | 13806 | Alpha-enolase | - | -1.54 | 47.1 | 6.37 |
| **603** | ANXA1_MOUSE | 16952 | Annexin A1 | - | -1.71 | 38.7 | 6.97 |
| **656*** | ANXA5_MOUSE | 11747 | Annexin A5 | -1.73 | -1.74 | 35.7 | 4.83 |
| **741** | CATB_MOUSE | 13030 | Cathepsin B | -1.72 | - | 37.3 | 5.57 |
| **747*** | CATD_MOUSE | 13033 | Cathepsin D | 2.46 | 2.49 | 44.9 | 6.71 |
| **777*** | CATD_MOUSE | 13033 | Cathepsin D | 2.34 | 2.37 | 44.9 | 6.71 |
| **975*** | CATD_MOUSE | 13033 | Cathepsin D | 1.73 | 1.72 | 44.9 | 6.71 |
| **772*** | CATS_MOUSE | 13040 | Cathepsin S | 1.70 | 1.57 | 38.4 | 6.51 |
| **783*** | CATS_MOUSE | 13040 | Cathepsin S | 2.02 | 1.84 | 38.4 | 6.51 |
| **799*** | CATS_MOUSE | 13040 | Cathepsin S | 2.15 | 2.27 | 38.4 | 6.51 |
| **666** | CATZ_MOUSE | 64138 | Cathepsin Z | 1.63 | - | 34.0 | 6.13 |
| **384*** | COR1A_MOUSE | 12721 | Coronin-1A | -1.77 | -2.14 | 51.0 | 6.05 |
| **407*** | CNDP2_MOUSE | 66054 | Cytosolic non-specific dipeptidase | -1.62 | -1.55 | 52.7 | 5.43 |
| **103** | ERAP1_MOUSE | 80898 | Endoplasmic reticulum aminopeptidase 1 | - | 1.65 | 106.5 | 5.77 |
| **499*** | HA12_MOUSE | 14964 | H-2 class I histocompatibility antigen, D-D alpha chain | -143.06 | -100.70 | 41.1 | 6.22 |
| **514*** | HA12_MOUSE | 14964 | H-2 class I histocompatibility antigen, D-D alpha chain | -5.56 | -3.64 | 41.1 | 6.22 |
| **241*** | HSP7C_MOUSE | 15481 | Heat shock cognate 71 kDa protein | -1.53 | -1.62 | 70.8 | 5.37 |
| **244** | HSP7C_MOUSE | 15481 | Heat shock cognate 71 kDa protein | - | -1.63 | 70.8 | 5.37 |
| **169*** | HS90B_MOUSE | 15516 | Heat shock protein HSP 90-beta | -1.89 | -2.11 | 83.3 | 4.97 |
| **1051** | ITAM_MOUSE | 16409 | Integrin alpha-M | -1.79 | - | 127.4 | 6.87 |
| **895*** | PPGB_MOUSE | 19025 | Lysosomal protective protein | -2.09 | -1.76 | 53.8 | 5.56 |
| **859** | PRDX1_MOUSE | 18477 | Peroxiredoxin-1 | 1.54 | - | 22.2 | 8.26 |
| **801*** | PRDX6_MOUSE | 11758 | Peroxiredoxin-6 | -2.15 | -2.26 | 24.9 | 5.71 |
| **652*** | PDIA6_MOUSE | 71853 | Protein disulfide-isomerase A6 | -10.19 | -7.48 | 48.1 | 5 |
| **1045** | PDIA6_MOUSE | 71853 | Protein disulfide-isomerase A6 | - | -1.57 | 48.1 | 5 |
| **708*** | TPM3_MOUSE | 59069 | Tropomyosin alpha-3 chain | -1.50 | -1.87 | 32.8 | 4.68 |

Each of 23 proteins had some but not all of identified isoforms existed in higher levels in BMMs of one mouse strain. Symbol ***** indicate protein spots which identified at different levels in BMM-BALB/c and BMM-C57BL/6 in both control and IFN-γ treatment condition. Positive fold change value means higher in BMM-C57BL/6, negative value means lower in BMM-C57BL/6.

**Table A.5: Thirty five proteins of which total amount was significant different in two strains**.

| *Spot* | *Accession Number* | *Gene entrez ID* | *Protein Name* | *Fold change ('C57BL/6' /'BALB/c')* | *Fold change ('C57BL/6+IFN' /'BALB/c+IFN')* | *MW (kDa)* | *Protein pI* |
|---|---|---|---|---|---|---|---|
| **716** | THTM_MOUSE | 246221 | 3-mercaptopyruvate sulfurtransferase | -6.15 | - | 33.0 | 6.11 |
| **524*** | CH60_MOUSE | 15510 | 60 kDa heat shock protein, mitochondrial | -1.84 | -1.70 | 60.9 | 5.91 |
| **959*** | ACTC_MOUSE | 11464 | Actin, alpha cardiac muscle 1 | -1.61 | -1.85 | 42.0 | 5.23 |
| **664** | ANXA4_MOUSE | 11746 | Annexin A4 | - | -1.66 | 36.0 | 5.43 |
| **647** | CATL1_MOUSE | 13039 | Cathepsin L1 | -3.36 | - | 37.5 | 6.37 |
| **732*** | CLIC1_MOUSE | 114584 | Chloride intracellular channel protein 1 | -1.54 | -1.98 | 27.0 | 5.09 |
| **960** | COTL1_MOUSE | 72042 | Coactosin-like protein | - | -1.68 | 15.9 | 5.28 |
| **938*** | CYB5_MOUSE | 109672 | Cytochrome b5 | 1.51 | 1.61 | 15.2 | 4.96 |
| **449*** | ODO2_MOUSE | 78920 | Dihydrolipoyllysine-residue succinyltransferase component of 2-oxoglutarate dehydrogenase complex, mitochondrial | 2.80 | 4.99 | 49.0 | 9.11 |
| **502** | OST48_MOUSE | 13200 | Dolichyl-diphosphooligosaccharide-protein glycosyltransferase 48kDa subunit | - | 1.78 | 49.0 | 5.52 |
| **711*** | EF1B_MOUSE | 55949 | Elongation factor 1-beta | -1.70 | -2.10 | 24.7 | 4.53 |
| **927*** | IF5A1_MOUSE | 276770 | Eukaryotic translation initiation factor 5A-1 | -1.76 | -2.21 | 16.8 | 5.08 |
| **973*** | LEG1_MOUSE | 16852 | Galectin-1 | -2.08 | -2.37 | 14.9 | 5.32 |
| **811*** | SAP3_MOUSE | 14667 | Ganglioside GM2 activator | 1.82 | 1.52 | 20.8 | 5.63 |
| **707** | GNPI1_MOUSE | 26384 | Glucosamine-6-phosphate isomerase 1 | -1.65 | - | 32.5 | 6 |
| **181** | HS90A_MOUSE | 15519 | Heat shock protein HSP 90-alpha | - | -1.97 | 84.7 | 4.93 |
| **166*** | HCLS1_MOUSE | 15163 | Hematopoietic lineage cell-specific protein | -4.50 | -4.49 | 54.2 | 4.73 |
| **172*** | HCLS1_MOUSE | 15163 | Hematopoietic lineage cell-specific protein | -3.30 | -3.85 | 54.2 | 4.73 |
| **868** | ROA3_MOUSE | 229279 | Heterogeneous nuclear ribonucleoprotein A3 | -1.62 | - | 39.6 | 9.1 |
| **469*** | HNRPF_MOUSE | 98758 | Heterogeneous nuclear ribonucleoprotein F | -1.76 | -2.03 | 45.7 | 5.31 |
| **1047*** | IVD_MOUSE | 56357 | Isovaleryl-CoA dehydrogenase, mitochondrial | 1.52 | 2.15 | 46.3 | 8.53 |
| **85** | LONM_MOUSE | 74142 | Lon protease homolog, mitochondrial | - | 1.60 | 105.8 | 6.15 |
| **104** | LONM_MOUSE | 74142 | Lon protease homolog, mitochondrial | - | 1.70 | 105.8 | 6.15 |
| **779*** | NDUS3_MOUSE | 68349 | NADH dehydrogenase [ubiquinone] iron-sulfur protein 3, mitochondrial | -1.51 | -1.53 | 30.1 | 6.67 |
| **911** | CNPY2_MOUSE | 56530 | Protein canopy homolog 2 | - | 1.60 | 20.8 | 4.95 |
| **177*** | PDPR_MOUSE | 319518 | Pyruvate dehydrogenase phosphatase regulatory subunit, mitochondrial | 6.23 | 4.80 | 99.2 | 5.93 |
| **473** | GDIB_MOUSE | 14569 | Rab GDP dissociation inhibitor beta | - | -1.62 | 50.5 | 5.93 |
| **785*** | GDIR2_MOUSE | 11857 | Rho GDP-dissociation inhibitor 2 | -1.55 | -2.16 | 22.8 | 4.97 |
| **222** | RHG25_MOUSE | 232201 | Rho GTPase-activating protein 25 | -2.18 | - | 73.3 | 6.03 |
| **466** | RINI_MOUSE | 107702 | Ribonuclease inhibitor | - | -2.21 | 49.8 | 4.69 |
| **511** | SPA3G_MOUSE | 20715 | Serine protease inhibitor A3G | - | -2.33 | 49.0 | 6.06 |
| **1030*** | ACDSB_MOUSE | 66885 | Short/branched chain specific acyl-CoA dehydrogenase, mitochondrial | 2.08 | 2.49 | 47.8 | 8 |
| **1029*** | ACADS_MOUSE | 11409 | Short-chain specific acyl-CoA dehydrogenase, mitochondrial | 3.90 | 3.24 | 44.9 | 8.96 |
| **948** | SODC_MOUSE | 20655 | Superoxide dismutase [Cu-Zn] | - | -1.73 | 15.9 | 6.02 |
| **820*** | TCTP_MOUSE | 22070 | Translationally-controlled tumor protein | -1.58 | -1.61 | 19.4 | 4.76 |
| **1050*** | TPP1_MOUSE | 12751 | Tripeptidyl-peptidase 1 | 2.01 | 2.32 | 61.3 | 6.1 |
| **564*** | MYG1_MOUSE | 60315 | UPF0160 protein MYG1 | -2.70 | -3.44 | 42.7 | 6.54 |

Each of 35 proteins had all of identified isoforms existed in higher levels in BMMs of one mouse strain. Symbol ***** indicate protein spots which identified at different levels in BMM-BALB/c and BMM-C57BL/6 in both control and IFN-γ treatment condition. Positive fold change value means higher in BMM-C57BL/6, negative value means lower in BMM-C57BL/6.

**Table A.6: Fold change of 136 protein spots being present at different levels in a strain dependent manner which were not identified by MALDI-MS/MS**

| *Spot* | *C57BL/6 vs BALB/c* | *C57BL/6+IFN vs BALB/c+IFN* |
|---|---|---|
| 1* | 2.76 | 3.19 |
| 4 | - | 2.23 |
| 5* | -1.63 | -2.16 |
| 14* | 1.80 | 1.68 |
| 19 | -1.57 | - |
| 26 | - | 2.29 |
| 28 | -2.12 | - |
| 32* | -1.75 | -1.55 |
| 44 | - | -1.68 |
| 46* | -2.04 | -1.89 |
| 60 | -1.50 | - |
| 62 | - | -1.64 |
| 65* | -1.51 | -1.68 |
| 66* | -1.71 | -2.21 |
| 69 | - | 1.56 |
| 71 | - | 1.65 |
| 73 | - | 1.98 |
| 74* | 2.01 | 2.49 |
| 83* | -1.52 | -1.56 |
| 89 | - | 1.95 |
| 90 | - | 2.32 |
| 92 | - | -1.52 |
| 94 | - | 1.60 |
| 96 | - | 2.32 |
| 99* | -1.56 | -1.57 |
| 101 | - | 2.03 |
| 106 | - | 1.73 |
| 107 | -1.81 | - |
| 108 | -1.79 | - |
| 119 | - | -1.68 |
| 121* | -1.52 | -1.78 |
| 125* | 2.04 | 2.30 |
| 134 | - | -1.67 |
| 139* | -1.99 | -2.01 |
| 151 | - | -1.64 |
| 157 | - | -1.82 |
| 160 | -1.63 | - |
| 164 | - | 1.56 |
| 168 | - | -1.66 |
| 174 | - | -1.50 |
| 175* | 2.86 | 2.32 |

| *Spot* | *C57BL/6 vs BALB/c* | *C57BL/6+IFN vs BALB/c+IFN* |
|---|---|---|
| 182* | -1.78 | -1.76 |
| 184* | -4.46 | -2.89 |
| 187 | 1.60 | - |
| 191 | -1.75 | - |
| 192 | - | 1.56 |
| 197* | -2.50 | -1.84 |
| 198 | - | 1.60 |
| 204 | - | 1.59 |
| 205* | -1.49 | -1.51 |
| 213 | - | 1.53 |
| 216* | -1.92 | -2.14 |
| 217 | - | -1.99 |
| 265 | - | -1.53 |
| 270 | - | 1.63 |
| 281 | 1.99 | - |
| 288* | -1.78 | -1.82 |
| 289 | 1.59 | - |
| 311* | -1.55 | -1.99 |
| 319* | -1.81 | -3.01 |
| 323 | -1.84 | - |
| 332 | -1.56 | - |
| 344 | - | -1.78 |
| 346* | -1.54 | -1.55 |
| 377* | -1.59 | -3.38 |
| 385* | -1.67 | -1.87 |
| 400* | -1.83 | -3.14 |
| 417* | -2.24 | -3.28 |
| 443* | 2.04 | 2.27 |
| 444* | 1.75 | 1.78 |
| 472* | -1.60 | -1.86 |
| 481 | - | -3.24 |
| 486 | -1.62 | - |
| 491 | - | -1.64 |
| 494* | -1.70 | -2.10 |
| 509* | -1.67 | -2.13 |
| 538* | -1.78 | -1.97 |
| 541 | - | 1.58 |
| 550 | 1.67 | - |
| 553 | - | -1.54 |
| 554* | -1.64 | -1.72 |
| 579 | - | -1.76 |

| *Spot* | *C57BL/6 vs BALB/c* | *C57BL/6+IFN vs BALB/c+IFN* |
|---|---|---|
| 581* | -1.98 | -2.83 |
| 600* | -2.26 | -1.74 |
| 601 | - | -1.75 |
| 653* | -2.36 | -2.46 |
| 668 | - | -2.95 |
| 669 | -1.85 | - |
| 670* | -13.41 | -2.13 |
| 671* | 2.00 | 1.72 |
| 679* | -1.61 | -1.54 |
| 685 | - | 1.50 |
| 690 | -2.19 | - |
| 695* | 1.82 | 2.27 |
| 703* | 1.54 | 1.91 |
| 713 | - | 2.07 |
| 715 | - | -1.78 |
| 748 | - | -1.68 |
| 755 | -1.78 | - |
| 761* | -1.59 | -1.58 |
| 764 | -1.50 | - |
| 768* | 2.34 | 2.60 |
| 771 | 2.49 | - |
| 774 | - | -1.72 |
| 781* | -1.97 | -1.65 |
| 786* | -1.59 | -1.58 |
| 807* | 2.54 | 1.82 |
| 852* | 2.34 | 1.73 |
| 864* | 4.11 | 3.15 |
| 917 | - | -2.29 |
| 926 | 1.70 | - |
| 931* | -1.59 | -1.64 |
| 962* | -2.71 | -3.99 |
| 964 | -1.55 | - |
| 982* | -1.58 | -1.59 |
| 983 | - | 1.98 |
| 988* | -2.90 | -3.19 |
| 990 | 1.51 | - |
| 992* | -2.42 | -3.02 |
| 996* | -1.64 | -3.07 |
| 1002 | - | -1.57 |
| 1003* | -1.56 | -2.10 |
| 1004 | - | -1.54 |

| *Spot* | *C57BL/6 vs BALB/c* | *C57BL/6+IFN vs BALB/c+IFN* |
|---|---|---|
| 1009* | -1.86 | -2.22 |
| 1013 | -2.02 | - |
| 1018* | -1.54 | -1.96 |
| 1023* | 4.22 | 4.27 |
| 1024* | 5.09 | 4.85 |
| 1025* | -1.57 | -1.85 |
| 1031 | - | -3.17 |
| 1042 | - | 1.52 |
| 1043 | - | 1.62 |
| 1046 | - | -2.25 |
| 1052* | 1.50 | 1.61 |
| 1060* | 1.92 | 2.32 |
| 1065 | - | -1.50 |

**Table A.7: A total of 343 proteins were identified at different levels in BMM-BALB/c and BMM-C57BL/6 in control and/or IFN-γ treatment condition by LC-MS/MS approach.**

| *Protein* | *Gene Entrez ID* | *Gene Symbol* | *Protein name* | *Fold change (C57BL/6' /'BALB/c')* | *Fold change (C57BL/6+IFN' /'BALB/c+IFN')* |
|---|---|---|---|---|---|
| IPI00330480 | 432987 | - | 35 kDa protein | - | 2.67 |
| IPI00153381* | 66152 | 1110020P15Rik | Cytochrome b-c1 complex subunit 9 | 1.52 | 1.66 |
| IPI00114945* | 18000 | 40422.0 | Septin-2 | -1.71 | -2.04 |
| IPI00224626* | 235072 | 40428.0 | Septin-7 | -1.79 | -1.82 |
| IPI00453792 | 319518 | 4930402E16Rik | Pyruvate dehydrogenase phosphatase regulatory subunit, mitochondrial | - | 1.71 |
| IPI00136293* | 67759 | 5033414D02Rik | Transmembrane protein C9orf46 homolog | 2.46 | 2.38 |
| IPI00857151* | 217830 | 9030617O03Rik | Isoform 1 of UPF0317 protein C14orf159 homolog, mitochondrial | 1.70 | 1.90 |
| IPI00135646* | 19299 | Abcd3 | ATP-binding cassette, sub-family D, member 3 | 1.95 | 1.50 |
| IPI00314069* | 56360 | Acot9 | Acyl-coenzyme A thioesterase 9, mitochondrial | 1.60 | 1.68 |
| IPI00857226* | 14081 | Acsl1 | Long-chain-fatty-acid--CoA ligase 1 | 1.73 | 1.98 |
| IPI00131701 | 50790 | Acsl4 | Isoform Long of Long-chain-fatty-acid--CoA ligase 4 | -1.78 | - |
| IPI00469942 | 68738 | Acss1 | Acetyl-coenzyme A synthetase 2-like, mitochondrial | - | 1.78 |
| IPI00380436* | 109711 | Actn1 | Alpha-actinin-1 | -1.58 | -1.78 |
| IPI00118899* | 60595 | Actn4 | Alpha-actinin-4 | -1.67 | -1.73 |
| IPI00125653 | 11520 | Adfp | adipose differentiation related protein | - | 1.54 |
| IPI00230440* | 269378 | Ahcy | Adenosylhomocysteinase | -1.70 | -1.67 |
| IPI00553798* | 66395 | Ahnak | AHNAK nucleoprotein isoform 1 | -1.82 | -1.71 |
| IPI00169980* | 107197 | AI462493 | UPF0723 protein C11orf83 homolog | 3.66 | 2.90 |
| IPI00116339* | 11629 | Aif1 | Allograft inflammatory factor 1 | -6.21 | -3.63 |
| IPI00466128 | 58810 | Akr1a4 | Alcohol dehydrogenase [NADP+] | - | -1.50 |
| IPI00223757 | 11677 | Akr1b3 | Aldose reductase | - | -2.17 |
| IPI00129350* | 56454 | Aldh18a1 | Isoform Short of Delta-1-pyrroline-5-carboxylate synthetase | 1.87 | 1.75 |
| IPI00330482 | 67689 | Aldh3b1 | Aldehyde dehydrogenase family 3 member B1 | - | 1.52 |
| IPI00405699* | 212647 | Aldh4a1 | Delta-1-pyrroline-5-carboxylate dehydrogenase, mitochondrial | 2.32 | 2.37 |
| IPI00856379 | 11674 | Aldoa | Fructose-bisphosphate aldolase | - | -1.93 |
| IPI00468203* | 12306 | Anxa2 | Annexin A2 | -1.55 | -1.60 |
| IPI00877279 | 11745 | Anxa3 | Annexin A3 | - | -1.75 |
| IPI00877291 | 11746 | Anxa4 | annexin A4 | - | -1.60 |
| IPI00317309* | 11747 | Anxa5 | Annexin A5 | -2.26 | -2.59 |
| IPI00121576 | 68316 | Apoo | Apolipoprotein O | 1.58 | - |
| IPI00625950 | 11821 | Aprt | adenine phosphoribosyl transferase | - | -1.96 |
| IPI00353418 | 232201 | Arhgap25 | Isoform 1 of Rho GTPase-activating protein 25 | - | -1.50 |
| IPI00322312* | 192662 | Arhgdia | Rho GDP-dissociation inhibitor 1 | -1.95 | -2.10 |
| IPI00122568 | 11857 | Arhgdib | Rho GDP-dissociation inhibitor 2 | - | -2.08 |
| IPI00133218 | 67166 | Arl8b | ADP-ribosylation factor-like protein 8B | - | 1.52 |

| *Protein* | *Gene Entrez ID* | *Gene Symbol* | *Protein name* | *Fold change (C57BL/6' /'BALB/c')* | *Fold change (C57BL/6+IFN' /'BALB/c+IFN')* |
|---|---|---|---|---|---|
| IPI00125266* | 11886 | Asah1 | Acid ceramidase | 1.83 | 2.02 |
| IPI00134746 | 11898 | Ass1 | Argininosuccinate synthase | 1.65 | - |
| IPI00330303 | 108147 | Atic | 5-aminoimidazole-4-carboxamide ribonucleotide formyltransferase/IMP cyclohydrolase | - | -2.00 |
| IPI00130280* | 11946 | Atp5a1 | ATP synthase subunit alpha, mitochondrial | 1.56 | 1.62 |
| IPI00468481* | 11947 | Atp5b | ATP synthase subunit beta, mitochondrial | 1.56 | 1.65 |
| IPI00341282* | 11950 | Atp5f1 | ATP synthase subunit b, mitochondrial | 1.58 | 1.62 |
| IPI00133342* | 27425 | Atp5l | ATP synthase subunit g, mitochondrial | 2.00 | 1.78 |
| IPI00407692 | 11964 | Atp6v1a | Isoform 1 of V-type proton ATPase catalytic subunit A | - | 1.52 |
| IPI00118787 | 73834 | Atp6v1d | V-type proton ATPase subunit D | - | -1.62 |
| IPI00120684 | 12028 | Bax | Apoptosis regulator BAX | -1.73 | - |
| IPI00230422 | 27061 | Bcap31 | B-cell receptor-associated protein 31 | - | 2.42 |
| IPI00122442 | 12036 | Bcat2 | Branched-chain-amino-acid aminotransferase, mitochondrial | - | 1.56 |
| IPI00415385 | 72567 | Bclaf1 | Isoform 2 of Bcl-2-associated transcription factor 1 | - | 2.70 |
| IPI00330627* | 109778 | Blvra | Biliverdin reductase A | -1.80 | -2.06 |
| IPI00399958 | 12321 | Calu | calumenin isoform 2 | - | -2.20 |
| IPI00406790 | 108058 | Camk2d | Isoform 4 of Calcium/calmodulin-dependent protein kinase type II delta chain | - | -1.90 |
| IPI00137331 | 12331 | Cap1 | Adenylyl cyclase-associated protein 1 | - | -1.65 |
| IPI00277930 | 12332 | Capg | Macrophage-capping protein | - | -1.76 |
| IPI00308938* | 12334 | Capn2 | Calpain-2 catalytic subunit | -1.68 | -2.09 |
| IPI00757359 | 53872 | Caprin1 | cytoplasmic activation/proliferation-associated protein 1 isoform c | - | -2.13 |
| IPI00125676 | 12362 | Casp1 | Caspase-1 | - | -2.65 |
| IPI00320217 | 12461 | Cct2 | T-complex protein 1 subunit beta | - | -1.67 |
| IPI00116283* | 12462 | Cct3 | T-complex protein 1 subunit gamma | -1.56 | -1.83 |
| IPI00331174 | 12468 | Cct7 | T-complex protein 1 subunit eta | - | -1.59 |
| IPI00469268* | 12469 | Cct8 | T-complex protein 1 subunit theta | -1.55 | -1.67 |
| IPI00112787 | 57781 | Cd200r1 | Cell surface glycoprotein CD200 receptor 1 | -1.67 | - |
| IPI00117031* | 12514 | Cd68 | Isoform Short of Macrosialin | 2.16 | 1.79 |
| IPI00113849 | 12540 | Cdc42 | Isoform 2 of Cell division control protein 42 homolog | 1.56 | - |
| IPI00890117* | 12631 | Cfl1 | Cofilin-1 | -1.83 | -2.05 |
| IPI00157508* | 12655 | Chi3l3 | Chitinase-3-like protein 3 | 12.99 | 13.89 |
| IPI00223047 | 216197 | Ckap4 | Cytoskeleton-associated protein 4 | 1.56 | - |
| IPI00136703* | 12709 | Ckb | Creatine kinase B-type | -1.90 | -2.55 |
| IPI00130344* | 114584 | Clic1 | Chloride intracellular channel protein 1 | -1.96 | -2.33 |
| IPI00153903* | 69634 | Clybl | Citrate lyase subunit beta-like protein, mitochondrial | 2.34 | 2.90 |
| IPI00315879 | 66054 | Cndp2 | Cytosolic non-specific dipeptidase | - | -1.60 |
| IPI00222125 | 69156 | Comtd1 | Catechol-O-methyltransferase domain-containing protein 1 | - | 1.59 |
| IPI00323600* | 12721 | Coro1a | Coronin-1A | -1.65 | -2.57 |
| IPI00124820 | 23790 | Coro1c | Coronin-1C | -1.78 | - |
| IPI00135390* | 78885 | Coro7 | Coronin-7 | -2.00 | -2.63 |
| IPI00117978* | 12857 | Cox4i1 | Cytochrome c oxidase subunit 4 isoform 1, mitochondrial | 1.69 | 1.50 |
| IPI00120719 | 12858 | Cox5a | Cytochrome c oxidase subunit 5A, mitochondrial | 1.63 | - |

| *Protein* | *Gene Entrez ID* | *Gene Symbol* | *Protein name* | *Fold change (C57BL/6' /'BALB/c')* | *Fold change (C57BL/6+IFN' /'BALB/c+IFN')* |
|---|---|---|---|---|---|
| IPI00116154* | 12859 | Cox5b | Cytochrome c oxidase subunit 5B, mitochondrial | 1.80 | 1.59 |
| IPI00225390 | 110323 | Cox6b1 | Cytochrome c oxidase subunit VIb isoform 1 | - | 2.36 |
| IPI00114377 | 12866 | Cox7a2 | Cytochrome c oxidase polypeptide 7A2, mitochondrial | - | 1.51 |
| IPI00330094 | 12894 | Cpt1a | Carnitine O-palmitoyltransferase 1, liver isoform | - | 1.53 |
| IPI00881401 | 12896 | Cpt2 | Carnitine O-palmitoyltransferase 2, mitochondrial | - | 1.76 |
| IPI00125931 | 13014 | Cstb | Cystatin-B | -1.52 | - |
| IPI00658539 | 19025 | Ctsa | cathepsin A isoform a | - | 2.04 |
| IPI00404551 | 13033 | Ctsd | Cathepsin D | - | 1.56 |
| IPI00118987* | 13036 | Ctsh | Cathepsin H | 4.37 | 3.34 |
| IPI00128154* | 13039 | Ctsl | Cathepsin L1 | -2.27 | -1.79 |
| IPI00309520* | 13040 | Ctss | Cathepsin S | 1.66 | 1.69 |
| IPI00230113* | 109672 | Cyb5 | 11 kDa protein | 1.66 | 1.63 |
| IPI00315794* | 66427 | Cyb5b | Cytochrome b5 type B | 1.96 | 2.82 |
| IPI00119131* | 72017 | Cyb5r1 | Isoform 1 of NADH-cytochrome b5 reductase 1 | 2.18 | 1.87 |
| IPI00121079* | 109754 | Cyb5r3 | Isoform 1 of NADH-cytochrome b5 reductase 3 | 1.96 | 1.63 |
| IPI00117117* | 13058 | Cybb | Cytochrome b-245 heavy chain | 2.89 | 2.19 |
| IPI00330476 | 20430 | Cyfip1 | Isoform 2 of Cytoplasmic FMR1-interacting protein 1 | - | -1.80 |
| IPI00230035 | 13205 | Ddx3x | ATP-dependent RNA helicase DDX3X | - | -1.55 |
| IPI00420363 | 13207 | Ddx5 | Probable ATP-dependent RNA helicase DDX5 | -1.50 | - |
| IPI00387379* | 67460 | Decr1 | 2,4-dienoyl-CoA reductase, mitochondrial | 1.68 | 1.72 |
| IPI00134506* | 27369 | Dguok | Isoform 2 of Deoxyguanosine kinase, mitochondrial | -2.73 | -1.87 |
| IPI00331549 | 52585 | Dhrs1 | Dehydrogenase/reductase SDR family member 1 | - | 1.61 |
| IPI00153660 | 235339 | Dlat | Dihydrolipoyllysine-residue acetyltransferase component of pyruvate dehydrogenase complex, mitochondrial | - | 1.51 |
| IPI00131445 | 13430 | Dnm2 | Isoform 1 of Dynamin-2 | - | -1.64 |
| IPI00114375 | 12934 | Dpysl2 | Dihydropyrimidinase-related protein 2 | - | -1.69 |
| IPI00127942 | 56431 | Dstn | Destrin | - | -1.82 |
| IPI00119876 | 13424 | Dync1h1 | Cytoplasmic dynein 1 heavy chain 1 | - | -1.64 |
| IPI00454049* | 93747 | Echs1 | Enoyl-CoA hydratase, mitochondrial | 1.79 | 1.69 |
| IPI00320208* | 55949 | Eef1b2 | Elongation factor 1-beta | -1.95 | -2.66 |
| IPI00118875* | 66656 | Eef1d | eukaryotic translation elongation factor 1 delta isoform b | -1.76 | -2.38 |
| IPI00466069 | 13629 | Eef2 | Elongation factor 2 | - | -1.58 |
| IPI00226872 | 27984 | Efhd2 | EF-hand domain-containing protein D2 | - | -2.67 |
| IPI00762705 | 233637 | EG233637 | similar to Twinfilin, actin-binding protein, homolog 1 | - | -1.97 |
| IPI00470152 | 78294 | Rps27a | ribosomal protein S27a | -1.59 | - |
| IPI00622837 | 621837 | EG621837 | hypothetical protein | - | 1.74 |
| IPI00626366* | 667618 | EG667618 | similar to Acidic ribosomal phosphoprotein P0 | -1.85 | -1.98 |
| IPI00318671* | 98878 | Ehd4 | EH-domain containing 4-KJR (Fragment) | -1.74 | -1.91 |
| IPI00265239* | 13063 | Cycs | Cytochrome c, somatic | 1.59 | 1.69 |
| IPI00137736* | 54127 | Rps28 | 40S ribosomal protein S28 | -2.05 | -2.85 |
| IPI00330289* | 13822 | Epb4.1l2 | Band 4.1-like protein 2 | -1.54 | -1.71 |

| *Protein* | *Gene Entrez ID* | *Gene Symbol* | *Protein name* | *Fold change (C57BL/6' /'BALB/c')* | *Fold change (C57BL/6+IFN' /'BALB/c+IFN')* |
|---|---|---|---|---|---|
| IPI00121440 | 110826 | Etfb | Electron transfer flavoprotein subunit beta | 1.56 | - |
| IPI00753434* | 100047333 | Evl | Isoform 2 of Ena/VASP-like protein | -1.81 | -2.50 |
| IPI00330862 | 22350 | Ezr | Ezrin | - | -1.55 |
| IPI00116705* | 11770 | Fabp4 | Fatty acid-binding protein, adipocyte | 1.75 | 2.52 |
| IPI00330695 | 227737 | Fam129b | Niban-like protein 1 | - | -1.60 |
| IPI00122015* | 223601 | Fam49b | Protein FAM49B | -1.60 | -1.90 |
| IPI00169731* | 108101 | Fermt3 | Fermitin family homolog 3 | -1.58 | -1.77 |
| IPI00921658* | 192176 | Flna | Isoform 1 of Filamin-A | -1.64 | -1.76 |
| IPI00117181* | 14251 | Flot1 | Flotillin-1 | 2.58 | 2.00 |
| IPI00673288* | 634386 | Ftl1 | ferritin light chain 1 | 1.73 | 1.72 |
| IPI00117063 | 233908 | Fus | 53 kDa protein | -2.66 | - |
| IPI00228385* | 14381 | G6pdx | Glucose-6-phosphate 1-dehydrogenase X | -1.54 | -1.93 |
| IPI00310090 | 50917 | Galns | N-acetylgalactosamine-6-sulfatase | - | 1.57 |
| IPI00112129* | 67092 | Gatm | Glycine amidinotransferase, mitochondrial | -2.55 | -4.28 |
| IPI00124675 | 14468 | Gbp1 | Interferon-induced guanylate-binding protein 1 | - | -24.01 |
| IPI00323251 | 14469 | Gbp2 | Interferon-induced guanylate-binding protein 2 | - | 2.77 |
| IPI00230283* | 28030 | Gfm1 | Elongation factor G 1, mitochondrial | 3.36 | 2.32 |
| IPI00123814 | 11605 | Gla | alpha-galactosidase A | - | 1.75 |
| IPI00464317* | 14660 | Gls | glutaminase isoform 1 | 1.99 | 1.81 |
| IPI00169870* | 234407 | Glt25d1 | Glycosyltransferase 25 family member 1 | 1.65 | 1.73 |
| IPI00119095* | 14667 | Gm2a | Ganglioside GM2 activator | 1.97 | 2.50 |
| IPI00347770* | 242851 | Gnat3 | Guanine nucleotide-binding protein G(t) subunit alpha-3 | 2.12 | 2.07 |
| IPI00775863 | 14693 | Gnb2 | Guanine nucleotide-binding protein G(I)/G(S)/G(T) subunit beta-2 | - | 1.68 |
| IPI00317740* | 14694 | Gnb2l1 | Guanine nucleotide-binding protein subunit beta-2-like 1 | -1.63 | -2.09 |
| IPI00221426 | 75612 | Gns | N-acetylglucosamine-6-sulfatase | - | 1.74 |
| IPI00877205 | 14718 | Got1 | Aspartate aminotransferase, cytoplasmic | - | -2.51 |
| IPI00228633 | 14751 | Gpi1 | Glucose-6-phosphate isomerase | - | -1.70 |
| IPI00890906* | 93695 | Gpnmb | glycoprotein (transmembrane) nmb | 8.13 | 6.25 |
| IPI00119058* | 14784 | Grb2 | Isoform 1 of Growth factor receptor-bound protein 2 | -1.71 | -2.41 |
| IPI00117083 | 17713 | Grpel1 | GrpE protein homolog 1, mitochondrial | - | 1.64 |
| IPI00117167* | 227753 | Gsn | Isoform 2 of Gelsolin | -1.69 | -1.57 |
| IPI00172039 | 14960 | H2-Aa | H-2 class II histocompatibility antigen, I-E alpha chain (Fragment) | -2.23 | - |
| IPI00378480 | 26914 | H2afy | Isoform 1 of Core histone macro-H2A.1 | 1.51 | - |
| IPI00110805* | 14964 | H2-D1 | H-2 class I histocompatibility antigen, D-D alpha chain | -2.97 | -1.56 |
| IPI00121908* | 14999 | H2-DMb1 | Class II histocompatibility antigen, M beta 1 chain | -2.84 | -2.33 |
| IPI00113299* | 14969 | H2-Eb1 | H-2 class II histocompatibility antigen, I-A beta chain | 4.78 | 15.63 |
| IPI00114492* | 14972 | H2-K1 | mRNA | 34.48 | 500.00 |
| IPI00850057* | 100044874 | H2-K1 | H-2 class I histocompatibility antigen, K-D alpha chain | -3.81 | -3.90 |
| IPI00624138* | 14964 | H2-L | H-2D cell surface glycoprotein (Fragment) | 3.79 | 3.86 |
| IPI00109996* | 14980 | H2-L | H-2 class I histocompatibility antigen, L-D alpha chain | -24.33 | -46.91 |
| IPI00222809* | 100198 | H6pd | Hexose-6-phosphate dehydrogenase | 3.34 | 4.22 |

| *Protein* | *Gene Entrez ID* | *Gene Symbol* | *Protein name* | *Fold change (C57BL/6' /'BALB/c')* | *Fold change (C57BL/6+IFN' /'BALB/c+IFN')* |
|---|---|---|---|---|---|
| IPI00762198* | 15129 | Hbb-b1 | Beta-globin | 5.65 | 5.21 |
| IPI00115530* | 15212 | Hexb | Beta-hexosaminidase subunit beta | 1.66 | 1.81 |
| IPI00317488* | 52120 | Hgsnat | Heparan-alpha-glucosaminide N-acetyltransferase | 4.93 | 4.39 |
| IPI00284806 | 15452 | Hprt1 | Hypoxanthine-guanine phosphoribosyltransferase | - | -1.83 |
| IPI00626132* | 15108 | Hsd17b10 | Hydroxysteroid (17-beta) dehydrogenase 10 | 1.93 | 1.82 |
| IPI00110224* | 114664 | Hsd17b11 | Isoform 1 of Estradiol 17-beta-dehydrogenase 11 | 1.63 | 1.58 |
| IPI00331628* | 15488 | Hsd17b4 | Peroxisomal multifunctional enzyme type 2 | 1.73 | 1.64 |
| IPI00330804* | 15519 | Hsp90aa1 | Heat shock protein HSP 90-alpha | -1.67 | -1.84 |
| IPI00229080* | 15516 | Hsp90ab1 | MCG18238 | -1.59 | -1.74 |
| IPI00320165 | 53415 | Htatip2 | Oxidoreductase HTATIP2 | - | 1.74 |
| IPI00453499* | 381314 | Iars2 | Isoleucyl-tRNA synthetase, mitochondrial | 1.79 | 1.69 |
| IPI00123570 | 15953 | Ifi47 | Interferon gamma inducible protein 47 | - | -1.90 |
| IPI00136858* | 16181 | Il1rn | Isoform 1 of Interleukin-1 receptor antagonist protein | -1.58 | -1.89 |
| IPI00467447* | 29875 | Iqgap1 | Ras GTPase-activating-like protein IQGAP1 | -1.70 | -1.76 |
| IPI00111285 | 16365 | Irg1 | Immune-responsive gene 1 protein | - | 1.79 |
| IPI00757372* | 664994 | Isoc2a | Isochorismatase domain-containing protein 2A, mitochondrial | 2.15 | 1.93 |
| IPI00761784 | 16409 | Itgam | Integrin alpha-M | 1.61 | - |
| IPI00471246* | 56357 | Ivd | Isovaleryl-CoA dehydrogenase, mitochondrial | 2.08 | 2.05 |
| IPI00421206 | 239217 | Kctd12 | BTB/POZ domain-containing protein KCTD12 | - | -1.64 |
| IPI00462934 | 16549 | Khsrp | Far upstream element-binding protein 2 | - | -1.68 |
| IPI00798492 | 16661 | Krt10 | keratin complex 1, acidic, gene 10 | 6.62 | - |
| IPI00622240 | 16681 | Krt2 | 71 kDa protein | - | 3.00 |
| IPI00466711* | 16784 | Lamp2 | Lysosomal membrane glycoprotein 2, isoform CRA_a | 1.61 | 1.58 |
| IPI00125091* | 16796 | Lasp1 | LIM and SH3 protein 1 | -1.72 | -2.41 |
| IPI00229517* | 16852 | Lgals1 | Galectin-1 | -2.19 | -2.15 |
| IPI00130627 | 19141 | Lgmn | Legumain | -1.60 | - |
| IPI00129265 | 16889 | Lipa | lysosomal acid lipase A | - | 1.62 |
| IPI00462072* | 13806 | Eno1 | Alpha-enolase | -1.53 | -1.89 |
| IPI00230507 | 71679 | LOC100044492 | hypothetical protein | 1.57 | - |
| IPI00139795* | 67186 | LOC100048062 | similar to LOC665931 protein isoform 1 | -1.77 | -1.72 |
| IPI00849349* | 100048461 | LOC100048461 | similar to dendritic cell-associated C-type lectin-1; DECTIN-1 | 5.75 | 6.06 |
| IPI00319188 | 16956 | Lpl | lipoprotein lipase | 1.54 | - |
| IPI00119063 | 16971 | Lrp1 | Prolow-density lipoprotein receptor-related protein 1 | 1.59 | - |
| IPI00469307 | 16976 | Lrpap1 | Alpha-2-macroglobulin receptor-associated protein | - | 1.68 |
| IPI00169818 | 211228 | Lrrc25 | Leucine-rich repeat-containing protein 25 | - | 1.83 |
| IPI00107952* | 17105 | Lyz2 | Lysozyme C-2 | 2.23 | 2.88 |
| IPI00118011* | 110173 | Manba | Beta-mannosidase | 2.87 | 2.56 |
| IPI00117896* | 13589 | Mapre1 | Microtubule-associated protein RP/EB family member 1 | -1.79 | -2.48 |
| IPI00229534* | 17118 | Marcks | Myristoylated alanine-rich C-kinase substrate | -2.00 | -3.02 |
| IPI00128450* | 23943 | Mbc2 | Isoform 1 of Extended synaptotagmin-1 | 1.94 | 1.89 |
| IPI00222546 | 19934 | Rpl22 | 60S ribosomal protein L22 | - | -1.78 |

| *Protein* | *Gene Entrez ID* | *Gene Symbol* | *Protein name* | *Fold change (C57BL/6' /'BALB/c')* | *Fold change (C57BL/6+IFN' /'BALB/c+IFN')* |
|---|---|---|---|---|---|
| IPI00849952 | 269878 | Megf8 | similar to Multiple epidermal growth factor-like domains 8 | - | 1.63 |
| IPI00411071* | 17304 | Mfge8 | Isoform 2 of Lactadherin | 3.02 | 2.93 |
| IPI00132874 | 23945 | Mgll | Monoglyceride lipase | - | 1.58 |
| IPI00137706* | 17524 | Mpp1 | 55 kDa erythrocyte membrane protein | -1.52 | -1.50 |
| IPI00604945 | 246221 | Mpst | 3-mercaptopyruvate sulfurtransferase | - | -1.94 |
| IPI00118963* | 56282 | Mrpl12 | 39S ribosomal protein L12, mitochondrial | 1.58 | 1.53 |
| IPI00754363* | 64656 | Mrps23 | Mrps23 protein (Fragment) | 2.15 | 1.80 |
| IPI00222514 | 218506 | Mrps27 | 28S ribosomal protein S27, mitochondrial | 1.60 | - |
| IPI00750596* | 56428 | Mtch2 | Mitochondrial carrier homolog 2 | 2.16 | 1.68 |
| IPI00355248* | 17708 | mt-Co1 | cytochrome c oxidase subunit I | 1.68 | 1.56 |
| IPI00131176 | 17709 | mt-Co2 | Cytochrome c oxidase subunit 2 | 1.75 | - |
| IPI00480233* | 17721 | mt-Nd6 | NADH dehydrogenase subunit 5 | -2.29 | -2.32 |
| IPI00380896* | 17879 | Myh1 | Myosin-1 | 2.55 | 1.93 |
| IPI00123181 | 17886 | Myh9 | Myosin-9 | 1.58 | - |
| IPI00109044 | 67268 | Mylc2b | Myosin regulatory light chain MRLC2 | 1.51 | - |
| IPI00118120* | 17918 | Myo5a | Myosin-Va | 1.87 | 1.86 |
| IPI00320157* | 67111 | Naaa | N-acylethanolamine-hydrolyzing acid amidase | 2.26 | 2.29 |
| IPI00111831* | 17938 | Naca | Nascent polypeptide-associated complex subunit alpha | -1.89 | -2.74 |
| IPI00315593 | 17939 | Naga | Alpha-N-acetylgalactosaminidase | - | 1.51 |
| IPI00314726* | 27419 | Naglu | Alpha-N-acetylglucosaminidase | 1.53 | 1.61 |
| IPI00124203* | 17972 | Ncf4 | Neutrophil cytosol factor 4 | -2.52 | -3.09 |
| IPI00125960* | 17988 | Ndrg1 | Protein NDRG1 | -5.83 | -6.74 |
| IPI00116748* | 67273 | Ndufa10 | NADH dehydrogenase [ubiquinone] 1 alpha subcomplex subunit 10, mitochondrial | -1.70 | -1.85 |
| IPI00230715 | 67184 | Ndufa13 | NADH dehydrogenase [ubiquinone] 1 alpha subcomplex subunit 13 | - | -2.20 |
| IPI00121288* | 68342 | Ndufb10 | NADH dehydrogenase [ubiquinone] 1 beta subcomplex subunit 10 | -1.57 | -1.98 |
| IPI00308882* | 227197 | Ndufs1 | NADH-ubiquinone oxidoreductase 75 kDa subunit, mitochondrial | -2.60 | -2.62 |
| IPI00229008 | 17993 | Ndufs4 | NADH dehydrogenase [ubiquinone] iron-sulfur protein 4, mitochondrial | - | -1.88 |
| IPI00170093 | 225887 | Ndufs8 | NADH dehydrogenase [ubiquinone] iron-sulfur protein 8, mitochondrial | - | -2.24 |
| IPI00228567* | 212114 | Nhlrc3 | NHL repeat-containing protein 3 | 1.70 | 1.55 |
| IPI00132444* | 66536 | Nipsnap3a | Protein NipSnap homolog 3A | 1.56 | 1.67 |
| IPI00132600 | 18145 | Npc1 | Niemann Pick type C1 | 2.08 | - |
| IPI00129186 | 67963 | Npc2 | Epididymal secretory protein E1 | - | 1.74 |
| IPI00132314 | 18220 | Nucb1 | Nucleobindin-1 | - | 1.51 |
| IPI00321058* | 246730 | Oas1a | 2'-5'-oligoadenylate synthetase 1A | -2.37 | -1.92 |
| IPI00626237* | 18293 | Ogdh | Isoform 1 of 2-oxoglutarate dehydrogenase E1 component, mitochondrial | 1.73 | 1.87 |
| IPI00475158* | 624814 | OTTMUSG00000005734 | similar to NADH dehydrogenase (ubiquinone) Fe-S protein 3 | -1.89 | -1.91 |
| IPI00458105 | 433745 | OTTMUSG00000008543 | similar to ribosomal protein L3 | - | 2.39 |
| IPI00453607* | 18733 | Pira11 | Paired-Ig-like receptor A11 | -28.88 | -100.58 |
| IPI00119305* | 18813 | Pa2g4 | Proliferation-associated protein 2G4 | -1.57 | -1.65 |
| IPI00331552 | 18458 | Pabpc1 | Polyadenylate-binding protein 1 | -1.56 | - |
| IPI00128904 | 23983 | Pcbp1 | Poly(rC)-binding protein 1 | - | -1.76 |

| *Protein* | *Gene Entrez ID* | *Gene Symbol* | *Protein name* | *Fold change (C57BL/6' /'BALB/c')* | *Fold change (C57BL/6+IFN' /'BALB/c+IFN')* |
|---|---|---|---|---|---|
| IPI00127707 | 18521 | Pcbp2 | Isoform 1 of Poly(rC)-binding protein 2 | - | -1.98 |
| IPI00918862* | 66904 | Pccb | Propionyl-CoA carboxylase beta chain, mitochondrial | 1.60 | 1.69 |
| IPI00923036 | 18571 | Pdcd6ip | Isoform 3 of Programmed cell death 6-interacting protein | - | -1.73 |
| IPI00222767 | 27402 | Pdhx | Pyruvate dehydrogenase protein X component, mitochondrial | - | 1.59 |
| IPI00222496* | 71853 | Pdia6 | Protein disulfide-isomerase A6 | 3.08 | 2.89 |
| IPI00283511* | 216134 | Pdxk | Pyridoxal kinase | -1.80 | -1.80 |
| IPI00121013 | 18611 | Pea15a | Isoform 1 of Astrocytic phosphoprotein PEA-15 | - | -2.11 |
| IPI00224740* | 18643 | Pfn1 | Profilin-1 | -1.50 | -1.59 |
| IPI00457898 | 18648 | Pgam1 | Phosphoglycerate mutase 1 | - | -1.88 |
| IPI00407130 | 18746 | Pkm2 | Isoform M2 of Pyruvate kinase isozymes M1/M2 | - | -1.66 |
| IPI00403031* | 102595 | Plekho2 | Pleckstrin homology domain-containing family O member 2 | -1.79 | -2.31 |
| IPI00776023 | 102866 | Pls3 | Plastin-3 | - | -1.85 |
| IPI00274656 | 73078 | Pmpcb | Mitochondrial-processing peptidase subunit beta | - | 1.53 |
| IPI00315452 | 18950 | Pnp1 | Purine nucleoside phosphorylase | - | -1.77 |
| IPI00310567* | 330260 | Pon2 | Serum paraoxonase/arylesterase 2 | 2.24 | 1.97 |
| IPI00400017 | 19024 | Ppfibp2 | Isoform 4 of Liprin-beta-2 | - | 1.76 |
| IPI00554989* | 268373 | Ppia | Peptidyl-prolyl cis-trans isomerase | -1.56 | -1.78 |
| IPI00132020 | 72461 | Prcp | Lysosomal Pro-X carboxypeptidase | - | 1.64 |
| IPI00116192* | 11757 | Prdx3 | Thioredoxin-dependent peroxide reductase, mitochondrial | 1.73 | 1.69 |
| IPI00915044* | 54683 | Prdx5 | Isoform Mitochondrial of Peroxiredoxin-5, mitochondrial | 1.68 | 1.59 |
| IPI00473190* | 19124 | Procr | Protein C receptor, endothelial, isoform CRA_b | 2.38 | 2.95 |
| IPI00654420 | 114863 | Prosc | Proline synthetase co-transcribed bacterial homolog protein | - | -1.63 |
| IPI00321190* | 19156 | Psap | Sulfated glycoprotein 1 | 1.93 | 2.36 |
| IPI00124223* | 19186 | Psme1 | Proteasome activator complex subunit 1 | -1.57 | -1.66 |
| IPI00225419 | 15170 | Ptpn6 | Isoform 2 of Tyrosine-protein phosphatase non-receptor type 6 | - | -1.98 |
| IPI00153702 | 217057 | Ptrh2 | Peptidyl-tRNA hydrolase 2, mitochondrial | 1.81 | - |
| IPI00123278* | 69051 | Pycr2 | Pyrroline-5-carboxylate reductase 2 | 2.00 | 1.96 |
| IPI00653254 | 110095 | Pygl | Phosphorylase | - | -1.88 |
| IPI00459279* | 110391 | Qdpr | Dihydropteridine reductase | -1.78 | -2.24 |
| IPI00116688 | 19340 | Rab3d | Ras-related protein Rab-3D | - | 1.61 |
| IPI00411115 | 235442 | Rab8b | Ras-related protein Rab-8B | 1.91 | - |
| IPI00137618 | 19354 | Rac2 | Ras-related C3 botulinum toxin substrate 2 | - | -1.82 |
| IPI00134621 | 19384 | Ran | GTP-binding nuclear protein Ran | - | -1.85 |
| IPI00110910* | 14961 | H2-Ab1 | H-2 class II histocompatibility antigen, A-D beta chain | -3.57 | -4.00 |
| IPI00113503* | 19893 | Rpgr | Retinitis pigmentosa GTPase regulator (Fragment) | 1.88 | 1.56 |
| IPI00225634* | 20042 | Rps12 | 40S ribosomal protein S12 | -1.77 | -2.04 |
| IPI00134599 | 27050 | Rps3 | 40S ribosomal protein S3 | - | -1.69 |
| IPI00136984 | 20115 | Rps7 | 40S ribosomal protein S7 | - | -1.90 |
| IPI00850840* | 16785 | Rpsa | 40S ribosomal protein SA | -1.58 | -2.54 |
| IPI00134131 | 20280 | Scp2 | Isoform SCP2 of Non-specific lipid-transfer protein | 1.57 | - |
| IPI00338536 | 67680 | Sdhb | Succinate dehydrogenase [ubiquinone] iron-sulfur subunit, mitochondrial | - | -1.77 |

| *Protein* | *Gene Entrez ID* | *Gene Symbol* | *Protein name* | *Fold change (C57BL/6' /'BALB/c')* | *Fold change (C57BL/6+IFN' /'BALB/c+IFN')* |
|---|---|---|---|---|---|
| IPI00454142 | 52398 | Sept11. | Isoform 3 of Septin-11 | - | -2.53 |
| IPI00669817 | 20715 | Serpina3g | Serine protease inhibitor A3G | - | -21.07 |
| IPI00121471 | 20719 | Serpinb6a | Serpin B6 | - | -2.27 |
| IPI00119079* | 20706 | Serpinb9b | Serine (Or cysteine) peptidase inhibitor, clade B, member 9b | -2.44 | -4.22 |
| IPI00115454* | 14057 | Sfxn1 | Sideroflexin-1 | 1.50 | 1.51 |
| IPI00318175 | 27029 | Sgsh | N-sulfoglucosamine sulfohydrolase | - | -2.08 |
| IPI00122265* | 56726 | Sh3bgrl | SH3 domain-binding glutamic acid-rich-like protein | -1.94 | -2.26 |
| IPI00875340* | 20514 | Slc1a5 | 58 kDa protein | -1.99 | -2.24 |
| IPI00308162* | 78830 | Slc25a12 | Calcium-binding mitochondrial carrier protein Aralar1 | 1.68 | 1.79 |
| IPI00131584 | 57279 | Slc25a20 | Mitochondrial carnitine/acylcarnitine carrier protein | - | 2.54 |
| IPI00404341 | 56857 | Slc37a2 | Isoform 1 of Sugar phosphate exchanger 2 | - | -2.20 |
| IPI00776208 | 57319 | Smpdl3a | acid sphingomyelinase-like phosphodiesterase 3a | - | 3.24 |
| IPI00420136* | 54198 | Snx3 | Sorting nexin-3 | -1.80 | -1.78 |
| IPI00112053 | 69178 | Snx5 | Sorting nexin-5 | - | -1.66 |
| IPI00130589* | 20655 | Sod1 | Superoxide dismutase [Cu-Zn] | -1.54 | -1.84 |
| IPI00109109* | 20656 | Sod2 | Superoxide dismutase [Mn], mitochondrial | 1.82 | 1.82 |
| IPI00313998* | 59010 | Sqrdl | Sulfide:quinone oxidoreductase, mitochondrial | 1.58 | 1.52 |
| IPI00318485 | 109552 | Sri | Isoform 2 of Sorcin | - | -2.23 |
| IPI00408243 | 381760 | Ssbp1 | single-stranded DNA binding protein 1 isoform 1 | 1.54 | - |
| IPI00110852* | 107513 | Ssr1 | Translocon-associated protein alpha, muscle specific isoform | 1.96 | 1.59 |
| IPI00122346 | 20832 | Ssr4 | Signal sequence receptor, delta, isoform CRA_c | 1.54 | - |
| IPI00467004* | 20846 | Stat1 | Signal transducer and activator of transcription 1 | -2.25 | -2.19 |
| IPI00121514 | 20867 | Stip1 | Stress-induced-phosphoprotein 1 | - | -1.60 |
| IPI00115117 | 66592 | Stoml2 | Stomatin-like protein 2 | 2.15 | - |
| IPI00125778 | 21346 | Tagln2 | Transgelin-2 | - | -1.82 |
| IPI00620227* | 21356 | Tapbp | Isoform Short of Tapasin | 2.79 | 2.64 |
| IPI00322543 | 21391 | Tbxas1 | Thromboxane-A synthase | 1.53 | - |
| IPI00459493* | 21454 | Tcp1 | Isoform 2 of T-complex protein 1 subunit alpha B | -1.65 | -1.60 |
| IPI00124700* | 22042 | Tfrc | Transferrin receptor protein 1 | -4.13 | -5.45 |
| IPI00126861* | 21817 | Tgm2 | Protein-glutamine gamma-glutamyltransferase 2 | -2.22 | -2.51 |
| IPI00132958* | 66834 | Them2 | Thioesterase superfamily member 2 | 1.90 | 2.04 |
| IPI00465786 | 21894 | Tln1 | Talin-1 | - | -1.69 |
| IPI00132768* | 66154 | Tmem14c | Transmembrane protein 14C | 1.61 | 1.77 |
| IPI00120083* | 74122 | Tmem43 | Transmembrane protein 43 | 1.55 | 1.58 |
| IPI00831626* | 22003 | Tpm1 | 29 kDa protein | -1.90 | -2.07 |
| IPI00421223* | 326618 | Tpm4 | Tropomyosin alpha-4 chain | -1.82 | -2.20 |
| IPI00403810* | 22146 | Tuba1c | Tubulin alpha-1C chain | -1.51 | -1.79 |
| IPI00338039 | 22151 | Tubb2a | Tubulin beta-2A chain | - | -2.38 |
| IPI00169463* | 227613 | Tubb2c | Tubulin beta-2C chain | -1.59 | -2.85 |
| IPI00117352* | 22154 | Tubb5 | Tubulin beta-5 chain | -1.68 | -2.37 |
| IPI00226993* | 22166 | Txn1 | Thioredoxin | -1.50 | -2.18 |

| *Protein* | *Gene Entrez ID* | *Gene Symbol* | *Protein name* | *Fold change (C57BL/6'/'BALB/c')* | *Fold change (C57BL/6+IFN' /'BALB/c+IFN')* |
|---|---|---|---|---|---|
| IPI00133110 | 66073 | Txndc12 | Thioredoxin domain-containing protein 12 | - | 1.55 |
| IPI00776252* | 50493 | Txnrd1 | Isoform 1 of Thioredoxin reductase 1, cytoplasmic | -1.69 | -2.26 |
| IPI00462482 | 227620 | Uap1l1 | Isoform 1 of UDP-N-acetylhexosamine pyrophosphorylase-like protein 1 | - | -1.58 |
| IPI00123313* | 22201 | Uba1 | Ubiquitin-like modifier-activating enzyme 1 | -1.51 | -1.69 |
| IPI00116718 | 22195 | Ube2l3 | Ubiquitin-conjugating enzyme E2 L3 | - | -1.50 |
| IPI00169448 | 22192 | Ube2m | NEDD8-conjugating enzyme Ubc12 | - | -2.35 |
| IPI00417181* | 394432 | Ugt1a5 | UDP-glucuronosyltransferase 1-7C | 1.75 | 1.72 |
| IPI00119138* | 67003 | Uqcrc2 | Cytochrome b-c1 complex subunit 2, mitochondrial | 1.75 | 1.68 |
| IPI00113214 | 22225 | Usp5 | Ubiquitin carboxyl-terminal hydrolase 5 | - | -2.19 |
| IPI00405227* | 22330 | Vcl | Vinculin | -1.86 | -2.32 |
| IPI00122548 | 22335 | Vdac3 | Voltage-dependent anion-selective channel protein 3 | - | 2.19 |
| IPI00120923* | 80743 | Vps16 | Isoform 2 of Vacuolar protein sorting-associated protein 16 homolog | -1.96 | -2.32 |
| IPI00329942 | 30930 | Vps26a | Isoform 2 of Vacuolar protein sorting-associated protein 26A | - | -2.10 |
| IPI00111181 | 65114 | Vps35 | Vacuolar protein sorting-associated protein 35 | - | -1.82 |
| IPI00221817 | 67776 | Vwa5a | Loss of heterozygosity 11 chromosomal region 2 gene A protein homolog | - | -1.80 |
| IPI00314748* | 22388 | Wdr1 | WD repeat-containing protein 1 | -1.95 | -2.09 |
| IPI00230682* | 54401 | Ywhab | Isoform Long of 14-3-3 protein beta/alpha | -1.61 | -2.01 |
| IPI00230707 | 22628 | Ywhag | 14-3-3 protein gamma | - | -1.88 |
| IPI00227392* | 22629 | Ywhah | 14-3-3 protein eta | -1.52 | -1.78 |
| IPI00853924* | 22630 | Ywhaq | Isoform 1 of 14-3-3 protein theta | -1.82 | -2.17 |
| IPI00116498 | 22631 | Ywhaz | 14-3-3 protein zeta/delta | - | -2.02 |
| IPI00387422* | 22793 | Zyx | Zyx protein | -1.99 | -3.67 |

Symbol * indicate proteins which differently expressed between two mouse strains in both control and IFN-γ treatment condition. Positive fold change value means higher in BMM-C57BL/6, negative value means lower in BMM-C57BL/6. Thresholds for considering differences as significant were a minimum 1.5 fold change, and $p \leq 0.01$.